MECHANICAL PROPERTIES AND FATIGUE BEHAVIOR OF UNITIZED COMPOSITE AIRFRAME STRUCTURES AT ELEVATED TEMPERATURE

THESIS

Michael P. Wilkinson, Captain, USAF

AFIT-ENY-14-M-51

DEPARTMENT OF THE AIR FORCE
AIR UNIVERSITY

AIR FORCE INSTITUTE OF TECHNOLOGY

Wright-Patterson Air Force Base, Ohio

AFIT-ENY-14-M-51

MECHANICAL PROPERTIES AND FATIGUE BEHAVIOR OF UNITIZED COMPOSITE AIRFRAME STRUCTURES AT ELEVATED TEMPERATURE

THESIS

Presented to the Faculty

Department of Aeronautics and Astronautics

Graduate School of Engineering and Management

Air Force Institute of Technology

Air University

Air Education and Training Command

in Partial Fulfillment of the Requirements for the

Degree of Master of Science in Aeronautical Engineering

Michael P. Wilkinson, B.S.M.E.

Captain, USAF

March 2014

AFIT-ENY-14-M-51

MECHANICAL PROPERTIES AND FATIGUE BEHAVIOR OF UNITIZED COMPOSITE AIRFRAME STRUCTURES AT ELEVATED TEMPERATURE

Michael P. Wilkinson, B.S.M.E.
Captain, USAF

Approved:

//signed//	12 Mar 2014
Marina B. Ruggles-Wrenn, PhD (Chairman)	Date
//signed//	10 Mar 2014
Thomas G. Eason, PhD (Member)	Date
//signed//	12 Mar 2014
Richard B. Hall, PhD (Member)	Date

AFIT-ENY-14-M-51

Abstract

The tension-tension fatigue behavior of newly developed polymer matrix composites (PMCs) and that of a unitized composite was studied. The PMCs investigated in this effort consisted of an NRPE (a high-temperature polyimide) matrix reinforced with carbon fibers. Two PMCs consisting of the aforementioned matrix with different fiber architectures were studied: one reinforced with a 2D woven fiber fabric and another reinforced with a non-crimp 3D orthogonal woven fiber fabric. The unitized composite consisted of a PMC co-cured with a ceramic matrix composite (CMC) layer, which acts as a thermal barrier. The PMC portion of the unitized composite had the same constituent properties and weave as the aforementioned 2D PMC. The CMC layer consisted of a zirconia-based matrix reinforced with a 2D woven quartz fiber fabric. For all three material systems (3D PMC, 2D PMC, and unitized composite), material properties were investigated for both on-axis [0/90°] and off-axis [±45°] fiber orientations. Tensile properties were evaluated at (1) room temperature and (2) with one side of the specimen at 329°C and the other side exposed to ambient air. Tension-tension fatigue tests were conducted at elevated temperature at a frequency of 1.0 Hz with a ratio of minimum stress to maximum stress of R= 0.05. Fatigue run-out for this effort was defined as 2×10^5 cycles. Both strain accumulation and modulus evolution during cycling were analyzed for each fatigue test. Elevated temperature had little effect on the tensile properties of all three material systems with the 0/90° fiber orientation; however, specimens with the ±45° fiber orientation exhibited a significant increase in failure strain at elevated temperature. The ultimate tensile strength (UTS) of both PMCs (2D weave and 3D weave) with the ±45° fiber orientation decreased slightly at elevated temperature, but the UTS of the unitized composite with ±45° fiber orientation showed no significant change. Neither the 3D PMC nor the unitized composite exhibited an increase in tensile strength and stiffness compared

to the 2D PMC. However, the 2D PMC with ±45° fiber orientation produced significantly greater failure strain. The 2D PMC showed slightly better fatigue resistance than both the 3D PMC and the unitized composite with 0/90° fiber orientation. For the ±45° fiber orientation, the fatigue limit for the 2D PMC was approximately two times greater than those for the 3D PMC and the unitized composite. Specimens that achieved fatigue run-out were subjected to tensile tests to failure to characterize the retained tensile properties. Microstructural investigation of tested specimens revealed delamination in the 2D PMC and very severe delamination in the unitized composite. However, the 3D PMC offered improved delamination resistance.

Acknowledgments

First and foremost, I would like to thank my Lord and Savior Jesus Christ for this opportunity and for sustaining me throughout the past year and a half. I would also like to thank my advisor, Dr. Ruggles-Wrenn, for her consistent tutoring and countless hours of support and guidance she has given me. In addition, I would like to thank my committee members, Dr. Thomas Eason (AFRL/RQHF) and Dr. Richard Hall (AFRL/RXCCP), for their time and support. My thanks are also extended to my research sponsor, Mr. Michael Falugi (AFRL/RQVS), for making this research effort possible by providing the material.

I would also like to thank Lt Col Ryther for his timely support and access to AFRL laboratories. I would like to thank the AFIT model shop personnel, namely Mr. Jan LeValley, Mr. Chris Harkless, and Mr. Dan Ryan, for their work and dedication to quality. Thanks also go to Mr. Barry Page and especially Mr. Chris Zickefoose for their lab support. Finally, I would like to thank my lab mate, Capt Skyler Hilburn, for his friendship and support throughout this endeavor.

Michael P. Wilkinson

Table of Contents

Page

Page

List of Figures

List of Tables

List of Symbols

Symbol	Definition
E	elastic modulus (GPa)
ϵ	strain (m/m or %)
N	cycles (number)
R	fatigue stress ratio
σ or S	stress (MPa)
T	temperature (°C)
V_f	fiber volume fraction (%)

List of Acronyms

Acronym	Definition
AFRL	Air Force Research Laboratory
AFIT	Air Force Institute of Technology
dpi	dents per inch
CMC	Ceramic Matrix Composite
HTPMC	High Temperature Polymer Matrix Composite
MS	Material System
MTS	Material Test Systems
PAN	Polyacrylonitrile
PMC	Polymer Matrix Composite
ppi	picks per inch
SiC	Silicon Carbide
TPS	Thermal Protection System
UTS	Ultimate Tensile Strength

MECHANICAL PROPERTIES AND FATIGUE BEHAVIOR OF
UNITIZED COMPOSITE AIRFRAME STRUCTURES
AT ELEVATED TEMPERATURE

I. Introduction

"The greatest revolution in aircraft structures since the all-aluminum Northrop Alpha has been the ongoing adoption of composite materials for primary structure" [25].

1.1 Motivation

The quest to find the optimum balance of low-weight structural materials with excellent mechanical properties, all at a reasonable cost, continues to elevate composite materials in the aerospace industry as potential replacements for existing metal alloy structures. Airframe structures and components on many existing and future Air Force systems reach elevated temperatures during operation. Examples include hypersonic vehicle airframes, engine related components (such as engine ducts, engine vanes, and exhaust flaps), and hot trailing edges of B-2 and C-17 wings. Material systems that show improved fatigue performance, excellent thermal resistance and damage tolerance, as well as resistance to corrosion are prime candidate materials for potential air vehicle structural components. Because of their impressive mechanical performance while being light weight (i.e. high strength to weight ratio), advanced composites are increasingly being researched, developed, and utilized for the aerospace applications mentioned above. As an example, the increased use of composite materials in fighter aircraft structures can be seen in Figure 1.

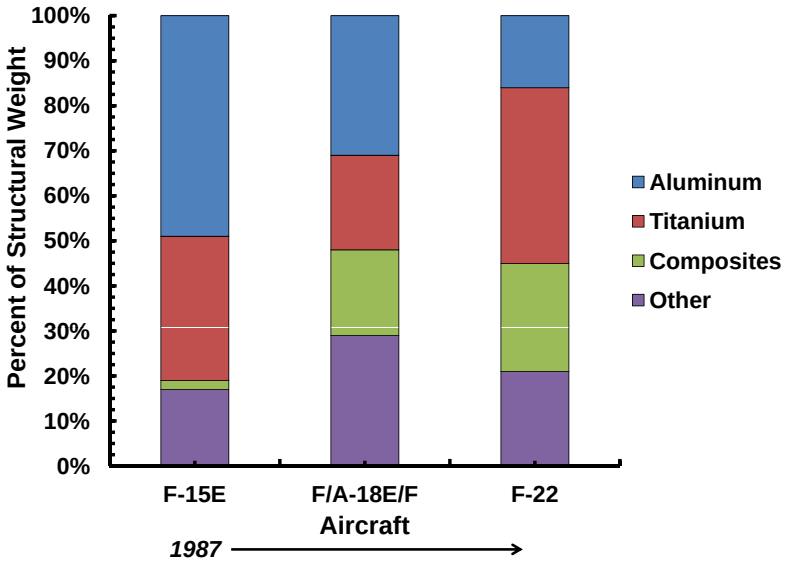

Figure 1: Aircraft structure material use over time. Data from [21].

Polymer Matrix Composites (PMCs) and Ceramic Matrix Composites (CMCs) are two types of composites used in aircraft structures subjected to high temperatures. The "state-of-the-art" polyimide resin used as the matrix constituent for High Temperature Polymer Matrix Composites (HTPMCs) in the aerospace industry is PMR-15 resin; however, replacement polyimide resins are being researched and developed partly due to the carcinogenic elements in PMR-15 [17]. One such polyimide is NRPE, which has been developed by Performance Polymer Solutions Inc. ($P^2SI^{®}$) of Moraine, OH as a possible replacement for PMR-15. $P^2SI^{®}$ has recently fabricated two carbon-reinforced NRPE-matrix composites for the Air Force Research Laboratory (AFRL), one with a two-dimensional (2D) weave and the other with a three-dimensional (3D) weave. 3D woven composites are of interest because of their mechanical properties and the ability to manufacture net preform shapes. The Beach Starship and the F-35 have both incorporated 3D woven composites [31]. Since the carbon/NRPE composites are new material systems intended for aerospace applications, they must be studied and tested to verify that the mechanical properties are sufficient for use in the operating environments. The Air Force

Institute of Technology (AFIT) has conducted extensive research on PMR-15 neat resin and some HTPMCs. This body of knowledge provides a basis for evaluating other similar materials.

Another composite recently developed by $P^2SI^{®}$ consists of a PMC and a thin CMC layer co-cured together to form a single material system. The purpose of combining these two types of composites together is to create a unitized material with a CMC layer that acts as a thermal barrier for the PMC. As can be seen in Figure 2, CMCs offer a dramatic increase in service temperature over carbon fiber reinforced plastics and other structural materials [32]. CMCs are a class of material that can perform at extreme temperatures and exhibit higher strength, elastic modulus, and hardness than PMCs [9, p. 4]. This research effort aims to investigate how well this CMC thermal barrier performs its intended function will be examined in this research effort.

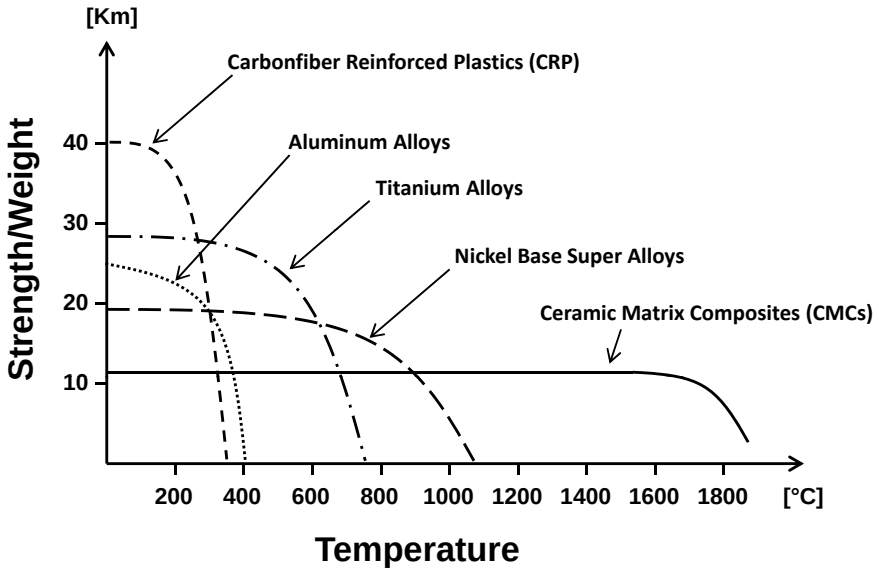

Figure 2: Strength to weight ratio vs. operating temperature comparison for various materials. Data from [32].

Advances in Thermal Protection Systems (TPSs) are vital to the success of many aerospace systems. Finding cost efficient yet functional replacements for current TPS materials and components is becoming more important as increased operating temperatures are required. Efforts are underway to develop new materials and methods for TPS systems, with many studies focusing on CMCs [4, 13, 16, 26]. This research is focused on experimental investigation of the mechanical properties and behavior of a new material system for possible use as a TPS material.

1.2 Problem Statement

PMCs are used in aircraft structure applications where high strength is required with a weight savings over legacy metal structural components. Many of these structural components are subjected to higher temperatures that exceed the melting temperature of the matrix constituent of HTPMCs. Thus, either a new material should be used or a TPS or thermal barrier should be employed to allow operation at these elevated temperatures. New material systems developed for these applications must have their mechanical properties evaluated through extensive testing in simulated environments to determine their ability to withstand complex loading and high temperature environments. Mechanical properties at room temperature are required to form a baseline with which to compare the material responses at elevated temperature. This mechanical property characterization will be performed on the new PMC and unitized composite material systems studied in this research effort.

1.3 Thesis Objective

The objective of this research was to experimentally determine the mechanical properties of three new composite material systems (referred to as MS1, MS2, and MS3) at room temperature and elevated temperature. The material systems evaluated in this research were:

MS1: PMC with 3D woven fibers

MS2: PMC with 2D woven fibers

MS3: Unitized PMC/CMC with 2D woven fibers

Monotonic tensile tests to failure were conducted at room temperature to assess the baseline material properties for each material system. The same tests were then conducted with one side of the specimen subjected to a temperature of 329°C with the other side open to ambient air to simulate actual operating environment. To assess fatigue performance, tension-tension fatigue tests were conducted under the same elevated temperature conditions. Note that in the case of elevated temperature tests conducted on MS3, the CMC side was the side subjected to 329°C. All tests were performed on specimens with 0/90° fiber orientation and on specimens with ±45° fiber orientation to assess both fiber- and matrix-dominated composite properties and behaviors.

1.4 Methodology

The key objectives outlined above were achieved as follows:

1. Perform room temperature modulus tests to assess specimen-to-specimen variability.

2. Perform monotonic tensile tests to failure to determine tensile properties for both 0/90° and ±45° fiber orientations at room temperature and at elevated temperature.

3. Compare results obtained for different material systems and assess whether one material system shows a marked improvement in performance compared to others.

4. Perform tension-tension fatigue tests to evaluate material fatigue behavior for both 0/90° and ±45° fiber orientations at elevated temperature. Construct S-N curves and determine fatigue limits for the run-out condition of 2×10^5.

5. Compare fatigue results obtained for different material systems and assess whether one material system offers improved fatigue durability compared to others.

6. Examine tested specimens under an optical microscope to assess damage and failure mechanisms.

II. Background

2.1 Composite Structure

In general terms, a *composite* is a material composed of two or more different constituent phases, each with different material properties. These phases are called the *matrix* (typically a polymer, metal, or ceramic resin) and the *reinforcement* (can also be polymeric, metallic, or ceramic) in the form of fibers, whiskers, or particulate. The motivation for combining two dissimilar materials lies in the fact that an improvement in mechanical performance and properties can be realized compared to the constituent materials acting alone [11]. As mentioned earlier, composites are used in aerospace applications because of their relatively high strength to weight ratio. However, this weight savings comes at a monetary cost as composites are more expensive to manufacture and there is a high cost associated with certifying new composite structural components. This cost, along with lower damage tolerance and low through-thickness strength, have made the metal-to-composite transition in aerospace applications a slower than expected process [31].

The purpose of the matrix phase in a composite is to transmit shear loads to the reinforcement fibers, provide strength in the direction normal to the fibers, and bind the fibers together. The reinforcement is the main load-bearing phase, and typically has greater tensile strength and stiffness than the matrix phase. One layer of fibers (whether unidirectional or as a woven fabric) with matrix material is termed a *lamina* or ply. When multiple plies are stacked and bonded together at various fiber orientations, it is known as a *laminate*. Laminated composites of different thicknesses can be made by changing the number of plies. An undesirable phenomenon observed in laminated composites is interlaminar separation or *delamination*. This delamination can also interact with transverse cracking during the failure process. [11]

2.2 Polymer Matrix Composites

The polymer matrix in PMCs can be either a thermoplastic or thermosetting resin. Thermoplastics become softer at higher temperatures, but then harden again upon cooling, a process that can be repeated and is reversible. Thermosets, in contrast, become permanently hard upon heating due to covalent crosslinks that form on a molecular level and retain much of their strength close to their melting temperatures. However, thermosets can be heated to the point where the crosslink bonds sever and the polymer degrades. Typically thermosets are stronger, harder, and have better dimensional stability than thermoplastics [5, pp. 467-468]. Thermosets can further be divided into polyesters, epoxies, and polyimides, with the latter having a maximum use temperature of 370 °C. High-temperature polymides are used in HTPMCs for aerospace applications in an effort to meet thrust-to-weight requirements of advanced fighters, which has driven a desire for polymer matrix materials to continuously operate at temperatures ranging from 371°C to 427°C [22]. PMR-15 and NRPE are both high-temperature polyimides.

Typical reinforcement materials used in PMCs are glass, carbon, silicon carbide (SiC) and aramid. The most frequently used reinforcement material is carbon [9, pp. 48,52]. The Material Systems (MSs) examined in this research contain carbon fibers.

2.3 Ceramic Matrix Composites

CMCs utilize a ceramix matrix and a ceramic fiber. High performance ceramics, such as oxides, nitrides, and carbides of silicon, aluminum, titanium, and zirconium are commonly used in CMCs. These advanced ceramics have very high resistance to heat, chemicals, and wear, but are difficult to fabricate simply and economically. Monolithic high performance ceramics also exhibit high strength and hardness while having a low density; however, they are very brittle and are prone to catastrophic failure under mechanical or thermal loading [9, pp. 2-3]. Therefore, ceramics are reinforced to create CMCs that can handle higher and more complex loading without failing catastrophically.

The CMC thermal protection layer in MS3 has a Silicon Carbide (SiC) matrix. Silicon carbide has excellent resistance to erosion and chemical attack, however, it also oxidizes readily in oxidizing environments at high temperatures. Reinforcements in CMCs are typically also ceramics. The most attractive form of reinforcement for high temperature structural ceramic composites is continuous ceramic fibers because they combine high strength and stiffness with high temperature capability [9].

2.4 Composite Interface Region

The interface region between the matrix and the fibers also plays an important part in PMCs and CMCs. A strong bond between matrix and fiber is desired for PMCs, whereas for CMCs a weak interface is needed to provide for crack deflection around the fibers and to prevent brittle failure of the CMC. It is desired that CMCs fail "gracefully", which is achieved by debonding at the fiber-matrix interface, crack deflection, and subsequent fiber pullout. [9]

2.5 Composite Tensile and Fatigue Response

A representative stress-strain curve for a composite and it's constituent materials is shown in Figure 3. The Young's Modulus (or Modulus of Elasticity), E, which is a measure of a material's stiffness, is defined as the slope of the stress-strain curve in the linear range of the material response. The stress-strain response may become nonlinear, and therefore, a tangent modulus can be found by taking the slope of a tangent line to the stress-strain curve. The ultimate tensile stress is the greatest stress supported by the material, although it does not necessarily have to be the point of failure.

Fatigue testing is important in characterizing material response under cyclic loading. Fatigue can be defined as the degradation of mechanical properties leading to failure under cyclic loading. The cyclic lifetime of a material under cyclic loading can be experimentally determined and plotted on a maximum stress vs. cycles to failure curve

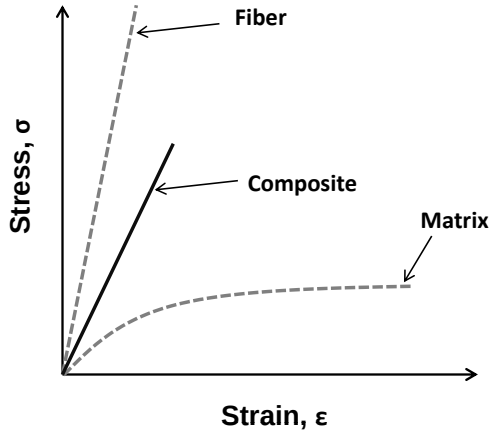

Figure 3: Representative tensile stress-strain curve
for a composite and its constituent materials

(S-N curve), as seen in Figure 4. A material might have an endurance limit, which means for stresses below such a limit, the material could theoretically be cycled indefinitely. [9]

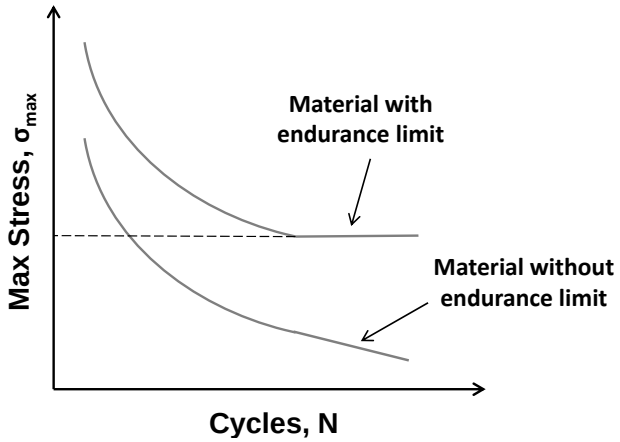

Figure 4: Example of S-N curves

2.6 Composite Weave Patterns

Initially, composites reinforced with a woven fabric only utilized a 2D weave. This weave pattern consists of two orthogonal sets of interlaced yarns. The fibers running in the

longitudinal direction of the fabric are called the *warp* fibers, and the fibers running transversely are termed *weft* or *fill* fibers [11]. Figure 5 shows examples of different 2D weave styles [14, p. 7-5].

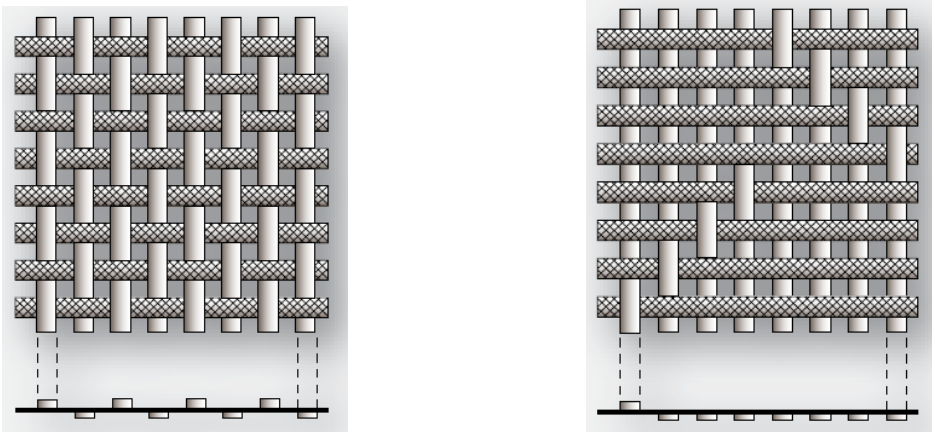

(a) plain weave (b) 8 harness satin weave

Figure 5: Examples of fabric weave patterns [14, p. 7-5]

The fabric *crimp*, a measure of the yarn waviness, is another variable that affects fabric reinforcement behavior. Crimp gives a relationship between fabric length and length of the yarn. For example, if the fibers are interlaced to form a woven fabric (as in most 2D composite structures), the actual fiber yarn length is slightly longer than the overall fabric length because the yarns are not perfectly straight. This waviness, or *crimp*, will cause reduced composite mechanical properties compared to those that could be obtained if the fibers were not interlaced and straight. [1]

In order to increase strength in the through-thickness direction of the composite and to reduce ply delamination, three-dimensional woven composites are being researched and utilized in composites. In 3D woven composites the fabric consists of in-plane yarns that are perpendicular to each other (standard 2D layup) and also contain through-thickness yarns (Z yarns), which can be angled through the thickness or perpendicular to the

in-plane yarns. This additional out-of-plane fiber orientation produces higher through-thickness strength and stiffness of the composite material. However, the introduction of through-thickness fiber tows usually decreases the in-plane fiber volume fraction, and thus, leads to lower in-plane strength and modulus [33]. In fact, Stig [34] found that compared to 2D laminates, the 3D woven fabric (with warp and weft yarns interlaced in a plain weave) reinforcements resulted in lower composite in-plane stiffness and strength, but increased out-of-plane strength by 22-40%. Therefore, composites with 3D fiber weaves would seem to be desirable in applications where complex out-of-plane loading occurs or for delamination resistance. In aircraft structures, most composites have been required to bear in-plane loads (as is the case with airframe structures). However, advances in composites have made them desirable for use in more structural components throughout the aircraft where out-of-plane loads may be seen.

Not all 3D weaves are created equal, however, and the mechanical properties of composites wth different 3D fiber weaves have been reported as both higher and lower compared to those of 2D woven composites [31]. A 3D weave composite investigated in this effort utilizes a non-crimp 3D orthogonal weave. In this weave, there is no interlacing of the warp and fill yarns, which means they are straight. The in-plane fiber layers are interlaced ("tied together") by through-thickness Z fiber yarns. Figure 6 schematically shows a non-crimp 3D orthogonal weave structure.

Although having the warp and fill yarns straight would serve to increase the in-plane mechanical properties, the in-plane properties should be naturally reduced due to the reduced in-plane fiber volume fraction. However, as will be discussed in Section 2.7.4, some experimental results have shown that non-crimp 3D orthogonal woven composites offer an improvement in the in-plane mechanical properties compared to their 2D weave counterparts. [1]

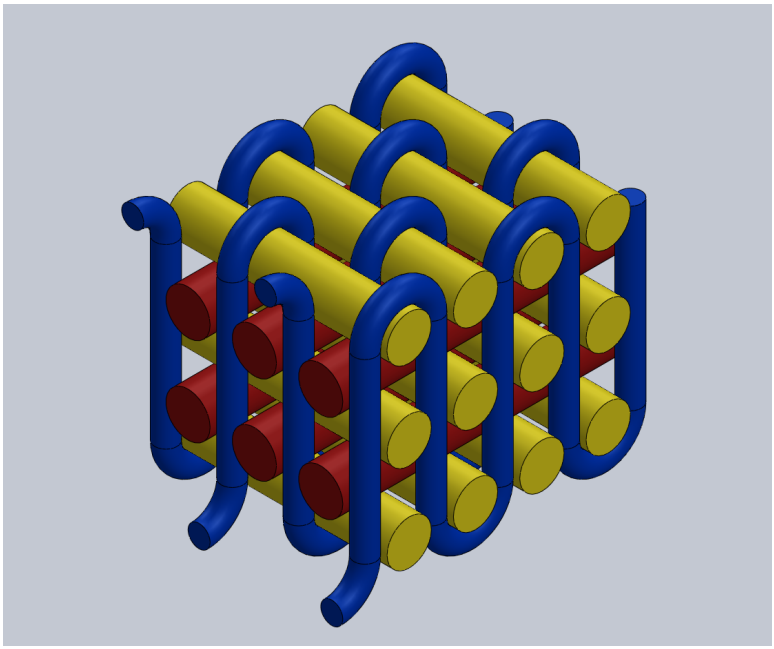

Figure 6: Schematic of a non-crimp 3D orthogonal weave. Warp yarns in red, fill yarns in yellow, and Z yarns in blue.

2.7 Previous Research: Experimental Investigations

Because the present study is focused on new material systems, there is no past research specifically addressing them. However, AFIT has conducted past research into mechanical behavior of PMR-15 polyimide resin, PMR-15/carbon fiber PMCs, and SiC based CMCs. These materials are similar to the constituents used in the present material systems, and therefore provide a baseline for this research. Several recent studies also focused on non-crimp 3D orthogonal weave composites. As the co-cured unitized composite is a novel material system, there is no known research on such unitized composites. However, related topics have been researched and will be briefly discussed.

2.7.1 PMR-15: Mechanical Behavior.

It is important to have a reference baseline when assessing whether a new material offers improvements over an existing one. The PMC in this research must operate at temperatures up to 329°C. Ryther [30] has examined PMR-15 resin (the leading polyimide

resin in HTPMC use) response to elevated temperatures in the range of 274-316°C. He observed that temperature had a significant effect on the stress-strain behavior of PMR-15, namely decrease in elastic modulus with increasing temperature (Figure 7) and earlier departure from the quasi-linear stress-strain behavior with increasing temperature [30].

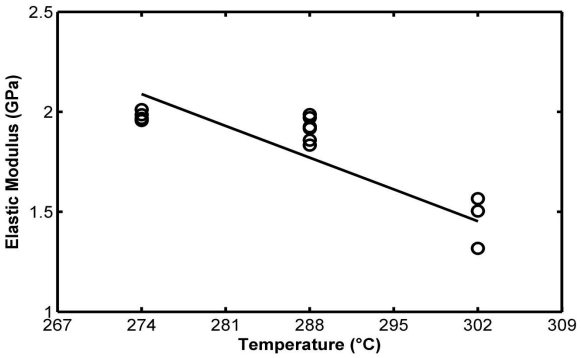

Figure 7: Elastic tensile modulus vs. temperature for PMR-15 neat resin (Reproduced from [30])

The change in the stress-strain curve for PMR-15 neat resin with increasing temperature can be seen in Figure 8. It is evident that the ultimate tensile strength of PMR-15 decreases significantly at 302°C which is closer to the elevated temperature used in the present effort.

2.7.2 HTPMC Research.

Response of a carbon/PMR-15 unidirectional composite at elevated temperature was studied by Odegard and Kumosa [23]. The carbon fibers in the composite were the same as those used in the 2D PMC of the present study. The authors performed tensile tests at temperatures ranging from room temperature to 316°C (the upper limit for retention of mechanical properties in PMR-15). It was observed that both longitudinal and transverse moduli decreased almost linearly with increasing temperature. The longitudinal modulus was reduced by 10% and the transverse modulus by 31% compared to the room temperature values. The shear modulus showed a nonlinear trend in reduction with

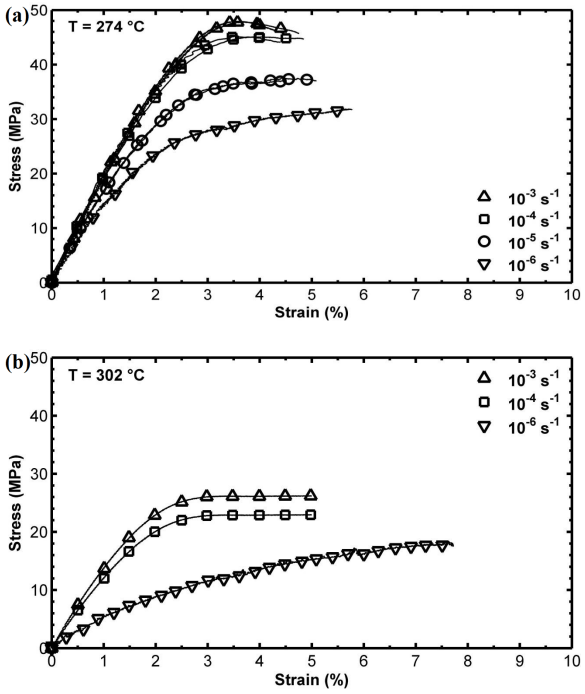

Figure 8: Tensile stress-strain curve for PMR-15 conducted at:
(a) 274°C, and (b) 302°C (Reproduced from [30])

increasing temperature. Plasticity parameters were determined and their dependence on temperature illustrate that the nonlinear behavior of the carbon/PMR-15 composite increases as a function of temperature. [23]

Tension-tension fatigue response of another HTPMC, IM7/BMI 5250-4 graphite/bismaleimide composite, at an elevated temperature of 191°C was studied by Ladrido at AFIT [19]. Tensile stress-strain response of this PMC in both the 0/90° and the ±45° fiber orientations can be seen in Figure 9. These stress-strain curves are typical for a PMC at elevated temperature where the strong fibers sustain the load in the 0/90° direction and the matrix bears most of the load in the ±45° orientation.

Ladrido actually observed stiffening of the ±45° specimens during fatigue tests (i.e. the modulus slightly increased). This phenomenon was attributed to the “scissoring” effect, where fibers were possibly realigning in the direction of load during cyclic loading.

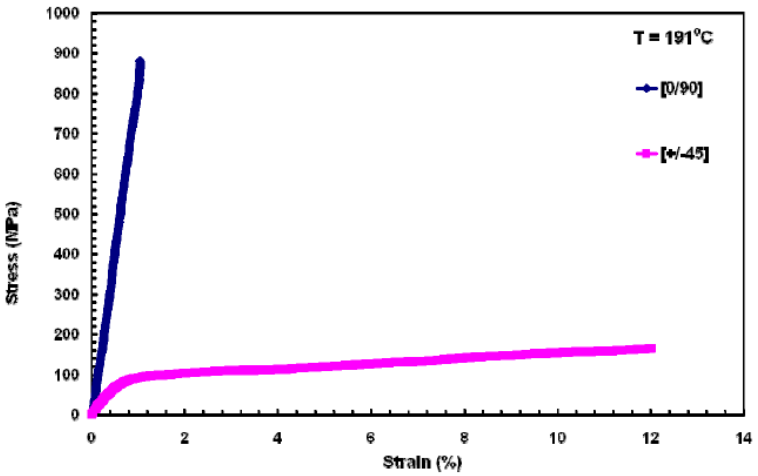

Figure 9: Stress-strain curves obtained in tension tests on as received specimens with 0/90° and ±45° fiber orientations (Reproduced from [19])

It was also observed that after a specimen reached fatigue run-out, its retained strength was lower, while its modulus remained unchanged [19].

2.7.3 CMC Research.

Numerous experimental studies of fatigue of CMCs at elevated temperature have been conducted at AFIT. These studies have focused on very high temperatures (from 1,000°C to 1,300°C) and most have explored operating in harsh environments, such as steam. Although such high temperatures and steam environment are not being explored in this effort, some useful insight into CMC performance can be gleaned from previous CMC studies. Therefore, results from a few of these past studies will be highlighted here.

Delapasse studied tension-tension fatigue of a Hi-Nicalon^{TM}/SiC-B_4C composite in air and steam [12]. Stress-strain response obtained in air at 1,200°C is shown in Figure 10. The composite exhibited a noticeable knee in the stress-strain curve near the proportional limit (the point at which the material response is no longer linear). Delapasse notes that this bi-linear characteristic is typical for tensile stress-strain curves for CMCs with the

dense matrix. During fatigue, a loss in stiffness was seen. For specimens that achieved run-out, significant reductions in the tensile strength and modulus were reported. [12, 28]

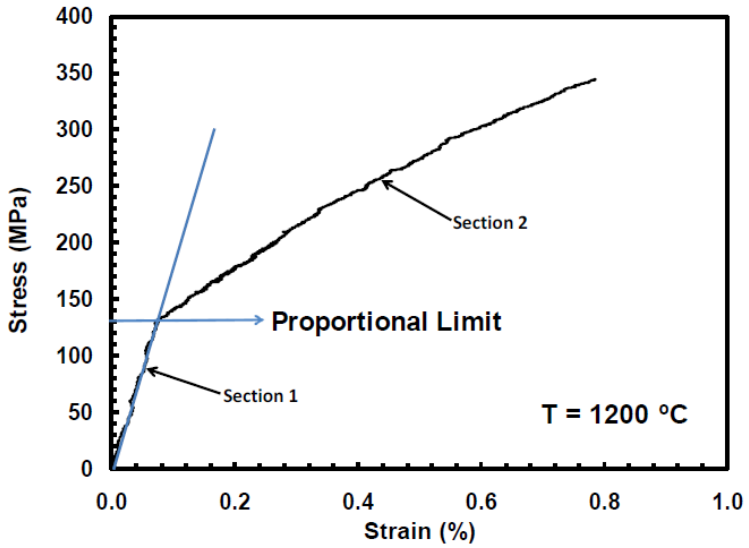

Figure 10: Tensile stress-strain curve obtained for the Hi-Nicalon/PyC/HyprSic composite at 1200°C showing the proportional limit. The bilinear nature of the stress-strain curve is evident. (Reproduced from [12])

Other studies of tension-tension fatigue of advanced CMCs such as those by Ruggles-Wrenn and Sharma [29] and Ruggles-Wrenn et al. [27] showed that those particular CMCs retained 100% of their tensile strength after being fatigued to the run-out condition. Again, loss of modulus during cyclic loading was seen [27, 29].

2.7.4 Three-Dimensional Woven Fabric Composites.

As discussed in Section 2.6, the addition of through-thickness (out-of-plane) fibers has been seen to reduce the in-plane mechanical properties of composites. However, surprising results were obtained for non-crimp 3D orthogonal woven composites. A detailed summary is presented elsewhere [1]. Carbon fiber/epoxy non-crimp 3D orthogonal woven composites were studied and compared to a laminated carbon fiber/epoxy 2D plain weave composite and a carbon fiber/epoxy 3D warp interlock weave

composite. As expected, the tensile modulus in the warp direction for both 3D woven composites was lower than that for the 2D woven composite. A 10-14% decrease of modulus was observed in the 3D orthogonal woven composite. Yet, the 3D orthogonal weave exhibited approximately a 22% higher modulus compared with the 3D interlock weave composite. Additionally, the 3D orthogonal woven composite exhibited a slightly higher modulus than the 2D woven composite in the weft direction. Surprisingly, the in-plane tensile strength of the 3D orthogonal woven composite was significantly higher than that for both the 2D woven and 3D interlock woven composites in both the warp and weft directions. In the warp direction, the improvement in tensile strength over the 2D woven composite was greater than 25%. Therefore, the authors concluded that non-crimp 3D woven composites could compete with tape-based laminates. [1, 3]

Carvelli et al. [8] conducted tension-to-failure tests on 2D plain woven and non-crimp 3D orthogonally woven E-glass composites. Their results again show an improvement of in-plane properties of the 3D orthogonal woven composite over that of the 2D weave. The Young's modulus values for both the warp and fill directions of the 3D weave were very similar to each other and were slightly higher than the modulus of the 2D weave composite. The 3D weave composite also exhibited significantly higher ultimate tensile strength and failure strain in the fill direction compared to the warp direction and compared to the 2D weave composite. The warp direction had higher ultimate stress and nearly the same failure strain as the 2D woven composite. The authors postulate that this increase in composite in-plane properties is due to absence of crimp in the 3D composite and the low fiber damage from weaving in the fill direction. [8]

Carvellie et al. also performed tension-tension fatigue tests on both the 2D plain weave and 3D non-crimp orthogonal weave composites. For a "high cycle" case (specimen sustained five million cycles at a low σ_{max}), the specimen lost stiffness continuously up to two million cycles, after which the stiffness remained nearly

unchanged. However, for a "high stress" case (specimen is cycled with a high σ_{max} and obtained failure), the stiffness continuously decreased and the hysteresis area increased up until failure. These trends were valid not only for the 3D warp direction, but also the 2D plain weave composite. The fill direction of the 3D weave exhibited the best fatigue performance, consistently sustaining more cycles than the 2D weave and 3D warp direction at the same maximum stress level. The fatigue performance of the 3D weave composite in the warp direction was worse than that of the 2D composite for low and moderate stresses, but showed improvement at higher stress levels. The authors submit some compelling reasons why there is a difference in performance in the warp and fill directions for the 3D weave composite. These possible explanations are given as [8]:

1. More fiber damage to the warp yarns from weaving than the to fill yarns
2. Presence of Z yarns creates many local pockets of pure matrix
3. Possible effect from differing frictional contact of Z yarns to warp yarns during cycling in the warp direction (where Z yarns are subjected to the in-plane loads) compared to frictional contact of Z yarns to fill yarns during cycling in the fill direction (where Z yarns are not loaded)

Another explanation could be the different types of damage and rates of damage development when loaded in each the warp and fill directions. This difference was said to be caused by the fabric architecture. When loaded in the warp direction, Z yarns would induce a stress concentration at the crossover sites with the fill yarn. [8]

It is important to note that the above comparisons of 3D non-crimp orthogonal weave composites against 2D plain weave composites can be made because the composites had similar thickness and fiber volume fraction and were comprised of the same constituent materials.

Experimental research conducted by Bogdanovich et al. [2] on a 3D non-crimp orthogonal woven carbon/epoxy composite revealed interesting characteristics of the stress-strain behavior. It was observed that the stress-strain curve for loading in the warp and fill directions actually exhibited a slight "S-shape". The modulus monotonically increased for low strains (< ~1.0%) and then monotonically decreased for higher strain levels (> ~1.0%). Possible explanations for this phenomenon were given as [2]:

1. A well-known carbon fiber "stiffening" effect with increasing strain (non-Hookean behavior)
2. A well-known fiber "straightening" effect
3. A "softening" of the composite from amassed damage during loading

Notably, the fill-directional modulus increase was about three times greater than the modulus increase in the warp direction [2].

Regarding tensile strength of the above carbon/epoxy 3D orthogonal weave composite, both warp and fill directions showed significantly higher strength than the in-plane strength values of 3D interlock weave carbon/epoxy composites. Also, the warp direction exhibited 5.8% higher strength than the fill direction. The authors note that the fibers used in the warp direction had a 6.3% higher strength than the fibers in the fill direction, but the volume of fill fibers was 11.1% larger than the warp fibers. Possible explanations for the higher strength in the warp direction include [2]:

1. Possible higher fill yarn damage from the weaving process
2. Stress concentrations at the surface fill yarns due to the interlaced Z yarns

Bogdanovich et al. also cite other studies on similar 3D non-crimp orthogonal woven composites that have resulted in the warp direction strength being higher than that of the fill direction despite the higher volume of fill fibers [2].

The same carbon/epoxy 3D non-crimp orthogonal weave composite was also tested in the off-axis direction (±45° fiber orientation). Results showed a highly nonlinear stress-strain response at strains exceeding 0.1%. The ultimate strength was significantly lower than the warp and fill direction strengths. The response followed the general trend of 2D orthogonal woven composites, cross-ply laminates, and 0/90° and ±45° stitch-bonded fabric composites when loaded in the off-axis direction. This stress-strain response is attributed to matrix micro-damage and the "scissoring" deformation effect [2].

It can thus be concluded that the mechanical properties of a 3D non-crimp woven composite in each of the principle directions is dependent on the fiber fabric architecture and the manufacturing process (or damage imparted to fibers during weaving), as well as the constituent volume fractions and material properties.

Relating to failure analysis of 3D woven composites, Quinn et al. [24] noted that Z-yarn failure in the specific 3D orthogonal woven composite occurred on the surface of the composite, where the Z-yarn enters the fabric. The authors hypothesized that failure of this type was caused by increased localized strain due to the matrix rich area around the point where Z-yarns entered the composite thickness. Despite this increased localized strain, the overall strain to failure was less than that for a 2D plain weave. This was thought to occur because of the weakened state of the 3D woven composite from crack initiation in the matrix rich area around the Z-yarns at the surface of the composite. Warp fiber pullout was also observed during tensile failure. [24]

2.7.5 Bonded Composites.

As the unitized composite is a novel material system, there is no past research into its mechanical properties. However, research has been performed on other bonded bimaterials. Mechanical properties and interface structure of fiber-metal laminates (alternating metal and PMC plies) have been studied [7, 10, 15], where volume fraction of the composite in the bimaterial was seen to affect the mechanical properties. Co-cured

composite joints have also been studied. See [6] for a thorough overview of bonded composite joints and failure analysis of epoxy/graphite composite co-cured joints.

III. Material and Test Specimen

This section discusses the material systems studied during this research effort, test specimen geometries used, and test specimen preparation. Two panels of each material system were manufactured by P^{2}SI® (Moraine, OH) and delivered to AFIT.

3.1 Material System 1: 3D Weave PMC

MS1 consists of NRPE matrix reinforced with carbon fibers in a three-dimensional woven fabric pattern. The matrix material, NRPE, is a high-temperature PMR-type polyimide resin manufactured by P^{2}SI®. NRPE exhibits low melt viscosity compared to PMR-15 and is advertised to maintain its mechanical integrity after continuous exposures up to 343 °C [20].

Details of the idealized carbon fabric design were provided by the manufacturer, P^{2}SI®, and can be seen in Table 1. The 3D weave structure consists of Z yarns that interlace warp yarns with multiple insertions of fill yarns in the cross direction. The carbon fibers used in the 3D woven fabric are Grafil 34-700WD for the warp and fill fibers, and AS4 for the Z fibers. As discussed in Section 2.6, the fabric pattern is a non-crimp weave, i.e. the warp and fill fibers are straight and do not have any waviness (as would occur if the fibers were interlaced together). Panel constituent properties were also provided by P^{2}SI® and are given in Table 2. The 3D woven fabric preforms were designed, fabricated, and delivered to P^{2}SI® by North Carolina State University. The method used to fabricate MS1 was resin film infusion.

Table 1: Three-dimensional fabric design with property predictions.
Data provided by manufacturer.

# Warps	Warp Tow	dpi[1]	# Fills	Fill Tow	ppi[2]	Z Tow	% of Warps	% of Fills	% of Z	h, mm	V_f, %
4	24K	8	5	12K	6.5	3K	47.9	48.6	3.5	4.9	58.1

[1] *dents per inch (dent - space between the wires of a reed on a loom through which the warp yarns pass)*

[2] *picks per inch (pick - single fiber fill yarn pulled through a weave)*

3.2 Material System 2: 2D Weave PMC

MS2 is made of similar constituent materials as MS1, with the main difference being the weave pattern. This material system consists of the NRPE matrix reinforced with 15 plies of 2D carbon de-sized Cytec T650-35 fibers woven in an 8 harness satin weave. The method of fabrication was prepreg. Panel properties were provided by the manufacturer and are given in Table 2.

Table 2: PMC panels constituent properties. Data provided by manufacturer.

	Resin Content	Fiber Volume Fraction	Resin Volume Fraction	Void Volume Fraction	Density (g/cc)
MS1-1	39.10%	52.87%	45.26%	1.87%	1.563
MS1-2	43.35%	49.18%	50.17%	0.64%	1.563
MS2-1	36.44%	55.29%	42.26%	2.45%	1.566
MS2-2	36.52%	55.23%	42.36%	2.41%	1.566

3.3 Material System 3: 2D Weave Unitized Composite

MS3 is a unitized composite consisting of a PMC and a thin CMC layer. Both the PMC and the CMC are reinforced with a 2D fabric with an 8 harness satin weave. However, the matrix and reinforcement materials differ. The PMC side utilizes the same material and fiber fabric pattern as MS2, but has only 12 plies; whereas the CMC portion has 3 plies of 2D fabric, made of 1059 HT sized JPS Astroquartz® III 4581. The ceramic matrix, C5 developed by P^{2}SI®, was produced by blending KDT HTT-1800

polysilazane-based pre-ceramic resin with yttria-stabilized zirconia and silica additives. The method of fabrication was prepreg. The co-curing process used to fabricate the unitized composite is proprietary, but it should be noted that these two joined materials are not merely bonded with an adhesive or other form of external bonding agent. The motivations for not having an adhesive are 1.) the two materials could come apart during operation due to mechanical loads and 2.) the adhesive could degrade when in elevated temperature environments. Panel properties such as constituent content percentages could not be measured for the unitized composite because of it having two dissimilar materials.

Another material system, MS4, has been fabricated, but was not available in time for this research effort. MS4 extends the technology of 3D woven fabric to the unitized composite. It will be of interest to investigate how the material behaves when the unitized composite has through-thickness fibers.

3.4 Specimen Geometry

Standard dog bone-shaped specimens (Figure 11) were used for all monotonic tension tests and tension-tension fatigue tests. This specimen geometry ensured that failure occurred within the gage section of the test specimen.

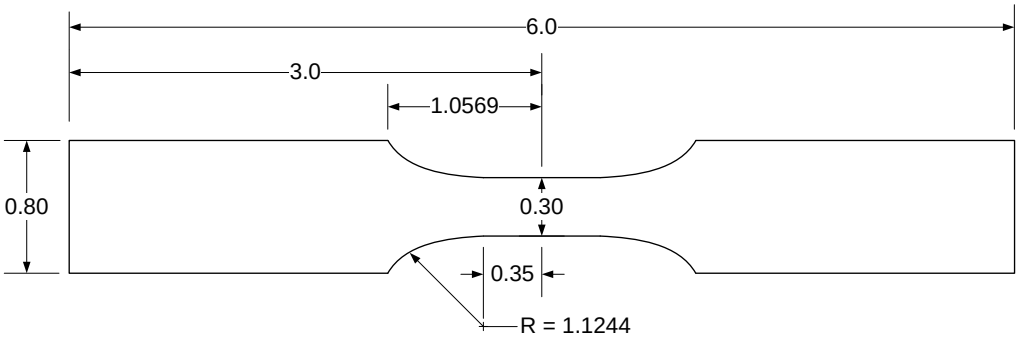

Figure 11: Tension-tension specimen geometry, all dimensions in inches

3.5 Specimen Preparation

Test specimens were machined from the composite panels by the AFIT Model and Fabrication Shop using diamond-grinding. One panel of each material system was cut into specimens with 0/90° fiber orientation, while the other was machined into specimens with ±45° fiber orientation for characterization of off-axis material performance. After specimen machining, every specimen was labeled. Specimen labels correspond to the geometry, material system, and fiber orientation. For example, label *T1-1* refers to tension-tension specimen number one from the 0/90° fiber orientation panel of the 2D PMC (panel MS2-1), whereas label *T4-5* refers to tension-tension specimen number five from the ±45° fiber orientation panel of the 3D PMC (panel MS1-2). Specimen labels corresponding to different material systems and fiber orientations can be seen in Table 3.

Table 3: Specimen labeling scheme

Material System	Material Type/ Fiber Weave	Panel ID	Fiber Orientation	Label	Example Specimen Labels	Total # of Specimens
MS1	3D PMC	MS1-1	0/90°	T3	T3-1	19
		MS1-2	±45°	T4	T4-5	11
MS2	2D PMC	MS2-1	0/90°	T1	T1-3	21
		MS2-2	±45°	T2	T2-4	14
MS3	2D PMC/CMC	MS3-1	0/90°	T5	T5-8	25
		MS3-2	±45°	T6	T6-2	19

After labeling, the gage section width and thickness was measured using a Mitutoyo Absolute Solar Digimatic Caliper, Model N0. CD-S6”CT. Specimen thickness varied slightly from panel to panel. Slight thickness variation within each panel was also observed and documented upon measurement of specimens. Average test specimen dimensions are given in Table 4. Tension-compression specimens were also machined from the same panels for use in future research efforts. These specimens have an

hourglass-shaped gage section, and the details and preparation are discussed in Appendix A.

Table 4: Average tensile specimen dimensions

Material System	Panel	Specimen Type	Avg Width (mm)	Avg Thickness (mm)	Avg Cross-Sect. Area (mm^2)
1	1	3D PMC, 0/90°	7.59	4.82	36.61
	2	3D PMC, ±45°	7.62	4.92	37.45
2	1	2D PMC, 0/90°	7.59	5.73	43.46
	2	2D PMC, ±45°	7.62	5.67	43.21
3	1	2D PMC/CMC, 0/90°	7.62	4.95	37.76
	2	2D PMC/CMC, ±45°	7.65	4.96	37.95

Four specimens from each panel of the unitized composite (MS3) were randomly selected to measure the the CMC layer thickness. This measurement was taken by using the *Measure* tool on the AxioVision software used with the optical microscope to be discussed in Section 4.4. The average CMC layer thickness was 1.06 mm for MS3-1 and 1.21 mm for MS3-2.

All specimens were cleaned with a solution of soap and water and thoroughly rinsed with distilled water in order to remove contaminants from the machining process. After cleaning, specimens were handled with nitrile gloves to prevent any contamination by skin oils. The specimens were then dried in an Isotemp Model 282A vacuum oven set to 105°C and approximately 2 inches Hg pressure. The drying was accomplished in three batches due to oven space limitations. Weight measurements for four specimens of each specimen type were recorded periodically during drying using a Mettler Toledo laboratory balance accurate to ± 0.9 mg to assess when all absorbed water was evaporated. Weight loss stabilized in less than 9 days as shown in Figure 12. The specimens were then removed

from the oven and stored at room temperature in a desiccator maintained at about 15% relative humidity in order to minimize reabsorption of moisture in the ambiant air.

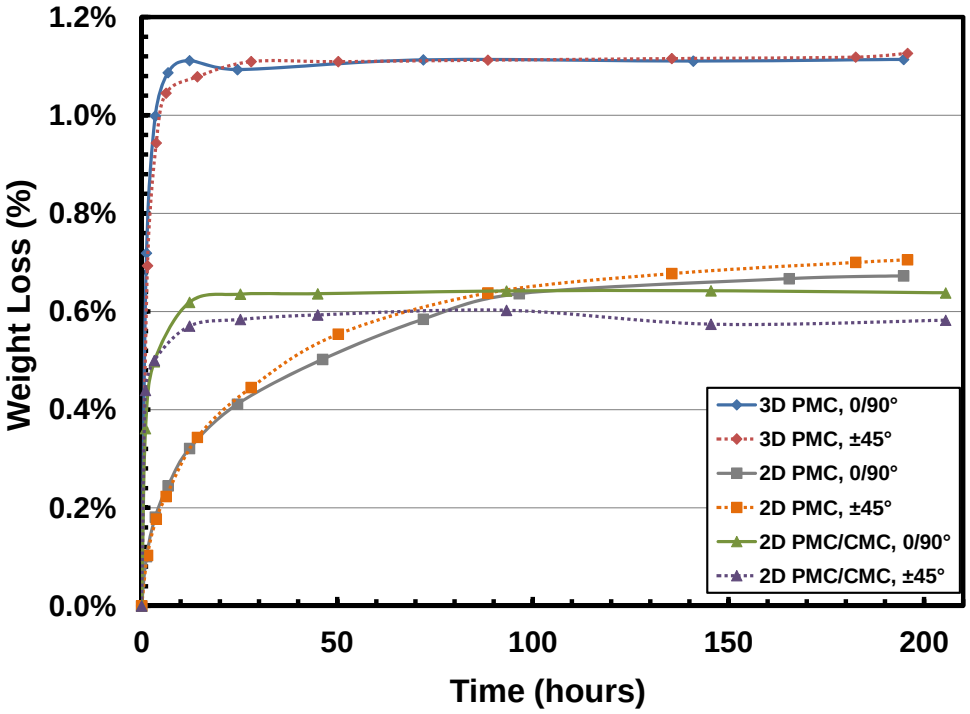

Figure 12: Specimen weight loss during drying

In order for the axial extensometer to stay in contact with the specimen during tests, two dimples were made in the side of the test specimen, 12.7 mm apart and centered in the middle of the gage section. Dimples were created using a hammer and a punch tool provided by Material Test Systems (MTS) and were kept to a minimal depth to avoid fracture initiation at the dimples. In the case of the unitized PMC/CMC, the dimples were made in the middle of the specimen thickness, which meant that the dimples were still in the PMC portion of the specimen.

Fiberglass tabs were installed on all specimens prior to testing in order to transfer the mechanical load to the test specimen and to avoid the wedge surface from damaging the

specimen. For the initial modulus tests, tabs were taped on the specimen with the tape only touching the top and bottom surfaces of the specimen. For all other testing, the tabs were bonded to the specimen grip area using M-bond 200, a room temperature cure epoxy. It was experimentally determined that a fiberglass tab thickness of $^{1}/_{16}$" was enough to keep the grip wedges from crushing the test specimen with the grip pressures required for testing. A close-up view of tabs bonded to a test specimen can be seen in Figure 13.

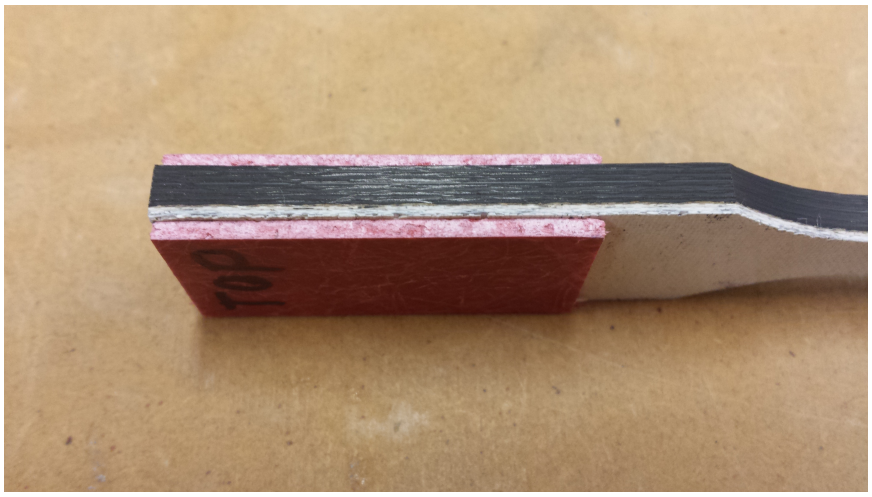

Figure 13: Specimen grip section showing fiberglass tabs

IV. Experimental Setup and Testing Procedures

This section describes the mechanical testing equipment, temperature calibrations, the test procedures, and the digital imaging and optical microscopy equipment used in this research effort.

4.1 Mechanical Testing Equipment

Room temperature modulus measurements were performed using a vertically configured model 810 MTS servo-hydraulic testing machine with a 100 kN (22 kip) model 647.10A load cell. MTS model 647.10 water-cooled hydraulic wedge grips were used with a grip pressure of 5 MPa. Strain was measured using an MTS model 632.53E-14 axial extensometer with a 12.7-mm gage section.

All further room temperature and elevated temperature tests were performed using the testing machine described above. This testing machine has a single zone MTS 653 furnace equipped with an MTS 409.83 Temperature Controller for elevated temperature tests. A grip pressure of 15 MPa was used for all tests except for tests on the 2D PMC specimens with 0/90° fiber orientation, which required a higher grip pressure of 20 MPa to avoid specimen pullout from the tabs/grips. The grips were continuously cooled with 15°C water supplied by a Neslab RTE7 chiller. The 100 kN (22 kip) hydraulic testing machine, furnace, and extensometer are depicted in Figure 14.

A Flex Test 40 digital controller was used for all data acquisition and input signal generation. A configuration file was created using the MTS station builder release 5.2B and operations were performed using the station manager interface. Procedures, which ran the desired test and collected the data, were developed for each type of test conducted. The following data were collected for all tests: force, force command, displacement,

Figure 14: Test apparatus setup

strain, right temperature, and time. The rate of time data acquisition was adjusted to ensure adequate capturing of the data.

4.2 Temperature Calibration

In order to maintain a temperature of 329°C in the gage section on the side of the specimen which faced the furnace, a temperature calibration was performed for each type of specimen geometry and material. Two type K thermocouples were attached to the specimen gage section, one on the side facing the furnace, and one on the opposite side open to ambient air. The thermocouples were fixed to the center of the specimen gage section by Kapton tape and secured with Nickel Chromium wire as seen in Figure 15 and Figure 16. The thermocouples were connected to a hand-held Omega HH501DK temperature sensor.

For the temperature calibration and all elevated temperature tests, the CMC side of the unitized composite faced the furnace. Care was taken to ensure the correct side of the 2D and 3D PMC was facing the furnace, and therefore exposed to heat. Since the PMC side (open to ambient air) of the unitized composite had a shiny surface, the shiny surface of the 2D and 3D PMC specimens were installed facing away from the furnace (open to ambient air).

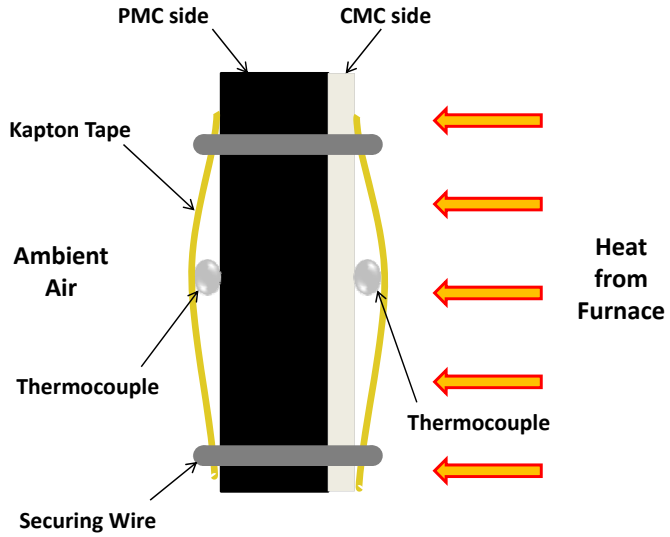

Figure 15: Thermocouple mounting schematic (shown for a unitized composite specimen)

Figure 16: MS2 temperature calibration specimen

Furnace insulation inserts were created consistent with the specimen geometry in order to keep the heat enclosed in the furnace and allow only one side (right side) of the specimen to see direct heat from the furnace heating element, with the other side (left side) open to ambient air. These inserts were glued in place using Rescor^{TM} 3901 ceramic adhesive. After the specimen was gripped and the extensometer rods placed on the specimen, another insulation piece was tied in place around the extensometer rods with wire. The purpose of this insulation was not so much to insulate (because it was on the side of the specimen open to ambient air), but to give support and prevent the main furnace insulation block from touching the specimen during a test. The insulation setup can be seen in Figure 17.

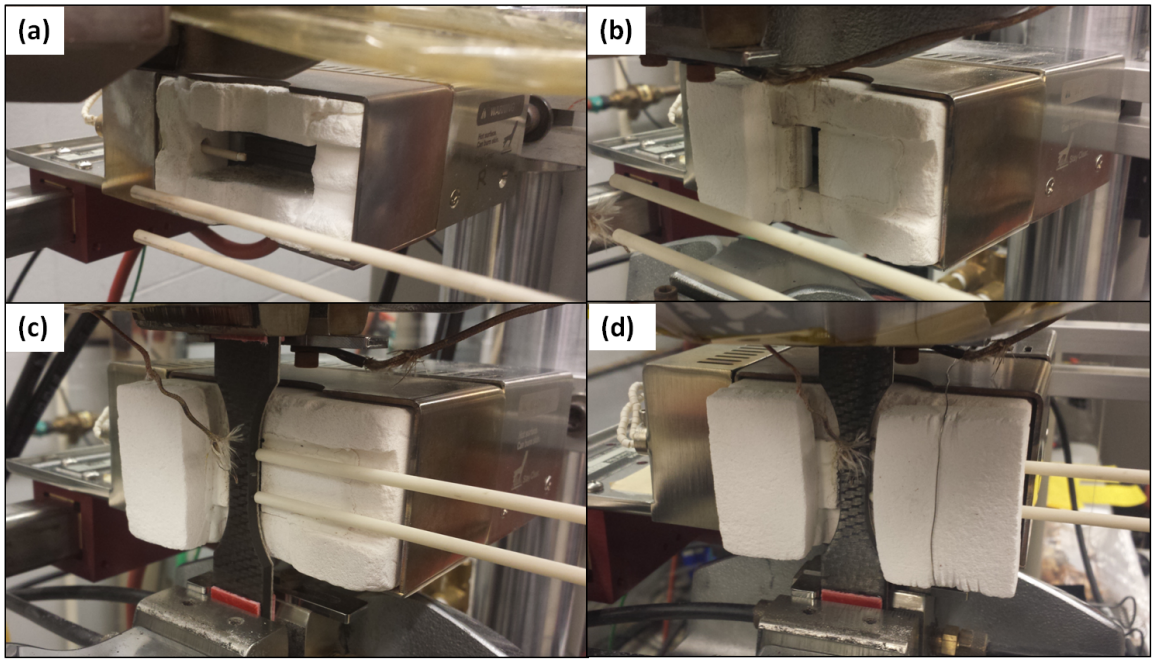

Figure 17: Furnace insulation setup: (a) without inserts, (b) with inserts, (c) with gripped specimen, (d) with supportive insulation

Temperature controller settings were adjusted until the desired temperature was obtained on the right face of the specimen gage section (side facing the furnace). This was

accomplished using a procedure developed using the MTS software, which ramped the temperature to a "guess" set temperature at a rate of 10°C per minute. Once the guess temperature was reached, the furnace temperature was manually raised until the temperature on the right face of the specimen gage section, T_{right}, was the desired 329°C. The temperature controller was then kept at this set temperature for 3 hours to ensure that the temperature stayed constant with no perturbation greater than 5°C. The furnace was then allowed to cool down to room temperature.

A second check was performed on the temperature calibration to ensure the same set point resulted in 329°C on the specimen face and to mimic procedures during an actual material test. This procedure involved ramping the temperature up to the set point previously determined at a rate of 10°C per minute, and then holding the set temperature for 45 minutes to ensure that the temperature stabilized. During the hold period, T_{right} stabilized to 329°C with no perturbation greater than 5°C. A separate temperature calibration was done for the 0/90° and ±45° specimens on the 3D PMC. It was found that the required temperature set point was the same in both instances. It was assumed that the other material system specimens would follow suit. Therefore, the same furnace temperature set point for the 0/90° specimens was used for the ±45° specimens.

Some issues were encountered when performing temperature calibrations. It was observed that the set point determined from the temperature calibration would not reproduce the desired 329°C on the specimen face when the second check was performed. This could have been due to two reasons. First, the insulation inserts that were created to isolate the heat to one side of the specimen were not initially glued. Each time a temperature calibration was performed, the insulation inserts would be set in place inside the furnace. This could potentially cause variability in the temperature set point since the inserts were not exactly in the same place every time. Therefore, the inserts were pasted to the regular furnace insulation using the ceramic adhesive in an effort to reduce temperature

variability each time a test was performed. Second, the ambient laboratory air conditions were slightly different each time a temperature calibration was performed. A plexi-glass shield (Figure 18) was installed around the MTS testing machine in order to isolate the test setup from any draft caused by laboratory doors opening and closing. This plexi-glass shield helped stabilize the temperature on the specimen face open to ambient air (T_{left}).

Figure 18: MTS machine with plexi-glass shield installed

Table 5 lists the required furnace temperature controller set points for each specimen type. Two set points for each material system are given. This is because after testing the 2D PMC/CMC 0/90° specimens in fatigue, the furnace insulation was worn down slightly; therefore, a recalibration of the temperature had to be accomplished.

Table 5: Furnace temperature set-points

Specimen Type	Furnace Set-points (°C)
3D PMC	564 / 547
2D PMC	580 / 553
2D PMC/CMC	548 / 534

4.3 Mechanical Test Procedures

4.3.1 Room Temperature Elastic Modulus Measurements.

In order to assess specimen-to-specimen and panel-to-panel variability, room temperature elastic modulus of each test specimen was measured. These modulus tests were completed before any other room-temperature or high-temperature testing began. To accomplish these tests, on-axis specimens were loaded in stress control to a stress of 20 MPa at a rate of 1 MPa/s, then unloaded to zero stress at the same rate. This ramp-up and ramp-down process was repeated three times to ensure an average modulus could be determined from the load and unload segments. For each segment, the modulus was determined by obtaining the slope of a best fit line on a stress-strain curve. The same procedure was used for the off-axis specimens, but a maximum load of 10 MPa was used to ensure that the material response stayed linear.

4.3.2 Monotonic Tensile Tests.

As previously stated, monotonic tension-to-failure tests were conducted first at room temperature (to determine as-processed mechanical properties) and then with the right side of the specimen at an elevated temperature of 329°C. One dog-bone shaped specimen of each MS and fiber orientation was tested at room temperature, and at least one specimen of each was tested at elevated temperature. The stress-strain response and Ultimate Tensile Strength (UTS) produced from these tests were used as a baseline for analyzing the material fatigue behavior.

Procedures were developed using the MTS software that would load the specimen in displacement control at a rate of 0.025 mm/s until failure. Failure was taken to occur when the load supported by the specimen dropped dramatically. For the elevated temperature tensile tests, the furnace temperature was first ramped to the required set point at a rate of 10°C/min and then held constant for 45 min before the specimen was loaded in displacement control to failure. Data collected during these tests included displacement, displacement command, force, strain, time, temperature, and temperature command.

4.3.3 Fatigue Tests.

Tension-tension fatigue tests were conducted at an elevated temp, T_{right}, of 329°C with a minimum to maximum stress ratio of $R = 0.05$ and frequency of 1 Hz. Different maximum stress levels were investigated for each MS and each fiber orientation (0/90° and ±45°), starting with 80% of the UTS determined from the elevated temperature monotonic tension-to-failure tests. If the specimen failed before achieving the run-out condition (2×10^5 cycles), then lower maximum stresses were explored until run-out was achieved. Once run-out was achieved for a particular MS and fiber orientation, additional tests were conducted in order to give a more complete characterization of the material response on a stress-cycle plot (S-N curve).

A procedure for fatigue testing was developed in the MTS software that would ramp the temperature to the required setpoint determined from the temperature calibration at a rate of 10°C/min. The temperature was held constant at the set point for 45 min before any loading began and was also held constant for the duration of the test. The specimen was then loaded in force control to the minimum stress level required for fatigue in 30 seconds. Once the minimum stress was reached, the procedure would immediately start cyclic loading of the specimen using a sine waveform in force control. If the specimen failed prior to reaching run-out (2×10^5 cycles), the procedure would stop. However, if the specimen sustained the full 2×10^5 cycles of loading, the load would be brought down to

zero in 30 seconds, and finally, the specimen would be tested in tension to failure using the method employed in monotonic tension-to-failure tests. This post-fatigue tension test was conducted in order to assess the retained properties (strength and stiffness) of the specimen subjected to prior cyclic fatigue loading.

Data collection during fatigue tests was included in the procedure developed in the MTS software and is outlined below.

- Warm-up: data collected every 15 seconds during temperature ramp up and 45 minute dwell period. Data was saved to the *specimen* data file.
- Ramp Load to Minimum Stress: data collected every 0.01 seconds. Data saved to the *specimen* data file.
- Fatigue Loading: data collected during cyclic loading
  - Peak & Valley Data: data collected for every cycle at the point of maximum or minimum force. Data saved to the *Peak_Valley* data file.
  - Cyclic Data: data collected every 0.01 seconds for the below cycles. Data saved to the *Cyclic* data file.
    - Cycles 1-25
    - Every 10^{th} cycle from cycle 30 to 100
    - Every 100^{th} cycle from cycle 100 to 1,000
    - Every $1,000^{th}$ cycle from cycle 1,000 to 10,000
    - Every $10,000^{th}$ cycle from cycle 10,000 to 200,000
- Unload to Zero Stress: data collected every 0.02 seconds (if fatigue run-out was achieved). Data saved to the *specimen* data file.
- Tension to Failure: data collected every 0.01 seconds (if fatigue run-out was achieved). Data saved to the *Tension_to_Failure* data file.

During the course of fatigue testing the ±45° specimens, it was observed that the force command and actual force applied to the specimen did not match as accurately as in the case of the 0/90° specimens (Figure 19). This difference between command and feedback was due to the fact that the matrix material carried the majority of the load in the ±45° specimens, and the MTS machine was better tuned for the stiffer 0/90° specimens. This tuning issue resulted in a slightly higher *R*-value for the ±45° specimens. However,

the percent difference in force command to force applied was deemed acceptable and and re-tuning of the MTS machine was not performed.

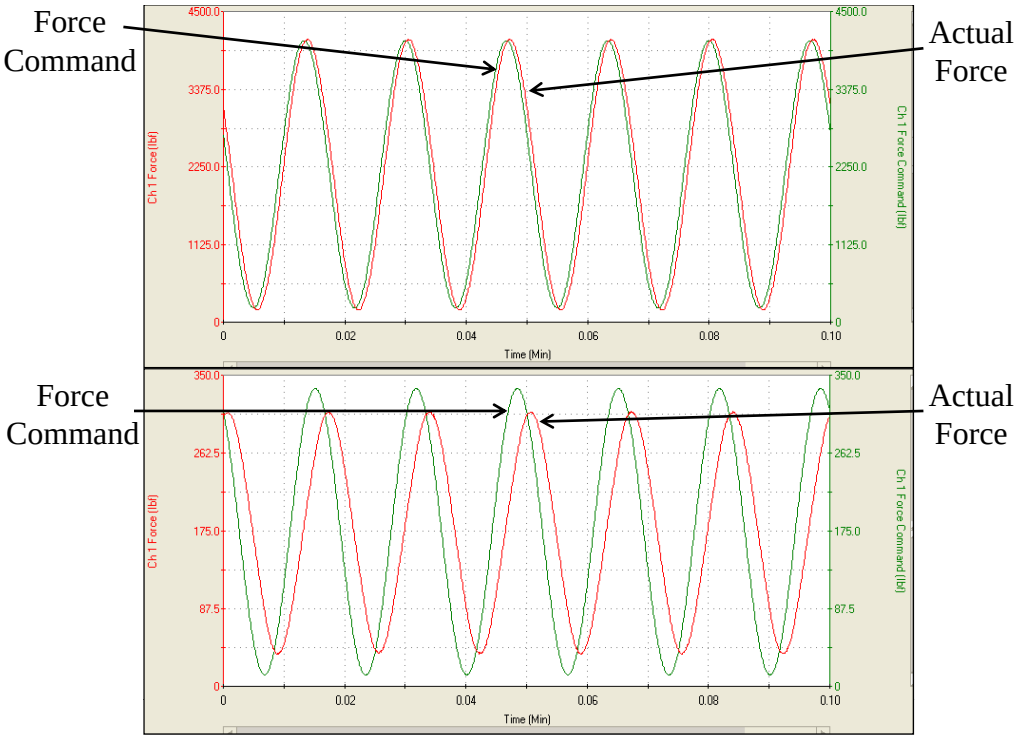

Figure 19: Screen shot of MTS scope during fatigue test:
0/90° specimen properly tuned (top), ±45° specimen improperly tuned (bottom)

4.4 Digital Imaging and Optical Microscopy Equipment

For one of the unitized composite [0/90°] specimens, digital images during load-up in tension at room temperature were captured using a Nikon ED digital camera utilizing PixelLINK Capture OEM software. The capture rate used was 1 frame per second. These pictures were taken to document the visual progression of damage of this novel material system under axial loading.

Specimens of each material type and fiber orientation tested in tension at room temperature and elevated temperature, as well as specimens tested in fatigue were examined under an optical microscope. The microscope used was a Zeiss Discovery.V12 stereoscopic optical microscope equipped with a Zeiss AxioCam HRc digital camera (Figure 20). Virgin specimens were examined for comparisons.

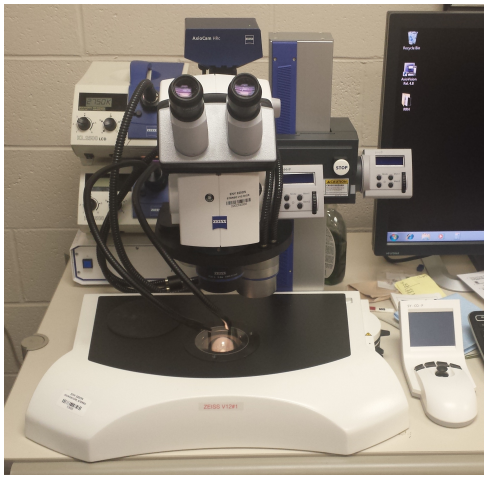

Figure 20: Zeiss optical microscope

V. Experimental Results and Discussion

5.1 Assessment of Specimen-to-Specimen Variability

Variability of mechanical properties between panels and even between specimens from the same panel is generally present in material systems due to slight differences and/or defects from manufacturing and processing. In this research, there were two panels of each material system. One panel was used to machine the 0/90° specimens while the other panel was used to machine the ±45° specimens. However, in some panels, slight defects and thickness changes could be seen by visual inspection. Therefore, it was vital to assess the specimen-to-specimen variability of each material system. This assessment was conducted by performing room temperature modulus tests as outlined in Section 4.3.1. Because there is inherent data scatter at very low stress levels, a linear best fit was computed using data gathered at stresses above 2 MPa. Results are shown in Table 6.

Table 6: Room temperature elastic modulus results

Panel	Specimen Type	Average Modulus (GPa)	Standard Deviation (GPa)	Coeff. of Variation
MS1-1	T3: 3D PMC, 0/90°	46.47	3.50	0.0753
MS1-2	T4: 3D PMC, ±45°	9.69	0.57	0.0592
MS2-1	T1: 2D PMC, 0/90°	59.01	1.47	0.0250
MS2-2	T2: 2D PMC, ±45°	16.90	0.52	0.0306
MS3-1	T5: 2D PMC/CMC, 0/90°	56.14	1.30	0.0231
MS3-2	T6: 2D PMC/CMC, ±45°	10.76	0.31	0.0284

It should be noted that the 3D PMC exhibited the most variation in modulus. This is likely caused by the introduction of through-thickness fibers and the complex nature of processing, which could result in more defects in the finished product. When analyzing results, it is important that comparisons only be made between the 3D PMC and 2D PMC

and between the 2D PMC and 2D PMC/CMC unitized composite. The 3D PMC can be compared to the 2D PMC because they both have the same matrix resin and PAN-based carbon fibers as reinforcement. These two material systems also have relatively close fiber volume fractions. Comparisons will show whether the 3D woven composite exhibits better mechanical performance than a standard 2D woven laminate. Likewise, the 2D PMC can be compared to the 2D unitized composite because they both have the same matrix and reinforcement for the PMC, while the unitized composite has an added CMC layer. Comparing these two material systems will show whether the unitized composite offers improvement in mechanical properties compared to the 2D PMC. One cannot compare the 3D PMC to the 2D unitized composite because there is more than one aspect that is different between them, namely reinforcement weave and the addition of the CMC layer. When future research is performed on the 3D unitized composite, then a comparison with the 3D PMC can be made.

It can be seen in Table 6 that the average modulus of the 3D PMC 0/90° specimens was about 12.5 GPa less than that of the 2D PMC. This is most likely due to the presence of the through-thickness *Z* fibers, which resulted in a smaller fiber volume fraction, V_f, for the 0° *warp* fibers. The ±45° modulus for the 3D PMC was also significantly less than that of the 2D PMC. The 2D PMC also had a higher modulus than the 2D unitized PMC/CMC, although the 0/90° values were closer (about 3 GPa difference).

In order to compare data from one specimen to another, the stresses obtained in tension-to-failure and fatigue tests were normalized in the following manner:

$$\sigma_{normalized} = \sigma_{actual} \frac{E_{avg}}{E_{specimen}} \tag{5.1}$$

where $\sigma_{normalized}$ is the normalized stress, σ_{actual} is the actual stress, E_{avg} is the average modulus for the material type (T1, T2, T3, etc.), and $E_{specimen}$ is the individual specimen initial modulus. This normalization procedure also revealed how the stiffness of a

particular specimen compared to the average. A $E_{avg}/E_{specimen}$ ratio less than 1 meant that the specimen was stiffer (had a higher modulus) than the average; and therefore, the normalized stress will be less than the actual stress. Normalized stresses, and the resulting normalized elastic moduli, are used in the majority of the data analysis for consistency and in order to have meaningful comparisons.

5.2 Thermal Expansion

All elevated temperature tests in this effort were conducted with a temperature of 329°C on the right face of the specimen, T_{right}. As discussed in Section 4.3, the temperature was ramped up to the required setpoint at a rate of 10°C/min and then held constant for 45 minutes while maintaining zero load. Thermal strain was recorded during this heat up and temperature dwell period. A representative plot of thermal strain versus time for the ramp up and dwell periods is shown in Figure 21.

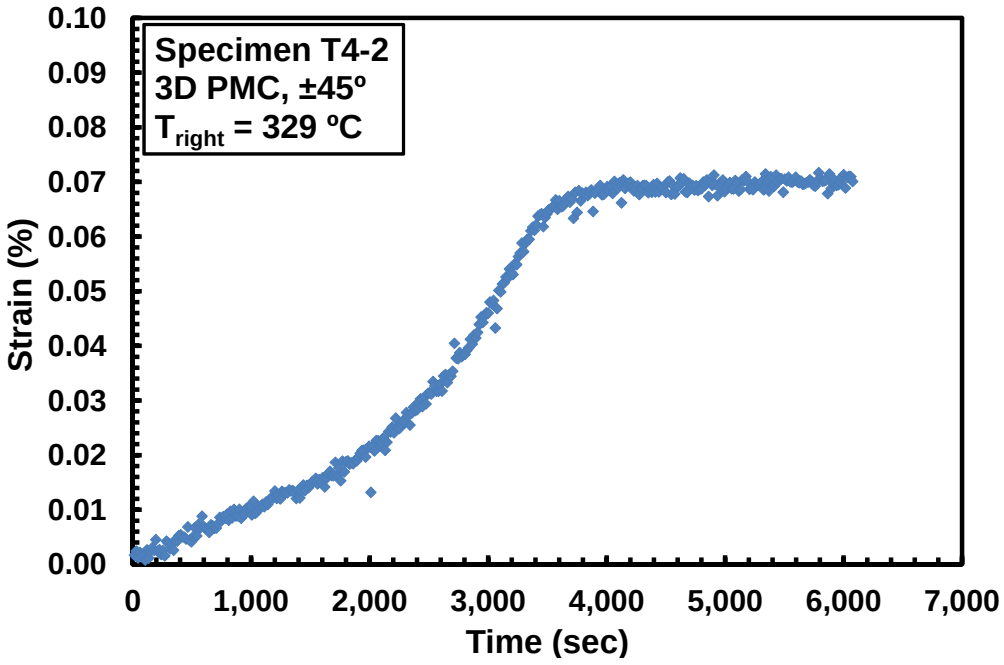

Figure 21: Representative thermal strain profile

A coefficient of thermal expansion was not calculated for this effort because of the uneven heating of the test specimens (only heating the right side with the left side open to ambient laboratory air). Due to different ambient laboratory air conditions, slight differences in specimen thickness, and possible differences in specimen distance from furnace insulation during setup, T_{left} varied from test to test. Thermal strains for all tested specimens are given in Tables 7 – 9. As can be seen, the unitized composite has produced less thermal strain than the 2D PMC on average, indicating that the CMC layer is indeed functioning as desired (as a thermal protection system).

Table 7: Thermal strain values obtained for the MS1 specimens

Material System 1: 3D PMC

Fiber Orientation	**Specimen #**	T_{left} **(°C)**	T_{right} **(°C)**	**Thermal Strain (%)**
0/90°	T3-2	173	329	0.101
	T3-4	154	329	0.068
	T3-6	165	329	0.075
	T3-7	179	329	0.104
	T3-8	190	329	0.088
	T3-9	167	329	0.031
	T3-10	196	329	0.129
	T3-11	192	329	0.081
	T3-12	195	329	0.120
	T3-13	194	329	0.089
	T3-14	194	329	0.075
	T3-15	196	329	0.082
	T3-17	197	329	0.095
	T3-18	191	329	0.106
	T3-19	201	329	0.058
	Average:	**186**	**329**	**0.087**
±45°	T4-2	186	329	0.070
	T4-3	179	329	0.062
	T4-4	168	329	0.110
	T4-5	151	329	0.018
	T4-6	200	329	0.137
	T4-7	204	329	0.048
	T4-8	197	329	0.177
	T4-9	207	329	0.108
	T4-11	205	329	0.078
	Average:	**189**	**329**	**0.090**

Table 8: Thermal strain values obtained for the MS2 specimens

Material System 2: 2D PMC

Fiber Orientation	**Specimen #**	T_{left} **(°C)**	T_{right} **(°C)**	**Thermal Strain (%)**
0/90°	T1-2	158	329	0.046
	T1-3	147	329	0.069
	T1-4	152	329	0.034
	T1-5	162	329	0.080
	T1-6	139	329	0.044
	T1-7	150	329	0.049
	T1-8	171	329	0.092
	T1-10	170	329	0.058
	T1-11	165	329	0.056
	T1-12	172	329	0.123
	Average:	**159**	**329**	**0.065**
±45°	T2-2	153	329	0.036
	T2-3	149	329	0.073
	T2-4	138	329	0.026
	T2-5	142	329	0.048
	T2-6	134	329	0.111
	T2-7	169	329	0.039
	T2-8	169	329	0.050
	T2-9	170	329	0.062
	T2-11	163	329	0.040
	Average:	**154**	**329**	**0.054**

Table 9: Thermal strain values obtained for the MS3 specimens

Material System 3: 2D PMC/CMC

Fiber Orientation	**Specimen #**	T_{left} **(°C)**	T_{right} **(°C)**	**Thermal Strain (%)**
0/90°	T5-4	151	329	0.026
	T5-5	159	329	0.028
	T5-6	165	329	0.035
	T5-7	152	329	0.018
	T5-8	166	329	0.026
	T5-9	145	329	0.015
	T5-10	142	329	0.042
	T5-11	146	329	0.037
	T5-13	143	329	0.014
	T5-14	154	329	0.052
	T5-16	141	329	0.022
	T5-17	165	329	0.004
	T5-18	163	329	0.018
	Average:	**153**	**329**	**0.026**
±45°	T6-2	159	329	0.078
	T6-3	167	329	0.076
	T6-4	163	329	0.016
	T6-5	160	329	0.031
	T6-6	200	329	0.064
	T6-7	165	329	0.007
	T6-8	165	329	0.044
	T6-9	166	329	0.045
	T6-10	166	329	0.010
	T6-11	162	329	0.059
	T6-12	163	329	0.058
	T6-13	170	329	0.017
	T6-14	164	329	0.055
	Average:	**167**	**329**	**0.043**

5.3 Monotonic Tensile Tests

The results of the tensile-to-failure tests at both room and elevated temperatures are given in Tables 10 – 12. The modulus of elasticity, E, was determined as the slope of a best fit line fitted to the initial linear region of a stress-strain curve. In some instances, the stress would drop slightly and then increase again before final failure. This was most likely due to one or more fiber failures or ply failures. For the purposes of this research, failure of a specimen was taken to occur when there was a dramatic instantaneous drop in sustained load. If a dramatic failure did not occur, then failure strain was taken as the

point at which the stress dropped below 50% of the UTS. This only occurred once, in the elevated temperature tensile test of the 2D PMC with ±45° fiber orientation. Although actual values and normalized values are given, only normalized values will be used in the discussion of results.

Table 10: Summary of tensile properties obtained for MS1 in laboratory air at room temperature (T = 23°C) and at elevated temperature (T_{right} = 329°C)

Material System 1: 3D PMC

Fiber Orientation	Specimen #	Elastic Modulus (GPa)	Normalized Modulus (GPa)	UTS (MPa)	Normalized UTS (MPa)	Failure Strain, ϵ_f (%)
0/90°	***Room Temperature:***					
	T3-1	39.99	47.17	699.3	824.9	1.645
	T3-3	52.31	48.42	772.9	715.5	1.172
	T3-5	41.46	46.31	713.8	797.2	1.644
	Elevated Temperature:					
	T3-2	48.40	46.65	762.5	734.9	1.407
	T3-4	47.44	49.53	746.4	779.3	1.405
	T3-6	41.30	45.66	681.9	753.9	1.602
±45°	***Room Temperature:***					
	T4-1	8.72	9.72	69.9	77.9	2.044
	Elevated Temperature:					
	T4-2	8.47	9.10	58.7	63.0	5.600

Table 11: Summary of tensile properties obtained for MS2 in laboratory air at room temperature (T = 23°C) and at elevated temperature (T_{right} = 329°C)

Material System 2: 2D PMC

Fiber Orientation	Specimen #	Elastic Modulus (GPa)	Normalized Modulus (GPa)	UTS (MPa)	Normalized UTS (MPa)	Failure Strain, ϵ_f (%)
0/90°	***Room Temperature:***					
	T1-1	56.87	57.29	831.8	837.9	1.401
	Elevated Temperature:					
	T1-2	60.93	61.88	834.4	847.3	1.276
	T1-6	59.04	58.03	809.6	795.7	1.287
±45°	***Room Temperature:***					
	T2-1	16.65	16.47	165.1	163.3	6.118
	Elevated Temperature:					
	T2-2	13.67	13.48	128.3	126.4	12.955*

** Failure strain taken at point where stress dropped to 50% UTS.*

Table 12: Summary of tensile properties obtained for MS3 in laboratory air at room temperature (T = 23°C) and at elevated temperature (T_{right} = 329°C)

Material System 3: 2D PMC/CMC

Fiber Orientation	Specimen #	Elastic Modulus (GPa)	Normalized Modulus (GPa)	UTS (MPa)	Normalized UTS (MPa)	Failure Strain, ϵ_f (%)
0/90°	***Room Temperature:***					
	T5-1	54.03	55.93	643.3	665.8	1.918
	T5-2	56.84	56.85	654.8	654.8	1.291
	T5-3	55.97	57.77	703.1	725.7	1.275
	Elevated Temperature:					
	T5-4	56.06	56.49	669.0	674.2	1.161
	T5-5	60.43	61.27	660.8	669.9	1.382
	T5-6	59.08	55.81	686.7	648.7	1.059
±45°	***Room Temperature:***					
	T6-1	11.45	10.76	61.7	58.0	1.390
	Elevated Temperature:					
	T6-2	9.41	9.39	57.1	57.0	2.131
	T6-3	9.38	9.06	57.7	55.7	2.947

5.3.1 Monotonic Tension at Room Temperature.

Tensile tests to failure were performed at room temperature on at least one specimen of every material system and fiber orientation. Figure 22 shows the stress-strain curves for the 3D woven PMC with 0/90° fiber orientation. For this research, the warp fibers were at 0° and the fill fibers at 90°. (i.e., all specimens were loaded axially along the warp direction). The average UTS was 779.20 MPa, the average modulus was 44.59 GPa, and the average failure strain was 1.487%. All specimens exhibited an initial linear response which transitioned to nonlinear stress-strain behavior around 0.8-0.85% strain. After this transition, the modulus began to increase (i.e., there was a stiffening effect). There are a few possible explanations for this stiffening. The warp fibers, which are theoretically straight, could have had slight waviness due to the Z-fibers pressing on the fill fiber yarns which in turn press on the warp fibers in its initial untested state. Therefore, there could be a slight straightening of the warp fibers during load up, which could cause the composite material to become stiffer. This case would be more likely for the outer surface yarns.

Another possible explanation for the stiffening is that the Z-fibers run parallel to the applied load. Therefore, the Z-fibers sustain some of the load, and the increase in modulus could be due to the Z-fibers straightening out slightly and carrying more and more load. Furthermore, it is known that carbon fibers exhibit stiffening under monotonic tension at high levels of stress and strain. Such stiffening of the reinforcing fibers would cause the composite stress-strain response in this 0/90° fiber orientation to follow suit.

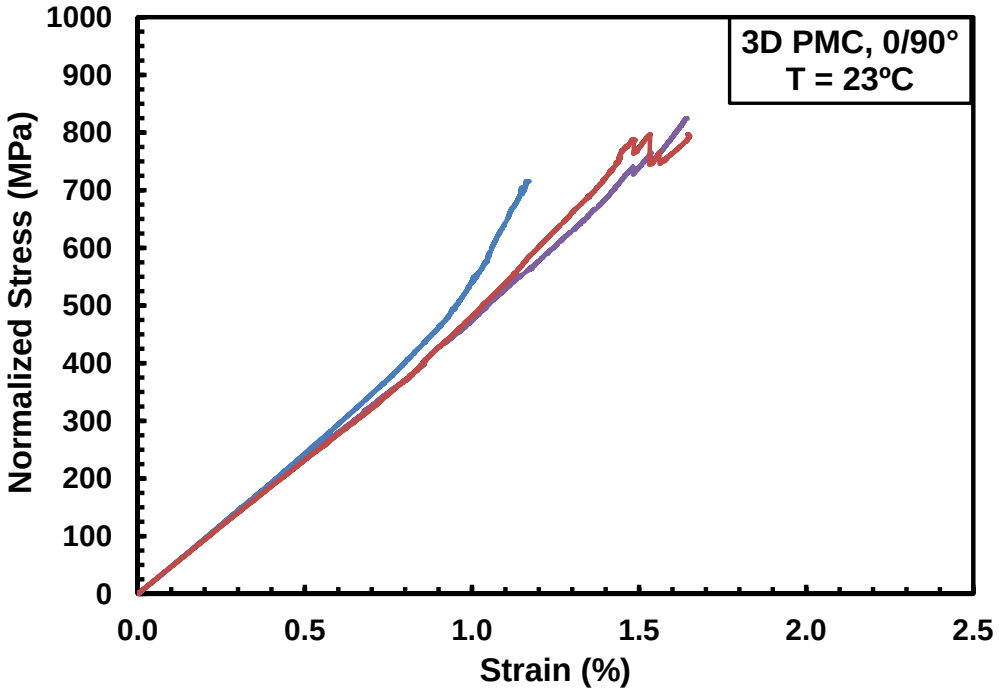

Figure 22: Tensile stress-strain curves obtained for the 3D PMC with 0/90° fiber orientation at room temperature

One specimen of the 3D PMC with ±45° fiber orientation was tested in tension to failure at room temperature. The stress-strain response is shown in Figure 23. The modulus was 8.72 GPa and the UTS was 77.93 MPa. Note that the ±45° UTS was only 10% of the 0/90° UTS. The strength for the ±45° fiber orientation is much lower compared to that for the 0/90° fiber orientation because the matrix material bears the majority of the load. The stress-strain response becomes nonlinear at a much lower load,

with the modulus decreasing until the ultimate strength is reached. Failure strain was 2.044% and did not occur at the point of maximum stress. Tensile stress-strain curves obtained for the 0/90° and ±45° fiber orientations for MS1 are compared in Figure 24.

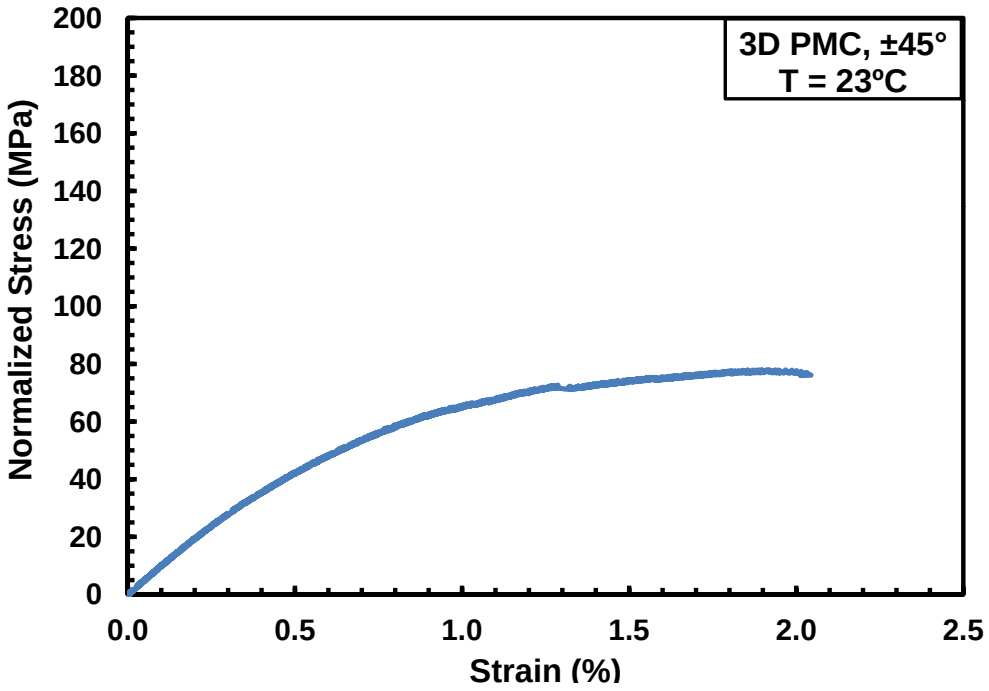

Figure 23: Tensile stress-strain curves obtained for the 3D PMC with ±45° fiber orientation at room temperature

The tensile stress-strain behavior of the 3D PMC is now compared to that of the 2D PMC. Figure 25 contrasts the tensile stress-strain curves obtained for the 2D PMC with those obtained for the 3D PMC for the 0/90° fiber orientation. The modulus of the 2D PMC is about 21% greater than that of the 3D PMC, and the UTS of the 2D PMC is approximately 59 MPa (or 7.5%) greater than the average UTS of the 3D PMC. It is evident that the 2D PMC stress-strain response is nearly linear to failure.

Figure 26 compares tensile stress-strain responses of the 2D and 3D PMC for the ±45° fiber orientation at room temperature. For the ±45° fiber orientation, the UTS of the 3D PMC is less than half of the UTS produced by the 2D PMC. The stiffness of the 2D

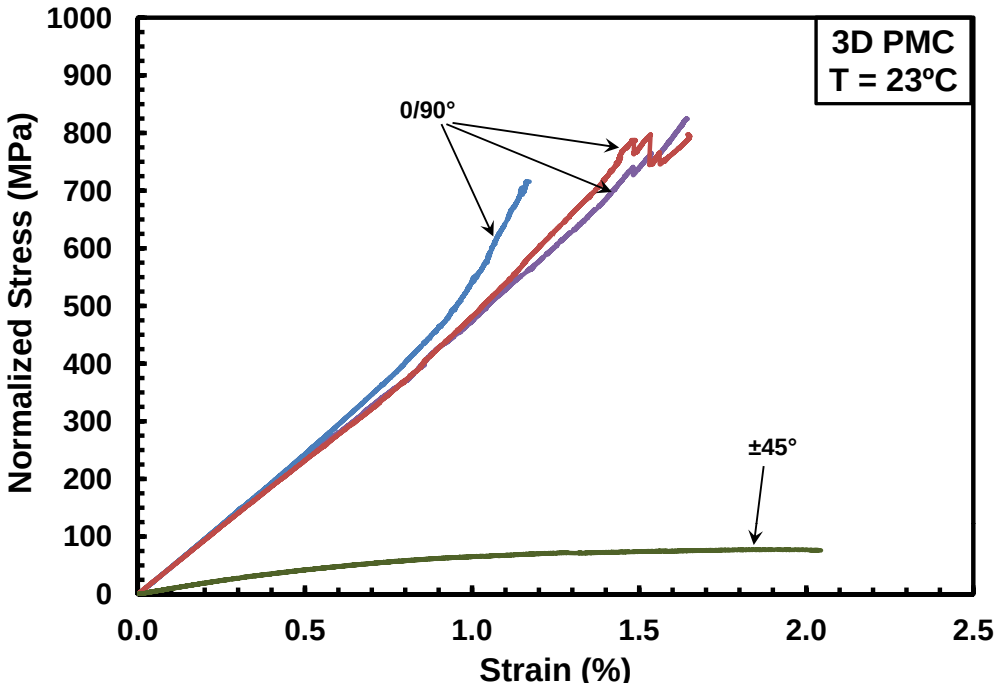

Figure 24: Tensile stress-strain curves obtained for the 3D PMC with 0/90° and ±45° fiber orientations at room temperature

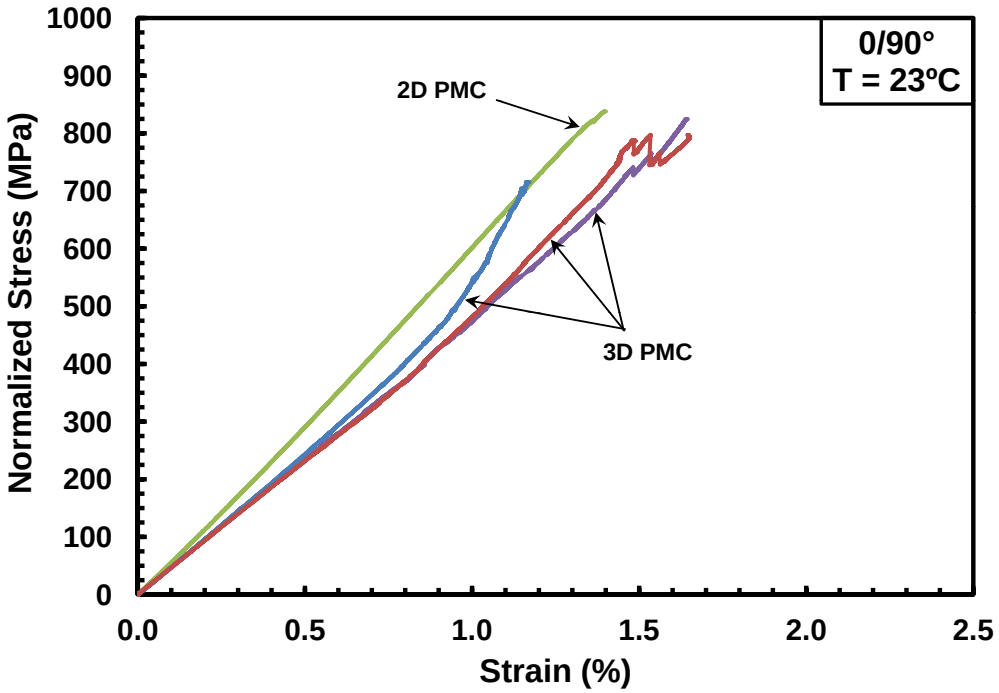

Figure 25: Tensile stress-strain curves obtained for the 2D and 3D PMC with 0/90° fiber orientation at room temperature

PMC is also nearly two times that of the 3D PMC. The failure strain obtained for the 2D PMC is approximately three times that of the 3D PMC. The tensile stress-strain curves obtained for the 2D PMC and 3D PMC with 0/90° and ±45° fiber orientations are shown in Figure 27. Note that the UTS obtained for the 2D PMC with ±45° fiber orientation is only ~19.5% of the UTS value obtained for the 0/90° fiber orientation.

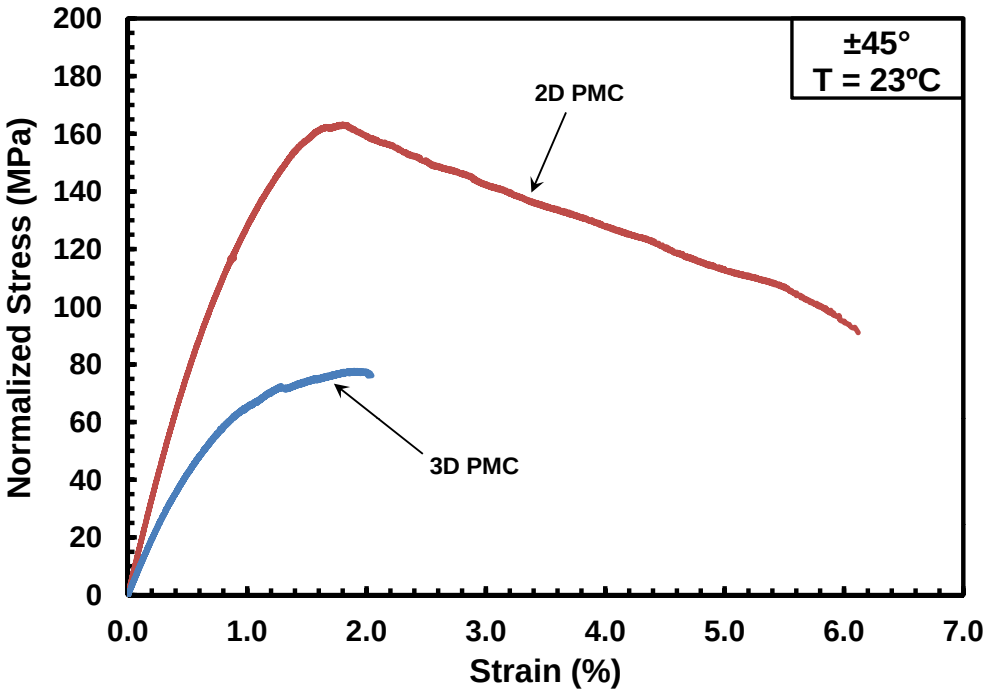

Figure 26: Tensile stress-strain curves obtained for the 2D and 3D PMCs with ±45° fiber orientation at room temperature

Three 0/90° specimens of the 2D unitized composite (PMC/CMC) were tested in tension at room temperature. The tensile stress-strain response is compared to that of the 2D PMC in Figure 28. It is evident that the initial modulus of both materials is nearly the same. However, the stress-strain curves produced by the unitized composite become nonlinear as the strain exceeds 0.55%. Notably one PMC/CMC specimen exhibits greater decrease in modulus than the other two. The other two PMC/CMC specimens exhibit more of a sporadic response at higher values of stress and strain. This behavior is most

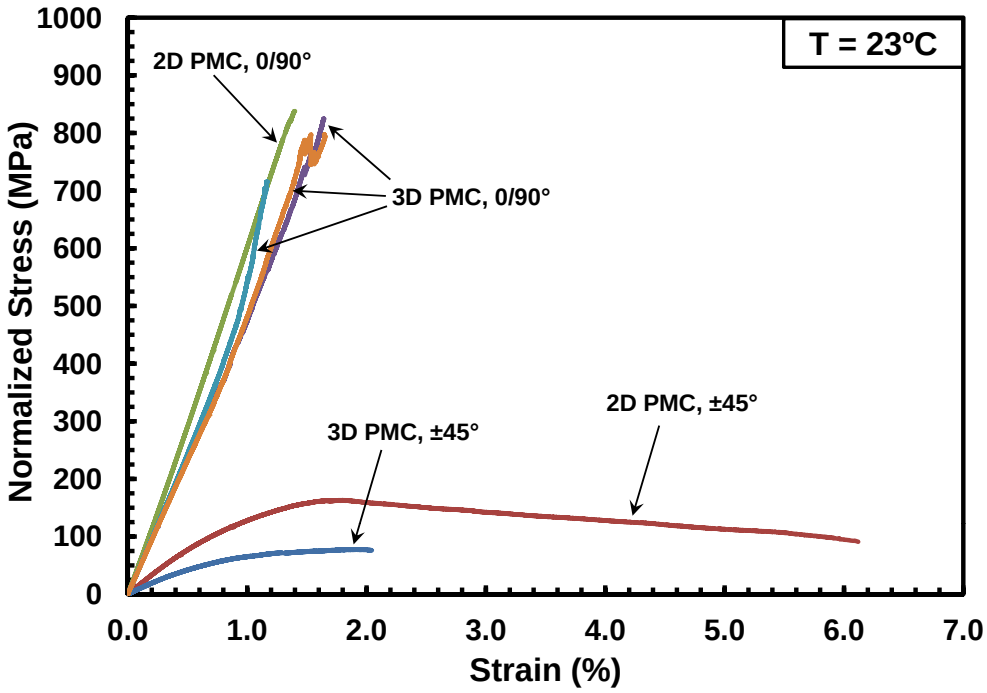

Figure 27: Tensile stress-strain curves obtained for the 2D and 3D PMCs with 0/90° and ±45° fiber orientations at room temperature

likely due to the interaction of the extensometer with the specimen because the material starts to delaminate severely. When such extensive delamination occurs, the extensometer rods most likely do not stay in the dimples, but become lodged between plies as the matrix cracks and the plies pull apart. This phenomenon was seen in all tests of the 2D unitized composite. Images in Section 5.6 show this delamination. The specimen's left and right sides tended to bow out when loaded in tension, with the third CMC ply (ply closest to the plane of co-curing with the PMC) staying relatively straight, indicating that it is stiffer than the rest of the plies. Note that this particular ply, was not located at the center of the specimen thickness, but at the point where the PMC and CMC were co-cured together.

The UTS of the 2D PMC is 22.8% higher than the UTS of the 2D unitized composite with the 0/90° orientation. This shows that the addition of the CMC layer on the unitized composite does not offer an improvement in strength. Strength loss is most likely due to

the complex nature of the material system which involves co-curing of two dissimilar matrix materials. The presence of two dissimilar materials results in non-uniform deformation across the specimen thickness, causing bending stresses in addition to the applied tension.

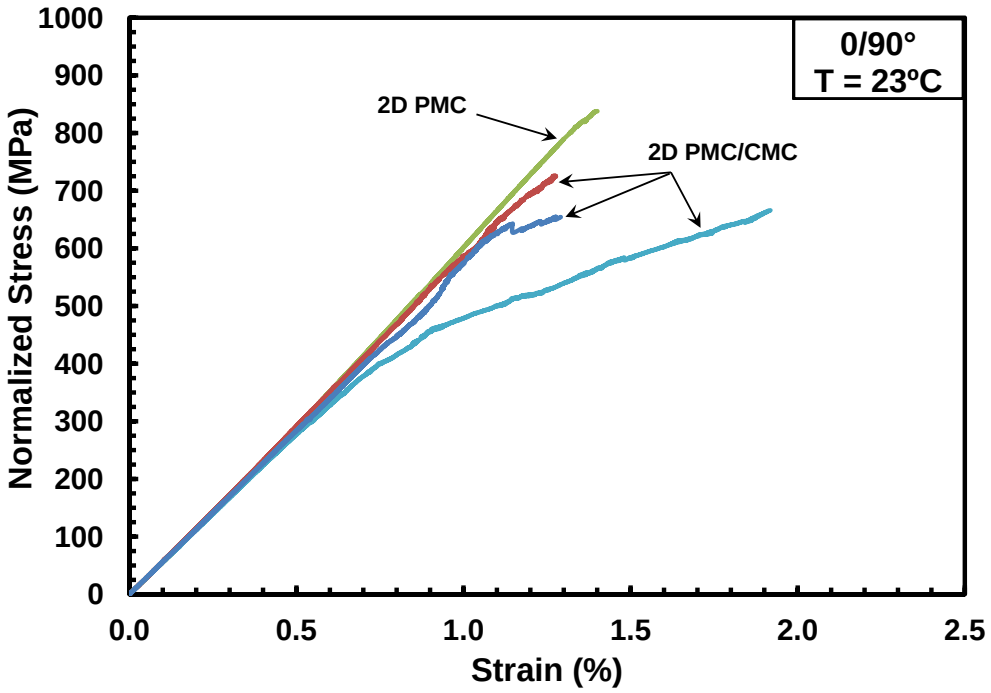

Figure 28: Tensile stress-strain curves obtained for the 2D PMC and 2D PMC/CMC unitized composite with 0/90° fiber orientation at room temperature

Comparing tensile properties obtained for the 2D unitized composite and the 2D PMC with the ±45° fiber orientation (Figure 29), it is evident that the UTS of the unitized composite is at least 100 MPa lower than that of the 2D PMC. The UTS of the unitized composite is only about 35.5% of the UTS value obtained for the 2D PMC. Furthermore, the 2D PMC exhibits stiffness that is 45.4% higher than that of the unitized composite. Figure 30 shows tensile stress-strain curves for the 2D PMC and 2D unitized composite. For the unitized composite, the UTS of the ±45° orientation is 8.5% that of the 0/90° orientation.

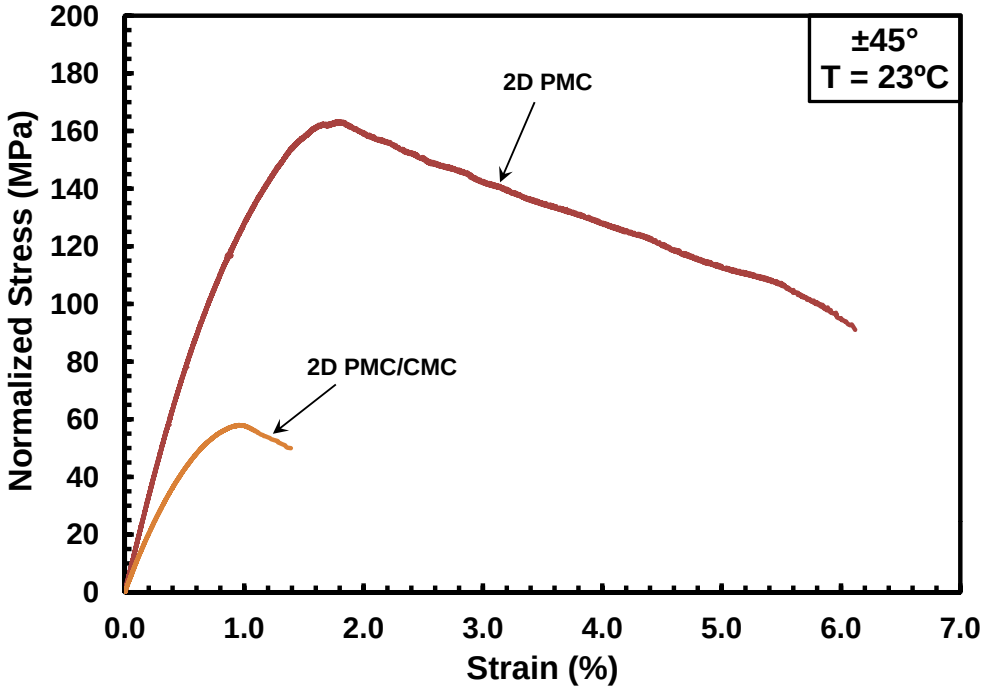

Figure 29: Tensile stress-strain curves obtained for the 2D PMC and 2D PMC/CMC unitized composite with ±45° fiber orientation at room temperature

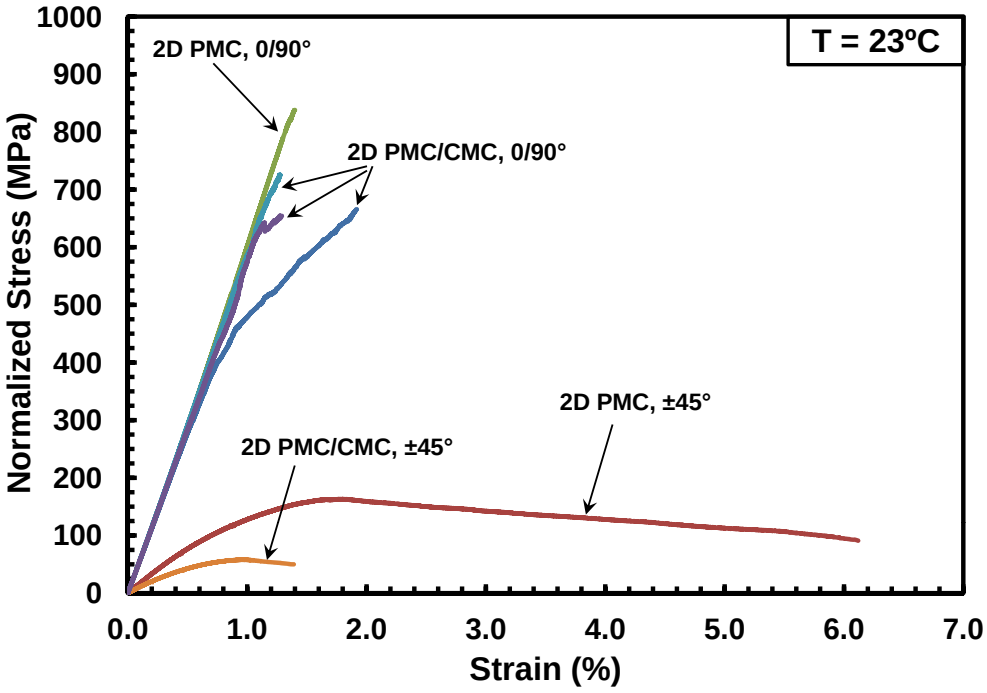

Figure 30: Tensile stress-strain curves obtained for the 2D PMC and 2D PMC/CMC unitized composite with 0/90° and ±45° fiber orientations at room temperature

Because the unitized composite is a novel material system, it was important to study the material behavior during testing. As mentioned previously, one specimen tested in tension at room temperature was photographed with a digital camera using PixelLINK Capture OEM software utilizing a capture rate of 1 frame per second. The progression of gage section damage during the tensile test can be seen in the images of Figure 31. Image (b), taken at 372 MPa, shows little visible damage to the PMC side; however, the CMC layer exhibits slight widening through the thickness, most likely due to the beginning of delamination. Progressive delamination of the CMC and PMC is seen in Figure 31(c)-(e). At 657 MPa (image (d)) one can easily see that the white mark in the PMC section is now altered as plies have moved. Image (e), taken directly after the load carrying capability of the specimen dramatically dropped after reaching the UTS, shows extensive delamination. The approximate corresponding points on the stress-strain curve are shown in Figure 32.

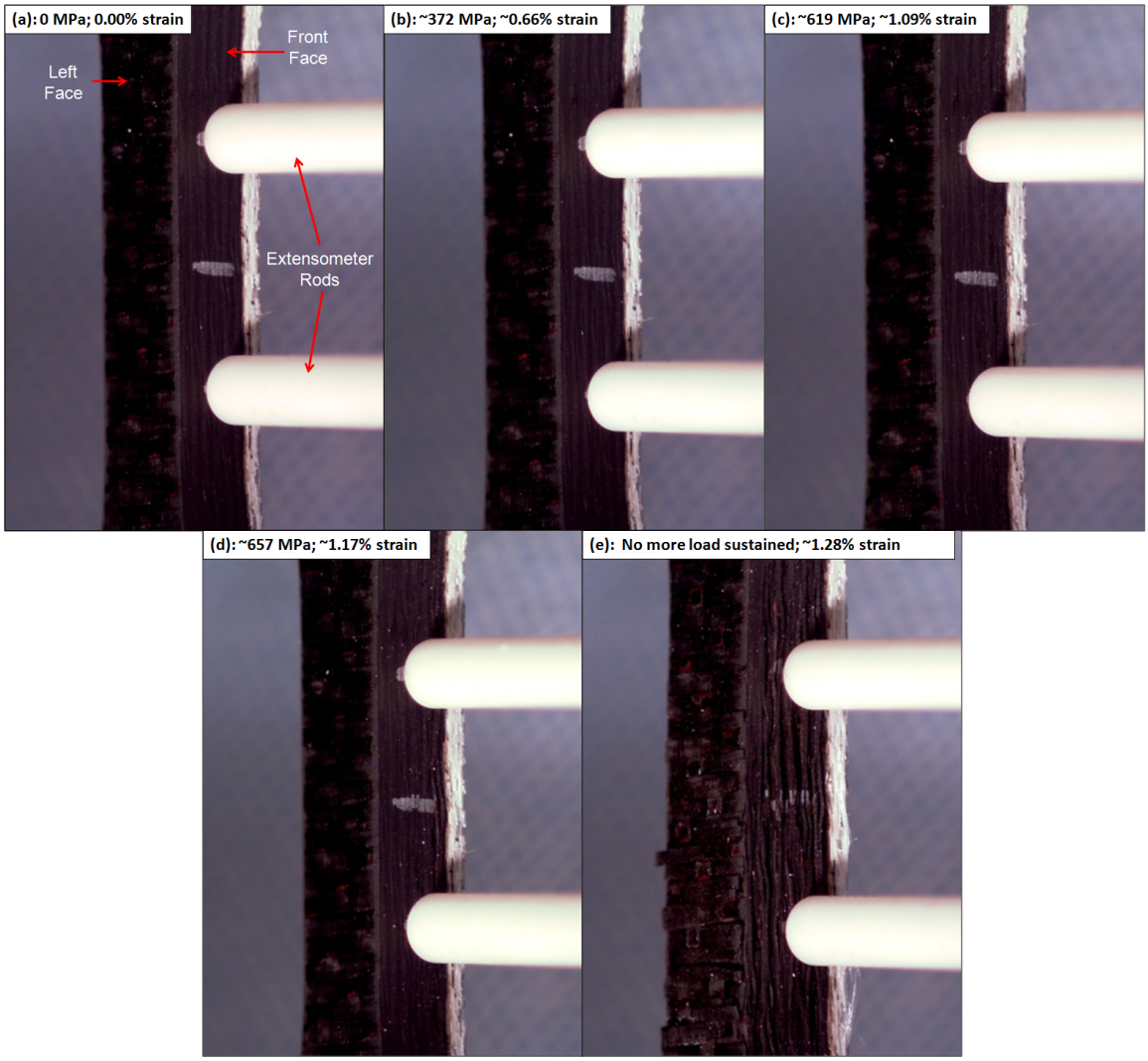

Figure 31: Damage progression during tension-to-failure test of specimen T5-3 (2D unitized composite, 0/90°)

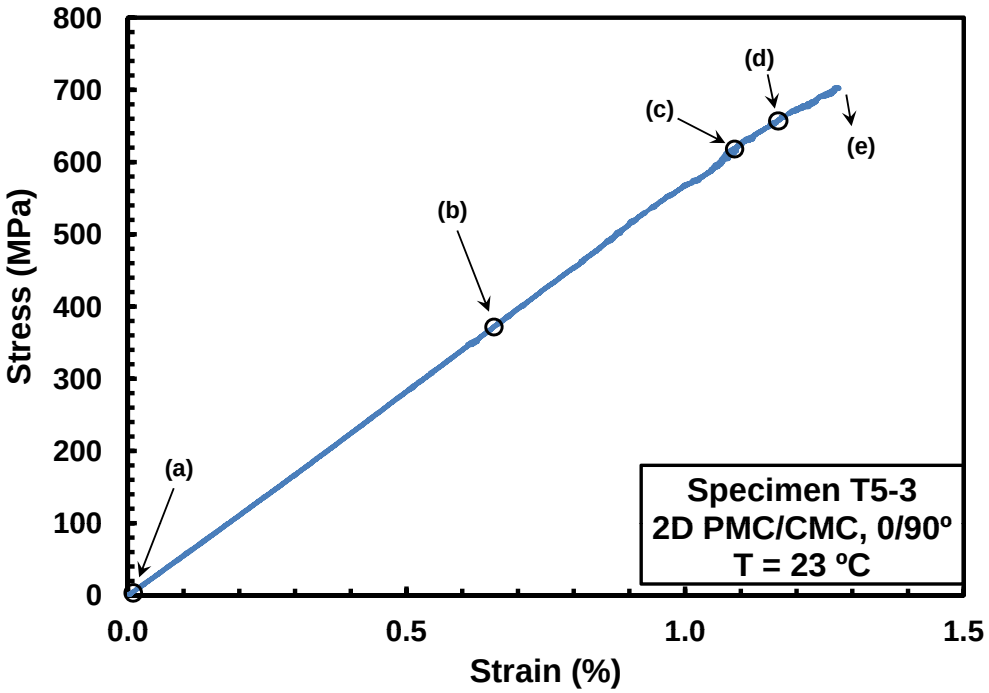

Figure 32: Tensile stress-strain curve obtained for specimen T5-3 at room temperature in laboratory air. Points (a), (b), (c), (d), and (e) on the graph correspond to images in Figure 31(a)-(e).

To summarize the room temperature tension-to-failure results, each material system exhibited significantly higher strength in the 0/90° fiber orientation than the ±45° orientation, as expected. The 2D PMC showed greater stiffness and strength than the 3D PMC for both fiber orientations. The 2D PMC also exhibited greater strength than the 2D unitized composite for both fiber orientations. The modulus of the ±45° orientation 2D PMC was greater than that of the 2D unitized composite; however, the modulus was roughly the same for the 0/90° orientation.

5.3.2 Monotonic Tension at Elevated Temperature.

Specimens of each material system and fiber orientation were tested in tension to failure at an elevated temperature, T_{right}, of 329°C. As mentioned previously, the left side of the specimen was open to ambient air, and consequently, T_{left} fluctuated from test to test. The results obtained in elevated temperature tensile tests are summarized in Tables 10 – 12 above. Figures 33 – 47 compare elevated temperature material response to room temperature material response for each material system, as well as responses obtained for different material systems at elevated temperature.

5.3.2.1 Room vs. Elevated Temperature Tensile Test Results.

Figure 33 shows the stress-strain response of the 0/90° 3D PMC at elevated temperature compared to that produced at room temperature. There is little difference between the material response at elevated temperature compared to that at room temperature. In all tests there is an initial linear behavior that transitions to nonlinear at approximately 0.75-0.85% strain. In the nonlinear regime the material exhibits an increase in modulus. This trend appears to be independent of temperature. The average normalized UTS at elevated temperature for the 0/90° 3D PMC is 756.01 MPa, only 3% lower than the room temperature UTS. This result when considered with the standard deviations of the UTS at room and elevated temperatures (56.89 MPa and 22.29 MPa respectively), shows no change in UTS with temperature. Average failure strain also remains nearly the same, namely 1.472% at elevated temperature and 1.487% for room temperature. In these tests the 0° fibers carry the majority of the load. These carbon fibers can operate at temperatures above the 329°C used in this research, so the effect of temperature increase from 23°C to 329°C (on one side of the specimen) is negligible.

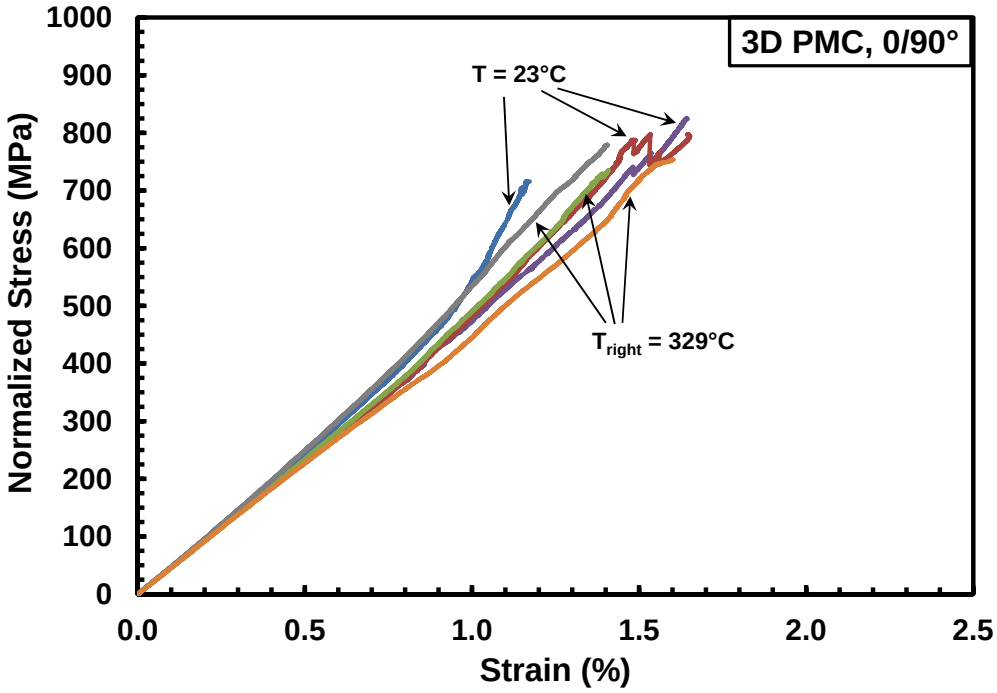

Figure 33: Tensile stress-strain curves obtained for the 3D PMC with 0/90° fiber orientation at room and elevated temperature

For the 3D PMC with ±45° fiber orientation (Figure 34), elevated temperature caused a 19% drop in UTS, although the modulus of the initial linear portion was very similar to that obtained at room temperature. Elevated temperature caused a large increase in failure strain; failure strain produced at elevated temperature was greater than 2.5 times that obtained at room temperature. This degradation in mechanical properties occurs because the polymer matrix material carries the majority of the load in the case of the ±45° orientation. Although the matrix material is a high temperature polyimide resin, 329°C approaches the maximum use temperature for most HTPMCs. The stress-strain curves obtained for the 3D PMC with 0/90° and ±45° fiber orientations at 23°C and at elevated temperature are plotted together in Figure 35 for comparison.

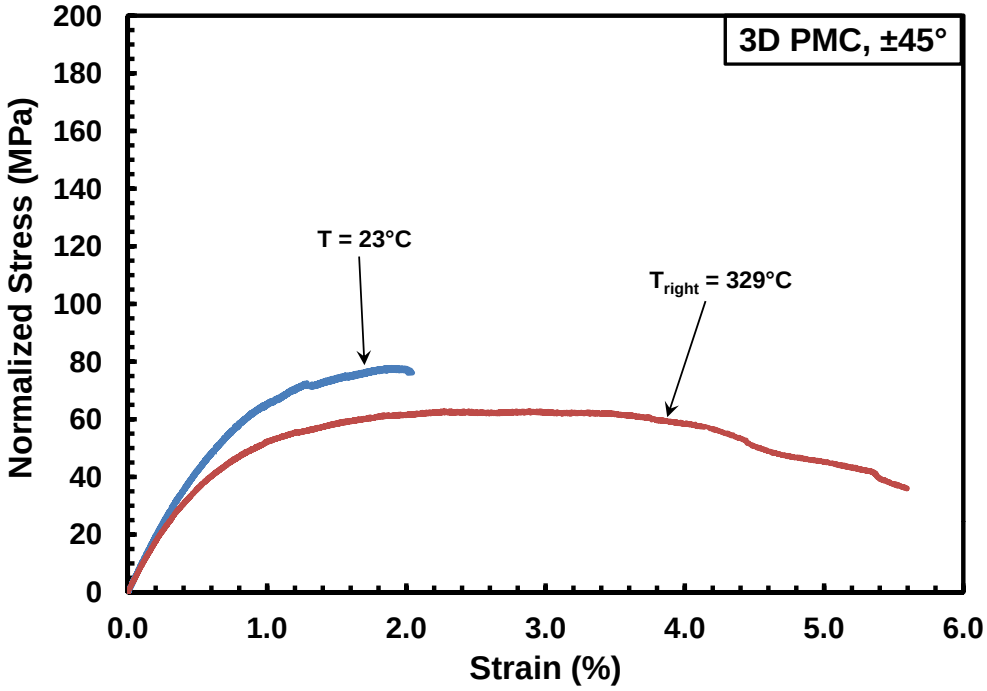

Figure 34: Tensile stress-strain curves obtained for the 3D PMC with ±45° fiber orientation at room and elevated temperature

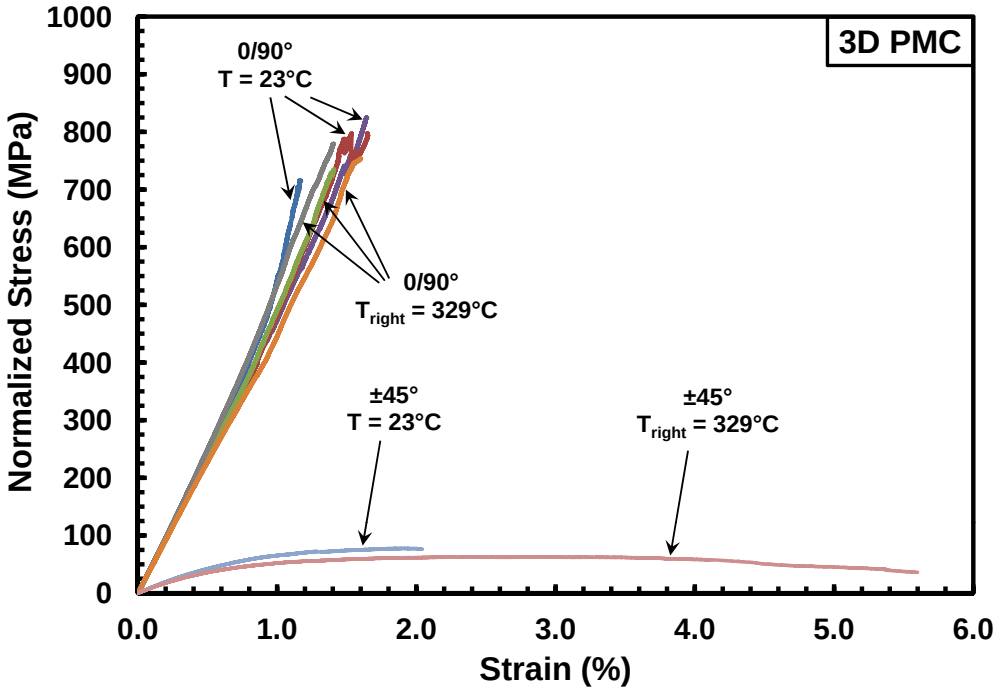

Figure 35: Tensile stress-strain curves obtained for the 3D PMC with 0/90° and ±45° fiber orientations at room and elevated temperature

The stress-strain response of the 2D PMC with 0/90° fiber orientation at elevated temperature also showed little difference compared to the room temperature response (Figure 36). The stress-strain curves are again nearly linear to failure. The room temperature UTS falls in between the two elevated temperature UTS values. The average failure strain obtained at elevated temperature is almost the same as that at room temperature (1.281% at elevated temperature compared to 1.401% at room temperature).

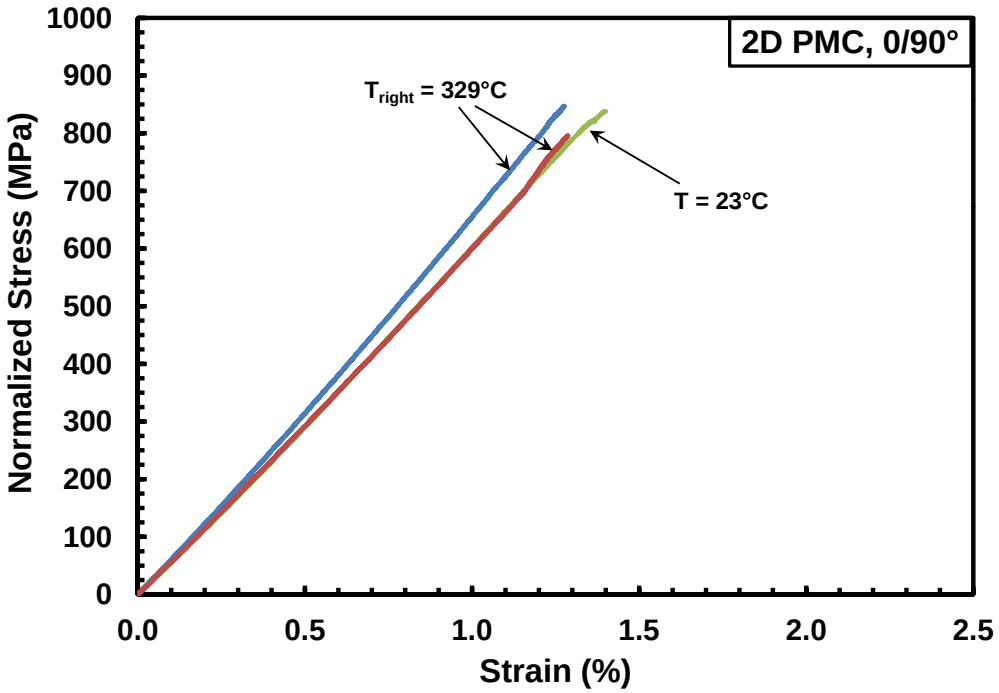

Figure 36: Tensile stress-strain curves obtained for the 2D PMC with 0/90° fiber orientation at room and elevated temperature

Figure 37 shows tensile stress-strain curves obtained for the 2D PMC with ±45° fiber orientation at room and elevated temperatures. It is evident that the UTS decreases (by 22.6%) and failure strain increases (by 112%) at elevated temperature. The stress-strain curve obtained at elevated temperature did not exhibit a dramatic instantaneous drop in stress at any point after the UTS was reached; therefore, the failure strain was taken as the strain at the point where the stress dropped to 50% of the UTS. The elevated temperature

caused a decrease in modulus by 18%. Additionally, the elevated temperature stress-strain curve shows a quicker decrease in stiffness compared to that produced at room temperature. Tensile stress-strain curves obtained for both 0/90° and ±45° fiber orientations of the 2D PMC at room temperature and elevated temperature are shown in Figure 38.

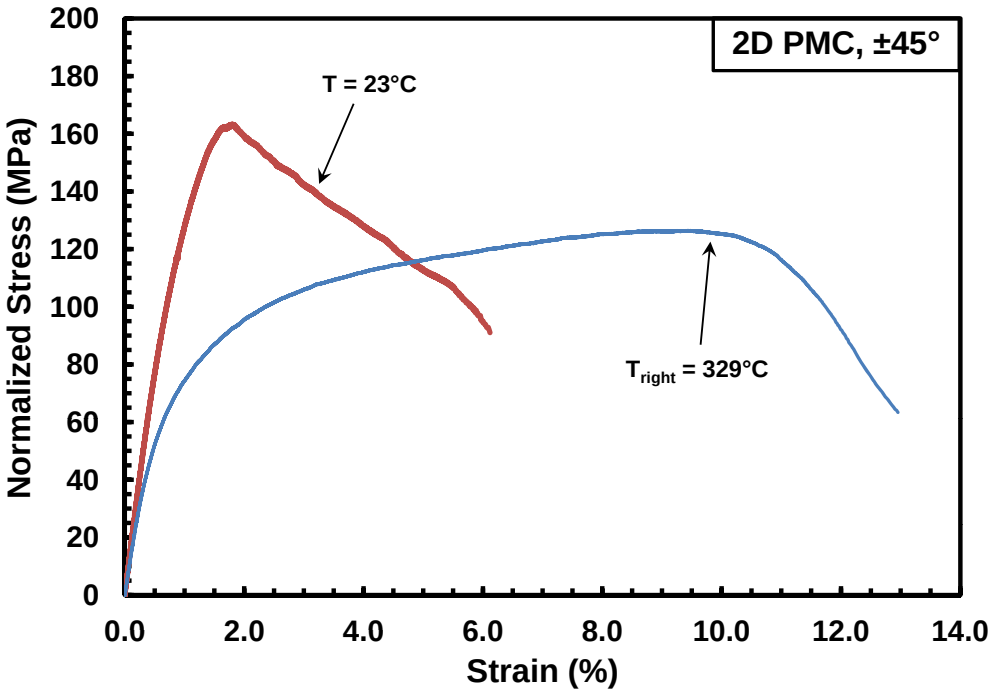

Figure 37: Tensile stress-strain curves obtained for the 2D PMC with ±45° fiber orientation at room and elevated temperature

For the 2D unitized composite, similar trends are seen. The tensile stress-strain behavior of the 0/90° fiber orientation was little influenced by temperature compared to room temperature (Figure 39), although the average normalized UTS obtained at elevated temperature was some 18 MPa lower than that produced at room temperature. However, the amount of data scatter (standard deviation of 38.13 MPa for room temperature UTS

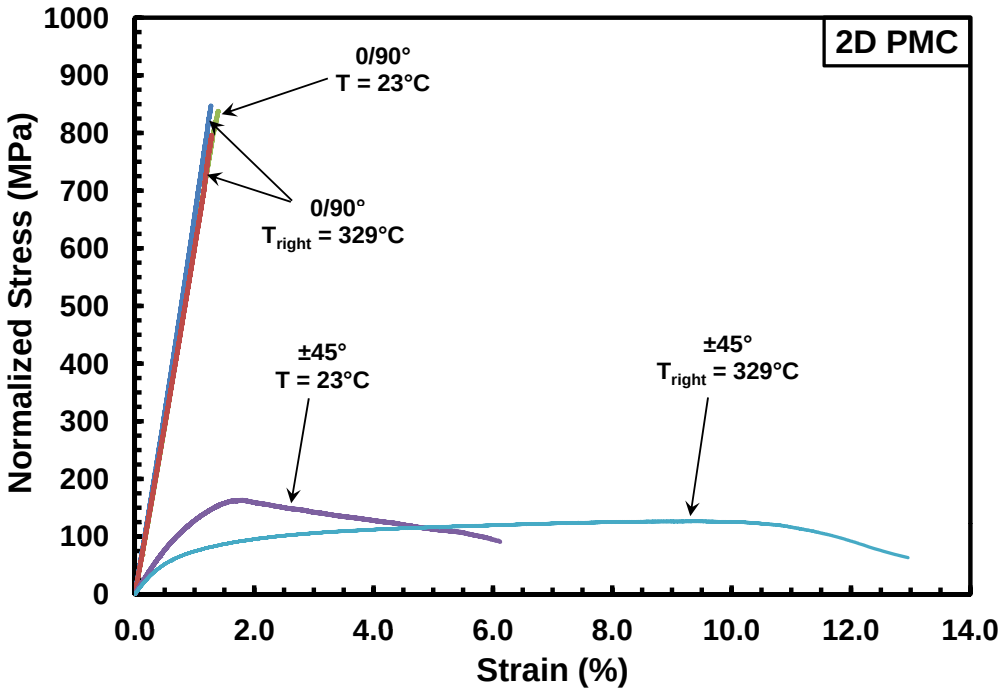

Figure 38: Tensile stress-strain curves obtained for the 2D PMC with 0/90° and ±45° fiber orientations at room and elevated temperature

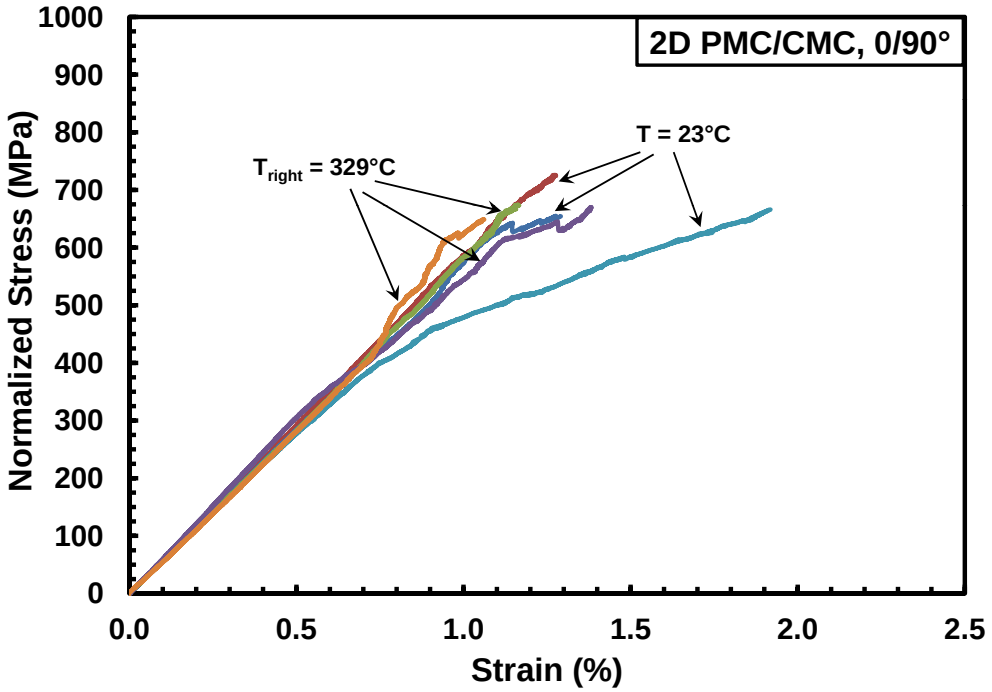

Figure 39: Tensile stress-strain curves obtained for the 2D PMC/CMC with 0/90° fiber orientation at room and elevated temperature

values and 13.67 MPa for elevated temperature UTS values) shows that the UTS changes little with temperature.

Two ±45° 2D unitized composite specimens were tested at elevated temperature. The resulting stress-strain response is plotted together with the stress-strain curves obtained at room temperature in Figure 40. Elevated temperature again causes an increase in failure strain by an average of 83%. The elastic modulus decreased by 14%. Although the elevated temperature UTS values appear to be lower than those obtained at room temperature, when normalized stresses are considered the UTS values obtained at elevated temperature are fairly close to those obtained at room temperature. This trend is more evident when the ±45° curves are plotted on the same graph as the 0/90° curves (Figure 41).

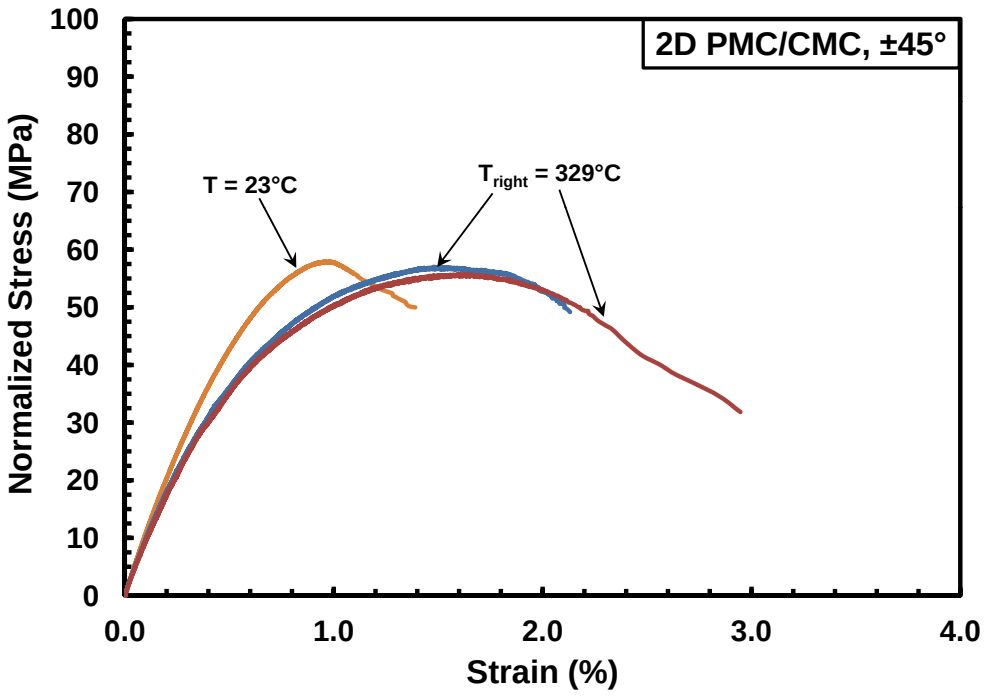

Figure 40: Tensile stress-strain curves obtained for the 2D PMC/CMC with ±45° fiber orientation at room and elevated temperature

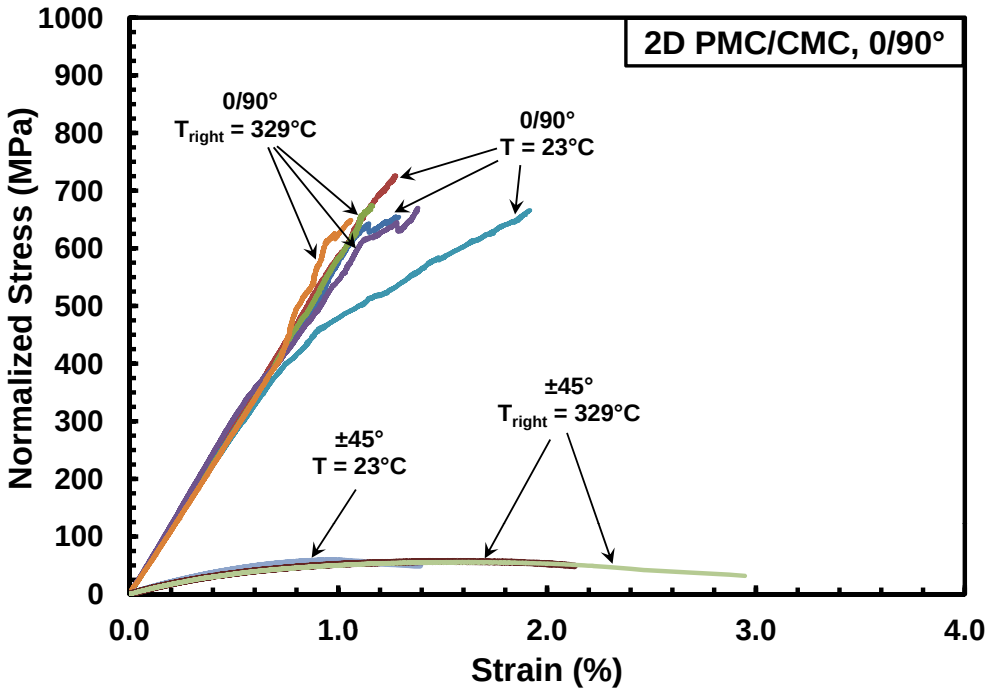

Figure 41: Tensile stress-strain curves obtained for the 2D PMC/CMC with 0/90° and ±45° fiber orientations at room and elevated temperature

To summarize the effect of elevated temperature on tensile properties, it appears that in the case of the 0/90° fiber orientation all three material systems did not exhibit significant degradation in tensile properties at elevated temperature. However, in the case of the ±45° fiber orientation, all three material systems exhibited significant increases in failure strain and a decrease in tensile strength at elevated temperature. Notably the loss of UTS for the unitized composite could be considered negligible. Finally, the modulus decreased in the 2D PMC and unitized composite due to elevated temperature, but stayed approximately the same in the 3D PMC.

5.3.2.2 Comparison of Tensile Properties at Elevated Temperature.

In this section, the elevated temperature mechanical response of the 3D PMC and 2D unitized composite are compared to that of the 2D PMC. Figure 42 compares tensile stress-strain behavior of the 3D PMC and of the 2D PMC with 0/90° fiber orientation at

elevated temperature. The average UTS of the 2D PMC is 8.6% greater than the average UTS of the 3D PMC. The 2D PMC is also stiffer, with the average modulus being 27% greater than that of the 3D PMC. These differences in UTS and modulus are similar to the differences observed at room temperature. The 3D PMC also exhibited greater failure strains than the 2D PMC (approximately 14.8% greater).

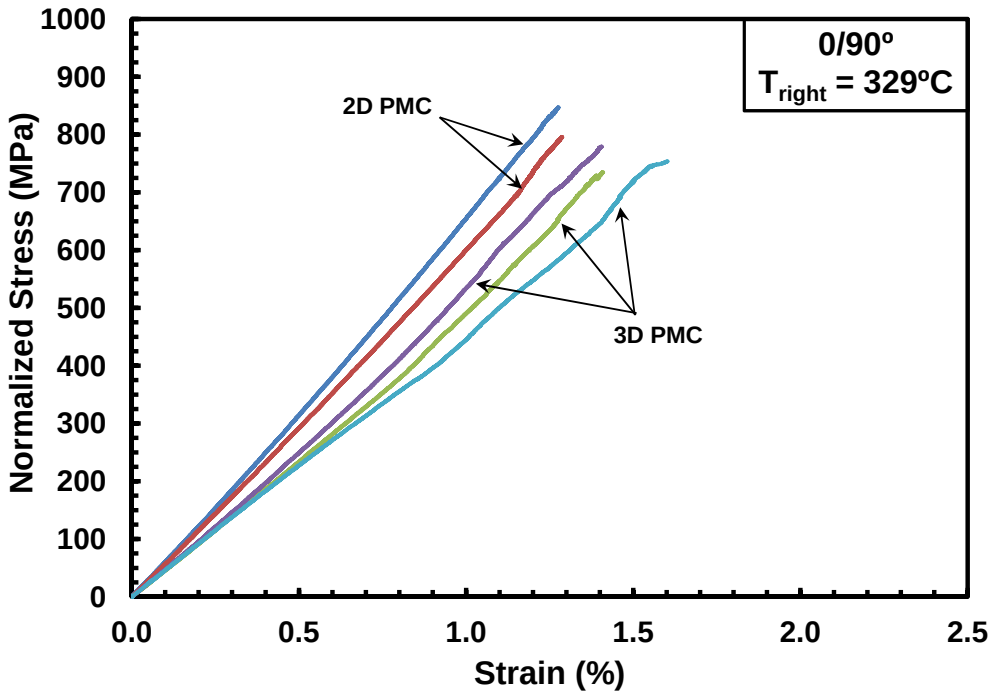

Figure 42: Tensile stress-strain curves obtained for the 2D and 3D PMC with 0/90° fiber orientation at elevated temperature

Figure 43 compares the tensile stress-strain behavior at elevated temperature of the 3D PMC and 2D PMC with ±45° fiber orientation. The UTS for the 2D PMC is two times that of the 3D PMC. The ±45° 2D PMC is stiffer as well, as evidenced by the higher modulus. Failure strain of the 2D PMC is significantly larger than that of the 3D PMC. Tensile stress-strain curves obtained for the 2D PMC and the 3D PMC at elevated temperature are presented in Figure 44.

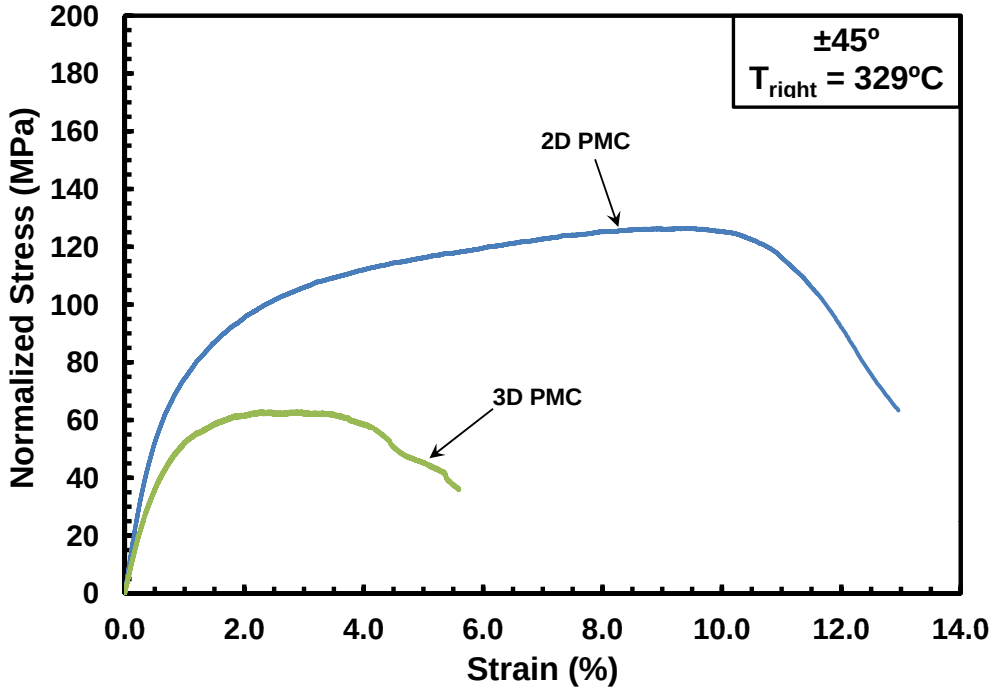

Figure 43: Tensile stress-strain curves obtained for the 2D and 3D PMC with ±45° fiber orientation at elevated temperature

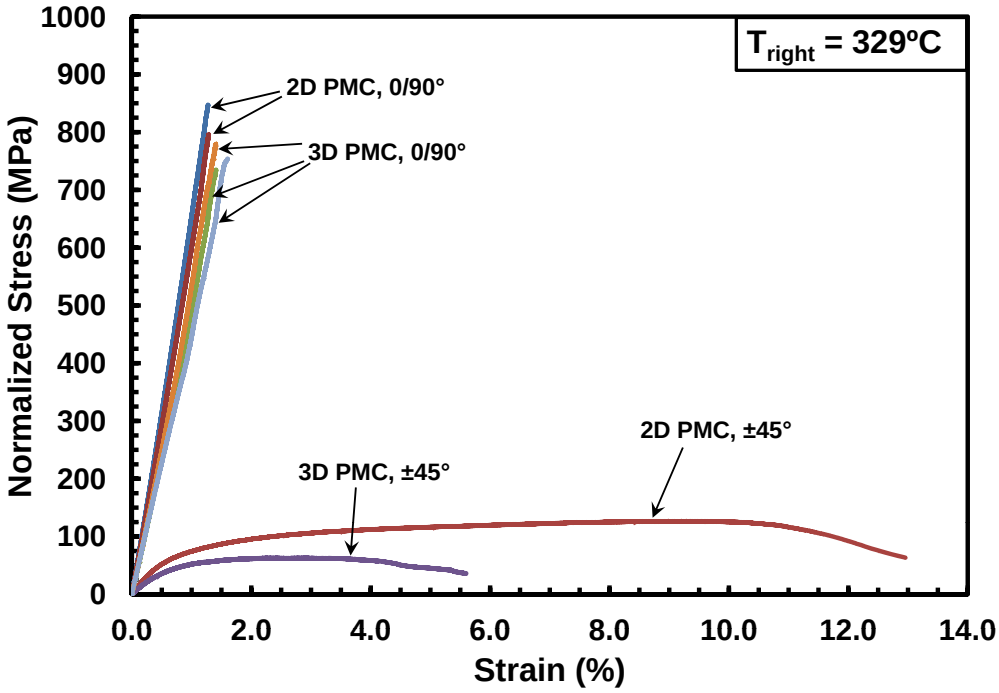

Figure 44: Tensile stress-strain curves obtained for the 2D and 3D PMC at elevated temperature

The tensile stress-strain curves obtained for the 2D PMC and 2D unitized composite with 0/90° fiber orientation at elevated temperature are compared in Figure 45. The average UTS of the 2D PMC is 23.7% greater than the average UTS of the 2D unitized composite, about the same difference as that noted at room temperature. This again shows that elevated temperature does not have much effect on the mechanical properties of the 0/90° fiber orientation. Both material systems show similar average stiffness and similar average failure strains.

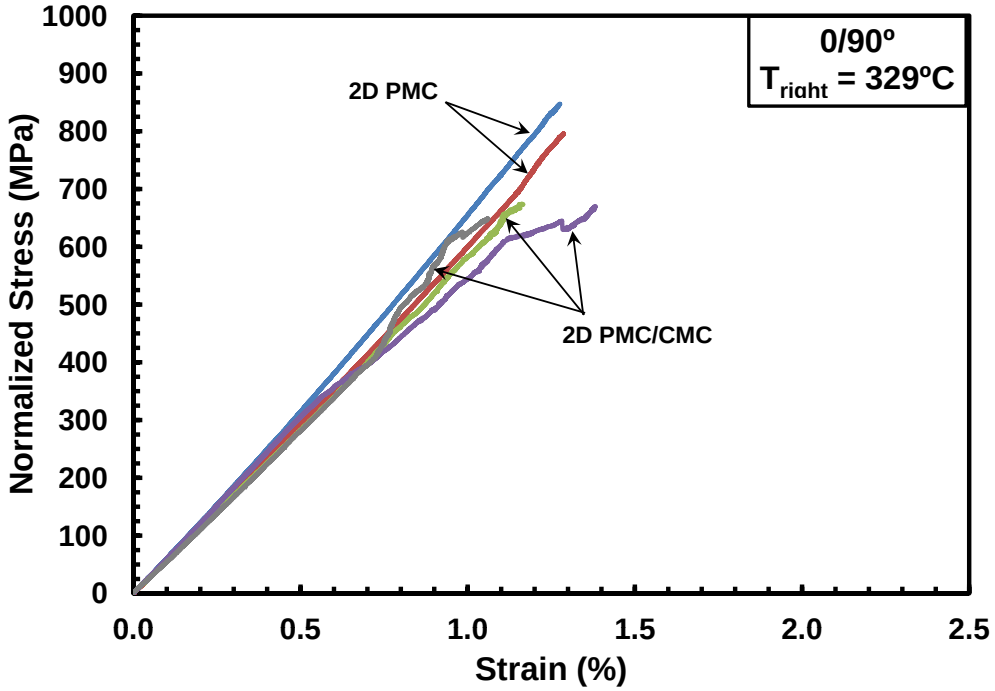

Figure 45: Tensile stress-strain curves obtained for the 2D PMC and 2D PMC/CMC unitized composite with 0/90° fiber orientation at elevated temperature

The 2D PMC exhibits greater strength, stiffness, and failure strain than the 2D unitized composite with the ±45° fiber orientation at elevated temperature (Figure 46). The average UTS of the 2D unitized composite is only 44.6% of the UTS produced by the 2D PMC, which is a greater percentage than observed at room temperature. The modulus of the 2D PMC is 46% greater than the average modulus of the 2D unitized composite.

Furthermore, the failure strain of the 2D PMC is over 5 times that of the 2D unitized composite. Tensile stress-strain curves for the 2D PMC and the 2D unitized composite are plotted together in Figure 47.

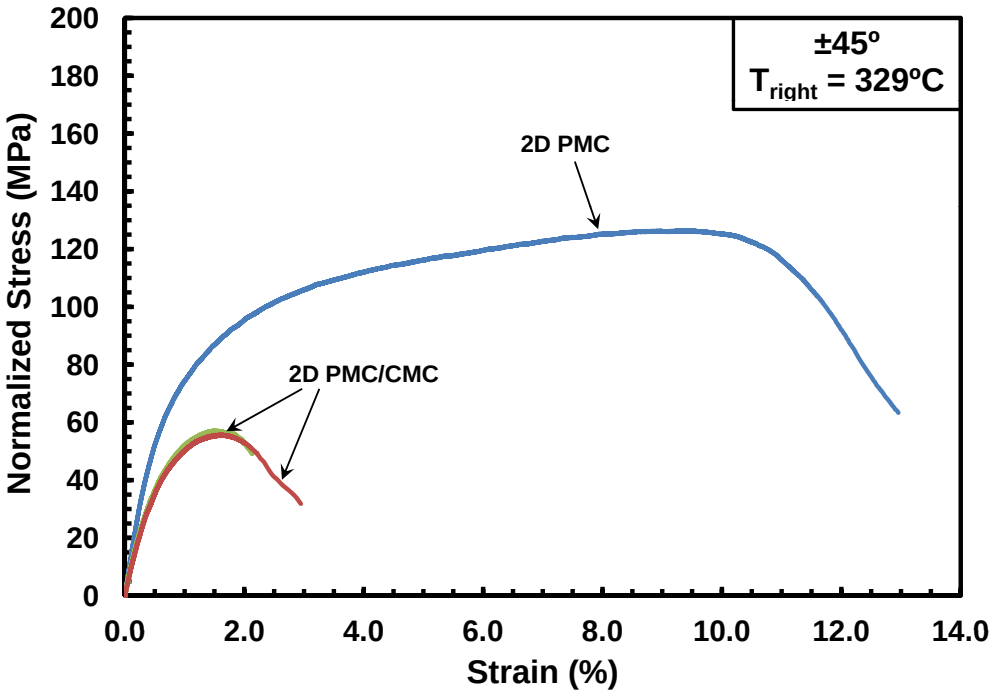

Figure 46: Tensile stress-strain curves obtained for the 2D PMC and 2D PMC/CMC unitized composite with ±45° fiber orientation at elevated temperature

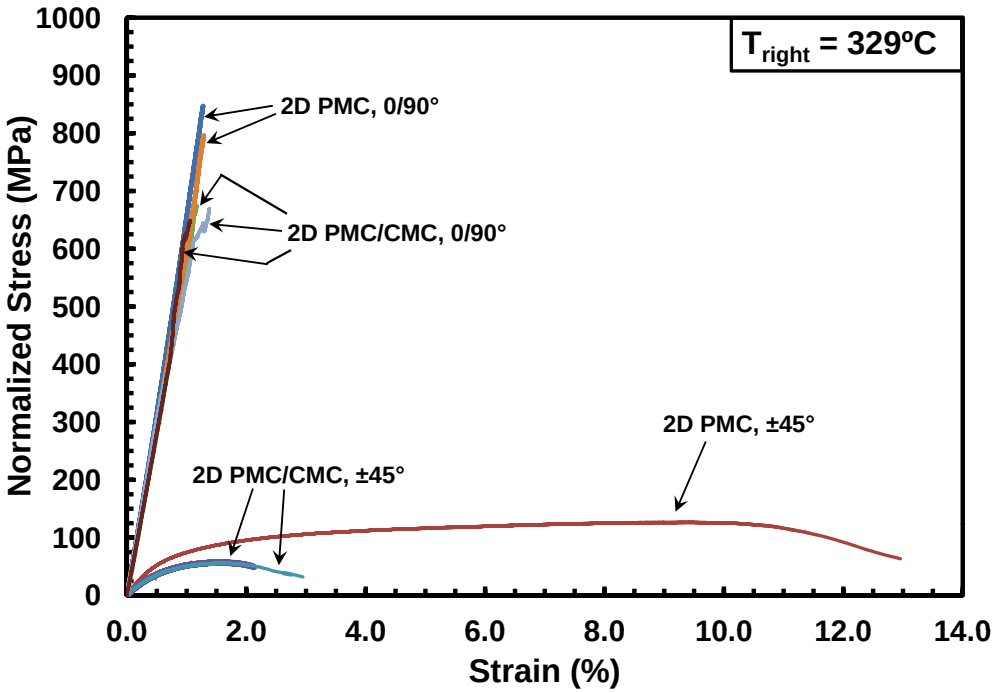

Figure 47: Tensile stress-strain curves obtained for the 2D PMC and 2D PMC/CMC unitized composite at elevated temperature

To summarize the comparisons of tensile behavior and properties produced by different material systems at elevated temperature, the 2D PMC exhibited greater UTS than both the 3D PMC and the unitized composite with the 0/90° orientation. No significant differences in failure strains were evident in the case of the 0/90° orientation at elevated temperature. The average modulus of the 2D PMC with the 0/90° orientation was greater than that of the 3D PMC, but nearly the same as that of the 2D unitized composite. For the ±45° fiber orientation, the 2D PMC exhibited a higher UTS, greater modulus, and significantly greater failure strain than both the 3D PMC and unitized composite.

5.4 Elevated Temperature Tension-Tension Fatigue Tests

All fatigue tests, were conducted at an elevated temperature, T_{right}, of 329°C with a minimum to maximum stress ratio of $R = 0.05$ at a frequency of 1 Hz. Fatigue run-out was defined as 2×10^5 cycles. The following sections will discuss the fatigue results for each individual material system and compare fatigue performance of the 3D PMC, the 2D PMC, and the 2D unitized composite.

5.4.1 Fatigue Performance of Material System 1 (3D PMC).

Fatigue results for the 3D PMC specimens are summarized in Table 13. Both measured and normalized stresses are shown.

Table 13: Tension-tension fatigue results for MS1 at T_{right} = 329°C in laboratory air

Specimen #	Maximum Stress (MPa)	Maximum Stress (% UTS)	Normalized Max. Stress (MPa)	Normalized Max. Stress (% Norm. UTS)	Cycles to Failure (N)	Failure Strain (%)
0/90° Fiber Orientation						
T3-18	621.2	85	661.0	88	1,159	0.051
T3-17	643.0	88	640.0	85	519	0.051
T3-15	621.7	85	609.9	81	10,141	0.258
T3-19	623.0	85	592.9	78	57,373	0.275
T3-11	584.8	80	575.1	76	75	0.089
T3-14	563.4	77	558.4	74	85,931	0.366
T3-12	549.4	75	551.0	73	159,828	0.091
T3-13	512.5	70	528.7	70	167,979	0.232
T3-8	586.4	80	526.0	70	45,091	0.015
T3-9	513.8	70	518.0	69	150,741	0.453
T3-10	476.0	65	482.9	64	200,000[a]	0.122[a]
T3-7	440.9	60	424.7	56	200,000[a]	0.047[a]
±45° Fiber Orientation						
T4-7	48.2	82	45.1	72	1,977	3.513
T4-5	43.9	75	43.4	69	1,899	2.476
T4-6	46.7	80	42.6	68	1,384	2.944
T4-9	41.1	70	41.4	66	7,843	2.751
T4-4	38.7	66	39.8	63	51,132	2.989
T4-11	36.1	61	35.1	56	53,922	3.316
T4-8	33.1	56	35.1	56	101,106	2.778
T4-3	32.2	55	33.0	52	200,000[a]	1.479[a]

[a] *Run-out; defined as 2×10^5 cycles. Failure of specimen did not occur when the test was terminated.*

Fatigue results are presented as the maximum stress vs. cycles to failure (S-N) curve in Figure 48. Fatigue run-out was achieved at 482.9 MPa for the 0/90° fiber orientation and at 33.0 MPa for the ±45° fiber orientation (a mere 7% that of the 0/90° orientation). Note that one specimen (specimen T3-11) failed much earlier than expected and is considered an outlier on the S-N curve. This short lifetime could be due to localized processing defects. Indeed, more matrix voids and thickness variation were noted in visual inspection for the 3D PMC than for the 2D PMC. The S-N curve obtained for the ±45° fiber orientation is shown in Figure 49. To show that normalization had little effect on the overall trend of the curve, S-N curves produced using measured and normalized stresses are provided in Appendix B.

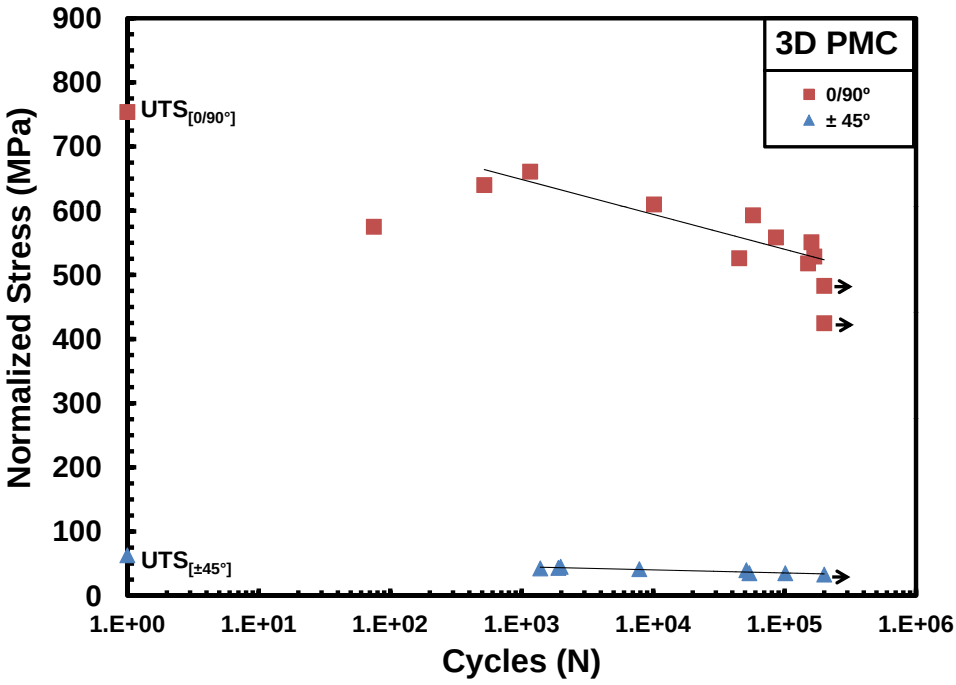

Figure 48: S-N curves for the 3D PMC at elevated temperature. Arrow indicates specimen achieved fatigue run-out.

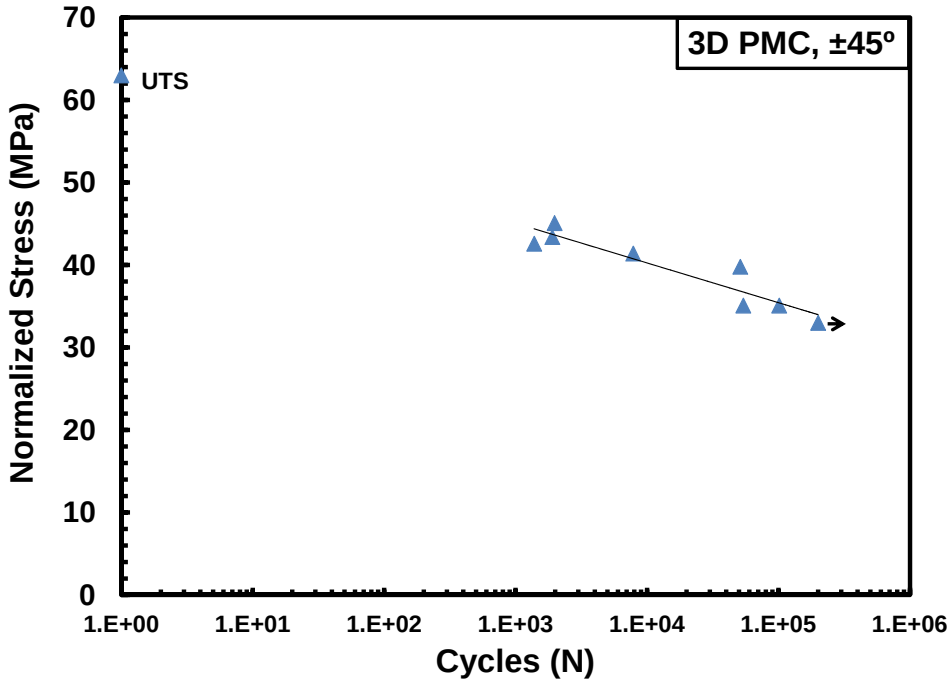

Figure 49: *S*-*N* curve for the 3D PMC with ±45° fiber orientation at elevated temperature. Arrow indicates specimen achieved fatigue run-out.

Fatigue results can also be assessed by plotting stress as percent UTS on an *S*-*N* curve. This allows insight into fatigue performance of the two fiber orientations relative to their respective UTS values. As can be seen in Figure 50, the *S*-*N* curve for the 0/90° fiber orientation occurs at a greater percent of the corresponding UTS than the *S*-*N* curve obtained for the ±45° fiber orientation. There is a 12% difference between the fatigue limits of the two fiber orientations when compared in this manner. The 0/90° orientation has better fatigue performance because the fibers carry the majority of the load and are stronger than the matrix, which dominates the fatigue response of the ±45° specimens. It is interesting to note, however, that the trendlines for both *S*-*N* curves have similar slopes.

Figure 51 shows evolution of stress-strain hysteresis loops with fatigue cycles at 526.0 MPa (70% normalized UTS) for the 3D PMC with 0/90° fiber orientation. The stress-strain curves in Figure 51 are representative of the results produced by all 3D PMC

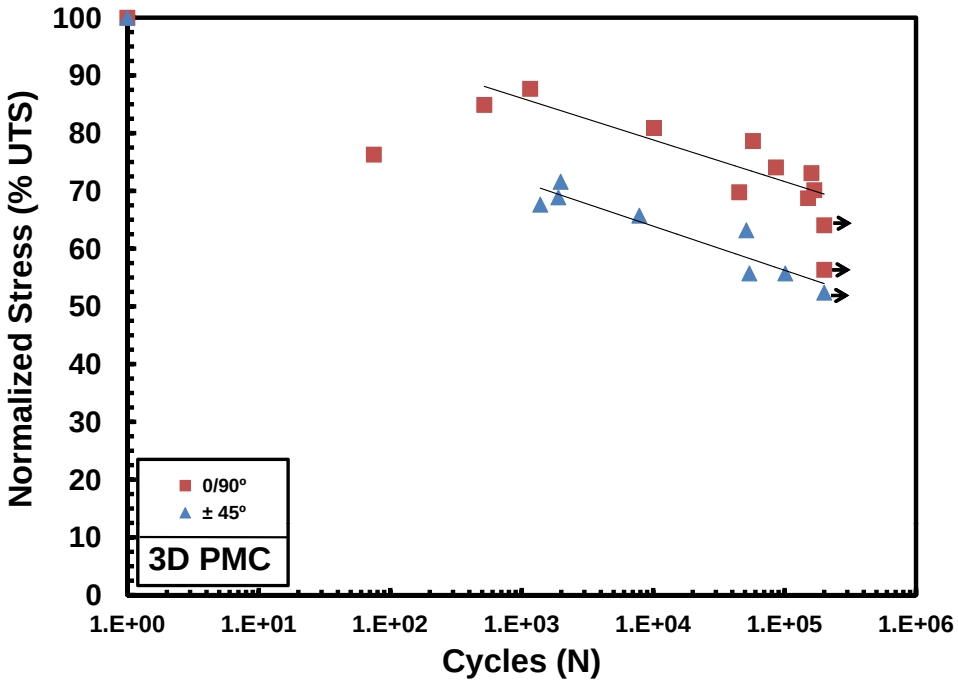

Figure 50: *S*-*N* curves obtained for the 3D PMC at elevated temperature. Maximum stress is shown as % UTS. Arrow indicates specimen achieved fatigue run-out.

specimens with 0/90° fiber orientation. There is very little strain ratcheting (strain accumulated during cycling) and a very slight loss in stiffness, as evident by the decrease in modulus with cycles. The modulus loss for the cycles shown is very small; however, the modulus decrease became accelerated for later cycles approaching final failure. These cycles were not captured with the cyclic data acquisition since failure of the specimen shown occurred between 40,000 and 50,000 cycles. Plots of stress-strain hysteresis response for all other 0/90° specimens are provided in Appendix B.

The overall loss in modulus is better seen by plotting the peak and valley acquisition data. A hysteresis modulus was determined from the maximum and minimum stress-strain data points during a load cycle. This hysteresis modulus was then normalized to the modulus of the second cycle instead of the first cycle due to increased strain accumulated during the first cycle. Modulus loss for 0/90° specimens can be seen in Figure 52. It can

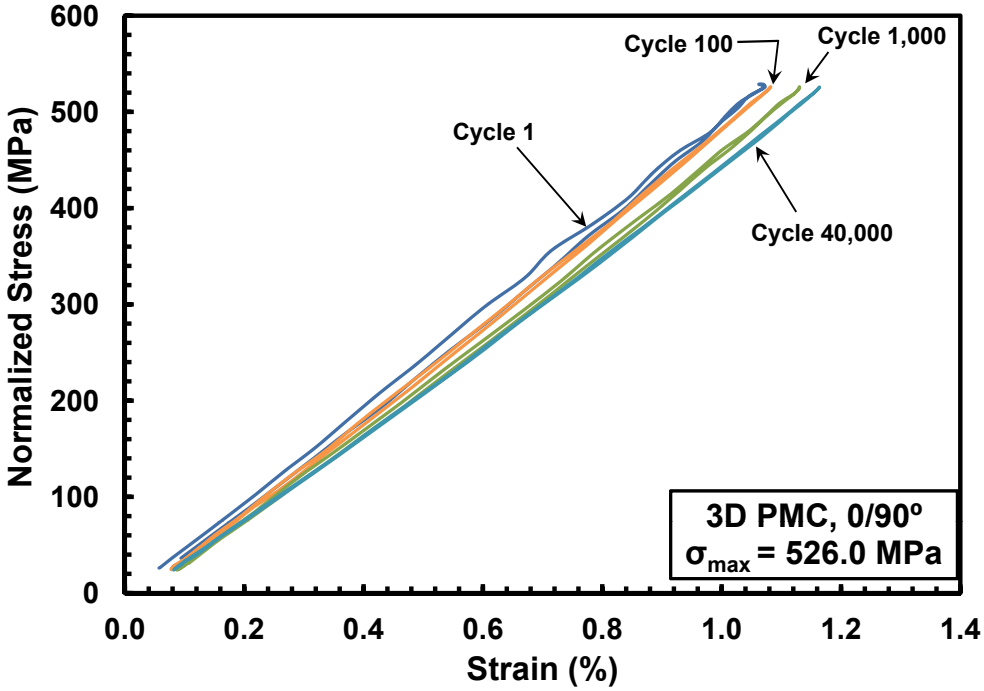

Figure 51: Evolution of stress-strain hysteresis response with fatigue cycles for specimen T3-8 of the 3D PMC with 0/90° fiber orientation at elevated temperature.

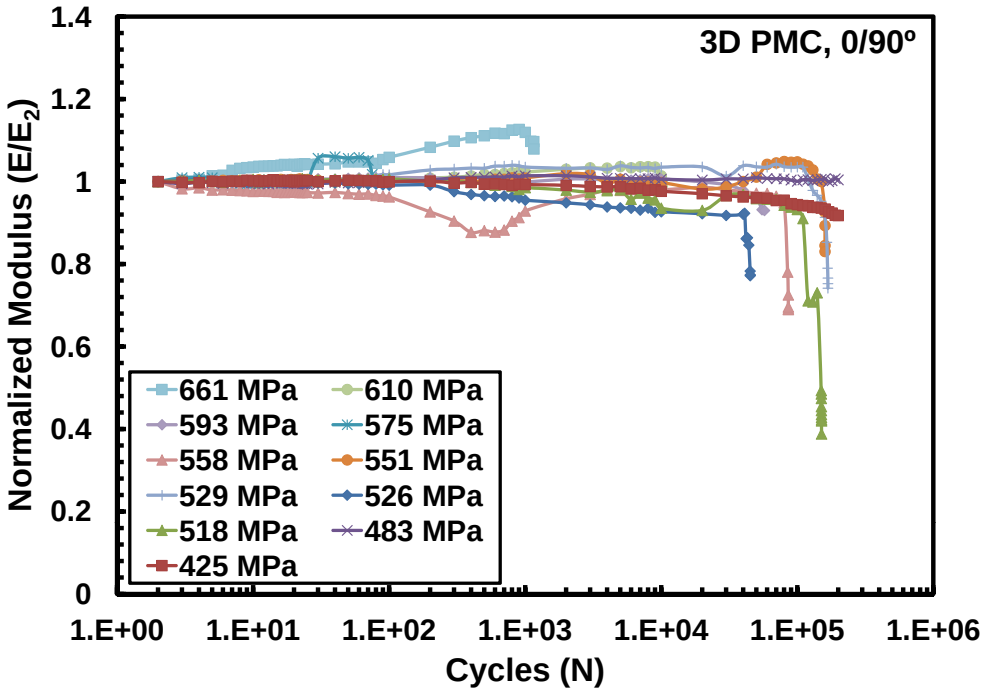

Figure 52: Normalized modulus vs. fatigue cycles for the 3D PMC with 0/90° fiber orientation at elevated temperature.

be seen that the modulus remains relatively constant until near failure. There was no apparent correlation between modulus loss and fatigue stress. The modulus loss varied from -7.9% (stiffening) to 61% (softening), with the majority of specimens having between 7% and 30% modulus loss at failure.

Maximum and minimum strains during cyclic loading for all tested 0/90° specimens are presented in Figure 53. The strains remain relatively constant until near failure. The minimum strain is the accumulated strain during cycling and represents strain ratcheting. Failure strains of all specimens were below 0.5%

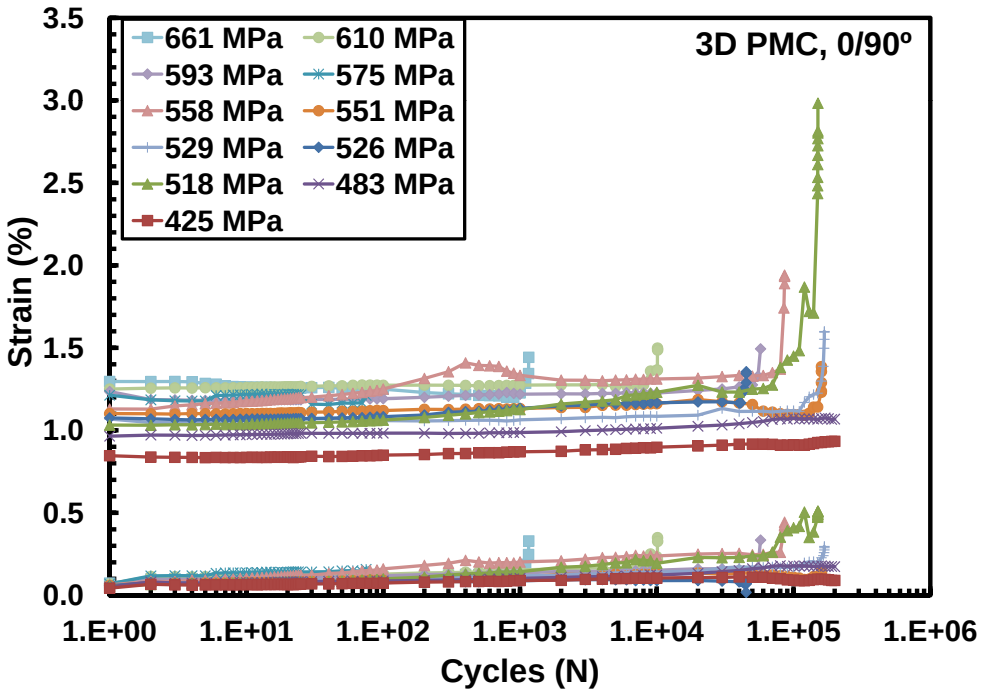

Figure 53: Maximum and minimum strains vs. fatigue cycles for the 3D PMC with 0/90° fiber orientation at elevated temperature.

Stress-strain hysteresis response of the 3D PMC with ±45° fiber orientation can be seen in Figure 54 for σ_{max} of 39.8 MPa (63% normalized UTS). More strain is accumulated with cycles in the case of this fiber orientation. Furthermore, modulus decreases as cycles increase, especially toward the end of the fatigue life. Plots of

stress-strain hysteresis response for other ±45° specimens follow similar trends and are provided in Appendix B.

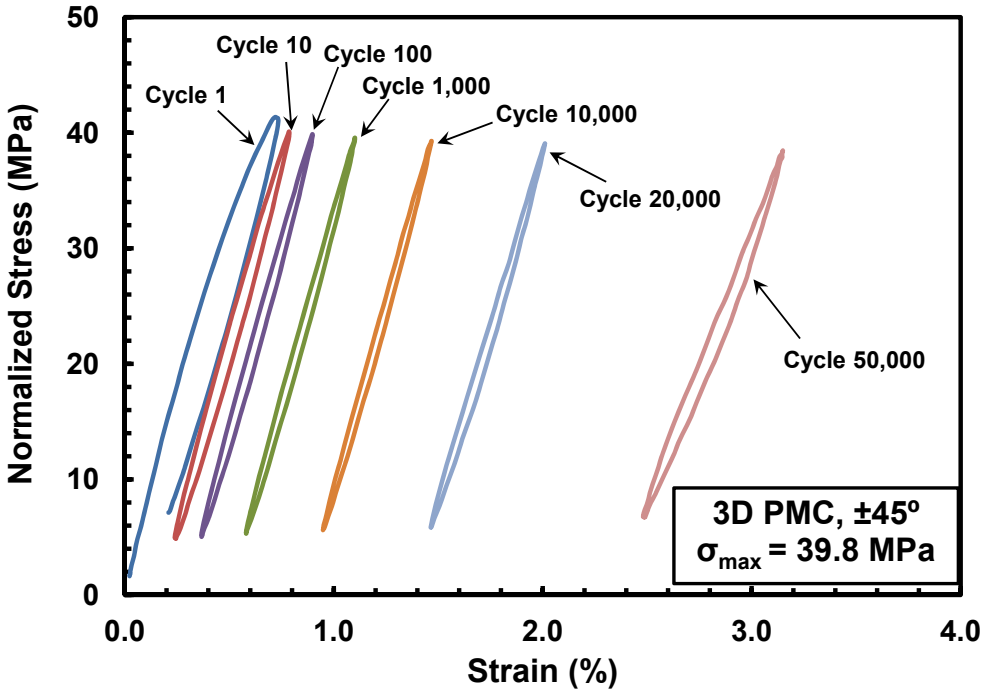

Figure 54: Evolution of stress-strain hysteresis response with fatigue cycles for specimen T4-4 of the 3D PMC with ±45° fiber orientation at elevated temperature.

Figure 54 also shows the effect of tuning previously mentioned in Section 4.3.3. Note the higher peak stress of the first cycle and higher than desired values of minimum stress. Consequently, the actual R value of the fatigue tests for the ±45° specimens was approximately 0.1 instead of 0.05. The percent difference between desired stress and actual stress output was about 7% for both maximum and minimum stresses. This difference is not believed to make a significant difference in the fatigue performance of the material. Another phenomenon observed for the ±45° specimens was the change in compliance of the material toward the end of the specimen fatigue life. As a result, the maximum stress sustained in cyclic loading started to decrease and the minimum stress started to increase. This change in maximum and minimum stresses is seen in Figure 54.

The compliance change is due to increased damage events in the matrix material as cycling progresses. Ideally, the MTS test system would be re-tuned to reflect the new specimen compliance. However, it was not desirable to interrupt the test for tuning. Figure 55 shows how the stresses changed due to the change in specimen material compliance.

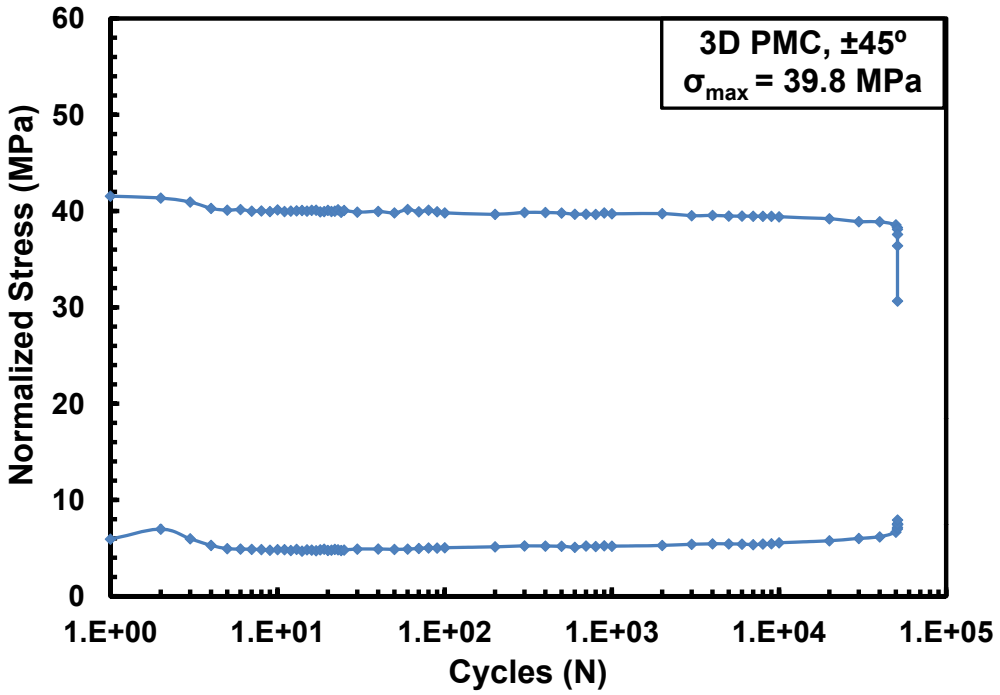

Figure 55: Stress vs. cycles for the 3D PMC with ±45° fiber orientation at elevated temperature showing material compliance change toward end of fatigue life.

Normalized modulus vs. fatigue cycles of all ±45° specimens can be seen in Figure 56. There is not an evident correlation between number of cycles and percent modulus loss. The average modulus loss for ±45° specimens is greater than that for the 0/90° specimens. The modulus loss ranges from 25-58%. The specimen that achieved a run-out represents an exception with modulus loss of 14%.

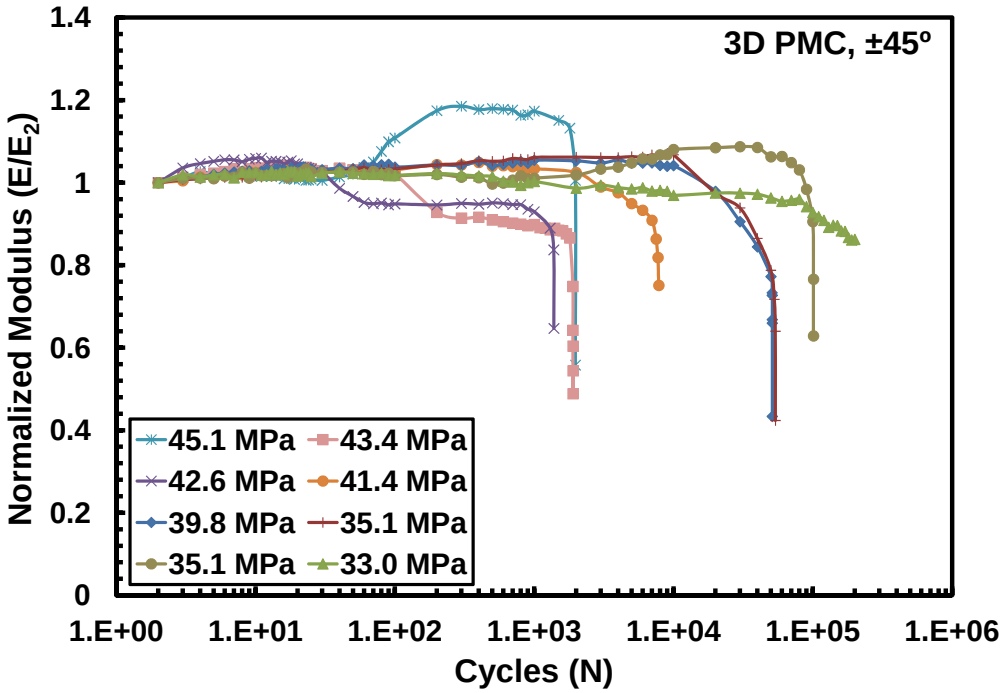

Figure 56: Normalized modulus vs. fatigue cycles for the 3D PMC with ±45° fiber orientation at elevated temperature.

Evolution of maximum and minimum strains with cycling for the 3D PMC specimens with ±45° fiber orientation is shown in Figure 57. Significant strain ratcheting is apparent. Strains accumulated during cycling ranged from 2.5 to 3.5%, with the exception of the run-out specimen, which accumulated 1.5% strain. It is also apparent that strain ratcheting began earlier than in the case of the 0/90° specimens, which accumulated little strain until near failure. The higher accumulated strains in the ±45° specimens are due to the fact that the matrix material carries the majority of the load and matrix cracks and damage are most likely introduced earlier in the cyclic loading.

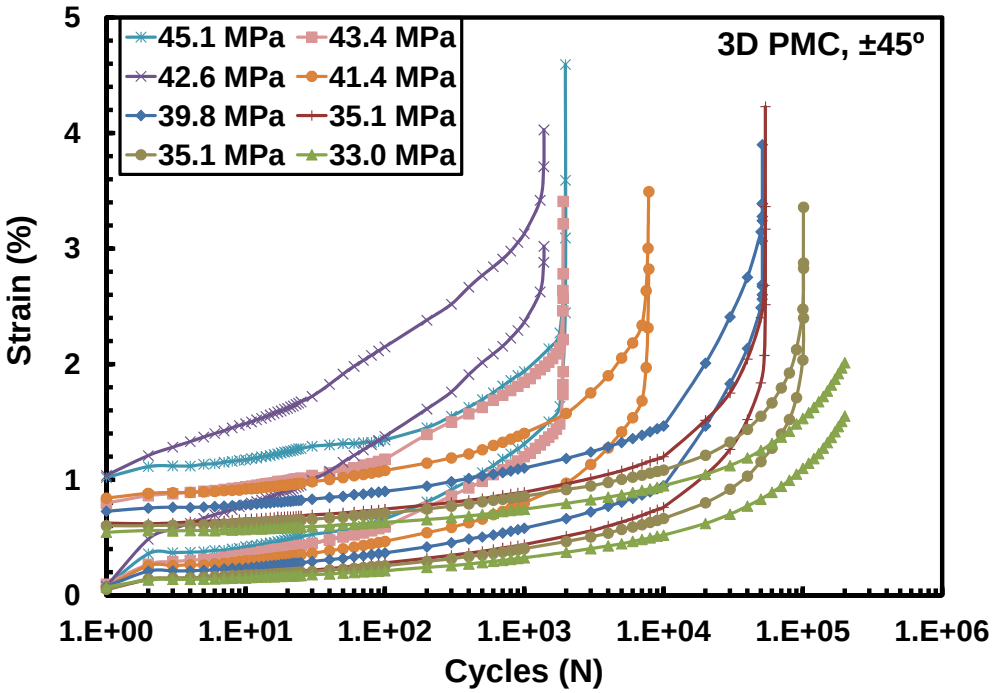

Figure 57: Maximum and minimum strains vs. fatigue cycles for the 3D PMC with ±45° fiber orientation at elevated temperature.

5.4.2 Fatigue Performance of Material System 2 (2D PMC).

Fatigue results for the 2D PMC specimens are given in Table 14. The *S*-*N* curves for the 2D PMC with 0/90° and ±45° fiber orientations are shown in Figure 58. The fatigue limit for the ±45° fiber orientation is 11% that of the 0/90° fiber orientation. The *S*-*N* curve for the ±45° fiber orientation is shown on a more appropriate scale in Figure 59.

The fatigue performance of the two fiber orientations is compared in Figure 60. The 0/90° fiber orientation again has a better fatigue performance, with the fatigue limit occuring at 71% UTS compared to the ±45° fatigue limit at 53% UTS. It is also noted that, like the 3D PMC, the two *S*-*N* curves have similar slopes.

Table 14: Tension-tension fatigue results for MS2 at T_{right} = 329°C in laboratory air

Specimen #	Maximum Stress (MPa)	Maximum Stress (% UTS)	Normalized Max. Stress (MPa)	Normalized Max. Stress (% Norm. UTS)	Cycles to Failure (N)	Failure Strain (%)
0/90° Fiber Orientation						
T1-5	740.1	90	759.7	92	2,756	0.130
T1-12	740.8	90	734.3	89	1,148	1.649
T1-11	723.9	88	719.8	88	10,916	—
T1-8	699.6	85	683.7	83	11,286	0.308
T1-3	658.0	80	663.0	81	23,768	1.111
T1-10	618.4	75	610.2	74	121,136	0.787
T1-7	576.3	70	585.3	71	200,000[a]	0.057[a]
T1-4	494.5	60	503.3	61	200,000[a]	0.167[a]
±45° Fiber Orientation						
T2-8	105.8	82	100.5	79	917	5.749
T2-7	94.0	73	99.0	78	2,291	6.434
T2-4	99.8	78	97.3	77	793	7.013
T2-6	87.6	68	89.2	71	4,888	7.183
T2-9	81.7	64	82.6	65	20,941	6.323
T2-3	75.7	59	76.1	60	102,372	7.050
T2-11	69.7	54	69.4	55	200,000[a]	1.471[a]
T2-5	63.4	49	66.4	53	200,000[a]	0.611[a]

[a] *Run-out; defined as 2×10^5 cycles. Failure of specimen did not occur when the test was terminated.*
[b] *Anomalous strain value.*

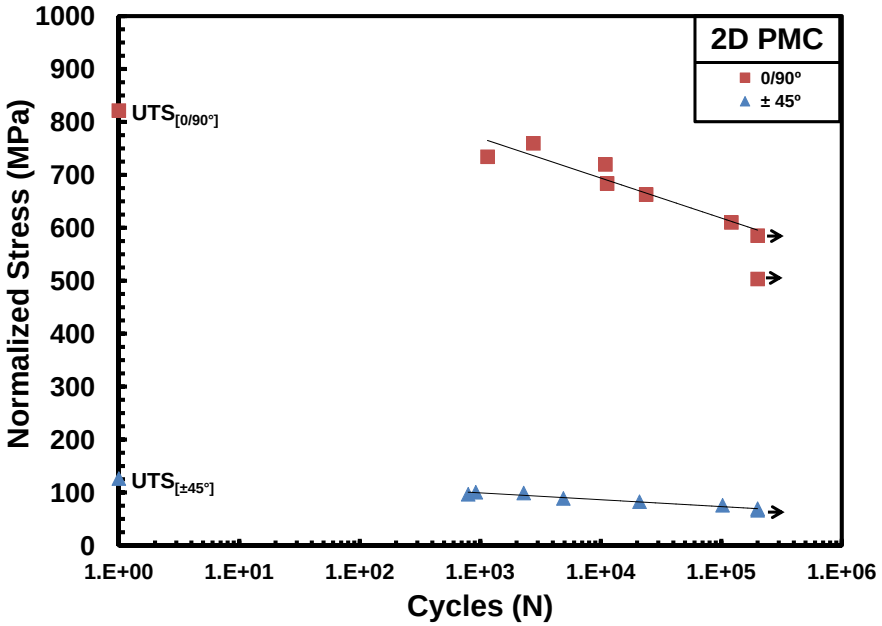

Figure 58: *S*-*N* curves for the 2D PMC at elevated temperature. Arrow indicates specimen achieved fatigue run-out.

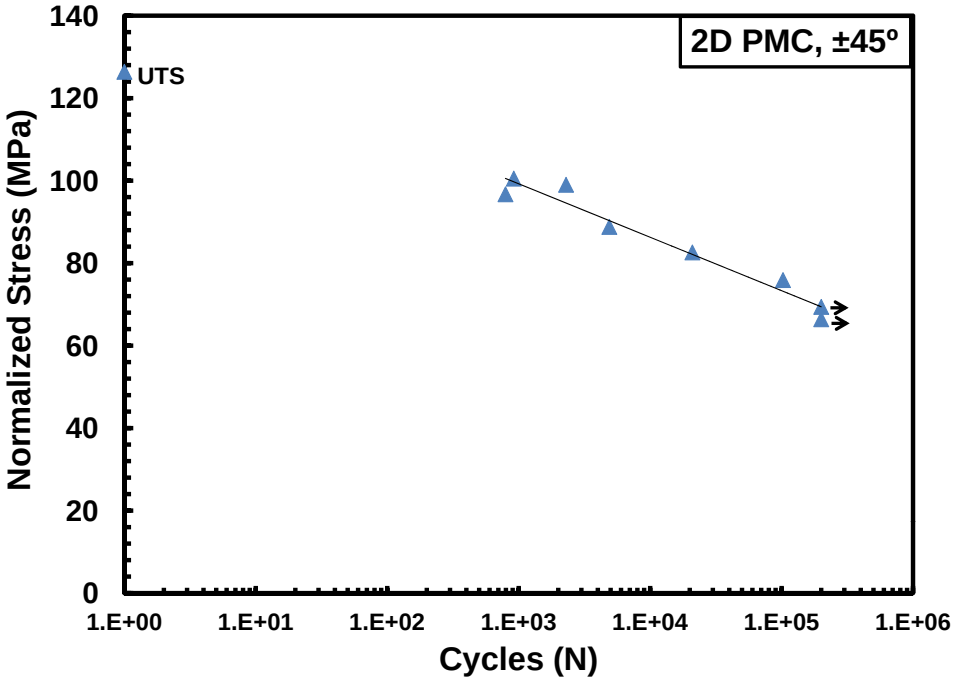

Figure 59: *S*-*N* curve for the 2D PMC with ±45° fiber orientation at elevated temperature. Arrow indicates specimen achieved fatigue run-out.

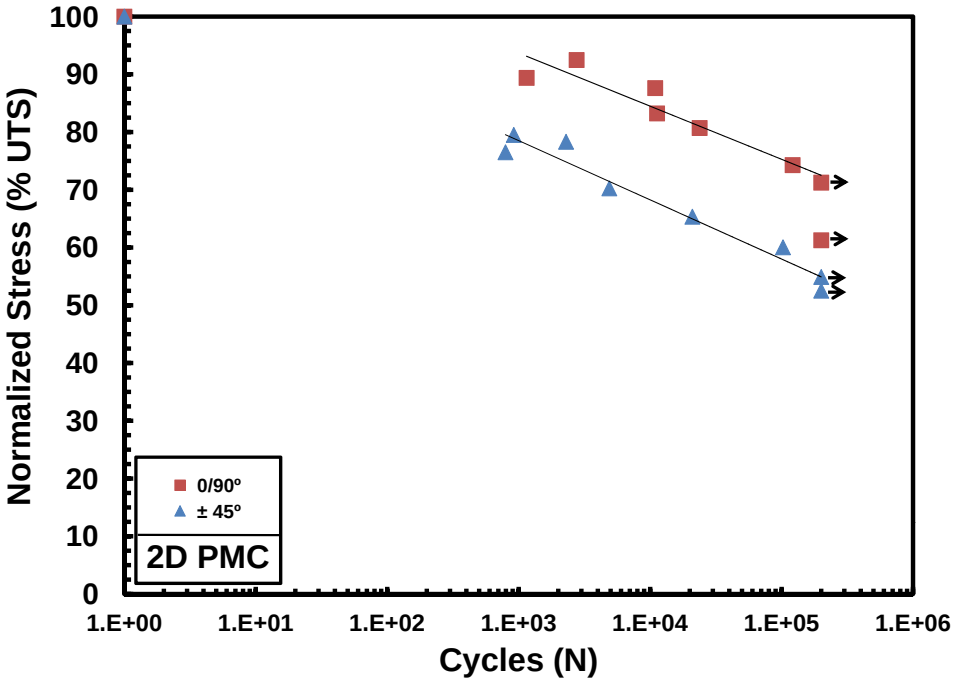

Figure 60: *S*-*N* curves for the 2D PMC at elevated temperature. Maximum stress is shown as % UTS. Arrow indicates specimen achieved fatigue run-out.

The evolution of stress-strain hysteresis response with fatigue cycles of the 2D PMC with 0/90° fiber orientation is shown in Figure 61 for a maximum fatigue stress of 585.3 MPa (71% UTS). Note that this specific specimen achieved run-out. The decrease in stiffness with increasing cycles is obvious. There is not much accumulated strain; most of the strain is accumulated during the first cycle. However, this was not always the case with this material system and fiber orientation. Stress-strain plots of the hysteresis response for other 2D PMC 0/90° specimens are included in Appendix B.

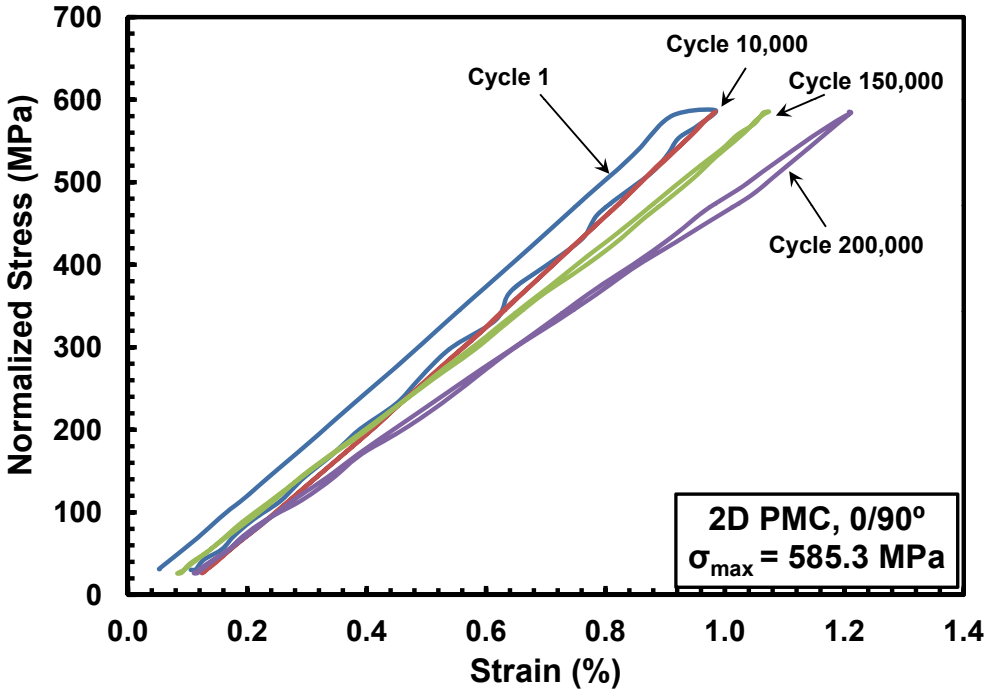

Figure 61: Evolution of stress-strain hysteresis response with fatigue cycles for specimen T1-7 of the 2D PMC with 0/90° fiber orientation at elevated temperature.

One of the specimens (T1-10) exhibited significantly more delamination than the others. This specimen was fatigued with the maximum stress of 610.2 MPa (74% normalized UTS). The stress-strain plot obtained for this specimen is shown in Figure 62. At first the response is very linear; however, as cycling continues, matrix cracking progresses which promotes ply delamination. The shape of the hysteresis loops changes

dramatically as more and more delamination occurs. This stress-strain response is attributed to the interaction of the extensometer with the specimen. Because the fiber plies delaminate from each other, the deformation of the gage section is non-homogeneous, as not all the plies deform in the same manner. Extensive delamination observed for this specimen could be due to localized processing defects. Strain accumulation and modulus loss produced by this specimen significantly exceed the corresponding results obtained for other specimens.

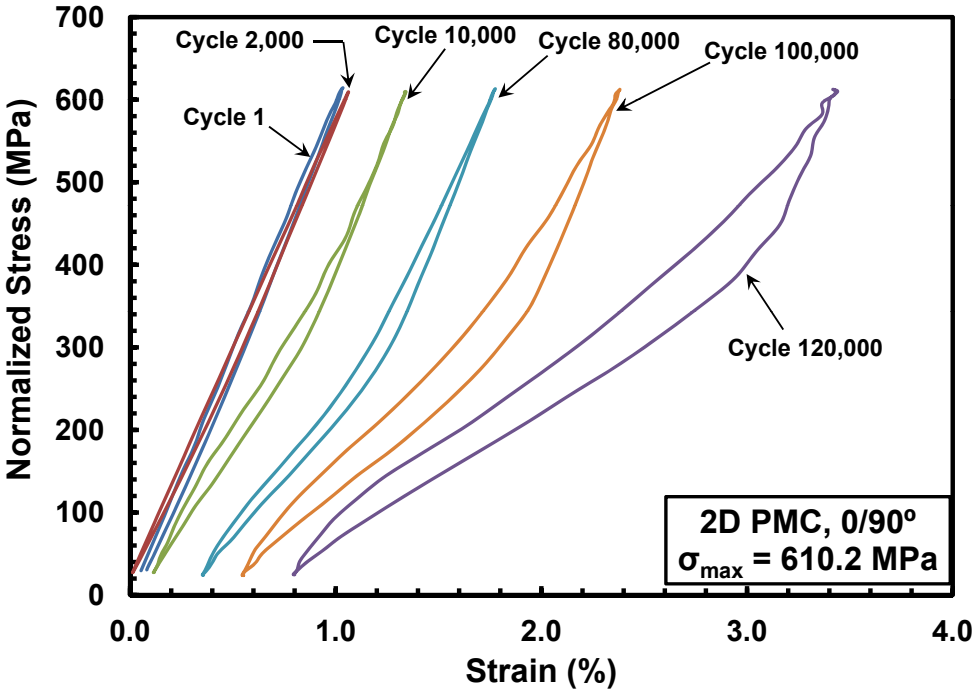

Figure 62: Evolution of stress-strain hysteresis response with fatigue cycles for specimen T1-10 of the 2D PMC with 0/90° fiber orientation at elevated temperature.

Change in normalized modulus with cycles of the 2D PMC specimens with 0/90° fiber orientation can be seen in Figure 63. It can be seen that the modulus stays relatively constant at the beginning of cycling, then starts to decrease steadily. The specimen with the most modulus loss is the specimen that exhibited extreme delamination. There is again no obvious correlation between modulus loss and number of cycles sustained. The amount

of modulus loss varied between 5% and 66%, with the majority of specimens producing near 20% modulus loss.

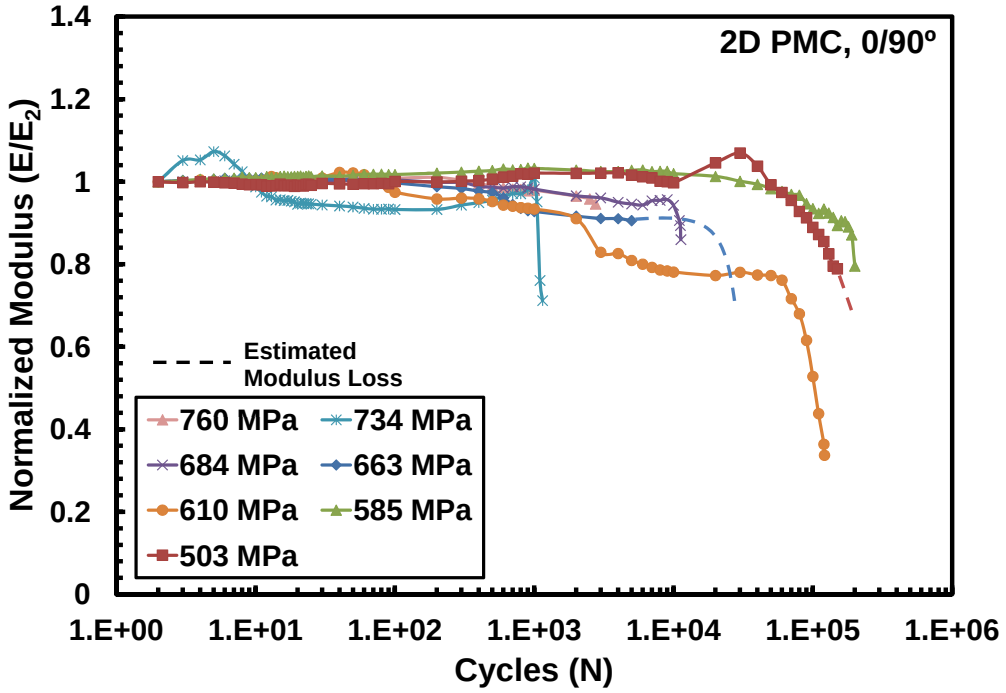

Figure 63: Normalized modulus vs. fatigue cycles for the 2D PMC with 0/90° fiber orientation at elevated temperature.

The maximum and minimum strains vs. fatigue cycles obtained for the 0/90° specimens are seen in Figure 64. The specimen tested at σ_{max} of 734 MPa exhibited significant strain early in its fatigue life, whereas the other specimens had an increase of strain later in their fatigue lives. Accumulated strains ranged from 0.06% to 1.6%.

For the ±45° fiber orientation of the 2D PMC, the evolution of hysteresis loops can be seen in Figure 65 for a fatigue stress of 76.1 MPa (60% normalized UTS). One can see that the material slightly stiffens at first. For example, compare cycle 10 with cycle 10,000. As cycling progresses toward failure, however, the modulus decreases and the

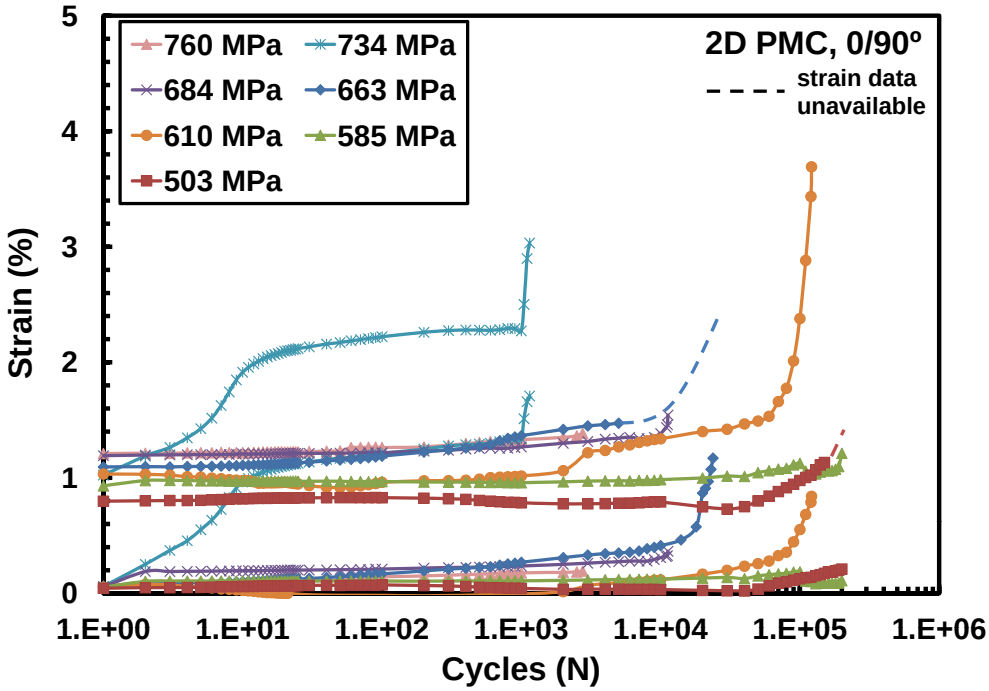

Figure 64: Maximum and minimum strains vs. fatigue cycles for the 2D PMC with 0/90° fiber orientation at elevated temperature.

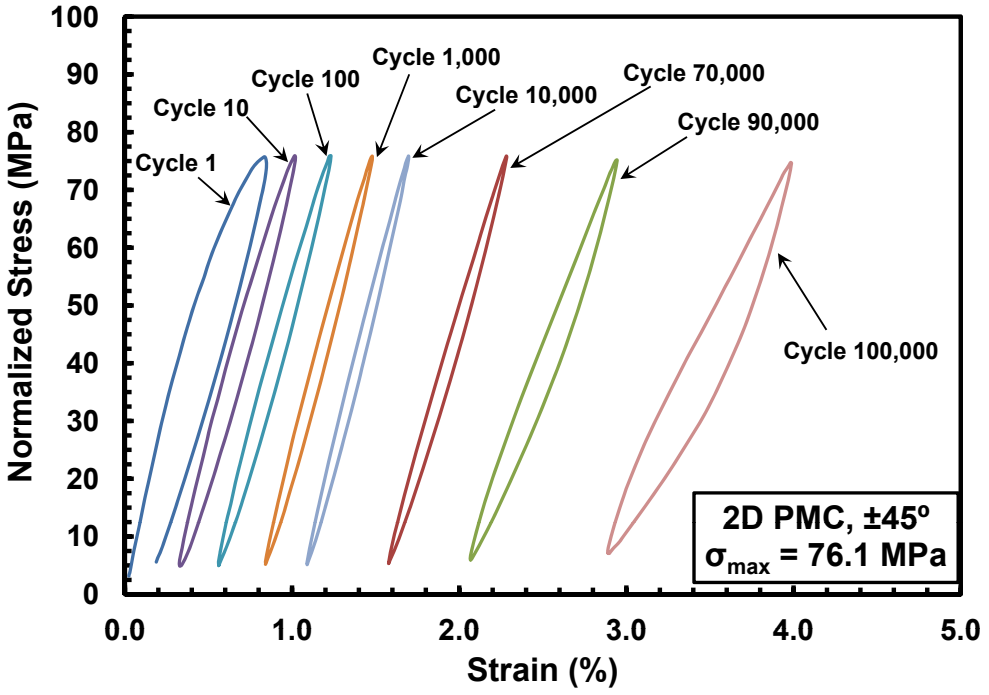

Figure 65: Evolution of stress-strain hysteresis response with fatigue cycles for specimen T2-3 of the 2D PMC with ±45° fiber orientation at elevated temperature.

hysteresis loops start opening up and exhibiting viscoelastic behavior. This response is typical for the ±45° fiber orientation specimens of the 2D PMC.

Normalized hysteresis modulus vs. fatigue cycles is given in Figure 66. The initial stiffening of the material is plainly evident. In fact, one of the run-out specimens exhibits continuous stiffening during the entire 200,000 cycles. It is hypothesized that this stiffening is due to a "scissoring" effect of the fibers in the ±45° orientation, during which the fibers start to slightly realign in the direction of applied load. As the cycling progresses, this stiffening effect is diminished and a dramatic drop in stiffness occurs most likely due to increased matrix damage. The amount of modulus loss ranged from 38% to 66%, except for the run-out specimens which saw increases in modulus of 18% and 2.5%.

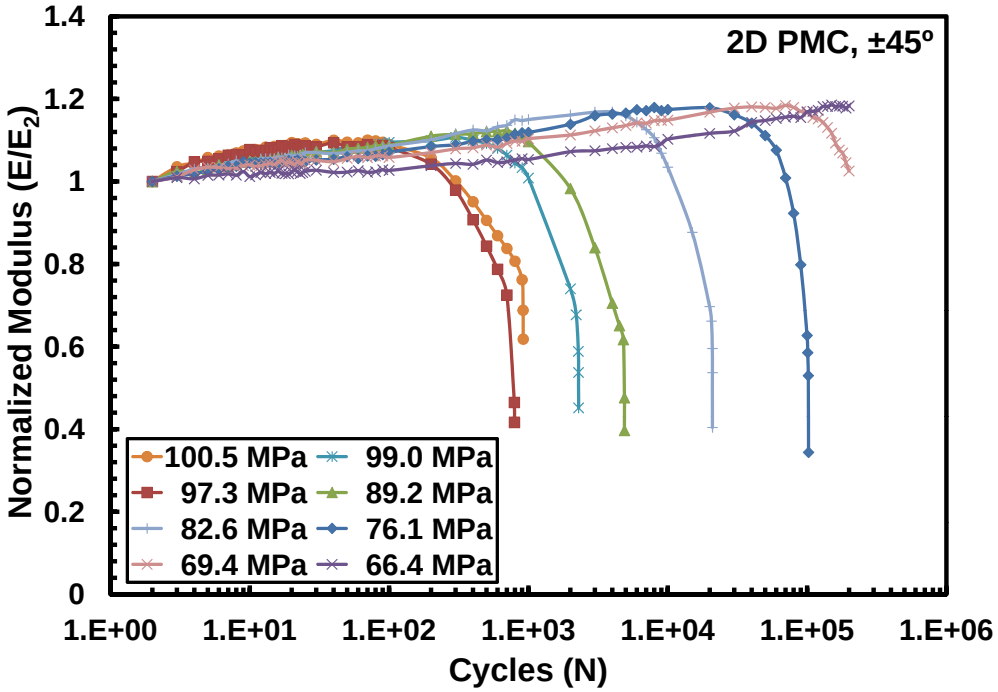

Figure 66: Normalized modulus vs. fatigue cycles for the 2D PMC with ±45° fiber orientation at elevated temperature.

Figure 67 shows the maximum and minimum strains during cycling. There is significant strain ratcheting, with a steady increase in strain throughout cycling and a

sharp increase in strain accumulation near failure. The run-out specimens did not accumulate much strain compared to the specimens that failed earlier. Failure strains ranged from 5.7% to 7.2%, with the exception of the run-out specimens which accumulated only 0.6% and 1.5% strain.

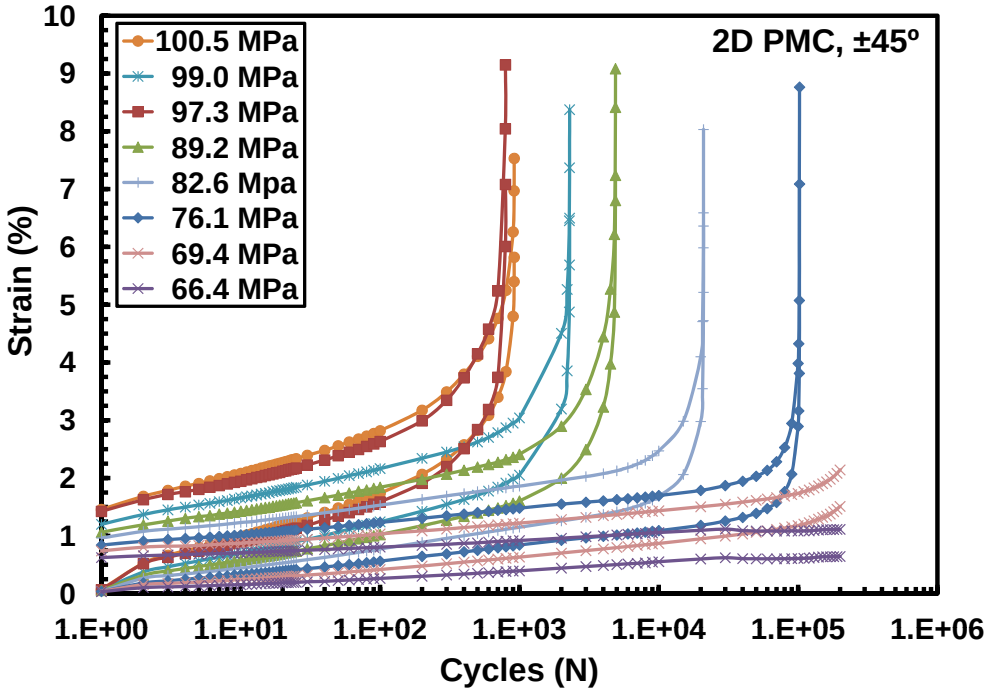

Figure 67: Maximum and minimum strains vs. fatigue cycles for the 2D PMC with ±45° fiber orientation at elevated temperature.

5.4.3 Comparison of Fatigue Performance of MS1 and MS2.

The fatigue performance of the 3D PMC and the 2D PMC can be compared using the *S*-*N* curves. Figure 68 contrasts the *S*-*N* curves for the 0/90° fiber orientation of the two material systems. The 2D PMC has a higher fatigue limit, as expected due to the greater UTS compared to the 3D PMC. The 3D PMC fatigue limit is 82.5% of the 2D PMC fatigue limit. Comparison of the results obtained at a given fatigue stress level reveals that the 2D PMC has better fatigue lifetimes. Specimens T3-15 and T1-10 were tested with a

normalized maximum fatigue stress of about 610 MPa. The 2D PMC specimen survived 121,136 cycles compared to 10,141 for the 3D PMC. Another two specimens that had relatively close fatigue stress levels are T3-18 and T1-3. Again, the 2D PMC outlasted the 3D PMC, 23,768 cycles to 1,159 cycles.

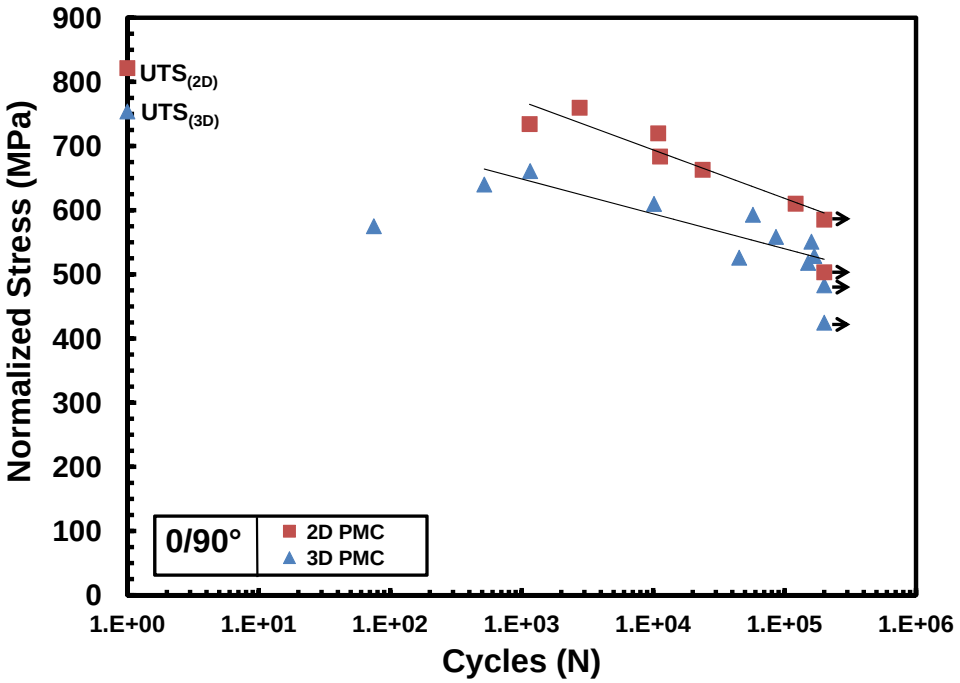

Figure 68: *S*-*N* curves for the 2D PMC and 3D PMC with 0/90° fiber orientation at elevated temperature. Arrow indicates specimen achieved fatigue run-out.

A comparison of the performance of the two material systems is given in Figure 69, which shows that relative to UTS, the 2D PMC still has a slightly better performance (fatigue limit of 71% UTS compared to 64% UTS for the 3D PMC).

The *S*-*N* curves obtained for the 2D PMC and 3D PMC with ±45° fiber orientation are compared in Figure 70. Because the UTS of the 2D PMC is twice that of the 3D PMC, it is not surprising that the fatigue limit for the 2D PMC is two times the fatigue limit of the 3D PMC. However, when the two material systems are compared on a percent

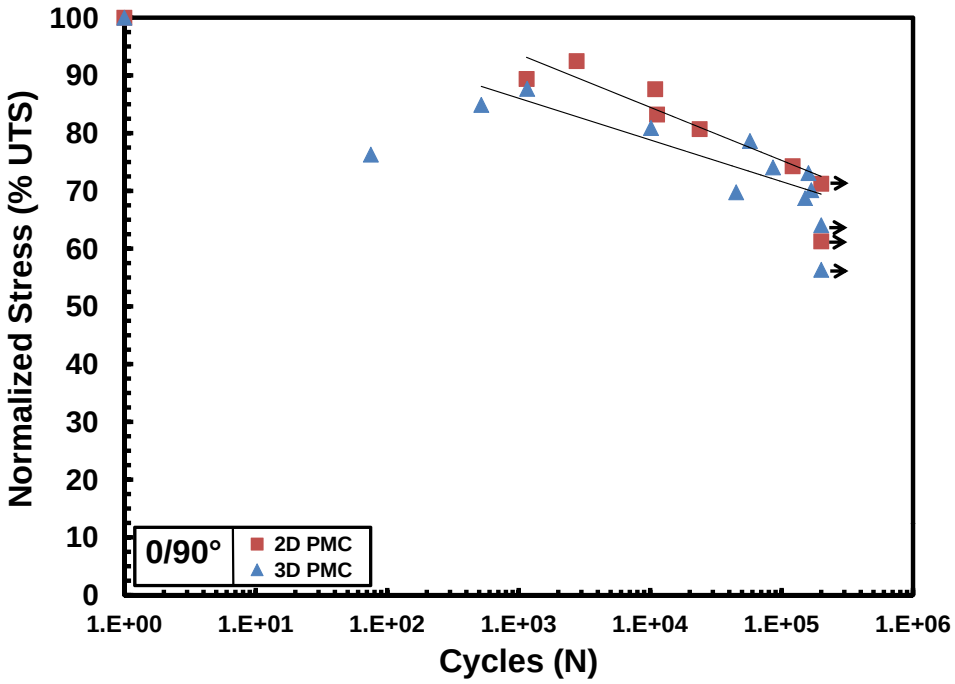

Figure 69: S-N curves for the 2D PMC and 3D PMC with 0/90° fiber orientation at elevated temperature. Maximum stress is shown as % UTS. Arrow indicates specimen achieved fatigue run-out.

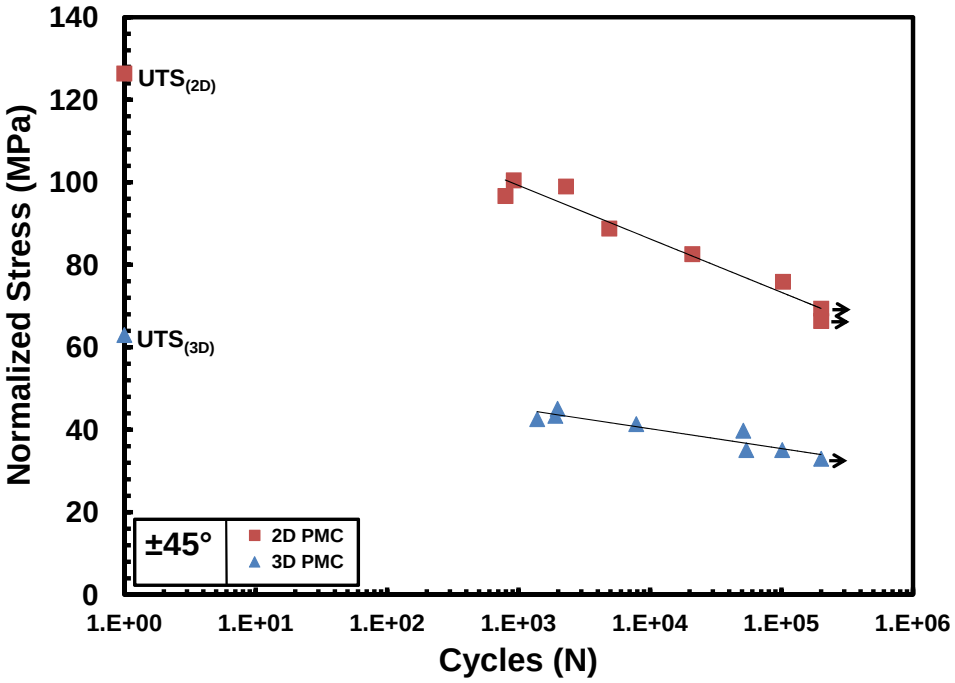

Figure 70: S-N curves for the 2D PMC and 3D PMC with ±45° fiber orientation at elevated temperature. Arrow indicates specimen achieved fatigue run-out.

normalized UTS basis (Figure 71), their fatigue performance is very similar. The 2D PMC only slightly outperforms the 3D PMC.

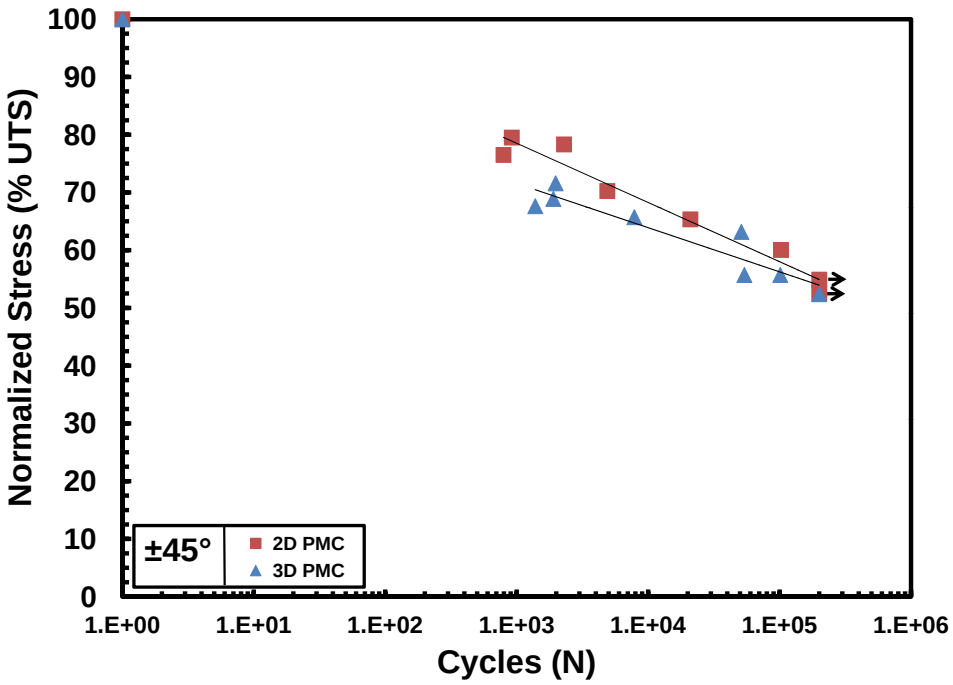

Figure 71: *S*-*N* curves for the 2D PMC and 3D PMC with ±45° fiber orientation at elevated temperature. Maximum stress is shown as % UTS. Arrow indicates specimen achieved fatigue run-out.

5.4.4 Fatigue Performance of Material System 3 (2D PMC/CMC).

Results for the 2D unitized composite specimens are given in Table 15. As seen for the 0/90° fiber orientation, there was significant variability in the number of cycles sustained for some of the lower and intermediate stress levels tested. For example, T5-15 (tested at 78% normalized UTS) sustained 190,580 cycles, whereas specimen T5-9 (tested at 77% normalized UTS) only sustained 4,152 cycles.

One explanation for the wide variation in results for the 0/90° fiber orientation can be proposed by examining the *S*-*N* curve (Figure 72). The *S*-*N* curve for the 0/90° orientation is very flat and shows that all results, despite the variations, still follow the

Table 15: Tension-tension fatigue results for MS3 at T_{right} = 329°C in laboratory air

Specimen #	Maximum Stress (MPa)	Maximum Stress (% UTS)	Normalized Max. Stress (MPa)	Normalized Max. Stress (% Norm. UTS)	Cycles to Failure (N)	Failure Strain (%)
0/90° Fiber Orientation						
T5-18	572.1	85	579.5	87	61	0.400
T5-16	572.6	85	557.3	84	297	0.325
T5-10	539.4	80	542.4	82	3,630	0.160
T5-13	538.7	80	532.5	80	425	0.162
T5-8	539.2	80	530.3	80	21,327	0.502
T5-14	505.4	75	520.7	78	190,580	0.397
T5-17	518.9	77	520.5	78	61,787	0.138
T5-9	505.1	75	508.9	77	4,152	0.631
T5-11	505.3	75	499.5	75	102,523	0.453
T5-7	471.8	70	471.7	71	200,000[a]	-0.165[a,b]
±45° Fiber Orientation						
T6-14	48.2	84	48.4	86	220	1.126
T6-12	46.5	81	46.7	83	664	1.345
T6-6	46.8	82	45.7	81	805	1.370
T6-11	41.2	72	42.5	75	5,604	1.564
T6-4	43.7	76	42.3	75	2,108	1.300
T6-7	41.3	72	41.4	73	3,972	1.259
T6-13	39.9	70	40.1	71	1,894	0.728
T6-8	38.7	67	39.2	70	40,423	1.420
T6-10	37.6	65	38.7	69	65,598	1.702
T6-9	35.7	62	35.7	63	185,365	1.022
T6-5	32.9	57	32.4	58	200,000[a]	0.327[a]

[a] *Run-out; defined as 2×10^5 cycles. Failure of specimen did not occur when the test was terminated.*
[b] *Anomalous strain value.*

general fatigue performance trend. Note that the material also exhibited very severe delamination. This could cause some specimens to fail earlier than expected. The fatigue limit for the ±45° fiber orientation is about 7% of the 0/90° fatigue limit. The *S*-*N* curve for the ±45° fiber orientation is plotted on a more appropriate scale in Figure 73.

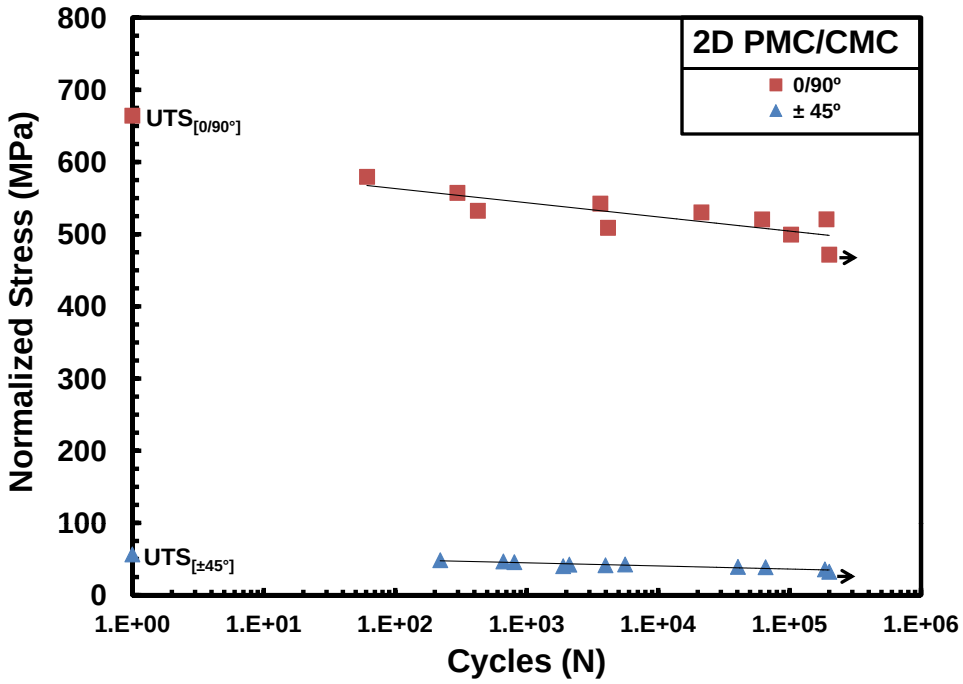

Figure 72: *S*-*N* curves for the 2D PMC/CMC at elevated temperature. Arrow indicates specimen achieved fatigue run-out.

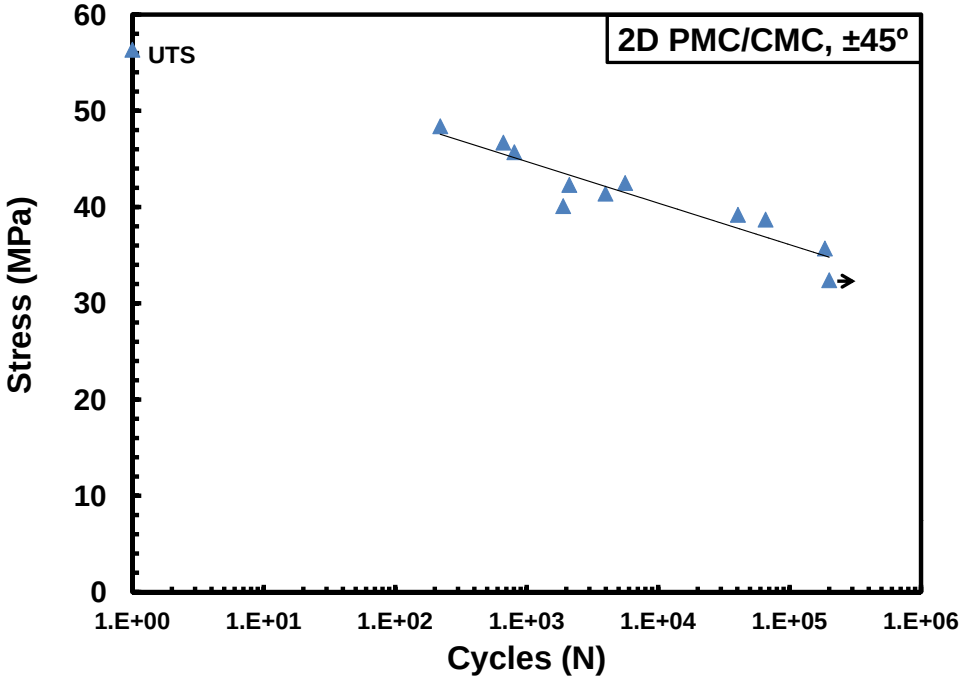

Figure 73: *S*-*N* curve for the 2D PMC/CMC with ±45° fiber orientation at elevated temperature. Arrow indicates specimen achieved fatigue run-out.

Comparing results obtained for the two fiber orientations on the basis of percent normalized UTS (Figure 74), it is seen that at higher fatigue stress levels they exhibit similar performance. In some cases, the ±45° specimens fair somewhat better. However, at lower stress levels, specimens with the 0/90° orientation exhibit a stronger performance. The fatigue limit of the 0/90° orientation is 71% normalized UTS while the fatigue limit of the ±45° orientation is 58% normalized UTS.

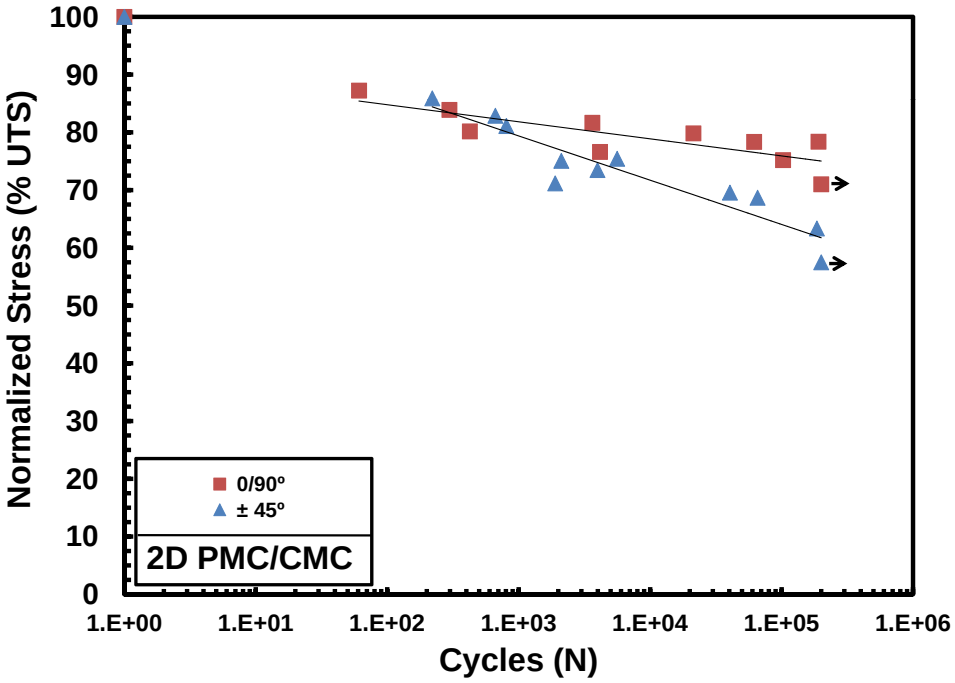

Figure 74: *S*-*N* curves for the 2D PMC/CMC at elevated temperature. Maximum stress is shown as % UTS. Arrow indicates specimen achieved fatigue run-out.

The evolution of stress-strain hysteresis response is presented in Figure 75 for a fatigue stress of 530.3 MPa (80% normalized UTS). After the first cycle, the response is nearly linear elastic. However, as cycling progresses with more and more damage events occurring in the material, the loops begin to open up slightly and stiffness loss is evident. Also later in cycling, the loops exhibit a lower modulus at lower stresses, then transition to an increased modulus, and then transition back slightly to a lower modulus (creating a

slight “S” shape of the hysteresis loop). This phenomenon has several possible explanations. First of all, this material system exhibited extensive delamination, so the extensometer contact with the specimen would be affected, as mentioned before, by the non-homogeneous deformation of the gage section. Another explanation is that this material system consists of two dissimilar materials co-cured together. This again causes non-homogeneous deformation of the material, especially since the PMC plies and the CMC plies bowed out on their respective sides when the specimen was stressed axially. This phenomenon was previously mentioned in Section 5.3.1, where it was explained that the CMC ply closest to where the two materials were co-cured together remained straight while the others bowed out. Translating this to cyclic loading, Figure 76 schematically shows the material bowing out during loading and returning to original shape during unloading. This bowing out is caused by ply delamination, but with two dissimilar material with two different thicknesses, the bowing of the sides is not even or symmetric. It is also noted in Figure 75 that the “S” shape of the hysteresis loop is different from the shape of the 2D PMC specimen that had extensive delamination. In that case, the modulus was larger at first, then transitioned to a lower modulus, and finally increased again before reaching the peak stress.

Figure 77 shows the evolution of hysteresis loops for a specimen fatigued at a maximum stress of 508.9 MPa (77% normalized UTS). The loops become highly nonlinear as cycling progresses, and the “S” shape is more pronounced, especially at the bottom of the loops. This specimen failed unusually early for the stress level at which it was tested. Plots of the evolution of hysteresis loops for other 2D PMC/CMC specimens are included in Appendix B.

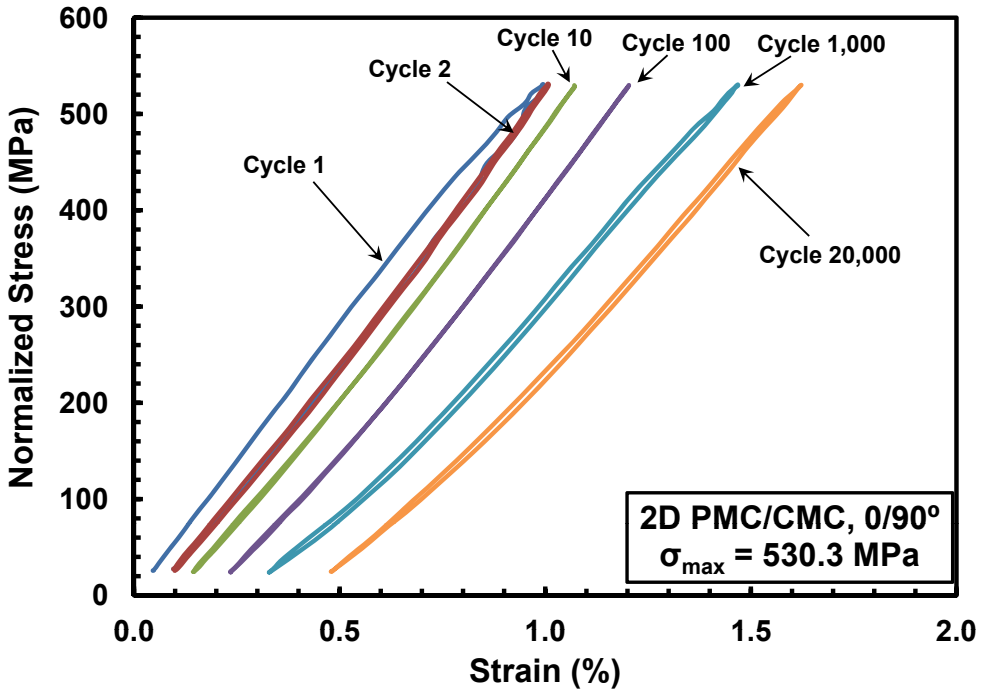

Figure 75: Evolution of stress-strain hysteresis response with fatigue cycles for specimen T5-8 of the 2D PMC/CMC with 0/90° fiber orientation at elevated temperature.

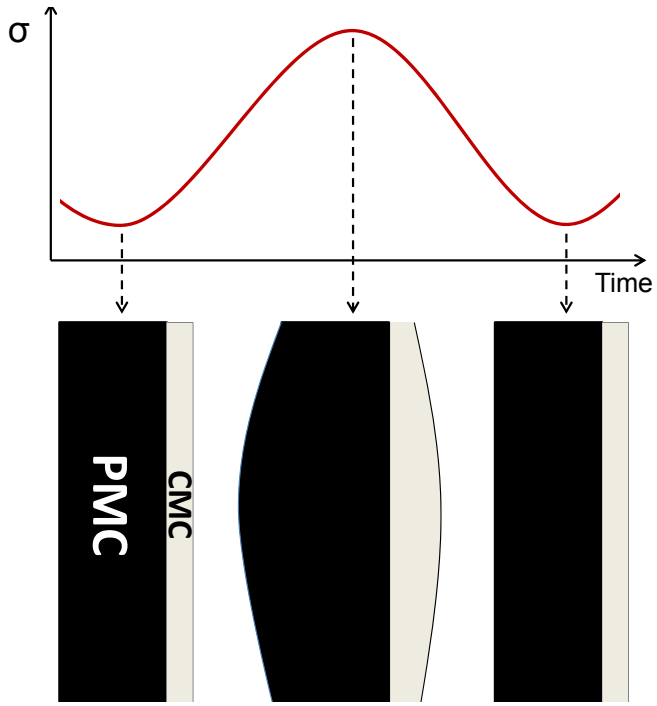

Figure 76: Schematic of unitized composite deformation behavior during cyclic loading. Individual plies not shown.

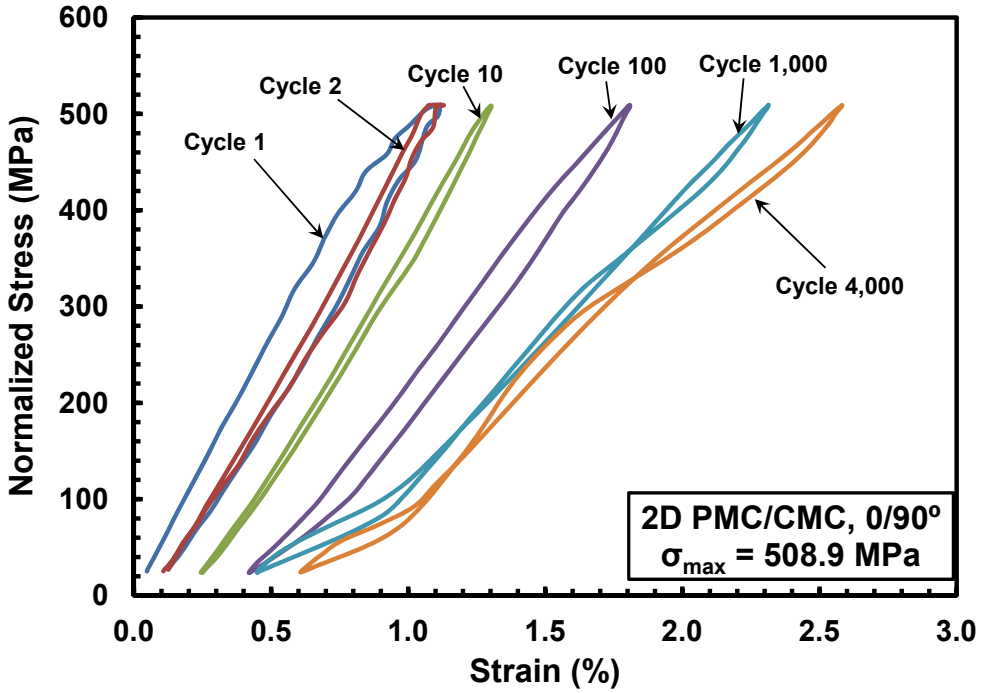

Figure 77: Evolution of stress-strain hysteresis response with fatigue cycles for specimen T5-9 of the 2D PMC/CMC with 0/90° fiber orientation at elevated temperature.

Normalized hysteresis modulus vs. fatigue cycles for the unitized composite specimens is shown in Figure 78. It is seen that the modulus in the majority of specimens seems to decrease with increasing number of cycles. There are stark differences in some of the curves, which is attributed to the extensive delamination. Nevertheless, the range of modulus loss for all specimens was between 4.2% and 57.2% with the average loss being 28.7% loss.

The maximum and minimum strains (shown in Figure 79) behave sporadically as cycling progresses. Because of the extensive delamination in this material system, it would be of interest in the future to explore means of strain measurement that does not involve physical contact with the specimen. Despite the wide variations in strain ratcheting progression, all specimens failed with an accumulated strain between 0.160% and 0.631%, with the exception of the run-out specimen, which did not accumulate strain.

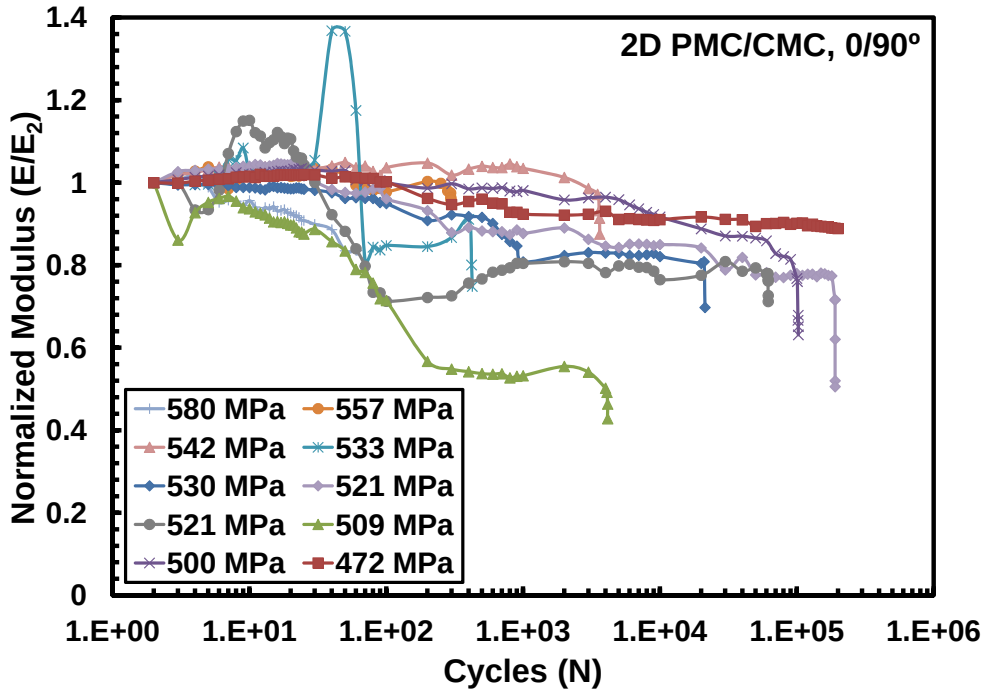

Figure 78: Normalized modulus vs. fatigue cycles for the 2D PMC/CMC with 0/90° fiber orientation at elevated temperature.

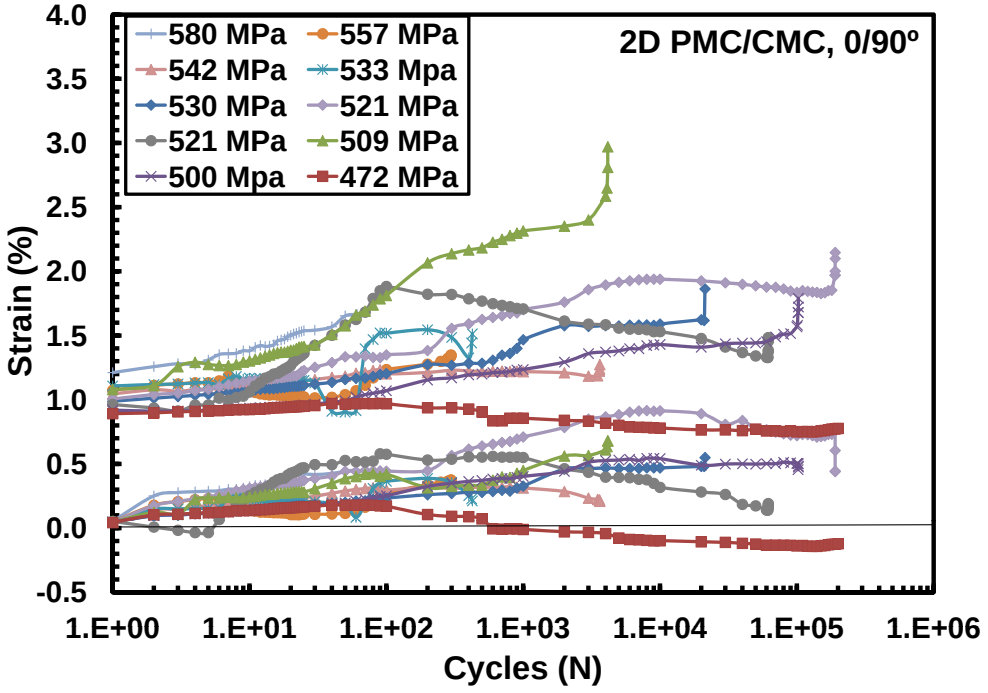

Figure 79: Maximum and minimum strains vs. fatigue cycles for the 2D PMC/CMC with 0/90° fiber orientation at elevated temperature.

A typical plot of the evolution of hysteresis loops with fatigue cycles for the ±45° fiber orientation is given in Figure 80 for a fatigue stress of 38.7 MPa (69% normalized UTS). The viscoelastic nature of the stress-strain response is evident as the loops are not linear on load-up or unloading. Furthermore, as cycling progresses, the loops become less steep and transition to having the three zones of modulus as seen before. However, with the ±45° fiber orientation, the modulus of the loops is greater at the bottom and top of the loops compared to the middle, which is the same trend as that seen for the 2D PMC 0/90° specimen that exhibited significant delamination. The ±45° specimens also showed signs of delamination along with slight bowing out of the sides upon load-up, but the delamination was more localized to the middle of the gage section, as will be seen in Section 5.6. One can also see the tuning issue again by the higher peak stress of the first cycle and by the minimum stress not returning to the initial minimum stress on the first cycle.

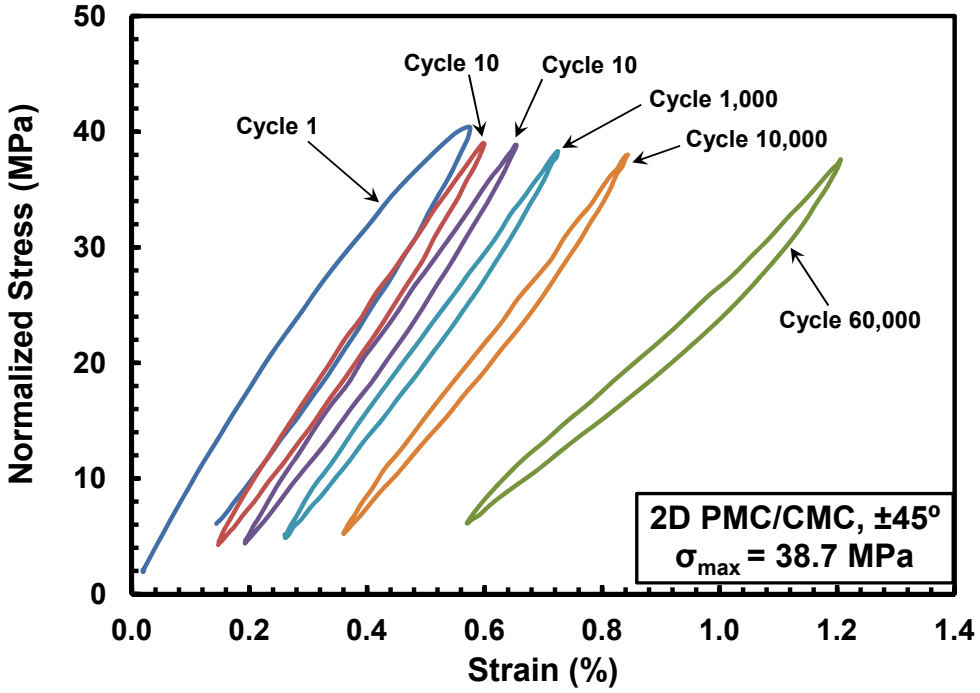

Figure 80: Evolution of stress-strain hysteresis response with fatigue cycles for specimen T6-10 of the 2D PMC/CMC with ±45° fiber orientation at elevated temperature.

The normalized hysteresis modulus is plotted against cycles in Figure 81. Modulus steadily decreased throughout the lifetime of each specimen and dropped dramatically when the specimen approached failure. There is no apparent correlation between modulus loss and cycles sustained. The modulus loss for all specimens that reached failure ranged between 44.4% and 61.9% with an average loss of 56.2%.

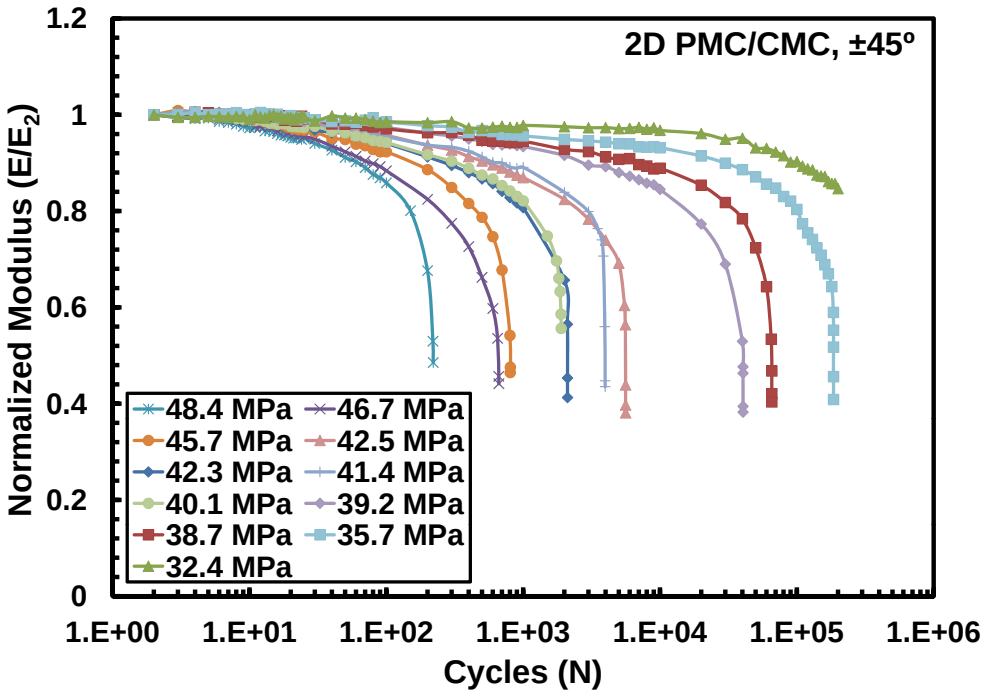

Figure 81: Normalized modulus vs. fatigue cycles for the 2D PMC/CMC with ±45° fiber orientation at elevated temperature.

Maximum and minimum strains vs. fatigue cycles are seen in Figure 82 for the ±45° unitized composite specimens. As expected, significant strain ratcheting is observed due to the material performance being matrix dominated in the direction of loading. Failure strains ranged from 0.728% to 1.702%, except for the run-out specimen, which accumulated 0.327% strain.

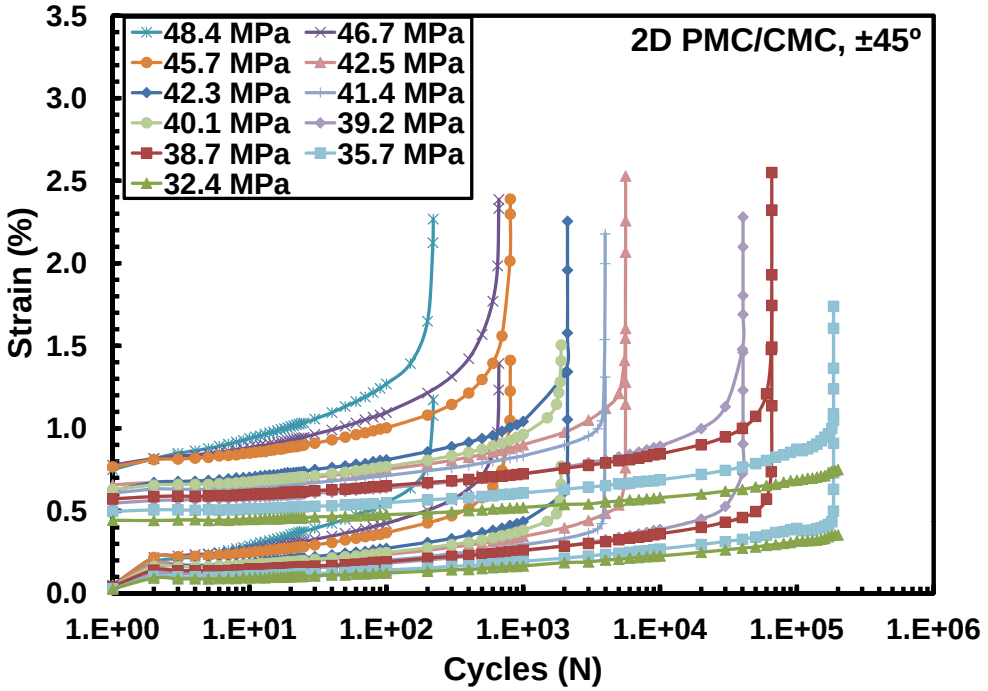

Figure 82: Maximum and minimum strains vs. fatigue cycles for the 2D PMC/CMC with ±45° fiber orientation at elevated temperature.

5.4.5 Comparison of Fatigue Performance of MS2 and MS3.

The fatigue performance of the 2D unitized composite is compared to that of the 2D PMC for the 0/90° fiber orientation in Figure 83. The *S*-*N* curve for the 2D PMC occurs at greater stress levels and has a fatigue limit about 24% higher than that of the unitized composite. When the *S*-*N* curve is viewed with maximum stress shown as % UTS (Figure 84), the two material systems have similar performance. However, at higher stresses, the 2D PMC still seems to perform better.

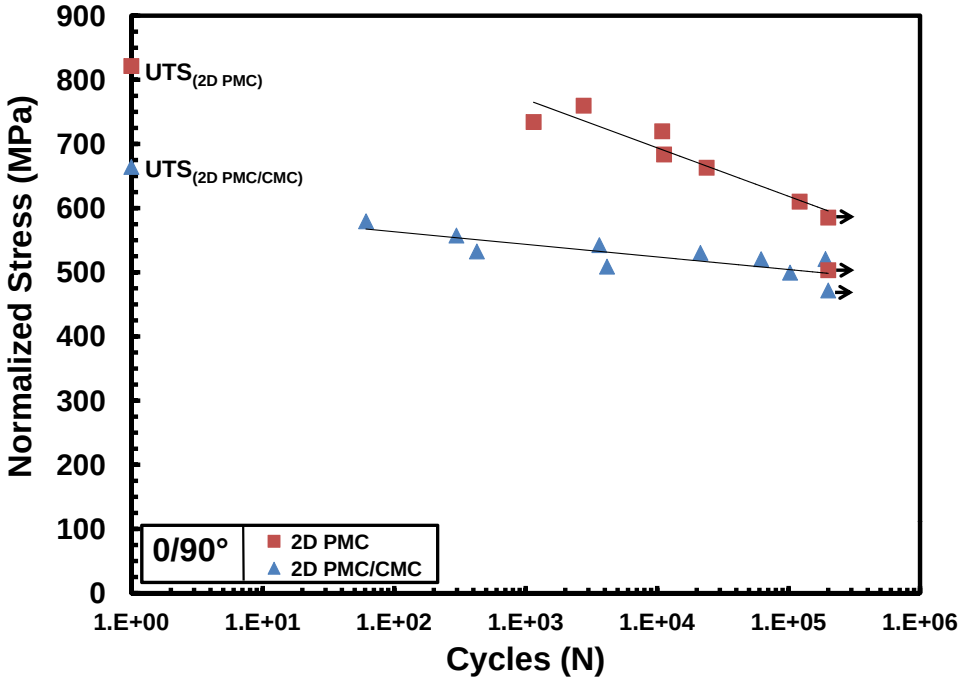

Figure 83: *S*-*N* curves for the 2D PMC and 2D PMC/CMC with 0/90° fiber orientation at elevated temperature. Arrow indicates specimen achieved fatigue run-out.

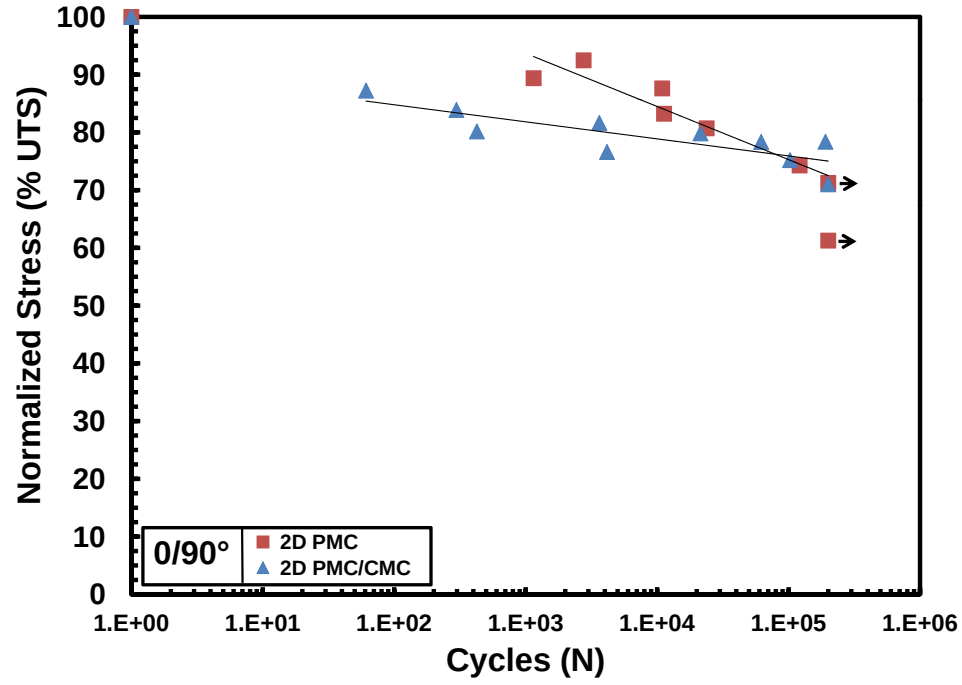

Figure 84: *S*-*N* curves for the 2D PMC and 2D PMC/CMC with 0/90° fiber orientation at elevated temperature. Maximum stress is shown as % UTS. Arrow indicates specimen achieved fatigue run-out.

Figure 85 compares the fatigue performance of the unitized composite and the 2D PMC for the ±45° fiber orientation. The fatigue limit of the unitized composite is 49% that of the 2D PMC fatigue limit. The fatigue performance of the two material systems is also compared in Figure 86. Their fatigue performance seems to be similar at higher stresses; however, the unitized composite reaches its fatigue limit at a slightly higher percent normalized UTS than the 2D PMC.

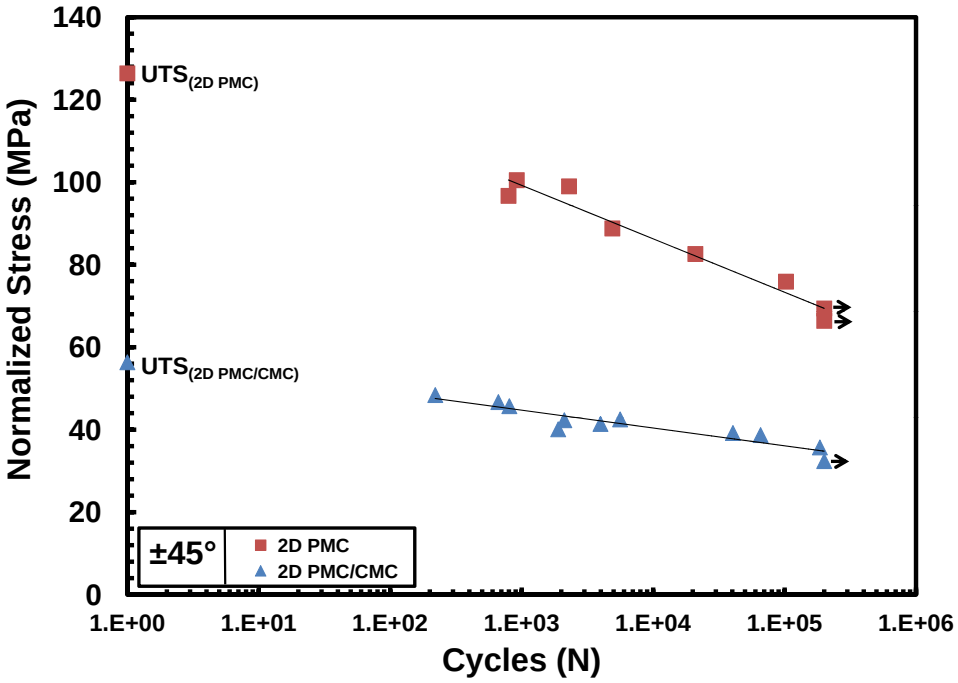

Figure 85: *S*-*N* curves for the 2D PMC and 2D PMC/CMC with ±45° fiber orientation at elevated temperature. Arrow indicates specimen achieved fatigue run-out.

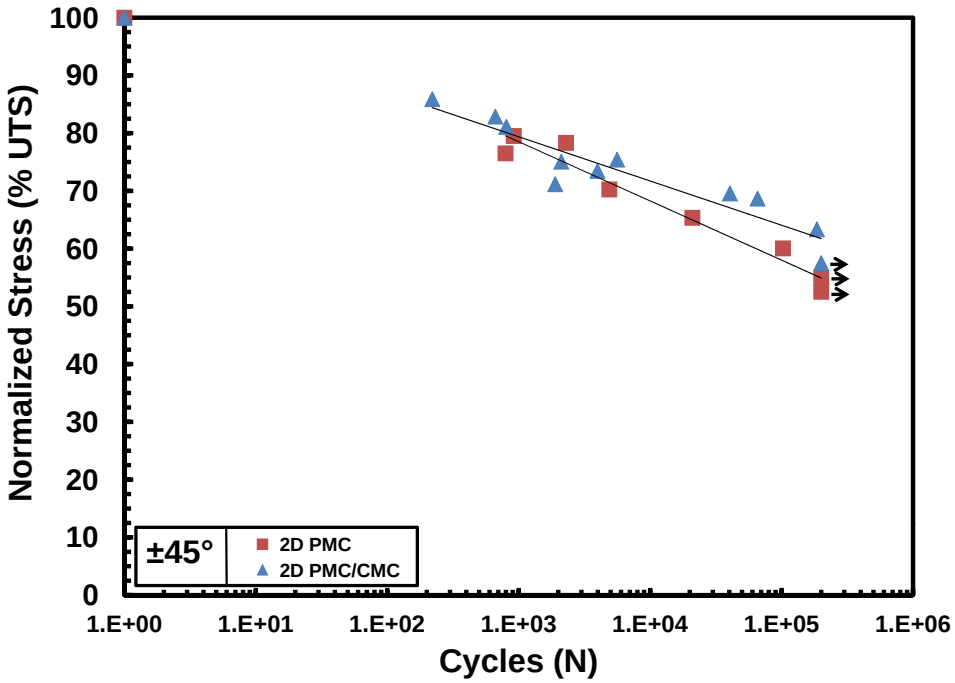

Figure 86: *S*-*N* curves for the 2D PMC and 2D PMC/CMC with ±45° fiber orientation at elevated temperature. Maximum stress is shown as % UTS. Arrow indicates specimen achieved fatigue run-out.

5.5 Retained Tensile Properties

Each specimen that achieved fatigue run-out was subjected to an elevated temperature tension-to-failure test in order to measure the retained tensile properties. The temperature during the tensile test was the same as during the fatigue test, namely T_{right} of 329°C. Retained properties are shown in Table 16.

The tensile stress-strain curves for the 3D PMC 0/90° specimens subjected to prior fatigue are plotted in Figure 87 along with the stress-strain curves for the as-processed material. It is observed that the pre-fatigued specimens retained 100% of their stiffness. It is clearly evident that prior fatigue caused a loss in strength. Strength retention for both specimens is around 85%. Interestingly, the stiffening effect found in the as-processed specimens is seen again in the pre-fatigued specimens; the tensile stress-strain curves exhibit the same characteristic of initially being linear and then showing modulus

Table 16: Retained properties of the MS1, MS2, and MS3 specimens subjected to prior fatigue at T_{right} = 329°C in laboratory air

Fiber Orientation	Fatigue Stress (MPa)	Retained Modulus (GPa)	Modulus Retention (%)	Retained Strength (MPa)	Strength Retention (%)	Failure Strain (%)
Material System 1: 3D PMC						
0/90°	482.9	44.81	94.8	640.0	84.7	1.207
0/90°	424.7	47.33	100.1	650.9	86.1	1.400
±45°	33.0	5.93	65.2	55.9	88.7	3.536
Material System 2: 2D PMC						
0/90°	585.3	50.89	84.9	682.1	83.0	1.367
0/90°	503.3	52.35	87.3	744.1	90.6	—
±45°	69.4	11.19	83.1	113.5	89.8	10.862*
±45°	66.4	13.93	103.4	138.2	109.3	10.916*
Material System 3: 2D PMC/CMC						
0/90°	471.7	39.20	67.7	591.1	89.0	1.194
±45°	32.4	7.88	85.4	54.8	97.3	1.968

Note: All stresses, moduli, and retention percentages are based on normalized values.
** Failure strain taken at point where stress dropped to 50% UTS.*

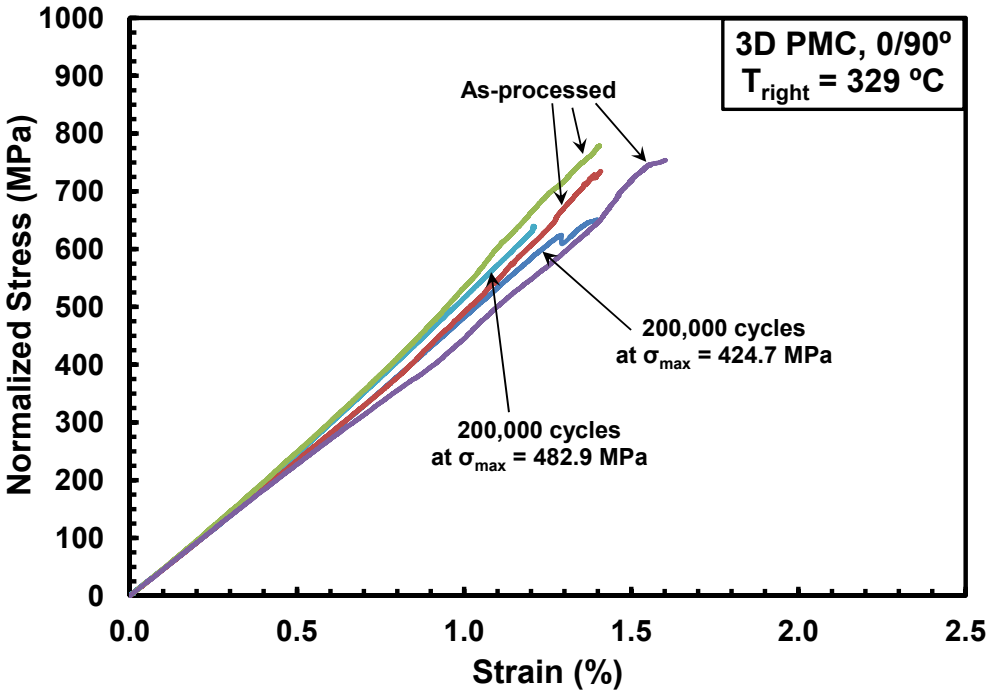

Figure 87: Stress vs. strain for the 3D PMC with 0/90° fiber orientation subjected to prior fatigue at elevated temperature. (as-processed curves shown for comparison)

increase. Failure strain of the specimen pre-fatigued at 424.7 MPa is close to the average failure strain for the as-processed material, but the specimen pre-fatigued at 482.9 MPa has slightly lower failure strain.

The retained tensile stress-strain curve for the ±45° fiber orientation of the 3D PMC is shown in Figure 88 together with the stress-strain curve for the as-processed material. There was significant modulus loss due to prior fatigue. The modulus was about 35% lower than that of the as-processed specimen. The retained strength is also lower by 11%. It is observed that once the UTS is reached, the stress-strain response of the pre-fatigued specimen is no longer a smooth curve like that for the as-processed specimen. Failure strain of the pre-fatigued specimen is 63% of the failure strain for the as-processed specimen.

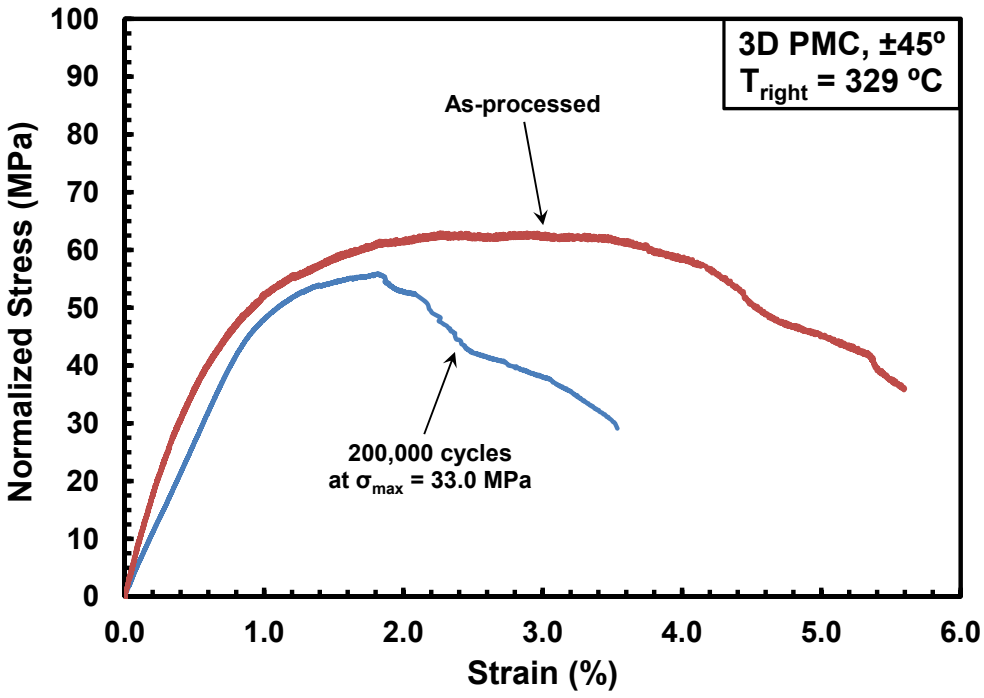

Figure 88: Stress vs. strain for the 3D PMC with ±45° fiber orientation subjected to prior fatigue at elevated temperature. (as-processed curve shown for comparison)

Tensile stress-strain curves for the 2D PMC with 0/90° fiber orientation subjected to prior fatigue are given in Figure 89. It is evident that prior fatigue caused a loss in stiffness and in strength. For the specimen pre-fatigued at 585.3 MPa, strength dropped by 17%, and for the specimen pre-fatigued at 503.3 MPa, the strength dropped by about 9%. There was no dramatic change in failure strain.

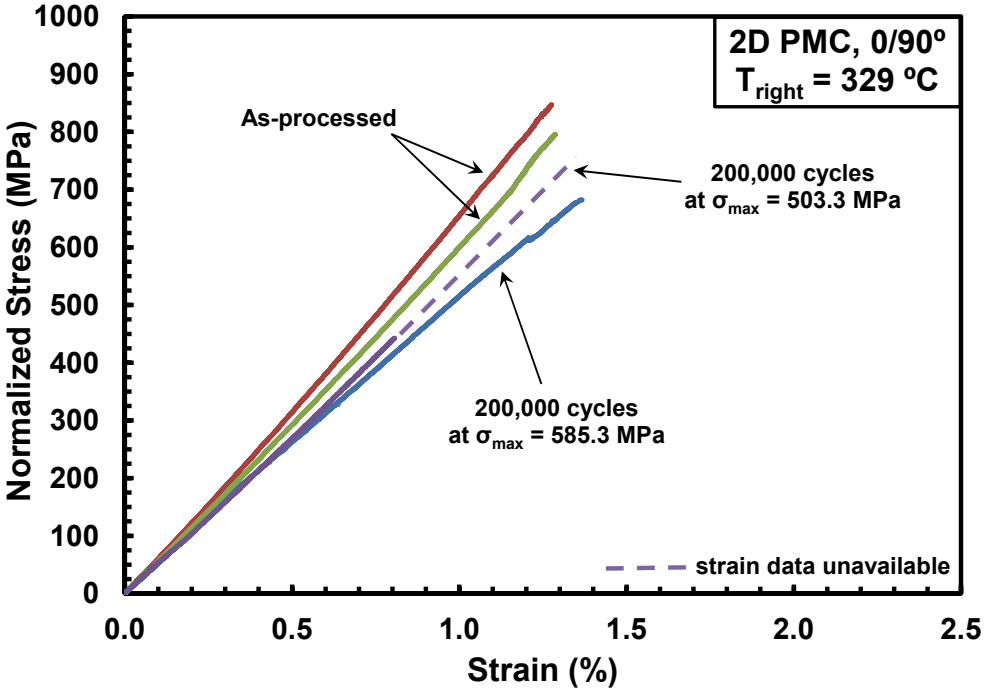

Figure 89: Stress vs. strain for the 2D PMC with 0/90° fiber orientation subjected to prior fatigue at elevated temperature. (as-processed curves shown for comparison)

For the ±45° fiber orientation of the 2D PMC (see Figure 90), the modulus and strength both increased slightly in the specimen subjected to prior fatigue at 66.4 MPa. This is not surprising as modulus increase was observed throughout cycling. The increases were slight — 3.4% and 9.3% respectively. For the specimen subjected to prior fatigue at 69.4 MPa, the modulus and strength both decreased, by 17% and 10% respectively. However, like the stress-strain response of the other pre-fatigued specimen, more stress is sustained before significant nonlinear response occurs compared to the

as-processed material. There was no dramatic drop in stress, so failure strain for each curve was taken at the point where the stress dropped to 50% of the UTS.

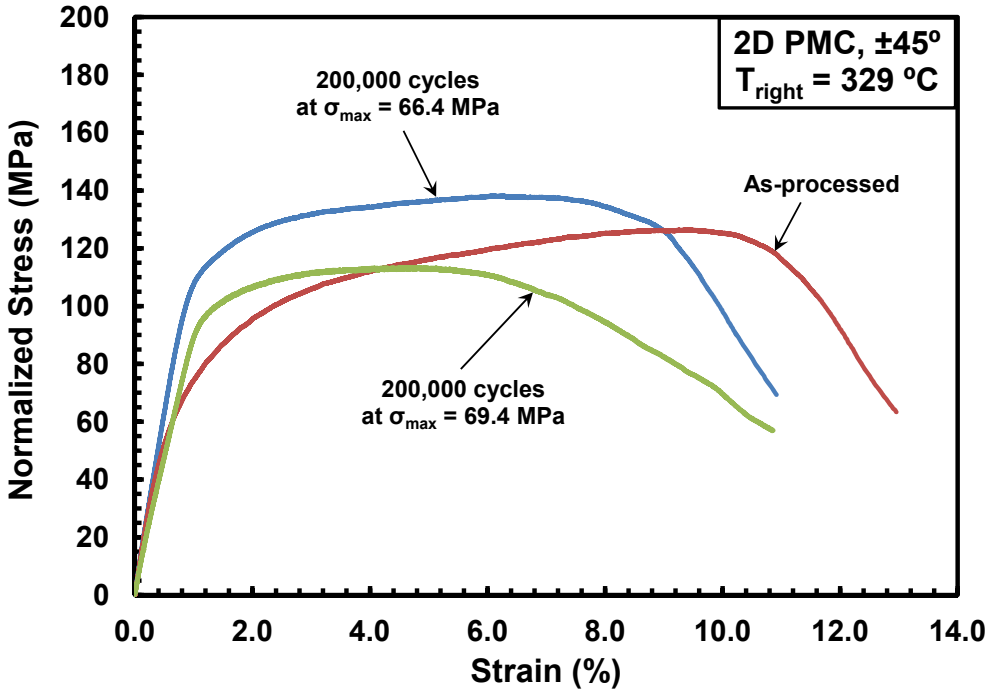

Figure 90: Stress vs. strain for the 2D PMC with ±45° fiber orientation subjected to prior fatigue at elevated temperature. (as-processed curve shown for comparison)

The tensile stress-strain curve for the pre-fatigued unitized composite with 0/90° fiber orientation is given in Figure 91 along with the results for the as-processed material. The retained curve exhibits the initial lower modulus that was seen in the hysteresis loops of this material during cyclic loading. However, at around 0.3% strain the modulus increased to about 52.7 GPa, which is 91% of the average modulus for the as-processed material. The strength decreased by 11%. There was no significant difference in failure strain.

The tensile stress-strain curve for the ±45° unitized composite subjected to prior fatigue is shown in Figure 92. The modulus decreased by 15%. The strength remained nearly unchanged.

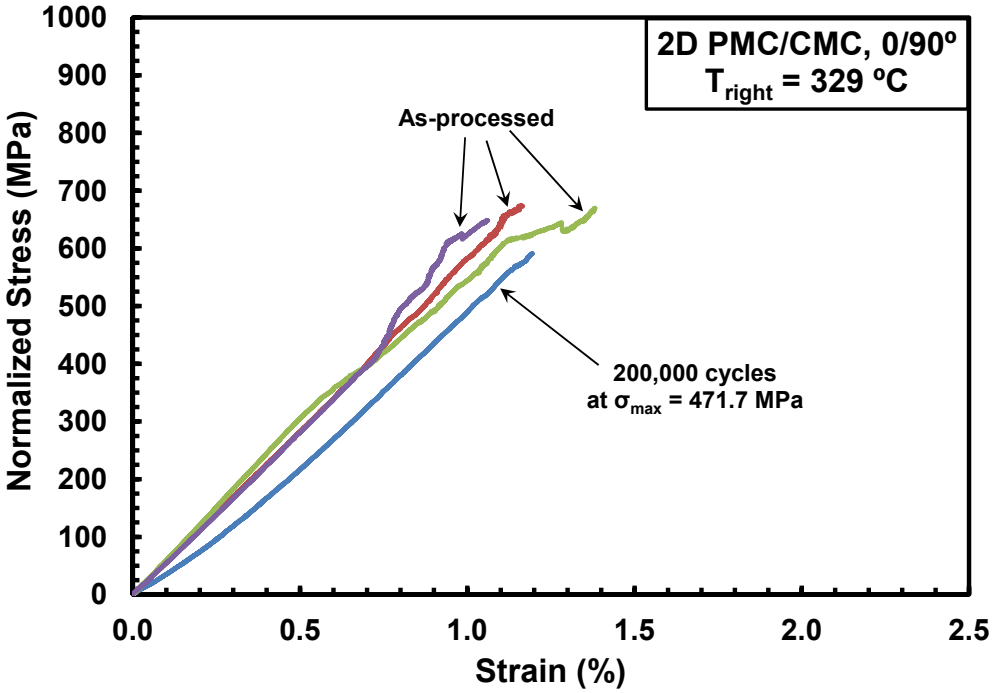

Figure 91: Stress vs. strain for 2D PMC/CMC unitized composite with 0/90° fiber orientation subjected to prior fatigue at elevated temperature. (as-processed curves shown for comparison)

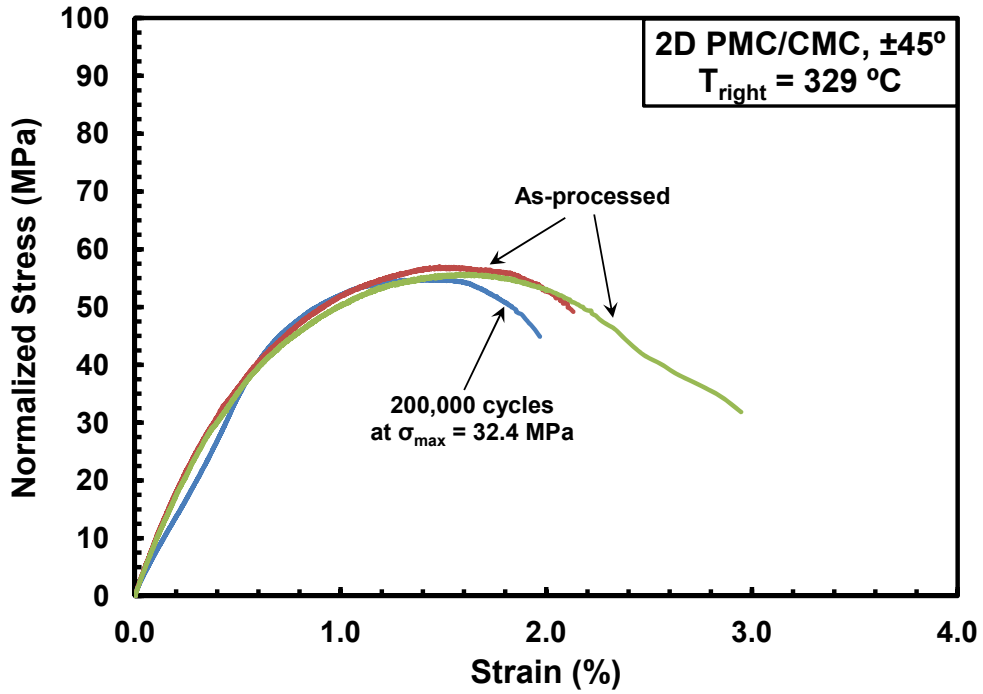

Figure 92: Stress vs. strain for 2D PMC/CMC unitized composite with ±45° fiber orientation subjected to prior fatigue at elevated temperature. (as-processed curves shown for comparison)

The retained modulus can also be compared to the modulus obtained from the first cycle of fatigue testing. Table 17 shows the modulus retention comparing the elastic modulus obtained during the first cycle to the modulus of the same specimen tested in tension-to-failure after fatigue run-out was achieved. By comparing the modulus retention percentages given in Table 17 to those given in Table 16, some insight is given into whether or not the modulus is dependent on the loading rate. The tension-to-failure test is performed at the displacement rate of 0.025 mm/s, whereas the fatigue cycling is much faster (0.5 s from minimum to maximum fatigue stress). It is seen that all retention percentages, whether calculated using as-processed tension-to-failure moduli or calculated using the first cycle load-up modulus had no significant differences except for the 3D PMC. One of the 0/90° specimens, T3-7, was slightly lower and the ±45° specimen shows a 19% difference in the retention percentages. This result suggests that the loading rate may have an effect on modulus, but should be studied more in-depth in the future.

Table 17: Modulus retention of the MS1, MS2, and MS3 specimens subjected to prior fatigue at T_{right} = 329°C in laboratory air

Specimen #	**Fiber Orientation**	**Fatigue Stress (MPa)**	**First Cycle Modulus (GPa)**	**Retained Modulus (GPa)**	**1^{st} Cycle Modulus Retention (%)**
Material System 1: 3D PMC					
T3-10	0/90°	482.9	47.95	44.81	93.4
T3-7	0/90°	424.7	50.57	47.33	93.6
T4-3	±45°	33.0	7.07	5.93	83.9
Material System 2: 2D PMC					
T1-7	0/90°	585.3	61.47	50.89	82.8
T1-4	0/90°	503.3	60.90	52.35	86.0
T2-5	±45°	66.4	13.95	13.93	99.8
T2-11	±45°	69.4	13.52	11.19	82.8
Material System 3: 2D PMC/CMC					
T5-7	0/90°	471.7	56.52	39.20	69.4
T6-5	±45°	32.4	9.61	7.88	82.0

Note: All stresses, moduli, and retention percentages are based on normalized values.
** Failure strain taken at point where stress dropped to 50% UTS.*

5.6 Optical Microscopy Examination

Each material system was examined under the Zeiss optical microscope for a qualitative analysis of the as-processed and tested specimens. One as-processed specimen was imaged along with one or more specimens that were tested in either tension-to-failure or fatigue.

5.6.1 Examination of MS1.

The gage section of a typical as-processed 3D PMC specimen with 0/90° fiber orientation is shown in Figure 93. One can clearly see the through-thickness Z-fibers, the uneven nature of the surface, and some matrix voids. On the left side of the specimen (c), matrix rich areas are seen between the fill fiber yarns, which have the Z-fibers passing over them. Figure 94 shows an angled view of the same specimen.

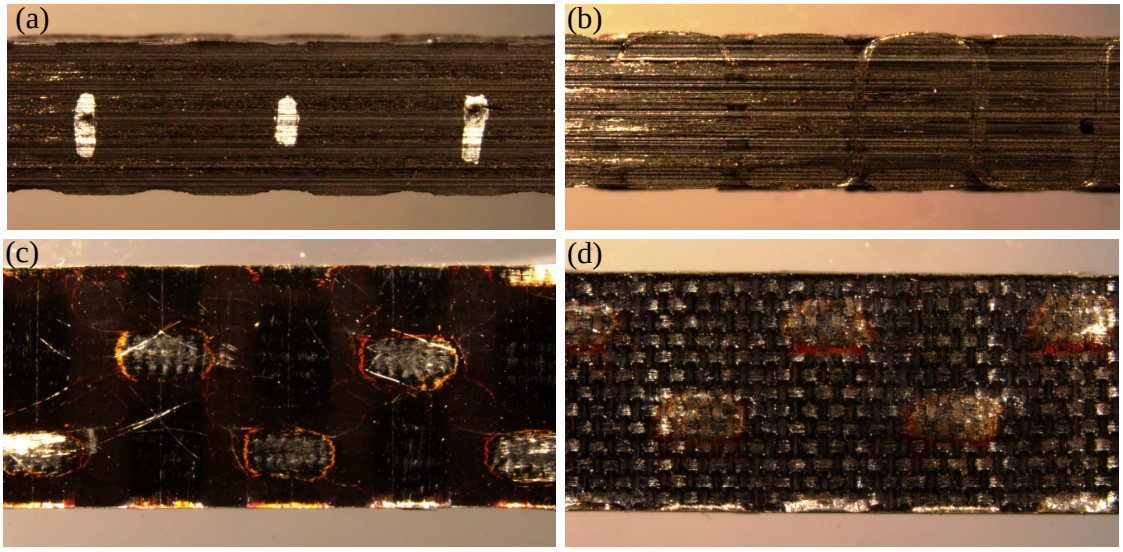

Figure 93: Optical micrographs of as-processed 3D PMC specimen with 0/90° fiber orientation (specimen T3-14): (a) front, (b) back, (c) left, and (d) right

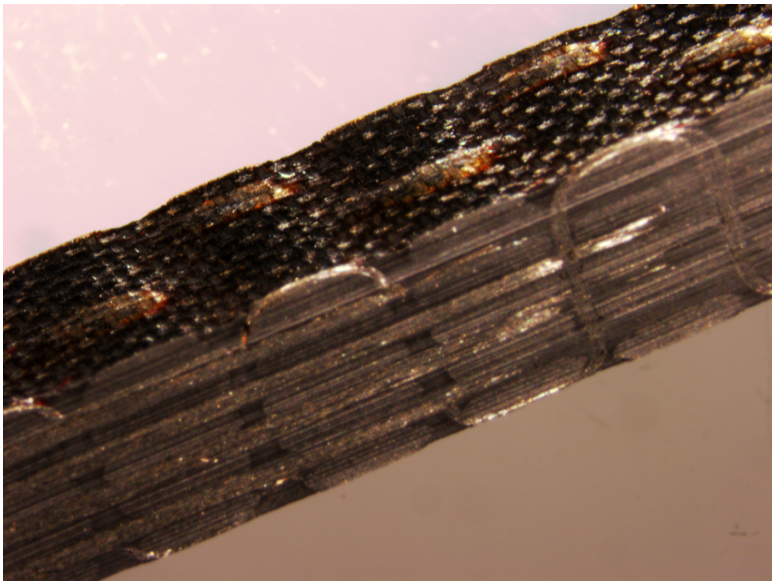

Figure 94: Optical micrograph of specimen T3-14 viewed from an angle

Failure of the 3D PMC specimens with 0/90° fiber orientation is typified in Figure 95. Numerous matrix cracks are evident on every surface of the specimen. Warp fiber pullout was observed, and in many cases the warp yarns extending into the specimen grip section pulled out, as is the case shown in Figure 95. If the specimen broke completely into two parts, the fracture in the 0/90° 3D PMC specimens occured predominantly along a plane where one or more Z-fibers protruded through the thickness of the specimen. No delamination was seen in these specimens.

An angled view of a tested specimen that was not fractured into two separate parts is shown in Figure 96. Although complete separation into two parts did not occur, failure of the specimen was still observed because there was a dramatic drop in sustained load. Matrix cracks and separation is observed between fill fibers, and the beginnings of warp fiber pullout is also visible.

The gage section of an as-processed 3D PMC specimen with ±45° fiber orientation is shown in Figure 97. The warp fiber yarns are evident in the front and back side images (a) and (b), along with some fine matrix cracks at the edge of some of the fiber yarns. Again,

Figure 95: Stitched optical micrographs of 3D PMC 0/90° specimen T3-8 after failure during fatigue at σ_{max} of 526.0 MPa. From left to right: front, back, left, right.

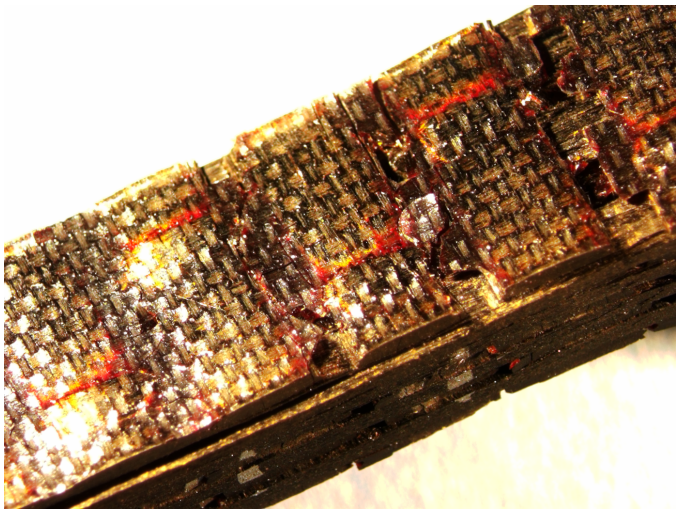

Figure 96: Optical micrograph of specimen T3-4 viewed from an angle after failure in tension at elevated temperature.

the Z-fibers are evident on the surface of the specimen in (c) and (d), along with the matrix rich areas between the fill fibers.

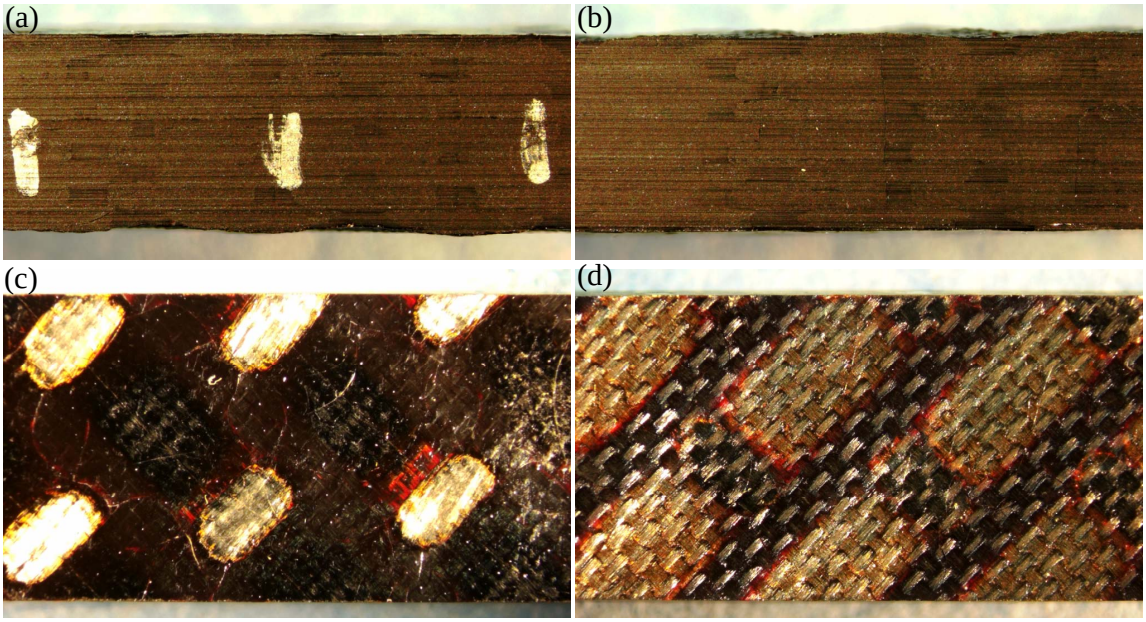

Figure 97: Optical micrographs of as-processed 3D PMC specimen with ±45° fiber orientation (specimen T4-10): (a) front, (b) back, (c) left, and (d) right.

Typical failure of the ±45° specimens of the 3D PMC is shown in Figure 98. Fracture occurs due to matrix cracking between fiber fill yarns and also between fiber warp yarns. Matrix cracking is evident in the front and back side views. As can be seen, there is little "scissoring" effect (i.e. the warp and fill fibers do not seem to realign into the direction of loading, but rather stay at their respective ±45° orientations). Compared to the 0/90° specimens, failure was more localized to the center of the gage section. Because Z-fibers were present at every intersection of warp and fill fiber yarns, one or more Z-fibers would be exposed upon fracture of the specimen. In Figure 98, the fractured Z-fiber is evident in all views. Figure 99 shows the fracture surface of specimen T4-6. The Z-fiber yarn and the rigid warp and fill fiber yarns are clearly visible.

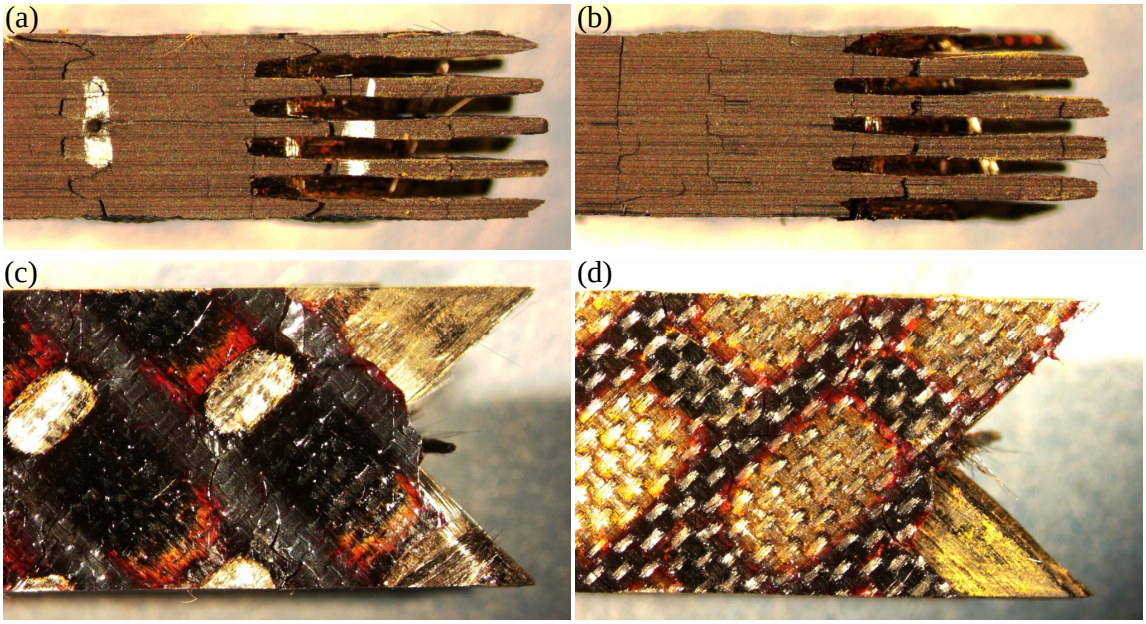

Figure 98: Optical micrographs of 3D PMC ±45° specimen T4-6 after failure from fatigue testing at 42.6 MPa: (a) front, (b) back, (c) left, and (d) right.

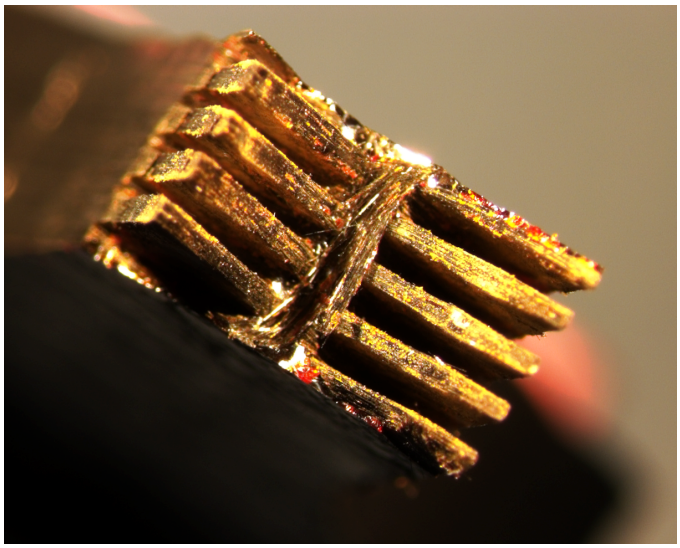

Figure 99: Optical micrograph of the fracture surface of specimen T4-6.

5.6.2 Examination of MS2.

An optical micrograph of an as-processed 2D PMC specimen with 0/90° fiber orientation is shown in Figure 100. These specimens showed no matrix voids or pre-existing cracks; only slight surface scratches were noted upon visual inspection.

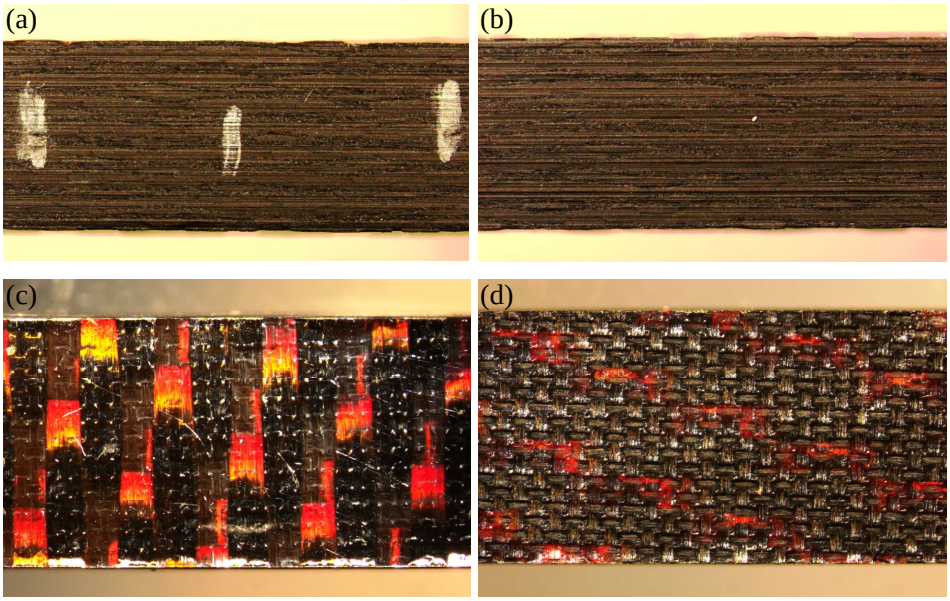

Figure 100: Optical micrographs of as-processed 2D PMC specimen with 0/90° fiber orientation (specimen T1-10): (a) front, (b) back, (c) left, and (d) right.

Some 0/90° specimens of the 2D PMC failed in a more localized brittle manner, but the majority showed failure mechanisms such as ply delamination and fiber pullout. Figure 101 shows a specimen that exhibited a more localized fracture with limited fiber pullout and limited delamination. However, matrix cracks and moderate delamination propagating through the length of the specimen are also observed. Figure 102 shows a specimen that exhibited more extensive delamination and fiber pullout. Numerous matrix cracks between fiber plies are seen.

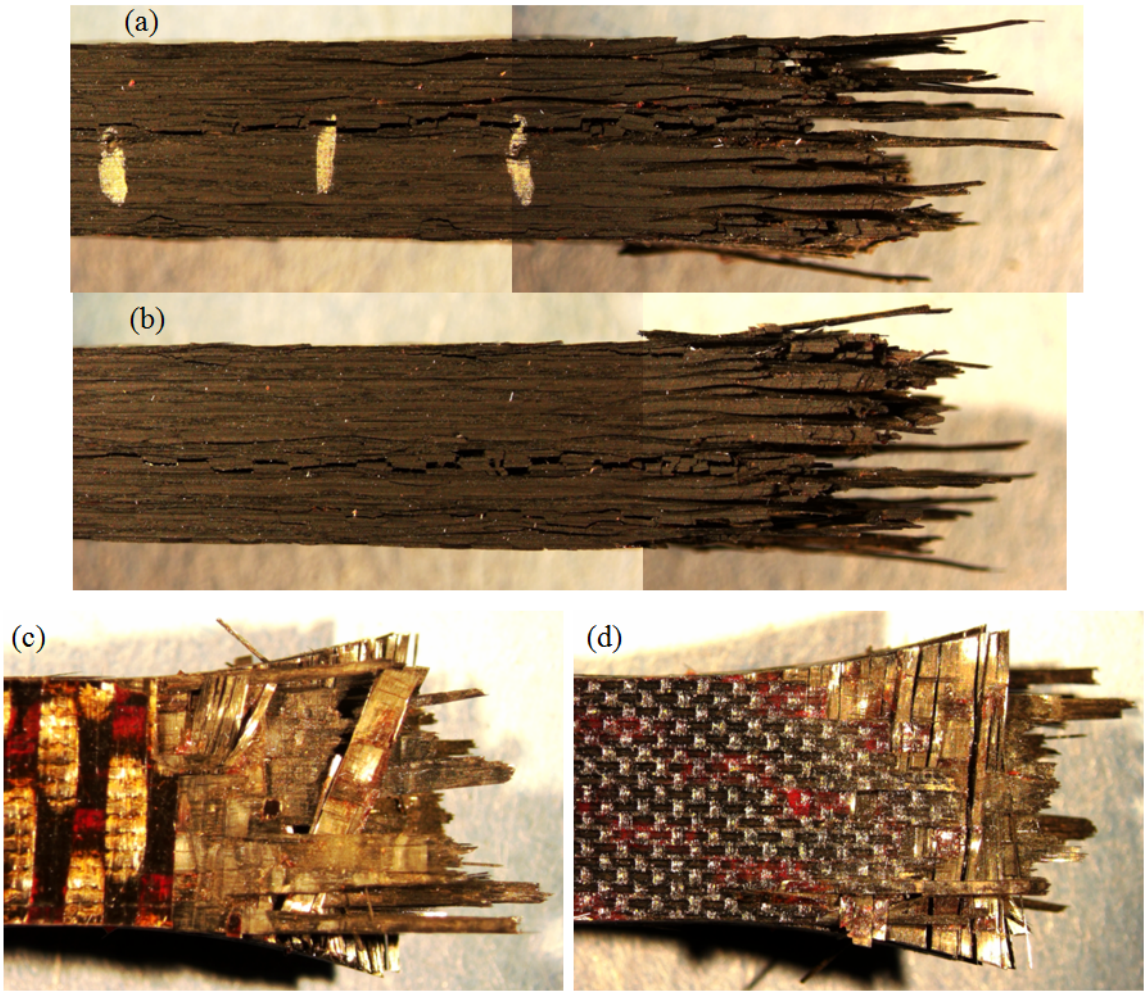

Figure 101: Stitched optical micrographs of 2D PMC 0/90° specimen T1-5 after failure during fatigue testing at 759.7 MPa: (a) front, (b) back, (c) left, and (d) right.

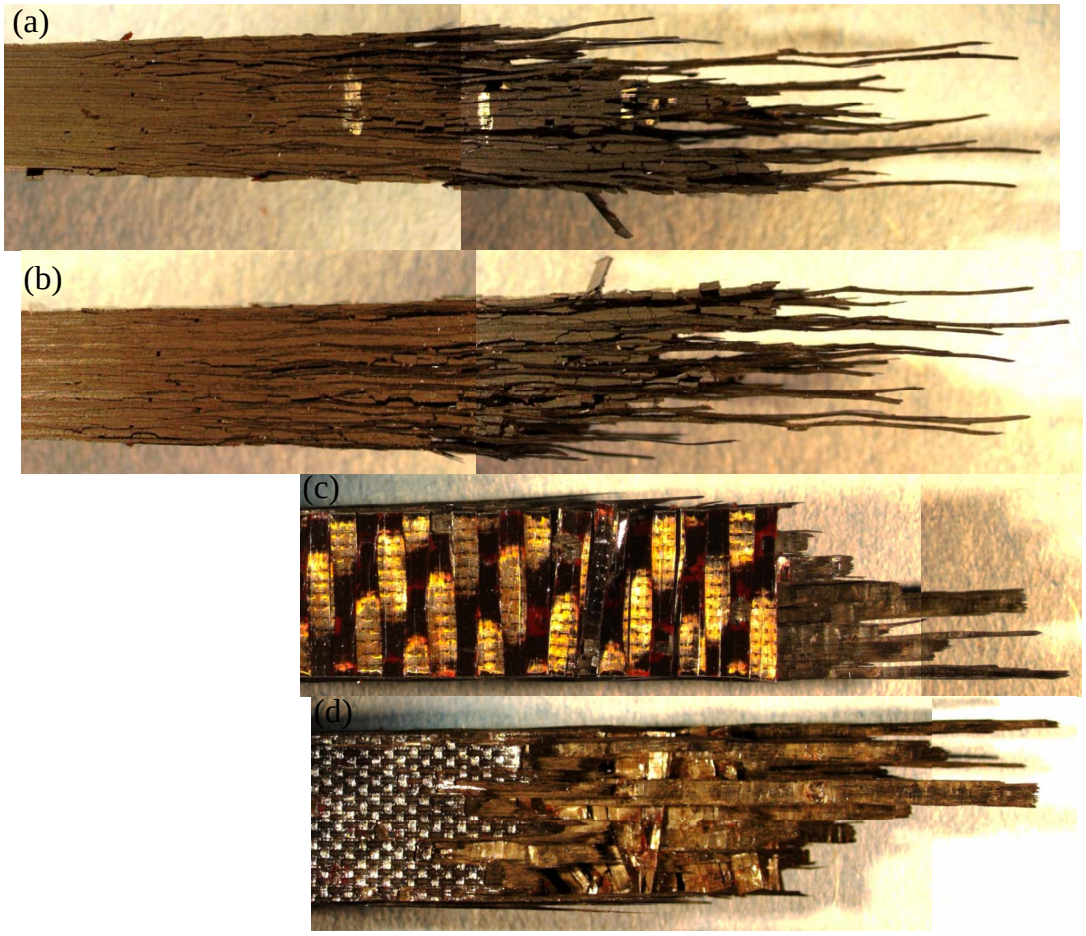

Figure 102: Stitched optical micrographs of 2D PMC 0/90° specimen T1-10 after failure during fatigue testing at 610.2 MPa: (a) front, (b) back, (c) left, and (d) right.

Figure 103 shows the gage section of an as-processed a ±45° specimen of the 2D PMC. Like the 0/90° specimens, no major flaws were noted upon visual examination, only slight surface scratches.

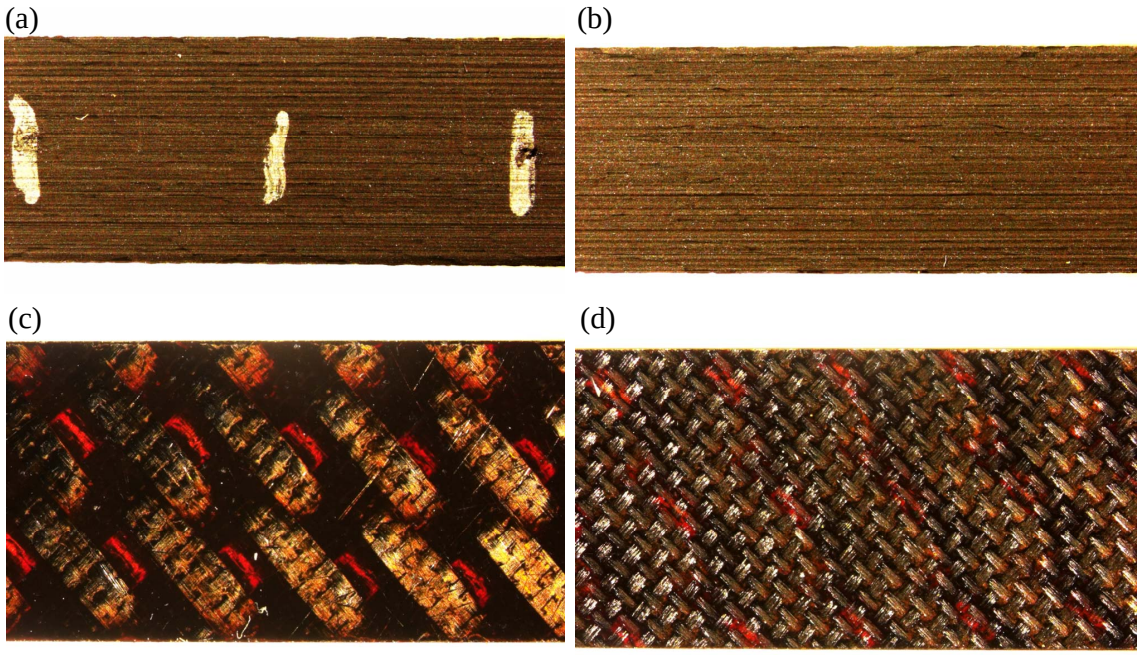

Figure 103: Optical micrographs of as-processed 2D PMC specimen with ±45° fiber orientation (specimen T2-8): (a) front, (b) back, (c) left, and (d) right.

Failure of the ±45° specimens is typified in Figure 104. As in the case of the 3D PMC specimens with ±45° fiber orientation, the failure was more localized in the gage section. Substantial matrix cracking is evident in all views shown. The resulting "scissoring" effect of the fibers can be clearly seen in the left and right face views. Some of the fibers have broken away from the edges and/or from their yarns and have realigned slightly in the direction of loading.

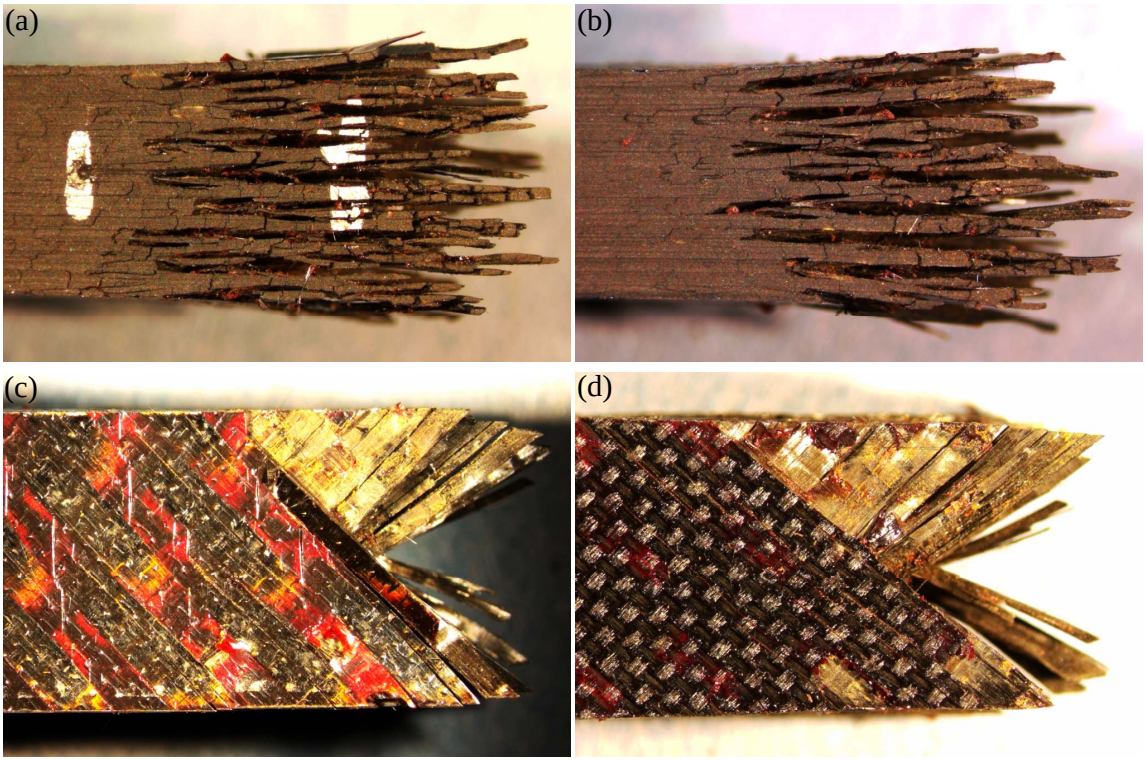

Figure 104: Optical micrographs of 2D PMC ±45° specimen T2-9 after failure from fatigue testing at 82.6 MPa: (a) front, (b) back, (c) left, and (d) right.

5.6.3 Examination of MS3.

Figure 105 shows a typical as-processed 2D unitized composite specimen with 0/90° fiber orientation. Uneven thickness of the CMC layer is evident. Additionally, the CMC surface had surface pits and matrix voids in many of the specimens, like the one shown.

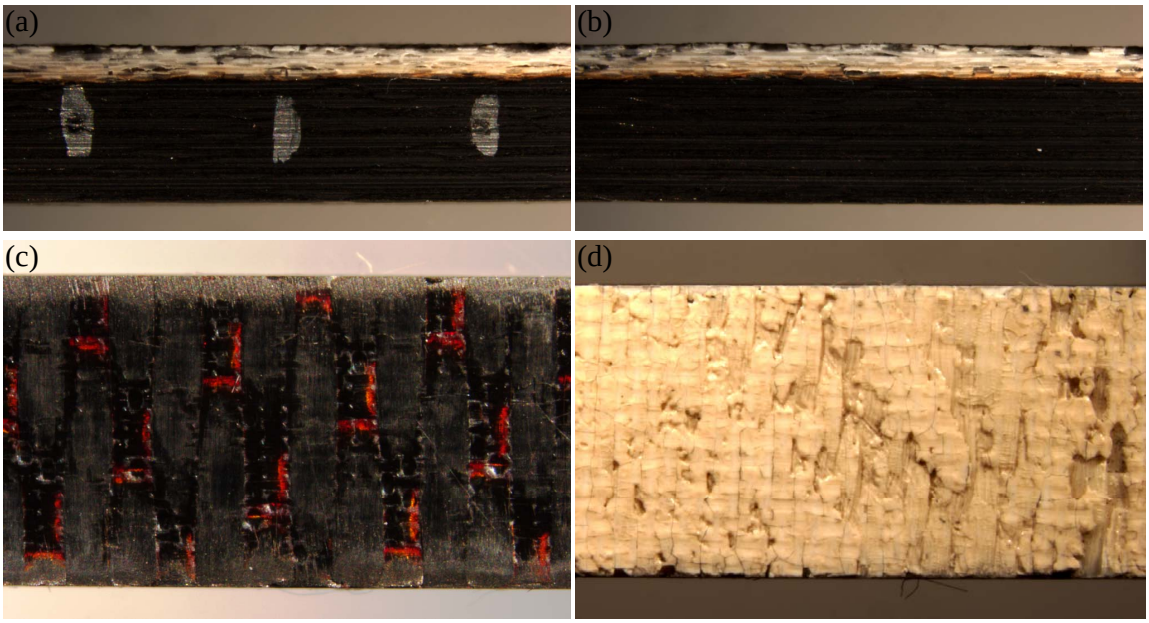

Figure 105: Optical micrographs of as-processed 2D PMC/CMC specimen with 0/90° fiber orientation (specimen T5-5): (a) front, (b) back, (c) left, and (d) right.

As mentioned previously, the unitized composite would bow out when large loads were applied axially. A few specimens tested in tension to failure were purposely not broken completely in two parts after failure in order to image this bowing effect. Figure 106 shows that the third CMC ply (the ply closest to the PMC and closest to the site of co-curing of the two materials) was stiffer than the other two CMC plies and the PMC plies. The image shown in Figure 106 was taken after failure and after any loads were removed from the specimen. Upon removal of all remaining loads, the specimen would attempt to regain its original length (most likely caused by the stiffer CMC ply),

resulting in an exaggerated bowing out of the fiber plies. Recall that the co-curing of two dissimilar matrix materials results in non-uniform deformation throughout the specimen thickness causing bending stresses in addition to the applied tension. Combined bending and tension, together with development of irreversible strains due to damage, are likely responsible for bowing out of the specimen. Extensive delamination is evident, and many of these specimens exhibited a large matrix crack propagating through the PMC layer extending to the grip sections, as seen in Figure 106.

Figure 106: Stitched optical micrographs of 2D PMC/CMC 0/90° specimen T5-2 following failure in tension at room temperature and load removal.

Figure 107 shows a 0/90° unitized composite specimen that broke completely in two upon failure, as did all specimens that failed in fatigue. The delamination in both the PMC and CMC portions is clearly seen. This delamination essentially caused a brooming out effect in the specimen, especially in the PMC portion. A large matrix crack extends through the middle of the PMC into the grip section. Failure of the PMC portion was expansive, and both halves of the failed specimen exhibited about equal carbon fiber pullout and ply delamination. Although the CMC layer exhibited extensive ply delamination as well, it had a more localized fracture. For specimens tested in tension-to-failure, the CMC fracture occurred in the straight gage section, but for specimens failed in fatigue, the CMC fracture occurred near the top or bottom of the gage section. Quartz fiber pullout is seen near the failure. It is interesting to note that the CMC

layer, which faced the furnace, did not fracture in the gage section directly exposed to heat. This result suggests that the 329°C temperature does not have a significant effect on the CMC. It is believed that the location of fracture in the CMC layer was caused by additional bending stresses resulting from the specimen repeatedly bowing in and out during cyclic loading.

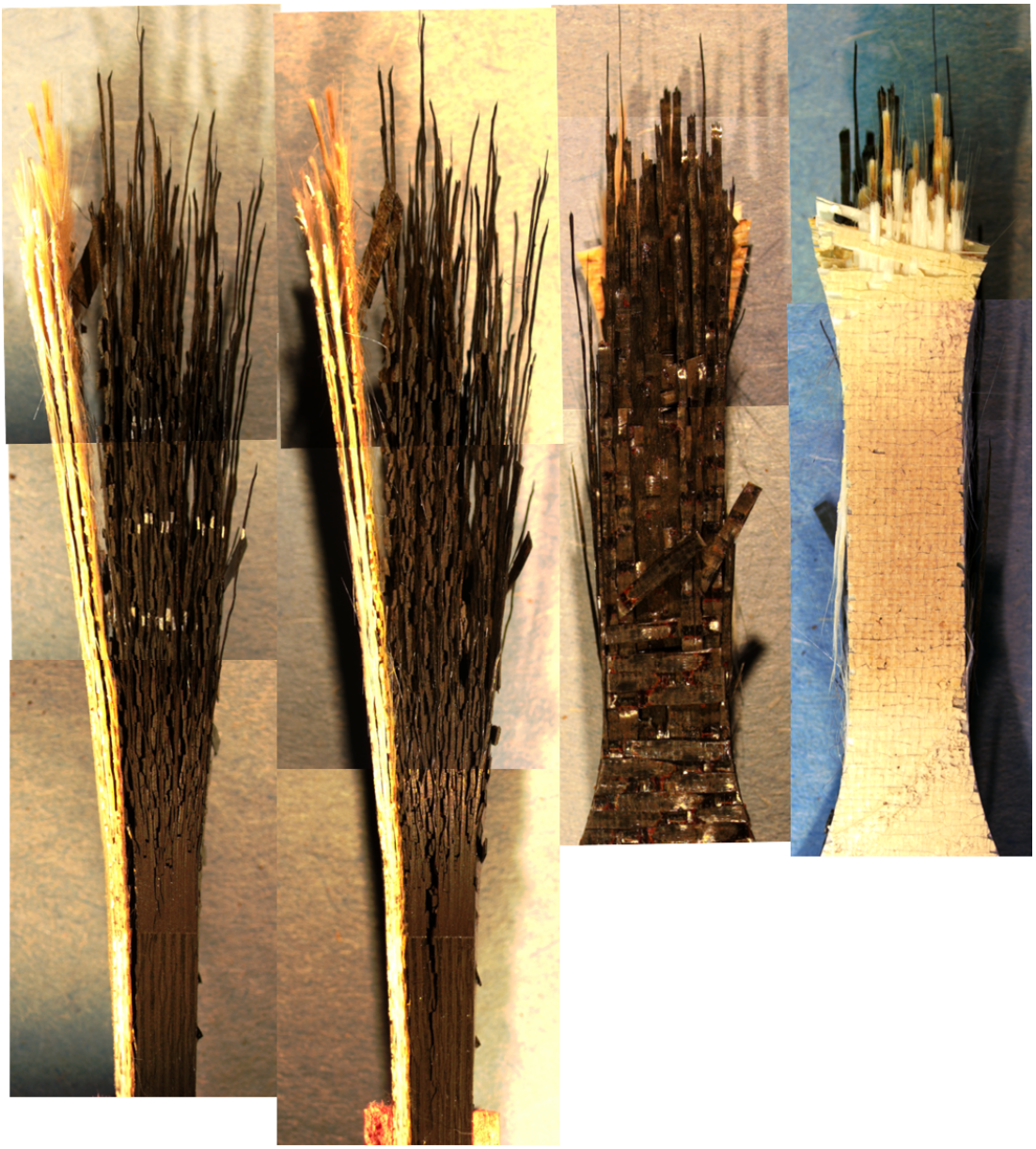

Figure 107: Stitched optical micrographs of 2D PMC/CMC 0/90° specimen T5-16 after failure during fatigue at 557.3 MPa. Left to right: front, back, left, right.

A typical as-processed 2D unitized composite specimen with ±45° fiber orientation is seen in Figure 108. More fiber fraying was evident on the CMC edge most likely due to machining. The CMC (right) surface had fewer voids and surface pits than the 0/90° panel; however, many specimens cut from the ±45° panel had NRPE polyimide resin overflow on the CMC surface (Figure 109). This polyimide resin overflow did not have any significant adverse effects on the mechanical performance of the material.

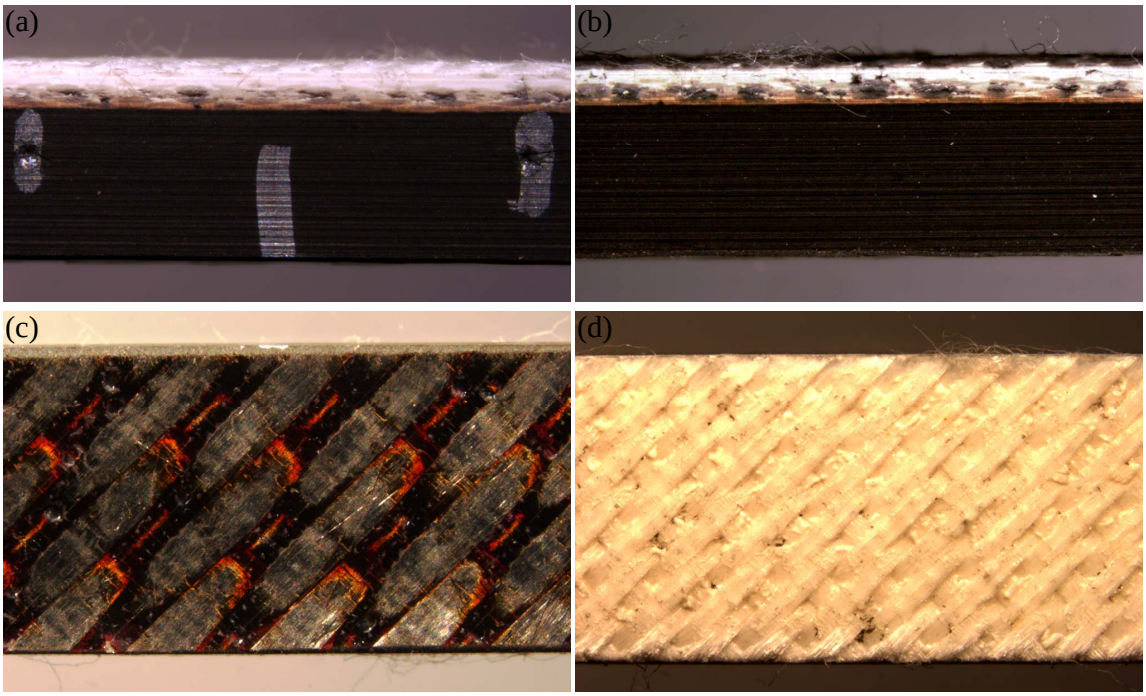

Figure 108: Optical micrographs of as-processed 2D PMC/CMC specimen with ±45° fiber orientation (specimen T6-13): (a) front, (b) back, (c) left, and (d) right.

Failure of the 2D unitized composite with ±45° fiber orientation is seen in Figure 110. Fracture of these specimens was localized in the gage section. As in the case of the 2D PMC, extensive matrix cracking is observed, but localized ply delamination is also evident. The “scissoring” effect of the fibers is again seen as fibers have become detached from the neighboring matrix material and align along the loading direction.

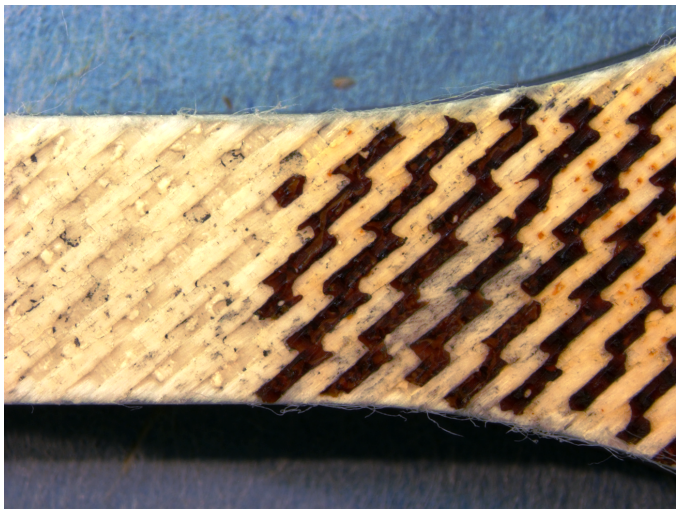

Figure 109: Optical micrograph of 2D PMC/CMC ±45° specimen T6-16 with NRPE resin overflow onto CMC surface.

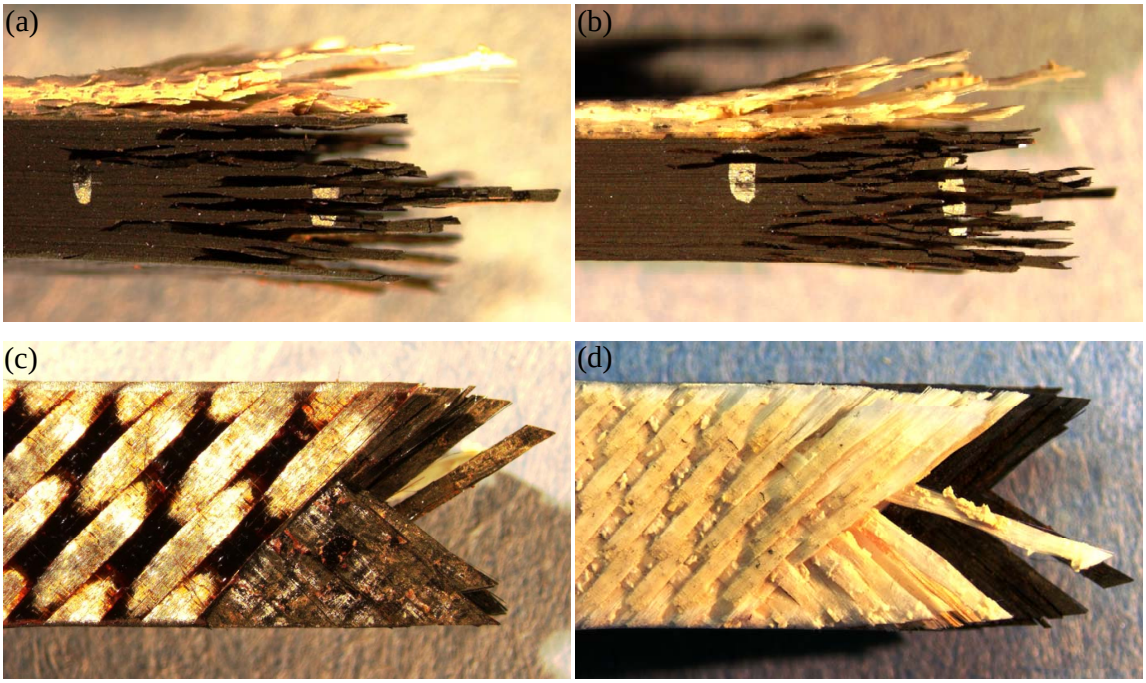

Figure 110: Optical micrographs of 2D PMC/CMC ±45° specimen T6-11 after failure during fatigue testing at 42.5 MPa: (a) front, (b) back, (c) left, and (d) right.

The bowing out of the plies upon load-up was also seen. A specimen tested in tension to failure, but not broken into two parts is seen in Figure 111. Note that the CMC ply closest to the PMC also deforms by bowing out, unlike in the case of the 0/90° orientation that exhibited a more rigid third CMC ply.

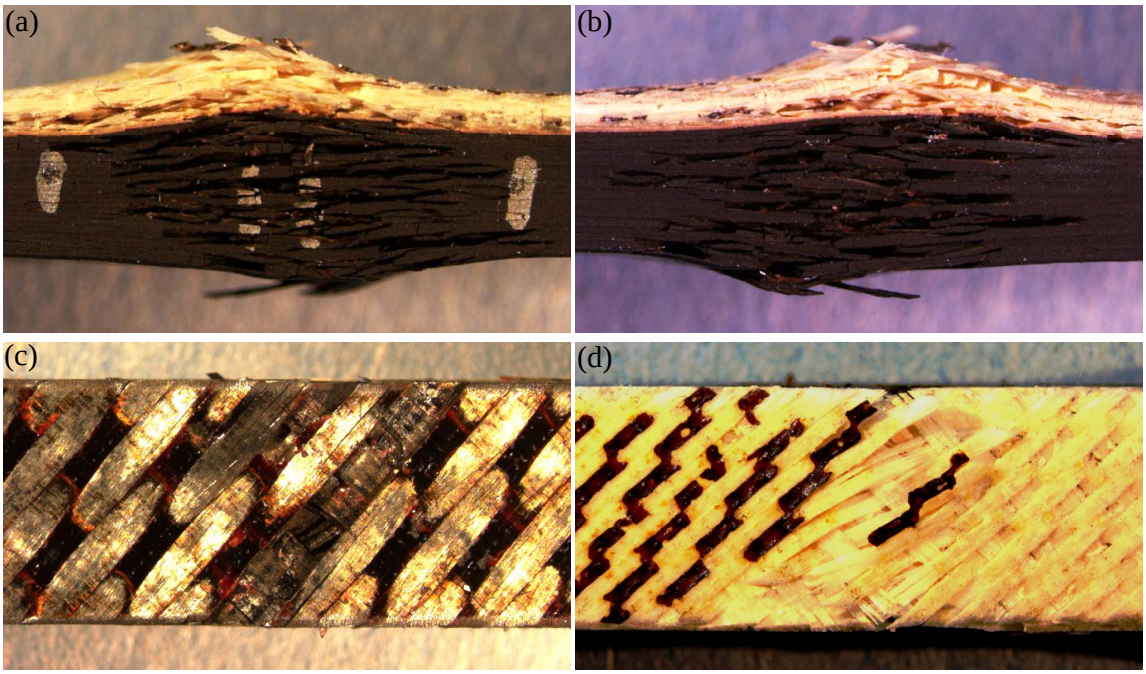

Figure 111: Optical micrographs of 2D PMC/CMC ±45° specimen T6-2 after failure in tension at elevated temperature: (a) front, (b) back, (c) left, and (d) right.

VI. Conclusions and Recommendations

6.1 Concluding Remarks

The tensile stress-strain behavior and tensile properties of the three material systems (3D PMC, 2D PMC, 2D unitized composite) were examined for both 0/90° and ±45° fiber orientations at room and elevated temperature. As expected, all three material systems produced significantly higher UTS values for the 0/90° fiber orientation than for the ±45° fiber orientation. In the case of the 0/90° fiber orientation, the increase in temperature from 23°C to T_{right} of 329°C had little effect on the UTS, modulus, or failure strain. However, in the case of the ±45° fiber orientation, the UTS of the 3D PMC and 2D PMC decreased with increasing temperature, while the UTS of the unitized composite remained largely unchanged. At elevated temperature, the tensile strength of the 0/90° 2D PMC was higher than that of both the 3D PMC and the 2D unitized composite. While the stiffness of the 3D PMC was noticeably lower than that of the 2D PMC, the stiffness of the 2D unitized composite was nearly the same as that of the 2D PMC. At elevated temperature, the UTS of the ±45° 3D PMC was only half of the UTS produced by the 2D PMC, whereas the modulus of the ±45° 3D PMC was only slightly lower than that of the 2D PMC. The ±45° 2D unitized composite also produced much lower UTS, modulus and failure strain values than the 2D PMC.

Tension-tension fatigue performance of the three material systems was also investigated. Fatigue tests were performed for both 0/90° and ±45° fiber orientations at elevated temperature. The fatigue performance of the 2D PMC was considerably better than that of the 3D PMC and of the 2D unitized composite for both 0/90° and ±45° fiber orientations. Furthermore, during fatigue loading the unitized composite exhibited highly non-homogeneous deformation, which led to extensive ply delamination.

Because the tensile properties and fatigue limit of the ±45° fiber orientation are much lower than the corresponding 0/90° values, any complex off-axis loading would result in diminished load carrying capability and fatigue performance. Additionally, results of the present study demonstrate that the 3D PMC and the 2D unitized composite do not offer significant advantages over the 2D PMC. While the 3D PMC offers improved delamination resistance, the tensile properties and tension-tension fatigue performance of the 2D PMC are considerably superior to those of the 3D PMC and the 2D unitized composite.

6.2 Recommendations

Further research is required in order to fully characterize the mechanical properties of the material systems examined in this effort. Damage initiation and development during tensile and tension-tension fatigue loading should be investigated. Additionally, mechanical performance in complex operating environments, for example over a range of elevated temperatures, should be studied. Effects of mean stress and/or frequency on tension-tension fatigue behavior should be examined. It is also recommended that compressive properties as well as tension-compression fatigue performance of these material systems be investigated. Other types of tests should be conducted, for example bending tests for the unitized composite which has an asymmetric lay-up of PMC and CMC layers. Lastly, it would be useful to characterize the mechanical performance of the 3D PMC in the 90° direction (the fill fiber direction).

Once the the 3D fiber architecture is extended to the unitized composite material, the characterization of that new material system should be undertaken. Panels of material system 4 (MS4), a unitized composite with a 3D weave in the CMC layer, have already been manufactured. However, because severe delamination was observed for MS3, it is suggested that the 3D weave architecture be extended to the PMC portion of the unitized composite as well. Moreover, because considerable bowing out of the MS3 specimens

was observed in most tests, design and fabrication of a material system with continuous through-thickness fibers (i. e. fibers extending through both the CMC and the PMC layers) should be considered. Of course this would be a challenging task. It would also be interesting to evaluate unitized composites with various thicknesses of the CMC layer should such material systems be fabricated.

Appendix A: Tension-Compression Specimen Geometry and Preparation

A.1 Specimen Geometry

Hourglass-shaped specimens (Figure 112) were machined out of the same panels along with the tension-tension dogbone-shaped specimens. These hourglass-shaped specimens will be used in future research to investigate mechanical behavior of the three material systems under monotonic compressive loading and tension-compression cyclic loading at elevated temperature. Buckling of a specimen is a failure mode that is often observed during compressive loading, but is undesirable. By using an hourglass shape, enough support is provided to prevent buckling of the specimen while still concentrating the maximum stress in the gage section. Finite-element analysis performed on the hourglass shape shows an axially stressed specimen will have 3.5% higher stress at the edges of the center of the gage section compared to the average axial stress. Hourglass specimens have also been used successfully in fatigue tests of glass strand composites and SiC/SiC composites with negative R ratios [18].

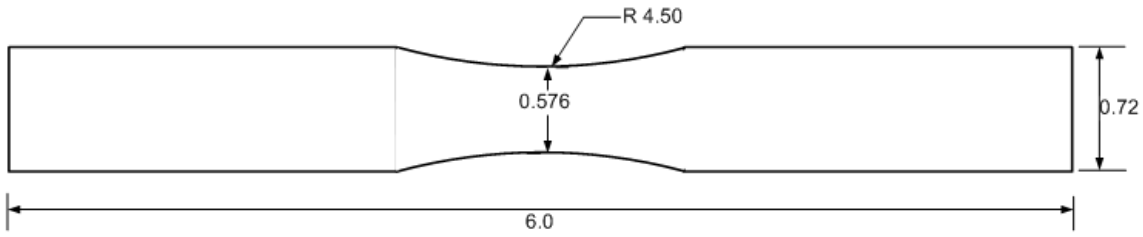

Figure 112: Tension-compression specimen geometry, all dimensions in inches

A.2 Specimen Preparation

Test specimens were machined from the composite panels by the AFIT Model and Fabrication Shop using diamond-grinding. One panel of each material system was cut into specimens with 0/90° fiber orientation, while the other was machined into specimens with ±45° fiber orientation for characterization of off-axis material performance. After specimen machining, every specimen was labeled. Specimen labels correspond to the geometry, material system, and fiber orientation. For example, label *C*1-1 refers to tension-compression specimen number one from the 0/90° fiber orientation panel of the 2D PMC (panel MS2-1), whereas label *C*4-5 refers to tension-compression specimen number five from the ±45° fiber orientation panel of the 3D PMC (panel MS1-2). Specimen labels corresponding to different material systems and fiber orientations can be seen in Table 18.

Table 18: Tension-compression specimen labeling scheme

Material System	Material Type/ Fiber Weave	Panel ID	Fiber Orientation	Label	Example Specimen Labels	Total # of Specimens
MS1	3D PMC	MS1-1	0/90°	C3	C3-1	11
		MS1-2	±45°	C4	C4-5	7
MS2	2D PMC	MS2-1	0/90°	C1	C1-3	10
		MS2-2	±45°	C2	C2-4	8
MS3	2D PMC/CMC	MS3-1	0/90°	C5	C5-8	14
		MS3-2	±45°	C6	C6-2	10

After specimen labeling, the gage section width and thickness was measured using a Mitutoyo Absolute Solar Digimatic Caliper, Model N0. CD-S6”CT. Specimen thickness varied slightly from panel to panel. Slight thickness variation within each panel was also observed and documented upon measurement of specimens. Average test specimen dimensions are given in Table 19.

Table 19: Average tension-compression specimen dimensions

Material System	Panel	Specimen Type	Avg Width (mm)	Avg Thickness (mm)	Avg Cross-Sect. Area (mm^2)
1	1	3D PMC, 0/90°	14.64	4.71	68.98
	2	3D PMC, ±45°	14.55	4.82	70.22
2	1	2D PMC, 0/90°	14.64	5.73	83.88
	2	2D PMC, ±45°	14.66	5.70	83.62
3	1	2D PMC/CMC, 0/90°	14.66	4.96	72.74
	2	2D PMC/CMC, ±45°	14.73	4.97	73.19

All specimens were cleaned with a solution of soap and water and thoroughly rinsed with distilled water in order to remove contaminants from the machining process. After cleaning, specimens were handled with nitrile gloves to prevent any contamination by skin oils. The specimens were then dried in an Isotemp Model 282A vacuum oven set to 105°C and approximately 2 inches Hg pressure. The drying was accomplished in three batches due to oven space limitations. Weight measurements for four specimens of each specimen type were recorded periodically during drying using a Mettler Toledo laboratory balance accurate to ± 0.9 mg to assess when all absorbed water was evaporated. Weight loss stabilized in less than 9 days as shown in Figure 113. The specimens were then removed from the oven and stored at room temperature in a desiccator maintained at about 15% relative humidity in order to minimize reabsorption of moisture in the ambiant air.

In order for the axial extensometer to stay in contact with the specimen during tests, two dimples were made in the side of the test specimen, 12.7 mm apart and centered in the middle of the gage section. Dimples were created using a hammer and a punch tool provided by MTS and were kept to a minimal depth to avoid fracture initiation at the dimples.

For the initial modulus tests, fiberglass tabs were taped on the specimen with the tape only touching the top and bottom surfaces of the specimen. The purpose of these tabs was

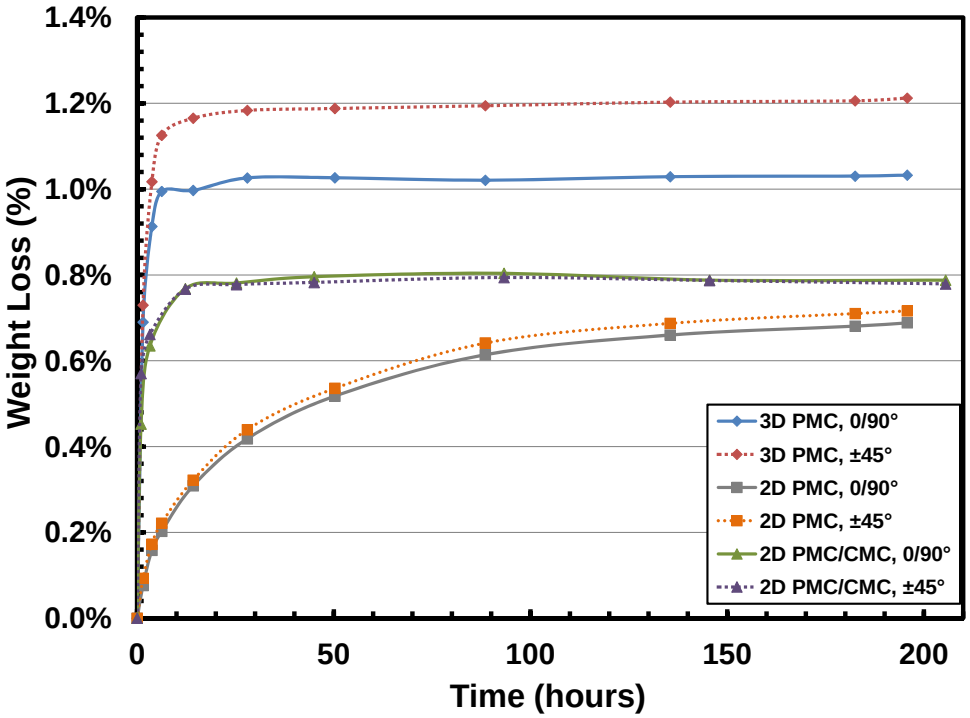

Figure 113: Tension-compression specimen weight loss during drying

to transfer the mechanical load to the test specimen and to avoid the wedge surface from damaging the specimen.

A.3 Assessment of Specimen-to-Specimen Variability

In this research, there were two panels of each material system. One panel was used to machine the 0/90° specimens while the other panel was used to machine the ±45° specimens. However, in some panels, slight defects and thickness changes could be seen by visual inspection. Therefore, it was vital to assess the specimen-to-specimen variability of each material system. This assessment was conducted by performing room temperature modulus tests as outlined in Section 4.3.1. Because there is inherent data scatter at very low stress levels, a linear best fit was computed using data gathered at stresses above 2 MPa. Results are shown in Table 20.

Table 20: Room temperature elastic modulus results obtained for tension-compression specimens

Panel	Specimen Type	Average Modulus (GPa)	Standard Deviation (GPa)	Coeff. of Variation
MS1-1	C3: 3D PMC, 0/90°	40.08	4.03	0.1006
MS1-2	C4: 3D PMC, ±45°	11.36	0.67	0.0590
MS2-1	C1: 2D PMC, 0/90°	52.11	1.81	0.0347
MS2-2	C2: 2D PMC, ±45°	17.66	0.50	0.0282
MS3-1	C5: 2D PMC/CMC, 0/90°	47.17	1.33	0.0282
MS3-2	C6: 2D PMC/CMC, ±45°	11.53	0.32	0.0274

It can be seen that the tension-compression modulus values follow the same trends as the tension-tension values. The 2D PMC modulus values are greater than both the 3D PMC and the 2D PMC/CMC. Also, as with the tension-tension specimens, the 3D PMC has the most variability in the modulus values.

When the initial room temperature modulus values of the tension-compression specimens are compared with the initial room temperature modulus values of the tension-tension specimens, it is observed that the 0/90° specimens had a slight difference between the two. This can be visualized in Figure 114 and occurred for all material systems, although it was less apparent in the 3D PMC because of the increased variability. It is postulated that this difference was due to the difference in geometry between the dogbone- and hourglass-shaped specimens and the resulting interaction between the specimen and extensometer. The modulus difference was not as pronounced at lower modulus values (for the ±45° specimens). Overall panel modulus values (combining tension-tension and tension-compression for each panel) are given in Table 21.

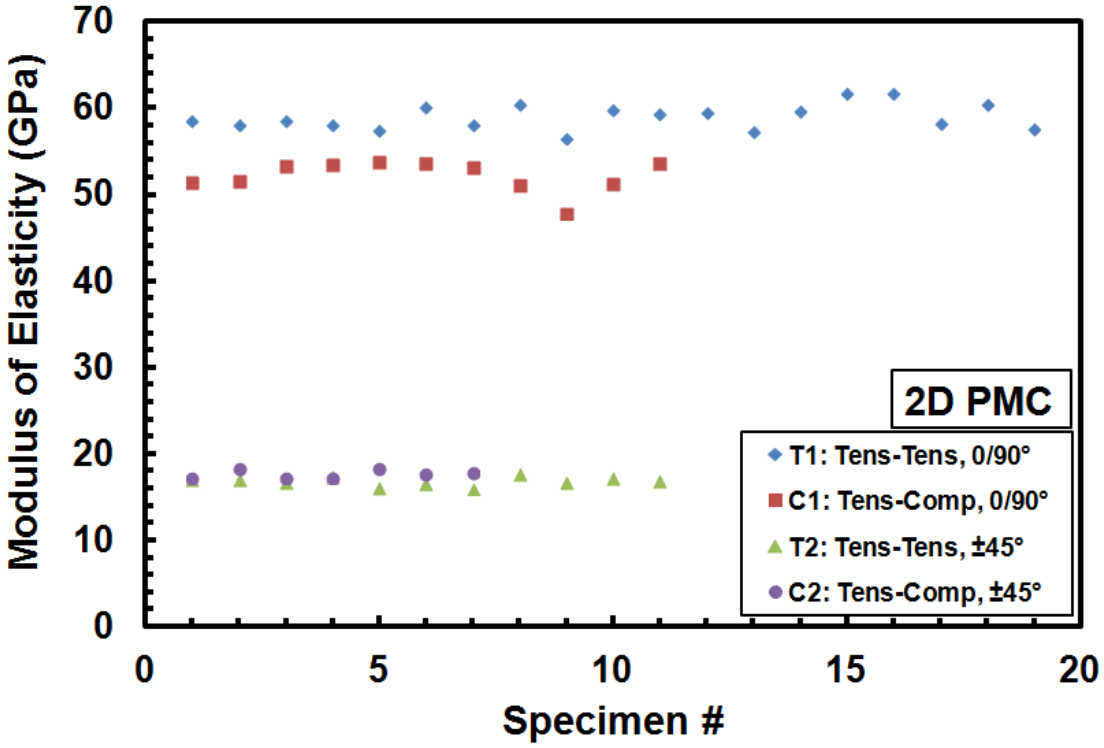

Figure 114: Room temperature modulus values obtained for the tension-tension and tension-compression specimens.

Table 21: Average panel room temperature modulus values

Panel	Specimen Type	Average Modulus (GPa)	Standard Deviation (GPa)	Coeff. of Variation
MS1-1	3D PMC, 0/90°	44.41	4.72	0.1062
MS1-2	3D PMC, ±45°	10.29	1.02	0.0986
MS2-1	2D PMC, 0/90°	56.48	3.73	0.0660
MS2-2	2D PMC, ±45°	17.20	0.62	0.0363
MS3-1	2D PMC/CMC, 0/90°	52.92	4.54	0.0859
MS3-2	2D PMC/CMC, ±45°	11.03	0.48	0.0435

Appendix B: Additional Fatigue Plots

In order to verify that the normalized stresses did not produce drastically different fatigue performance results, *S*-*N* curves comparing actual (measured) fatigue stresses to that of the normalized fatigue stresses are provided in Figures 115 – 120.

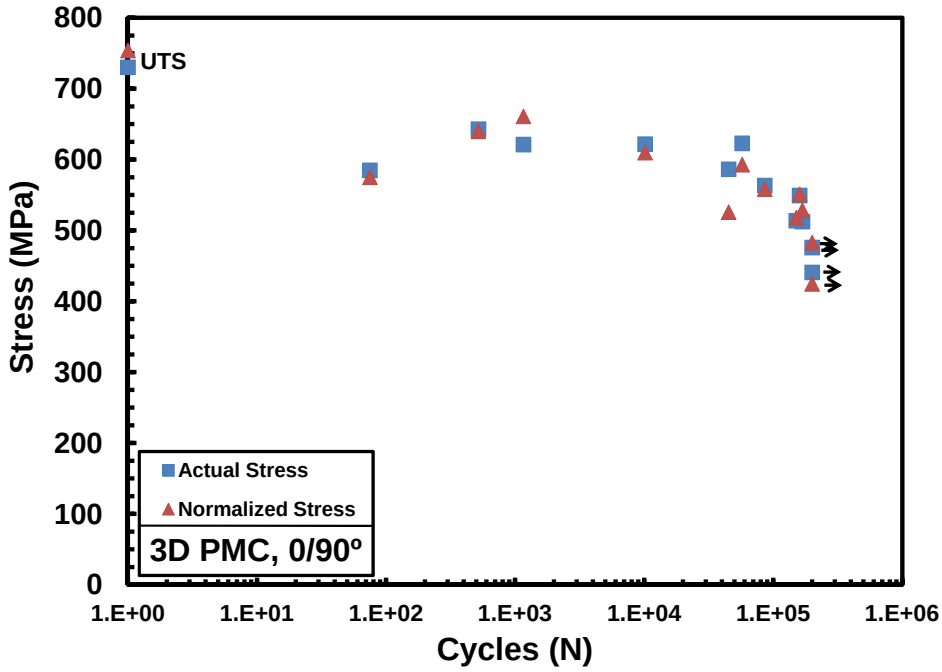

Figure 115: *S*-*N* curve for the 3D PMC with both 0/90° fiber orientation comparing actual and normalized stresses at elevated temperature. Arrow indicates specimen achieved fatigue run-out.

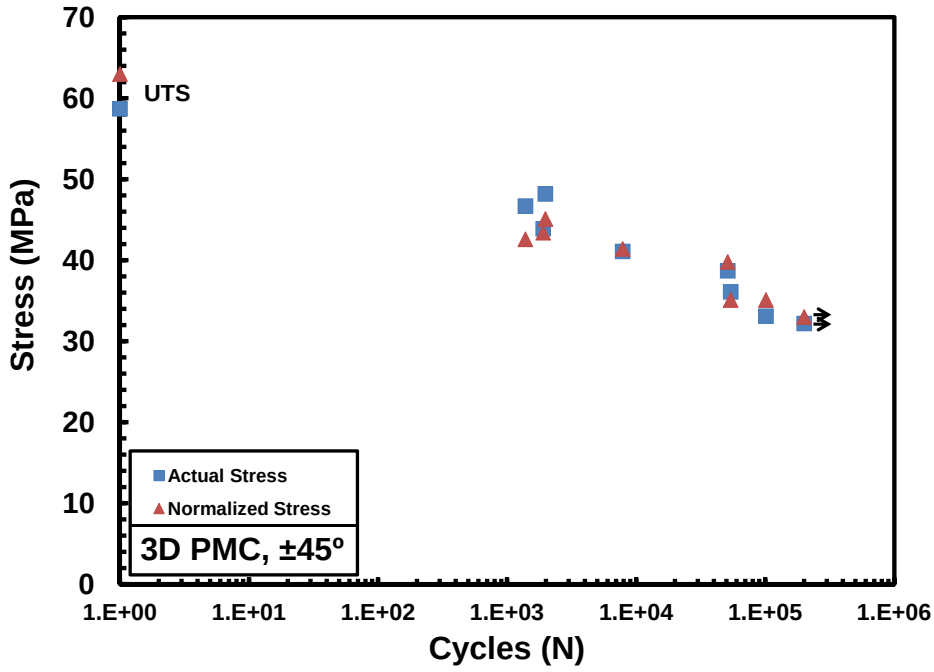

Figure 116: *S*-*N* curve for the 3D PMC with both ±45° fiber orientation comparing actual and normalized stresses at elevated temperature. Arrow indicates specimen achieved fatigue run-out.

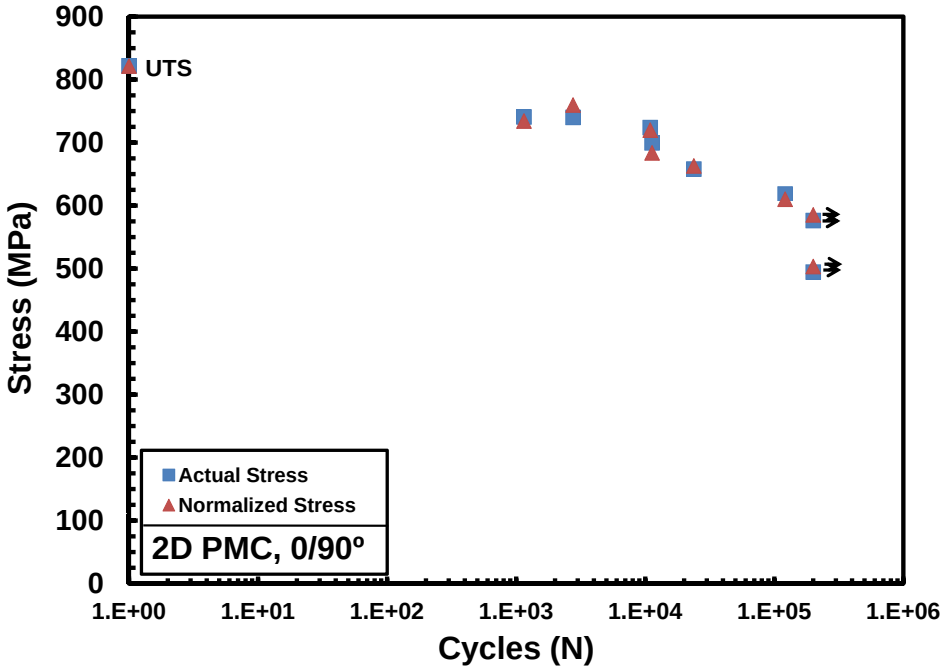

Figure 117: *S*-*N* curve for the 2D PMC with both 0/90° fiber orientation comparing actual and normalized stresses at elevated temperature. Arrow indicates specimen achieved fatigue run-out.

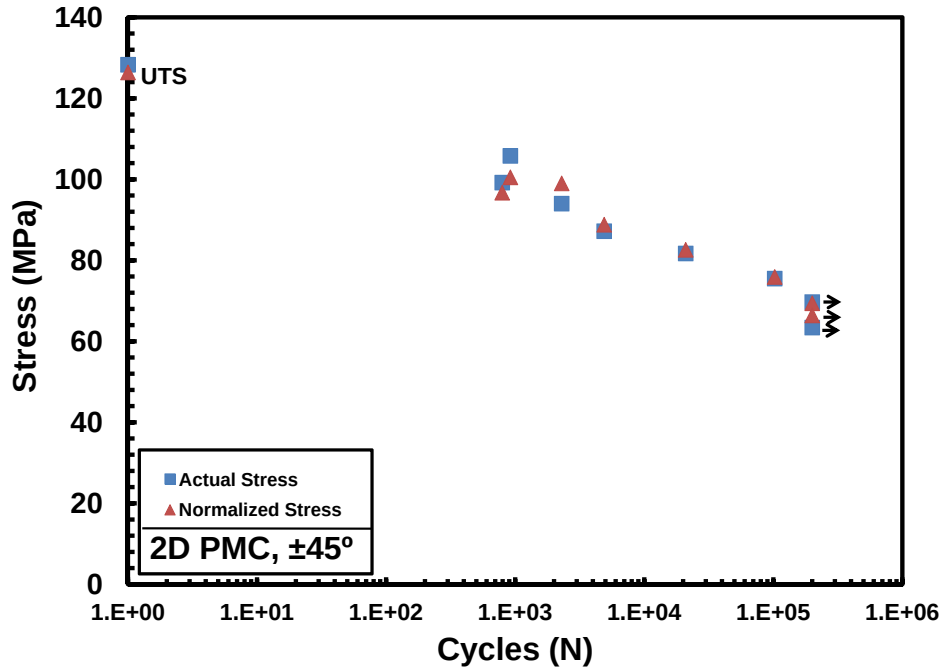

Figure 118: *S*-*N* curve for the 2D PMC with both ±45° fiber orientation comparing actual and normalized stresses at elevated temperature. Arrow indicates specimen achieved fatigue run-out.

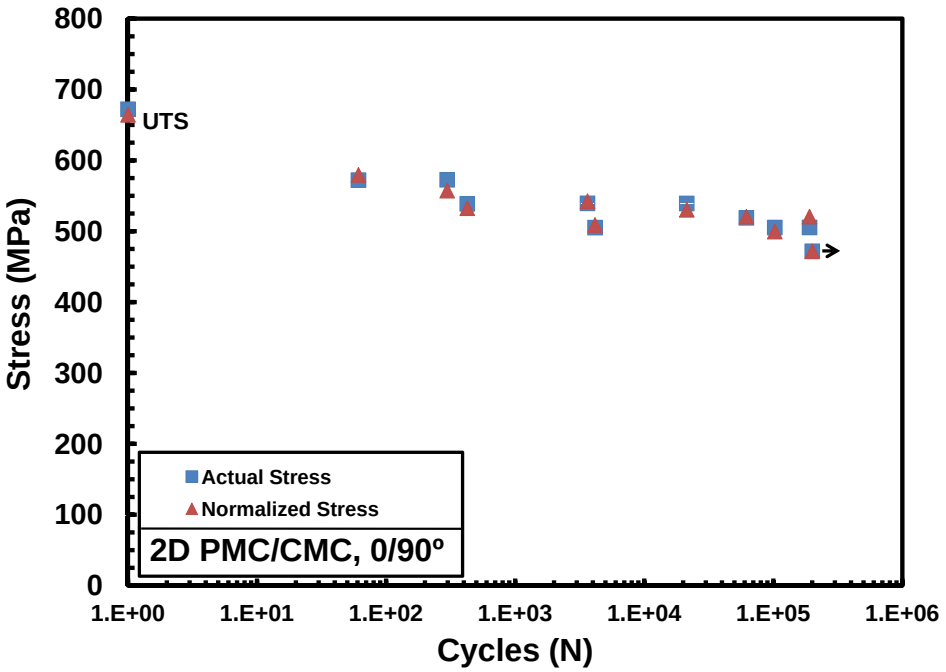

Figure 119: *S*-*N* curve for the 2D PMC/CMC with both 0/90° fiber orientation comparing actual and normalized stresses at elevated temperature. Arrow indicates specimen achieved fatigue run-out.

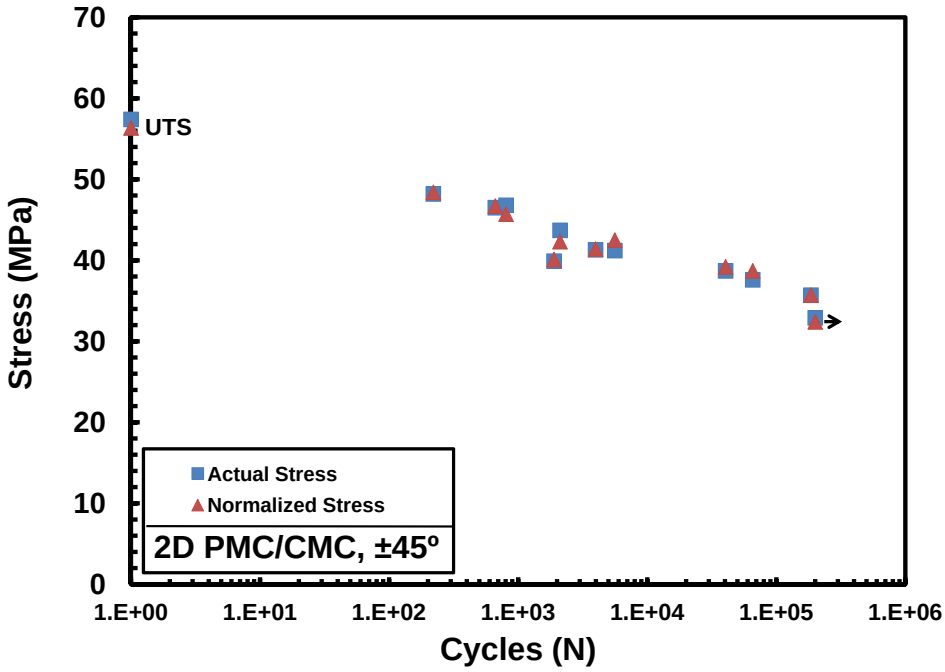

Figure 120: *S*-*N* curve for the 2D PMC/CMC with both ±45° fiber orientation comparing actual and normalized stresses at elevated temperature. Arrow indicates specimen achieved fatigue run-out.

Stress-strain hysteresis response for all remaining 3D PMC specimens are given in Figures 121 – 138.

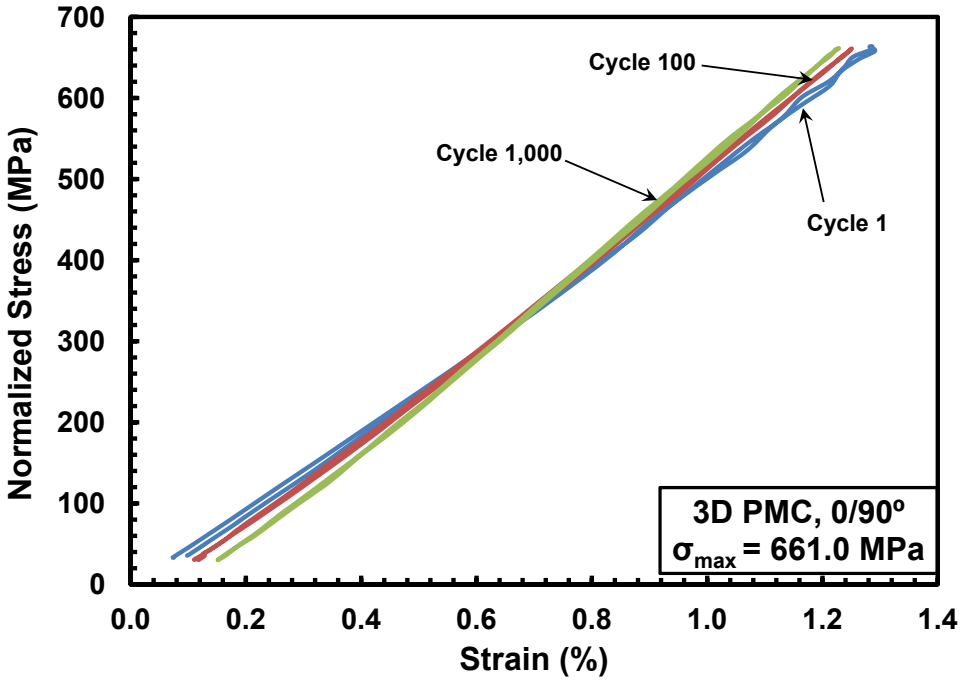

Figure 121: Evolution of stress-strain hysteresis response with fatigue cycles for specimen T3-18 of the 3D PMC with 0/90° fiber orientation at elevated temperature.

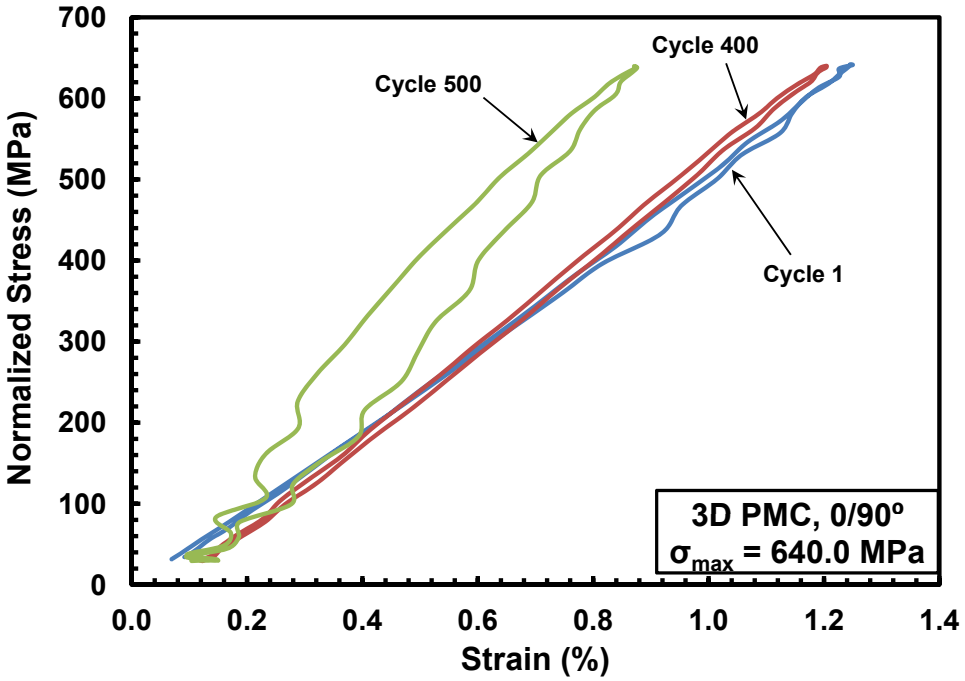

Figure 122: Evolution of stress-strain hysteresis response with fatigue cycles for specimen T3-17 of the 3D PMC with 0/90° fiber orientation at elevated temperature.

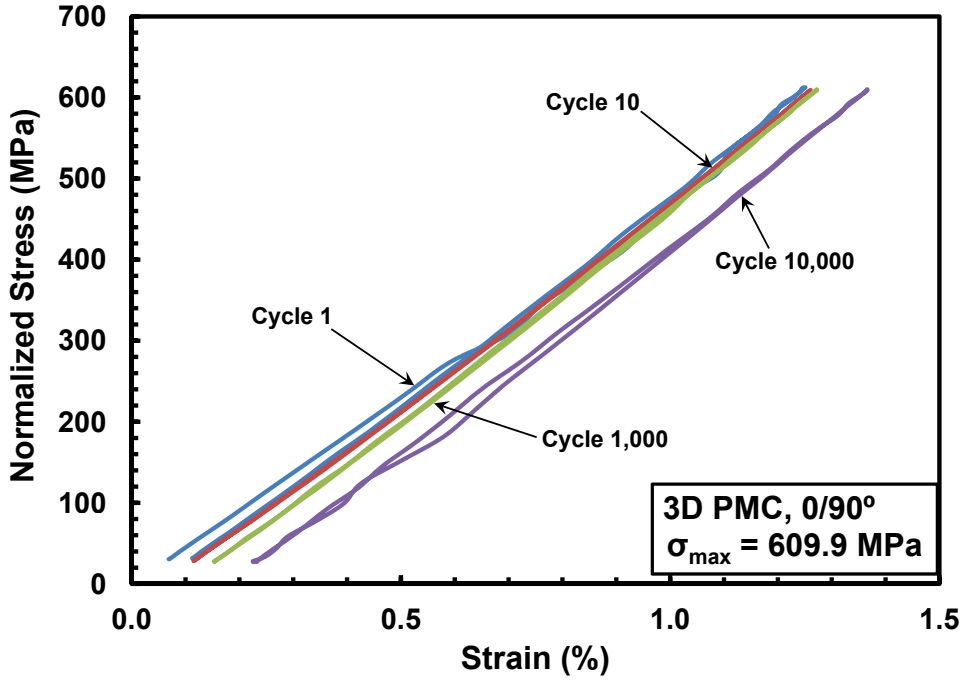

Figure 123: Evolution of stress-strain hysteresis response with fatigue cycles for specimen T3-15 of the 3D PMC with 0/90° fiber orientation at elevated temperature.

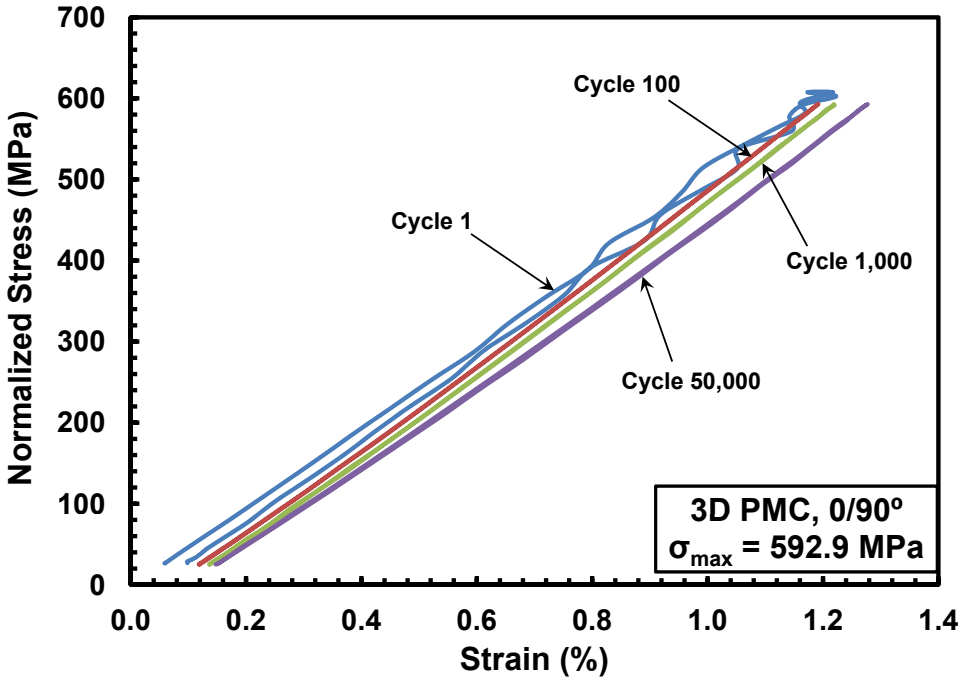

Figure 124: Evolution of stress-strain hysteresis response with fatigue cycles for specimen T3-19 of the 3D PMC with 0/90° fiber orientation at elevated temperature.

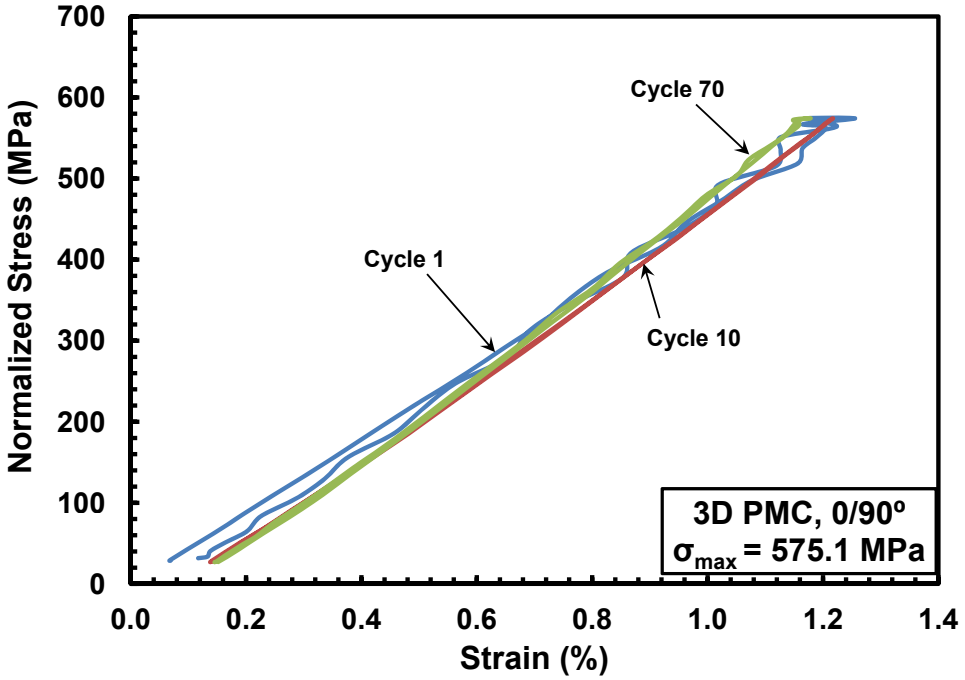

Figure 125: Evolution of stress-strain hysteresis response with fatigue cycles for specimen T3-11 of the 3D PMC with 0/90° fiber orientation at elevated temperature.

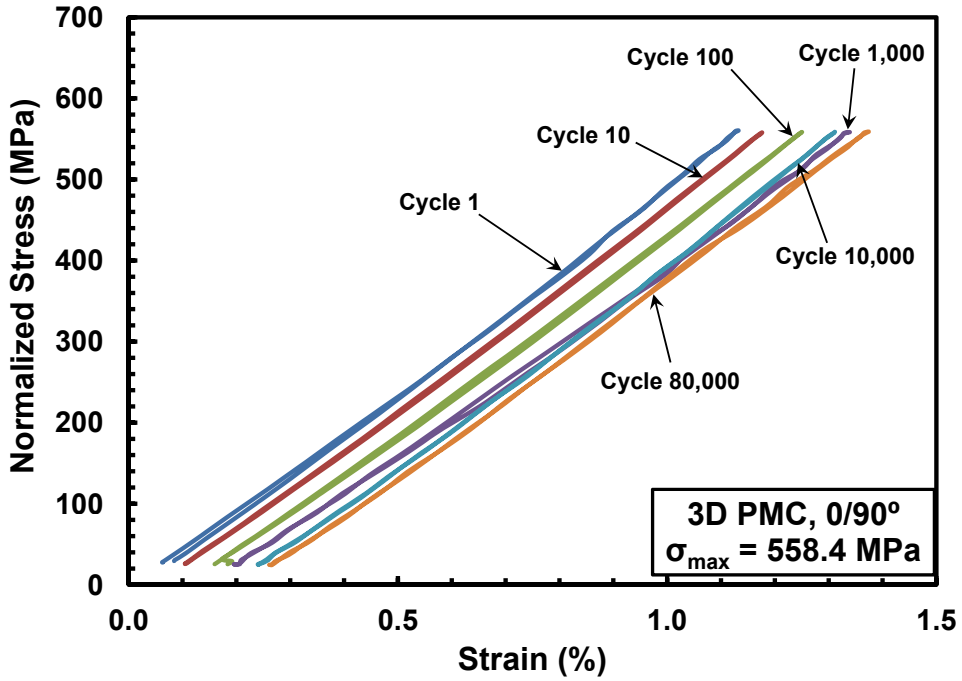

Figure 126: Evolution of stress-strain hysteresis response with fatigue cycles for specimen T3-14 of the 3D PMC with 0/90° fiber orientation at elevated temperature.

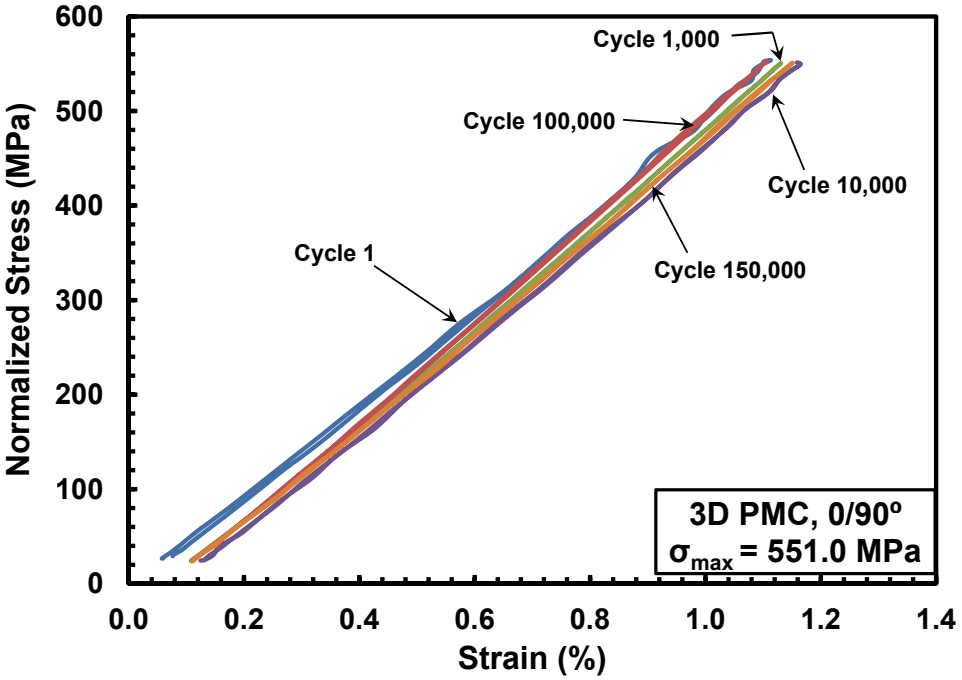

Figure 127: Evolution of stress-strain hysteresis response with fatigue cycles for specimen T3-12 of the 3D PMC with 0/90° fiber orientation at elevated temperature.

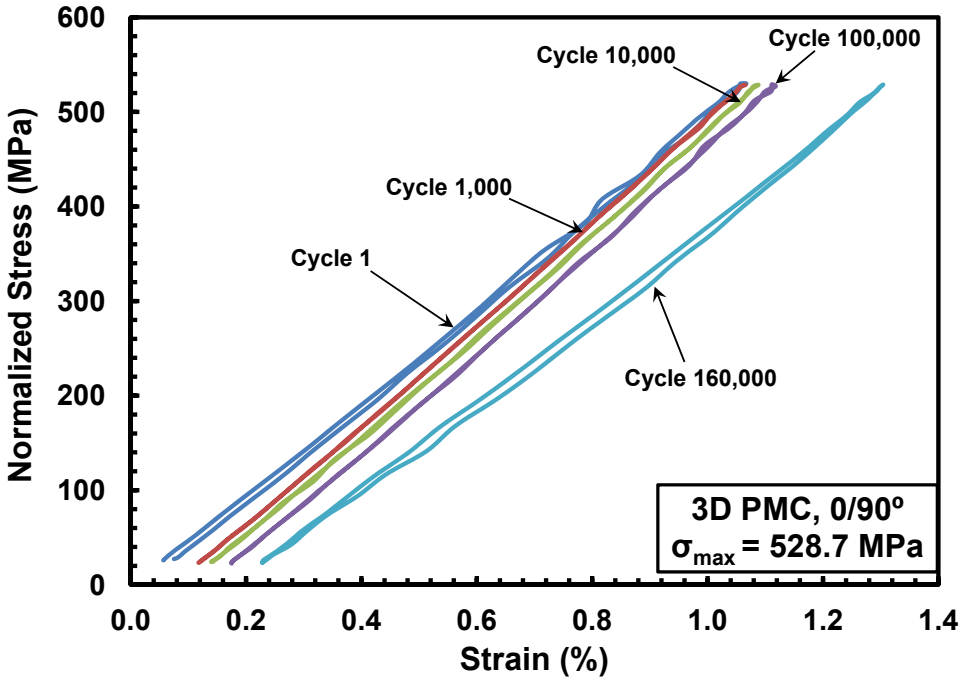

Figure 128: Evolution of stress-strain hysteresis response with fatigue cycles for specimen T3-13 of the 3D PMC with 0/90° fiber orientation at elevated temperature.

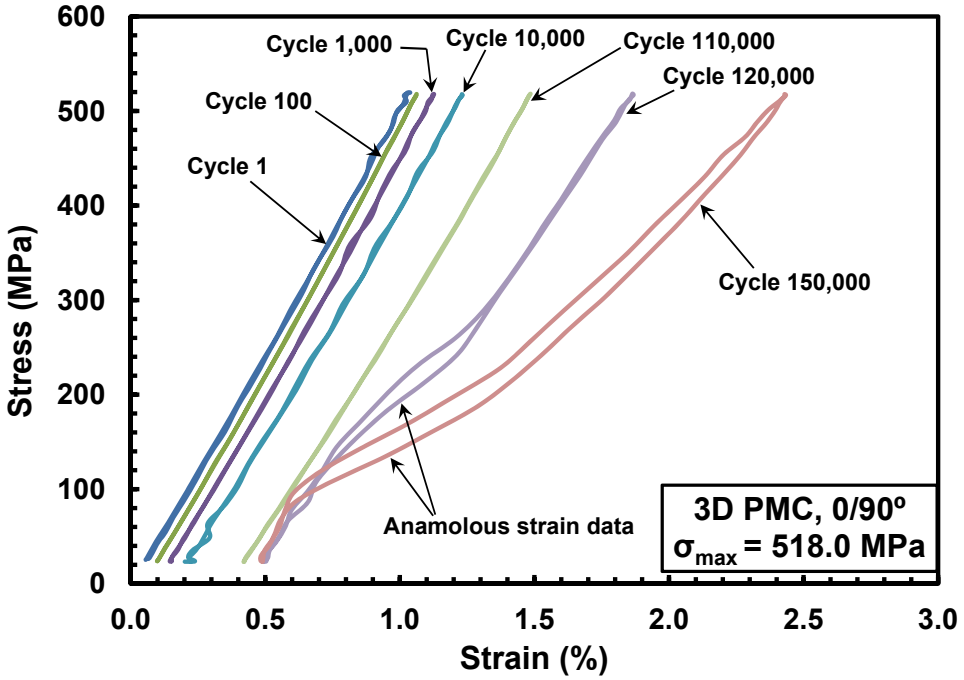

Figure 129: Evolution of stress-strain hysteresis response with fatigue cycles for specimen T3-9 of the 3D PMC with 0/90° fiber orientation at elevated temperature.

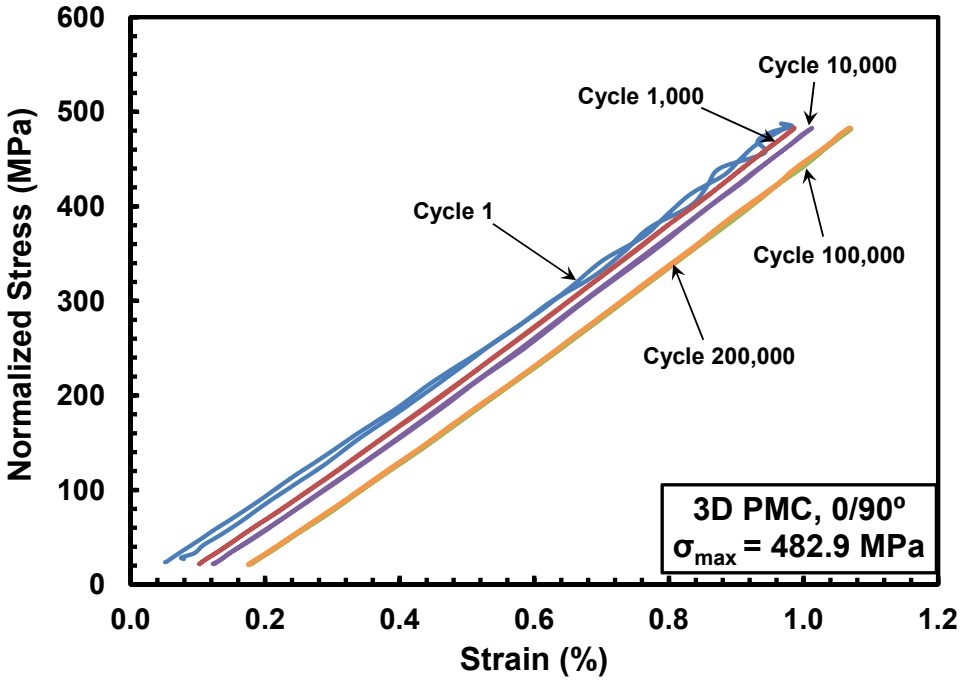

Figure 130: Evolution of stress-strain hysteresis response with fatigue cycles for specimen T3-10 of the 3D PMC with 0/90° fiber orientation at elevated temperature.

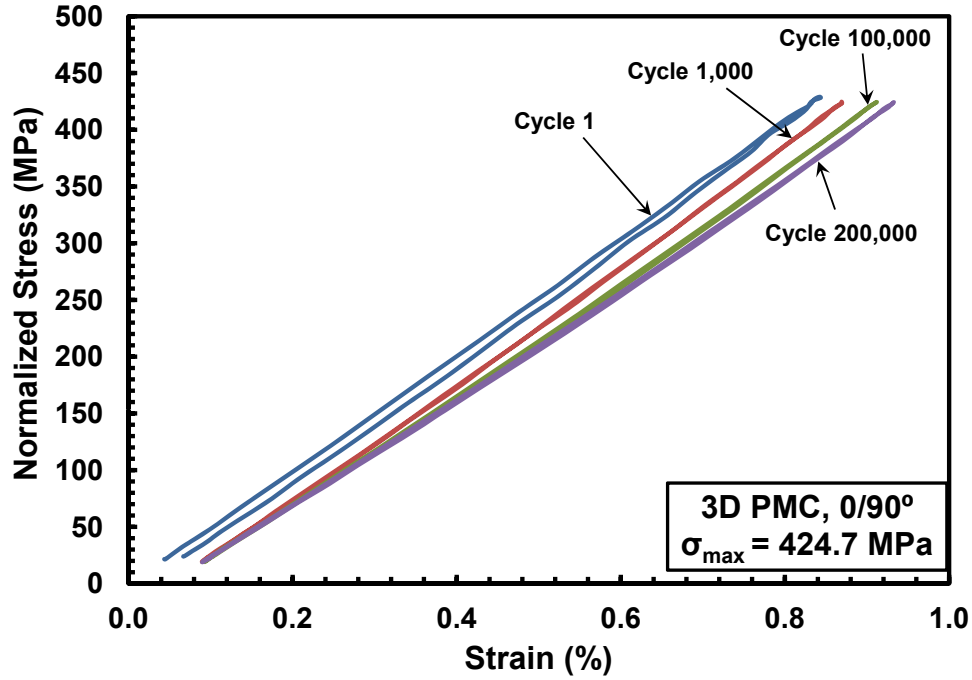

Figure 131: Evolution of stress-strain hysteresis response with fatigue cycles for specimen T3-7 of the 3D PMC with 0/90° fiber orientation at elevated temperature.

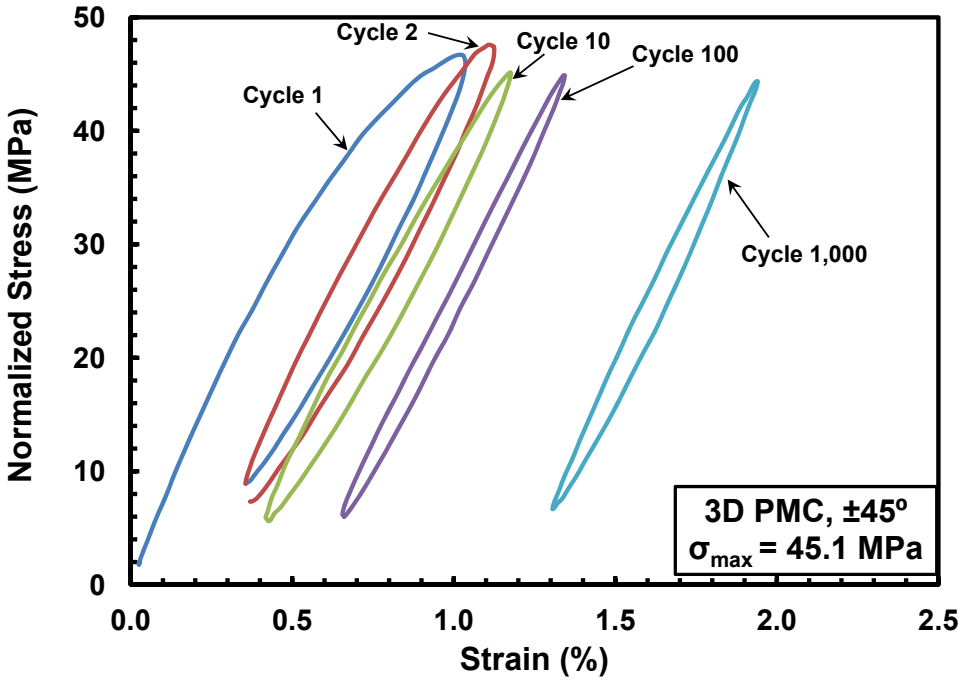

Figure 132: Evolution of stress-strain hysteresis response with fatigue cycles for specimen T4-7 of the 3D PMC with ±45° fiber orientation at elevated temperature.

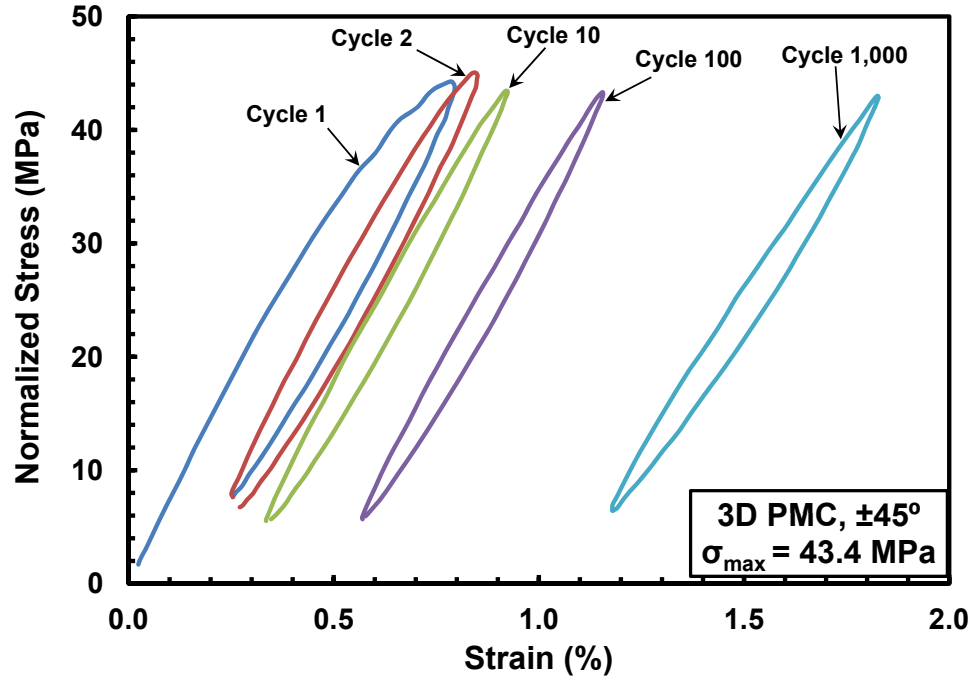

Figure 133: Evolution of stress-strain hysteresis response with fatigue cycles for specimen T4-5 of the 3D PMC with ±45° fiber orientation at elevated temperature.

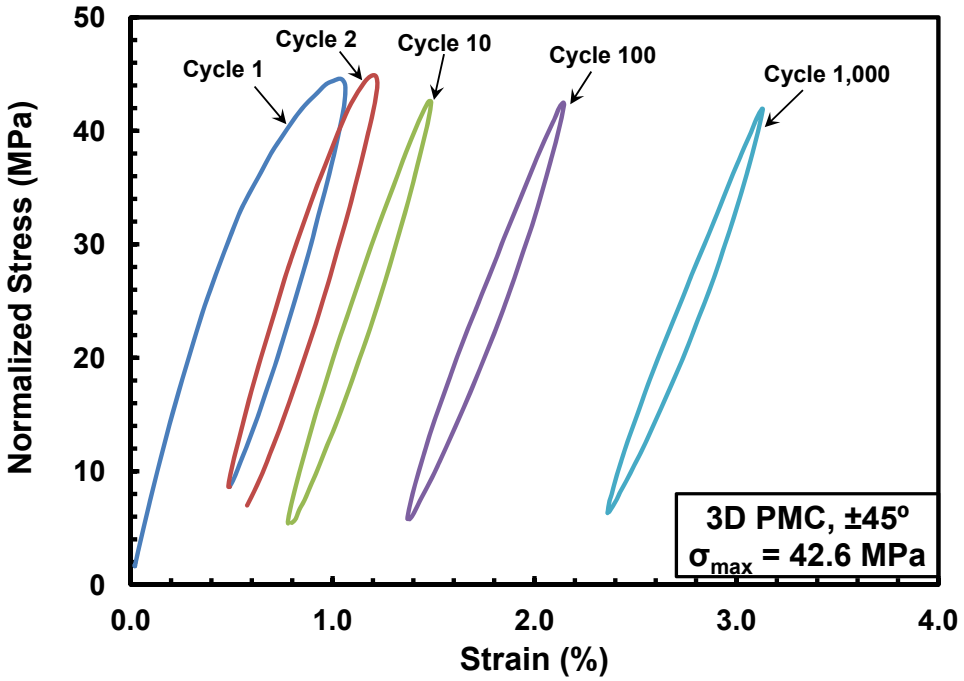

Figure 134: Evolution of stress-strain hysteresis response with fatigue cycles for specimen T4-6 of the 3D PMC with ±45° fiber orientation at elevated temperature.

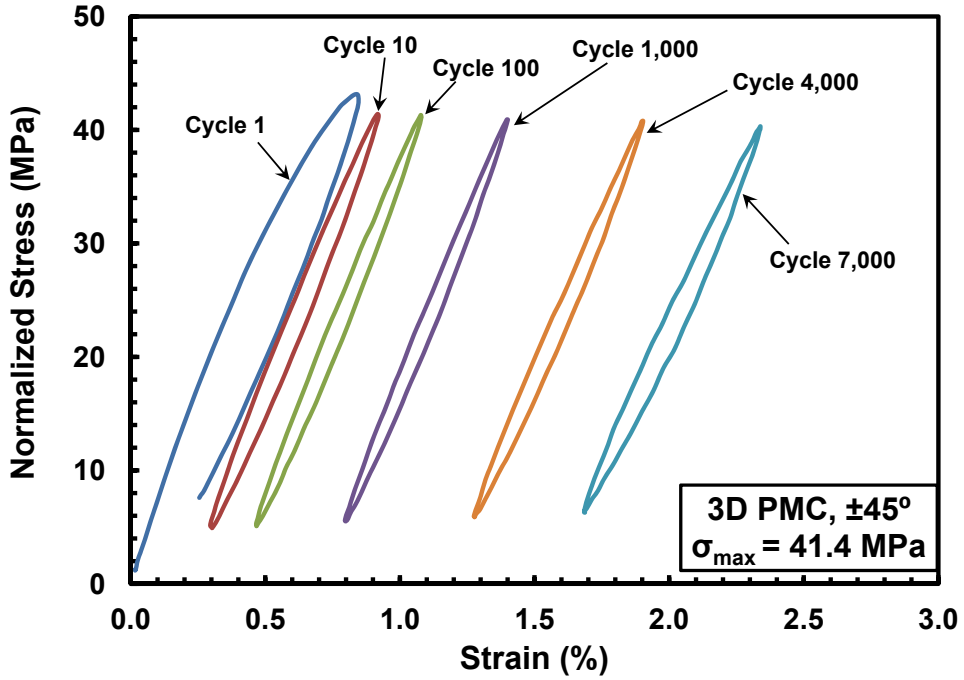

Figure 135: Evolution of stress-strain hysteresis response with fatigue cycles for specimen T4-9 of the 3D PMC with ±45° fiber orientation at elevated temperature.

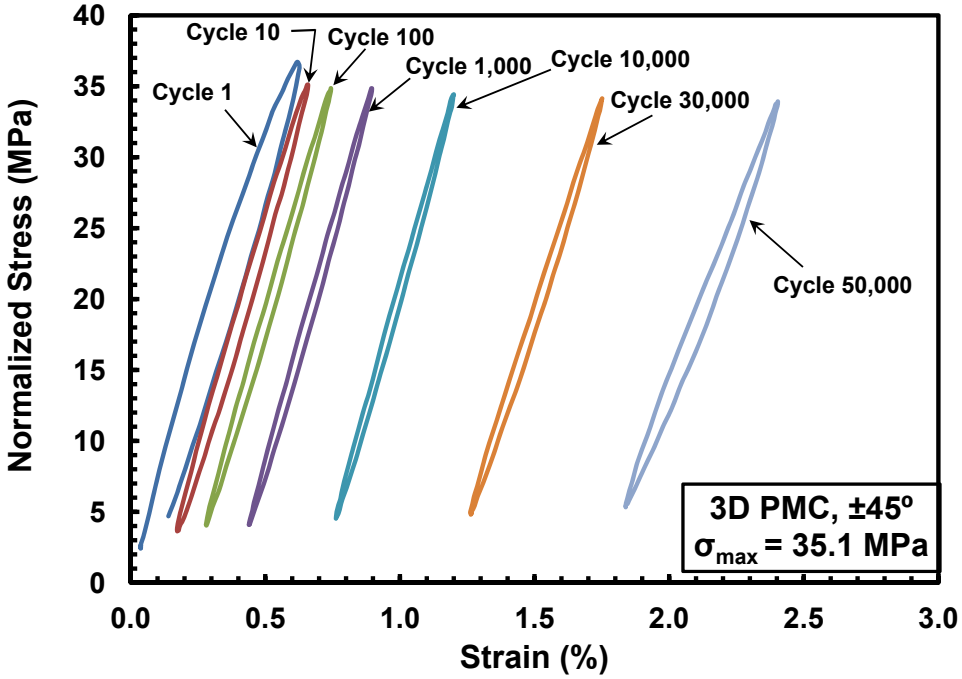

Figure 136: Evolution of stress-strain hysteresis response with fatigue cycles for specimen T4-11 of the 3D PMC with ±45° fiber orientation at elevated temperature.

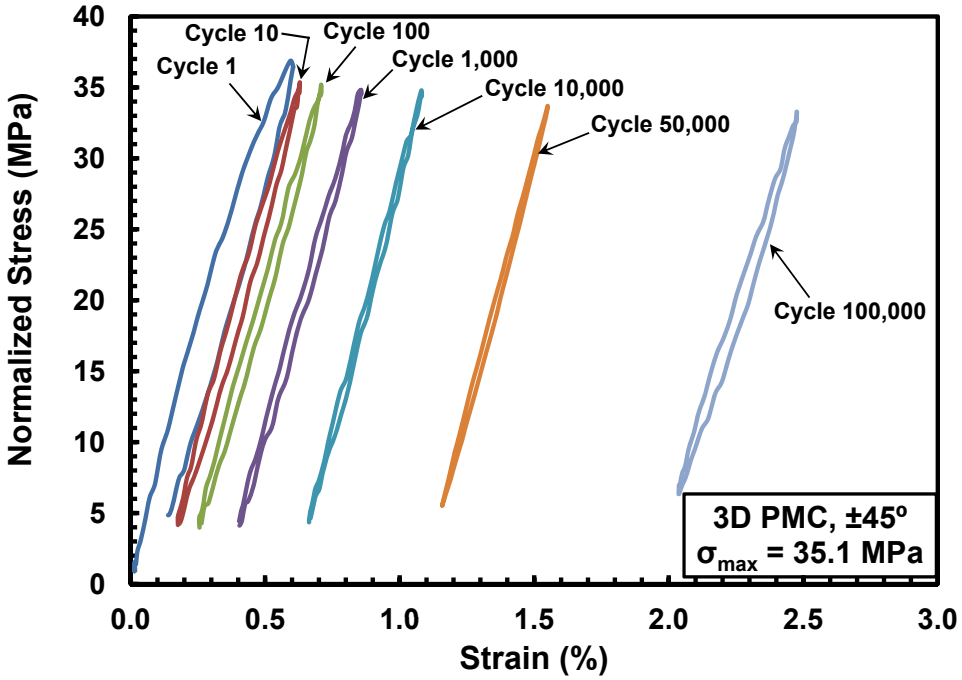

Figure 137: Evolution of stress-strain hysteresis response with fatigue cycles for specimen T4-8 of the 3D PMC with ±45° fiber orientation at elevated temperature.

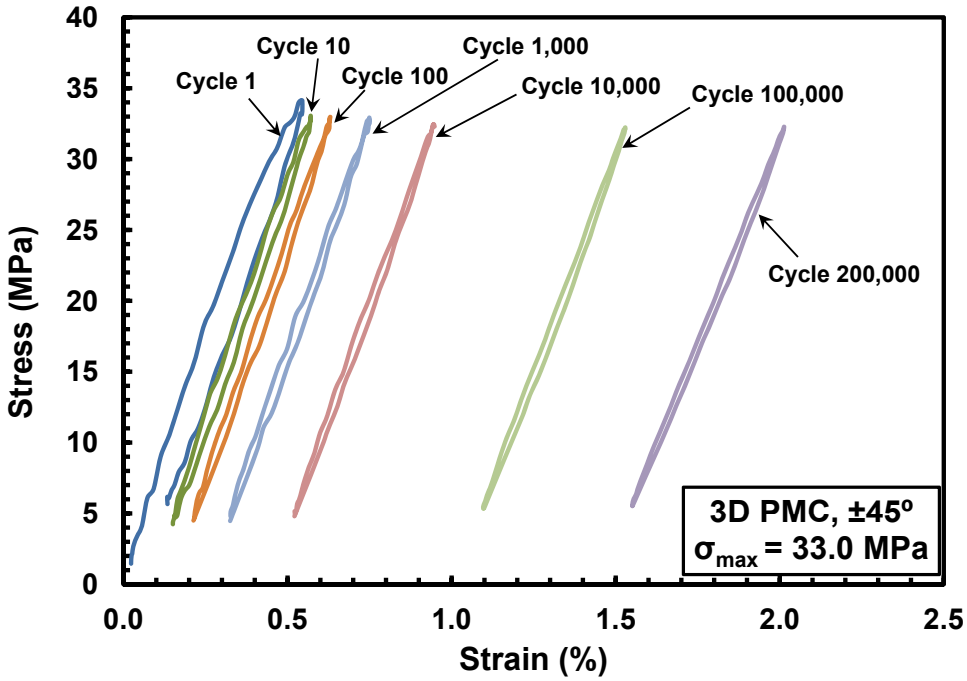

Figure 138: Evolution of stress-strain hysteresis response with fatigue cycles for specimen T4-3 of the 3D PMC with ±45° fiber orientation at elevated temperature.

Stress-strain hysteresis response for all remaining 2D PMC specimens are given in Figures 139 – 150.

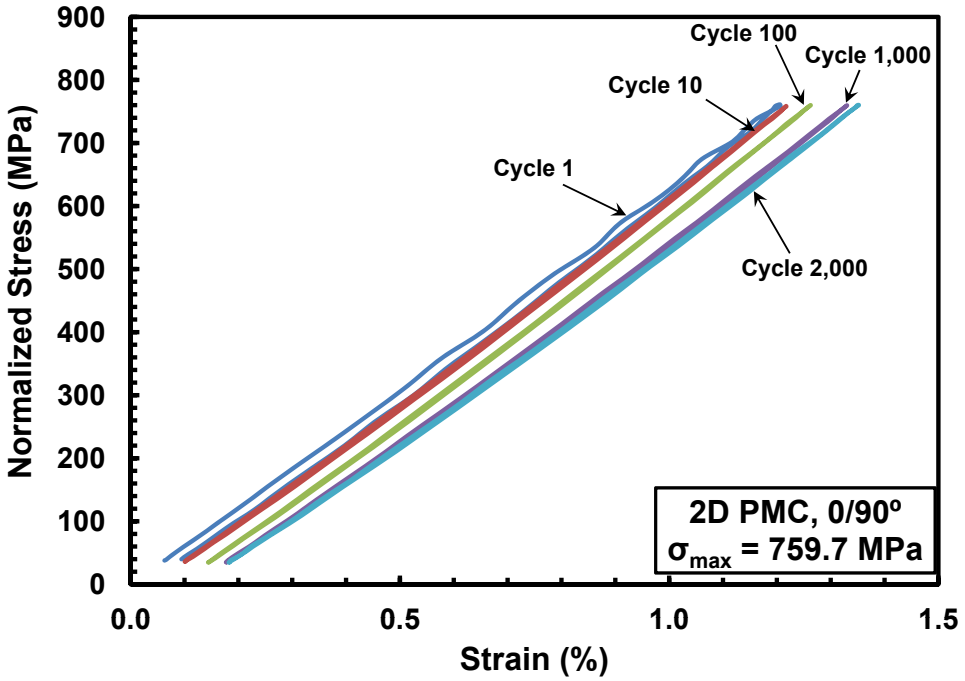

Figure 139: Evolution of stress-strain hysteresis response with fatigue cycles for specimen T1-5 of the 2D PMC with 0/90° fiber orientation at elevated temperature.

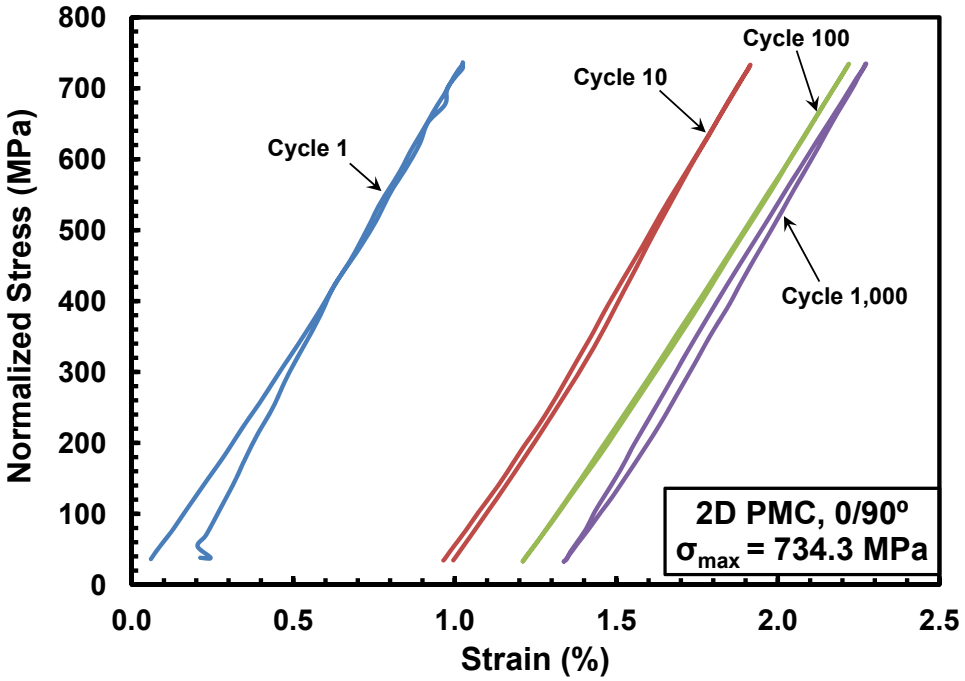

Figure 140: Evolution of stress-strain hysteresis response with fatigue cycles for specimen T1-12 of the 2D PMC with 0/90° fiber orientation at elevated temperature.

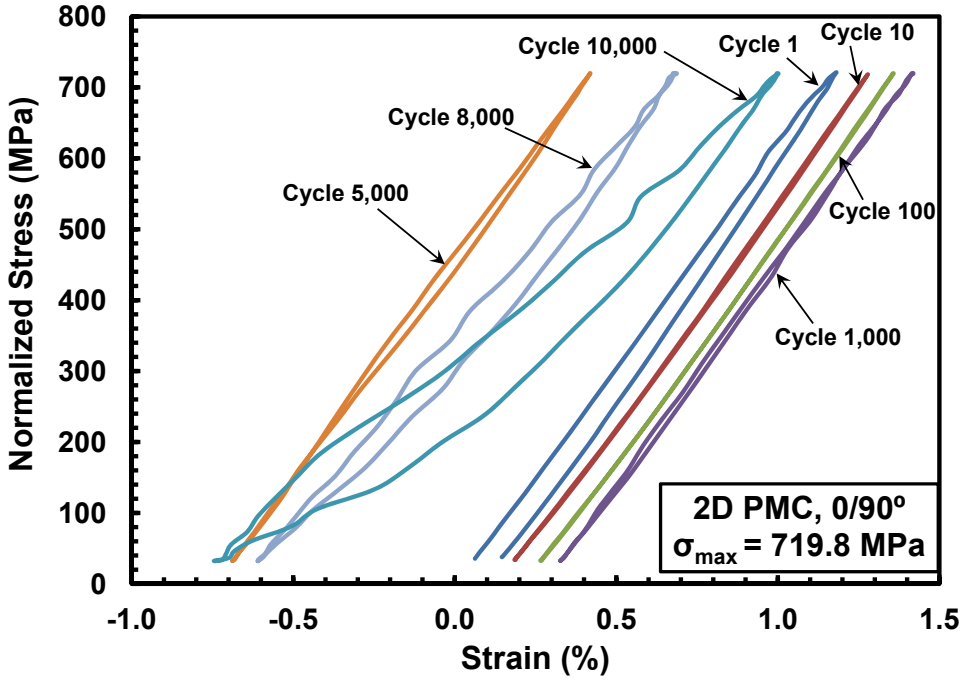

Figure 141: Evolution of stress-strain hysteresis response with fatigue cycles for specimen T1-11 of the 2D PMC with 0/90° fiber orientation at elevated temperature.

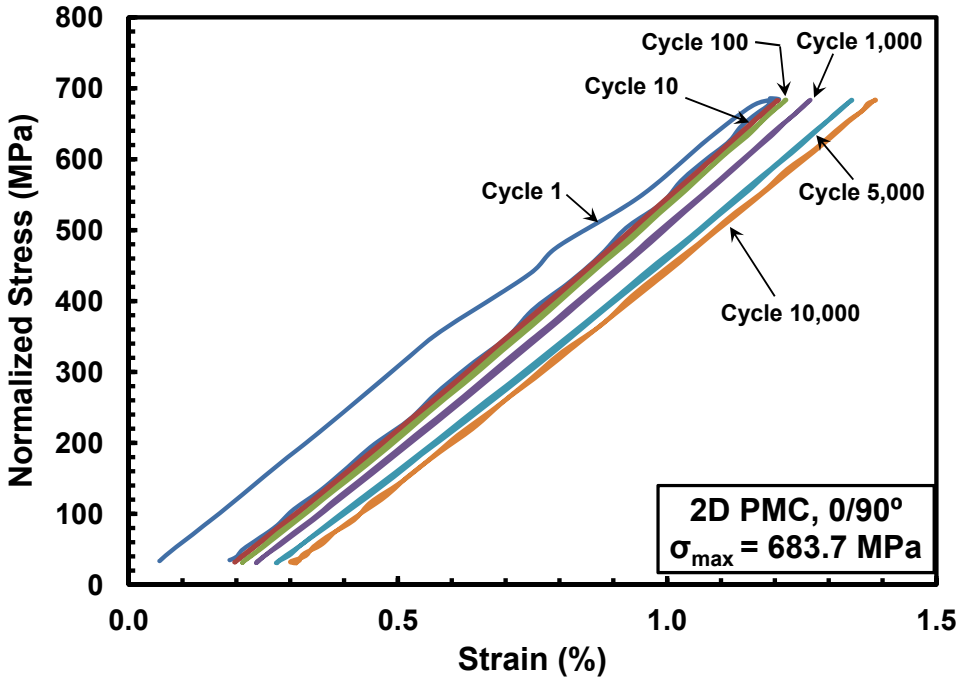

Figure 142: Evolution of stress-strain hysteresis response with fatigue cycles for specimen T1-8 of the 2D PMC with 0/90° fiber orientation at elevated temperature.

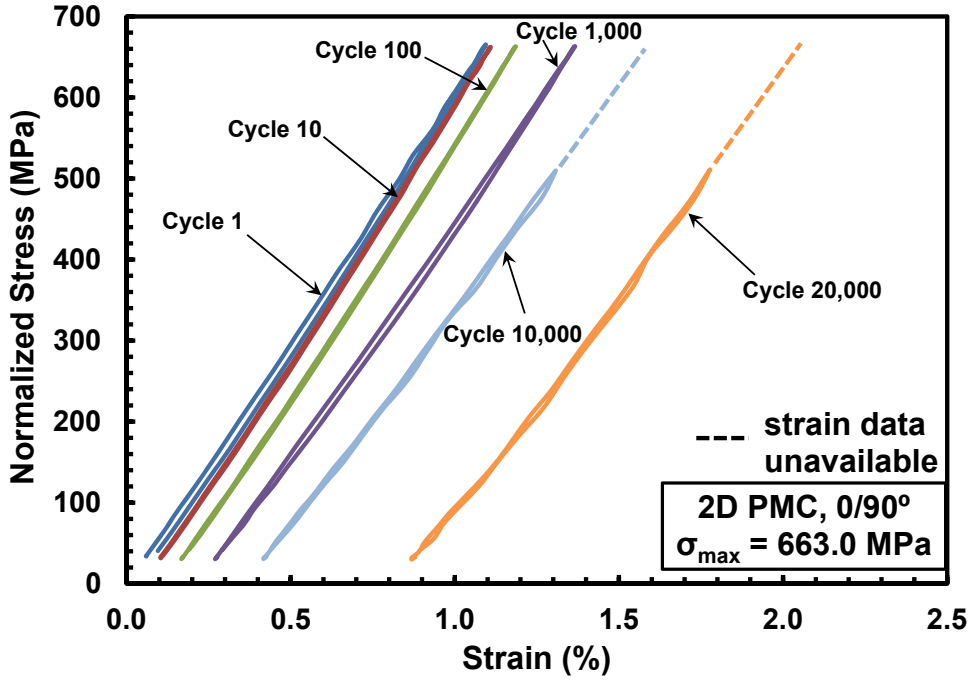

Figure 143: Evolution of stress-strain hysteresis response with fatigue cycles for specimen T1-3 of the 2D PMC with 0/90° fiber orientation at elevated temperature.

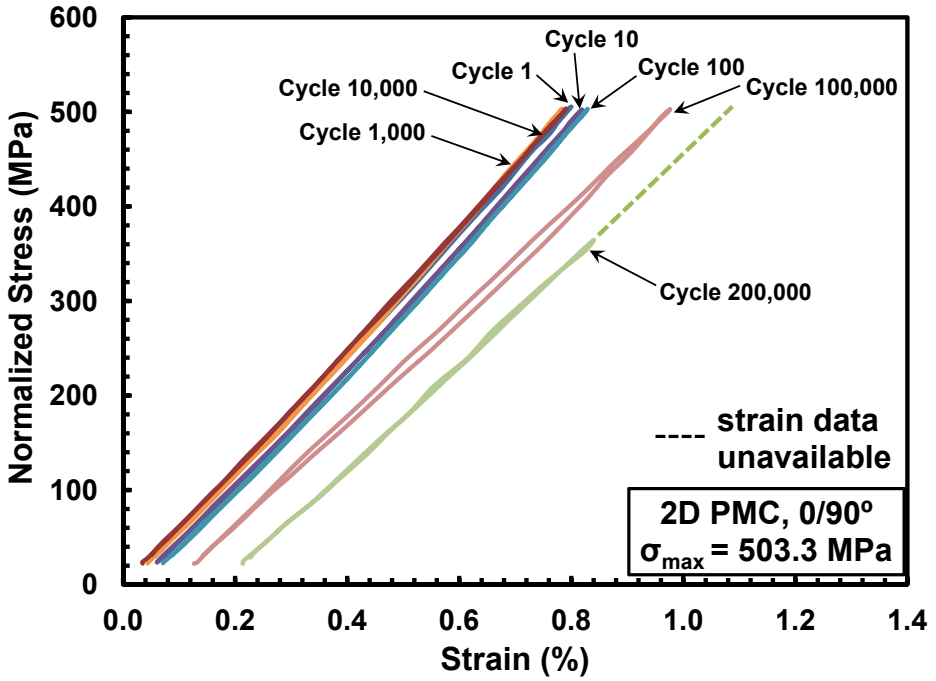

Figure 144: Evolution of stress-strain hysteresis response with fatigue cycles for specimen T1-4 of the 2D PMC with 0/90° fiber orientation at elevated temperature.

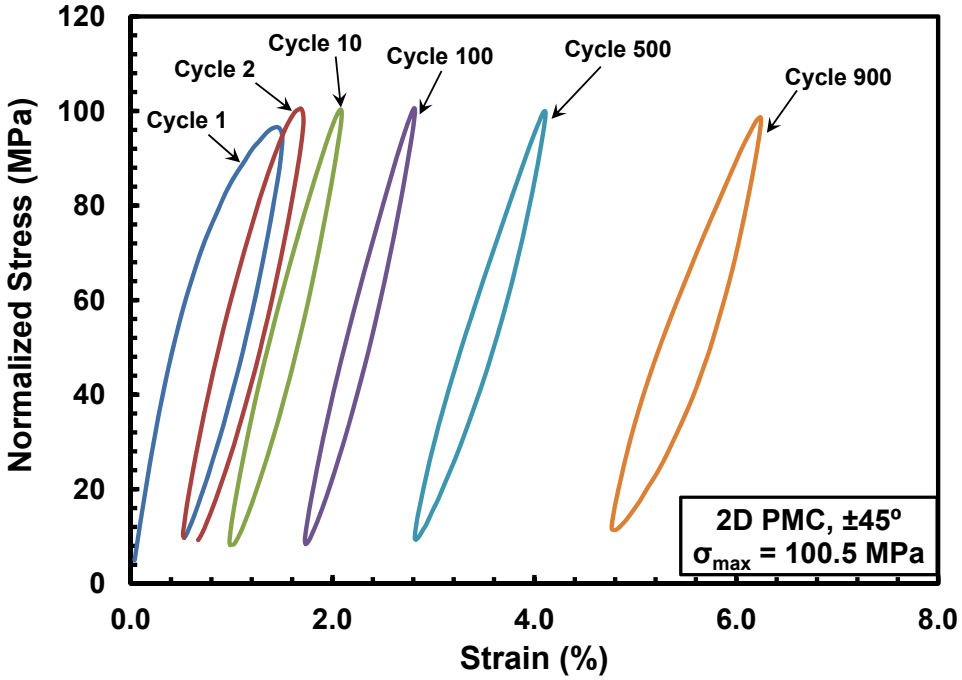

Figure 145: Evolution of stress-strain hysteresis response with fatigue cycles for specimen T2-8 of the 2D PMC with ±45° fiber orientation at elevated temperature.

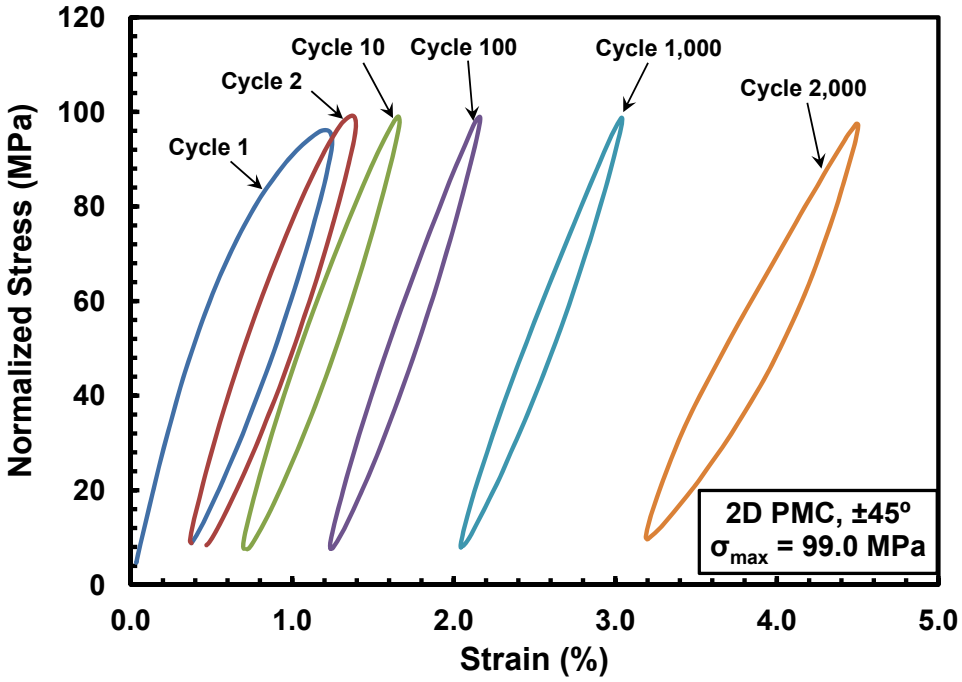

Figure 146: Evolution of stress-strain hysteresis response with fatigue cycles for specimen T2-7 of the 2D PMC with ±45° fiber orientation at elevated temperature.

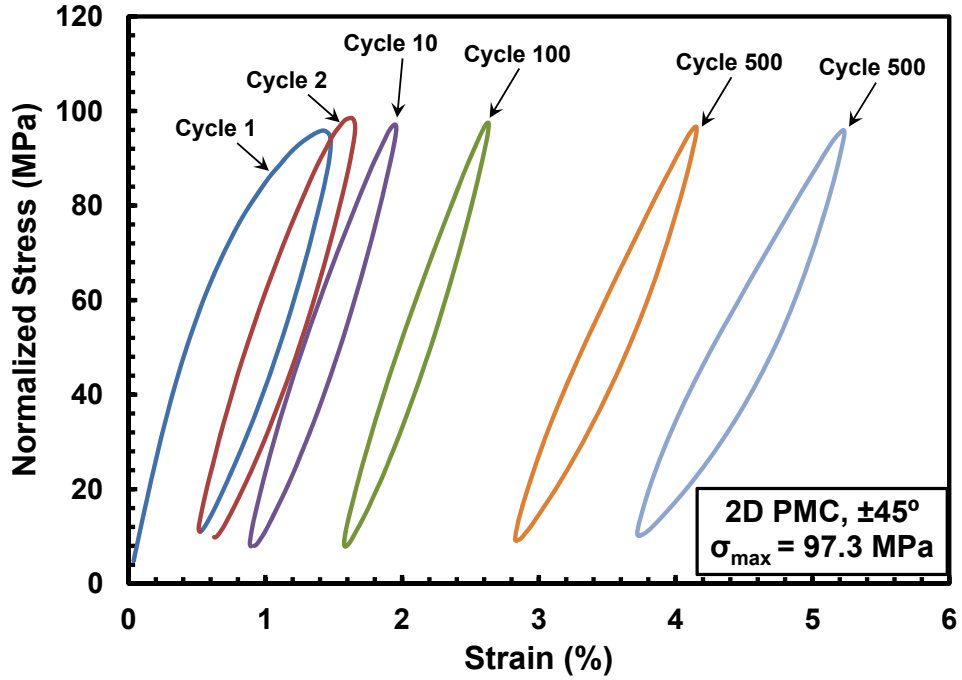

Figure 147: Evolution of stress-strain hysteresis response with fatigue cycles for specimen T2-4 of the 2D PMC with ±45° fiber orientation at elevated temperature.

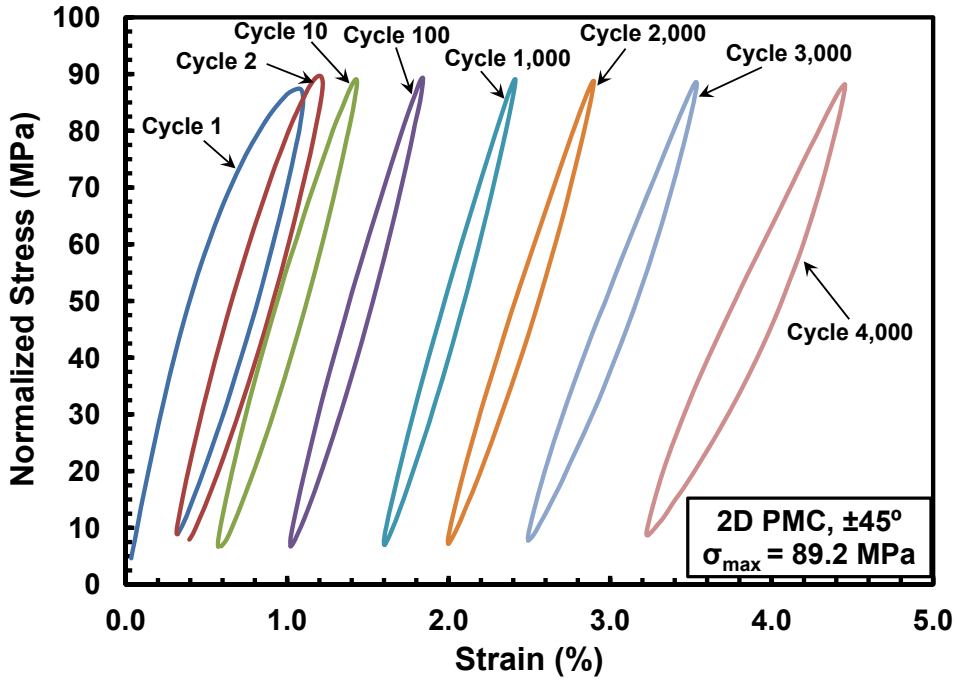

Figure 148: Evolution of stress-strain hysteresis response with fatigue cycles for specimen T2-6 of the 2D PMC with ±45° fiber orientation at elevated temperature.

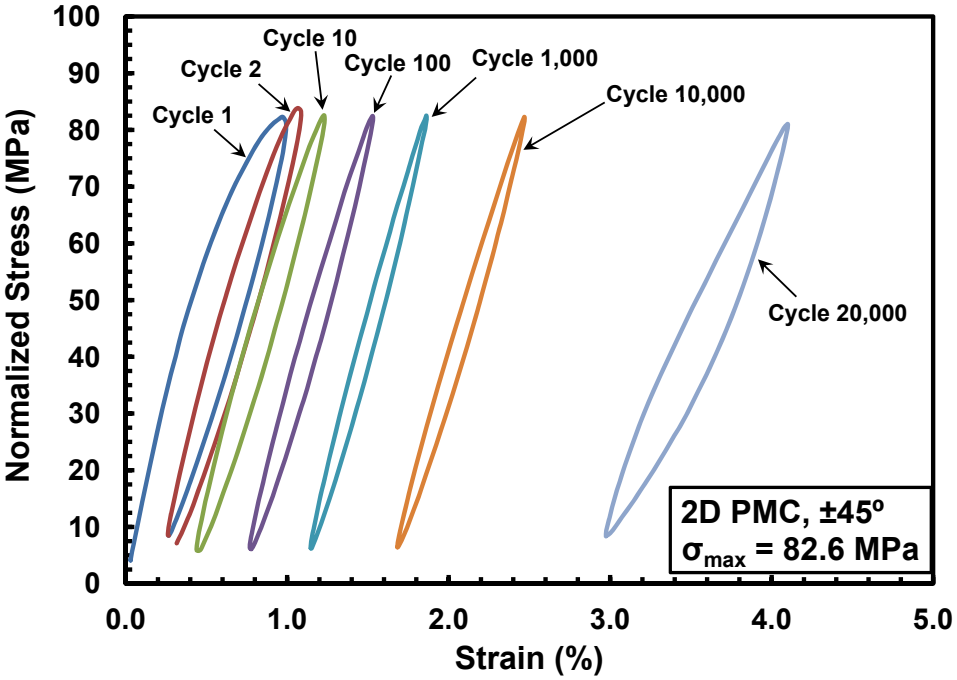

Figure 149: Evolution of stress-strain hysteresis response with fatigue cycles for specimen T2-9 of the 2D PMC with ±45° fiber orientation at elevated temperature.

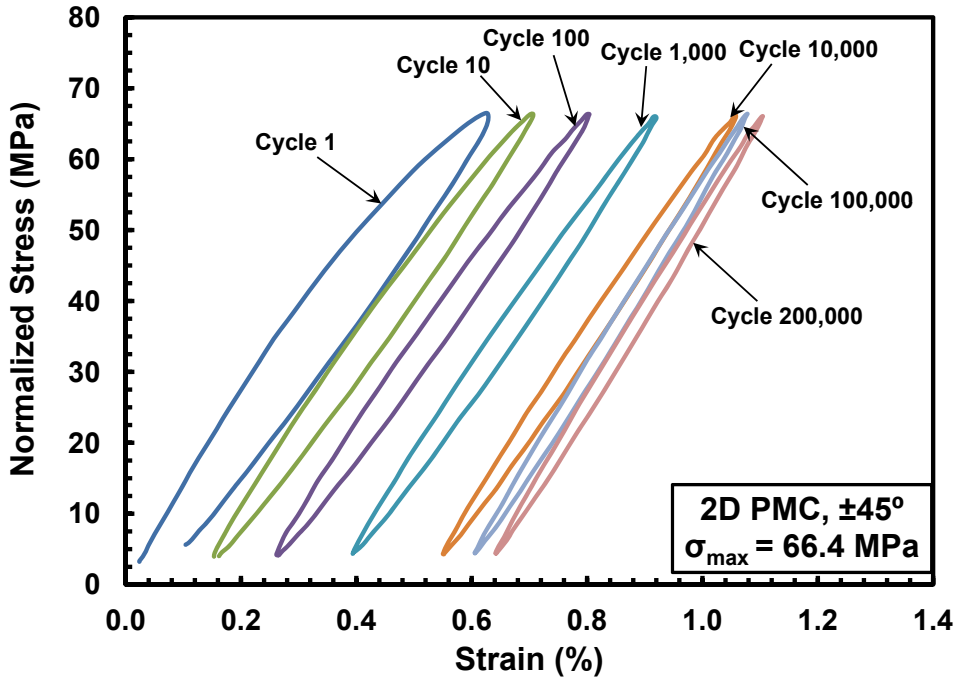

Figure 150: Evolution of stress-strain hysteresis response with fatigue cycles for specimen T2-5 of the 2D PMC with ±45° fiber orientation at elevated temperature.

Stress-strain hysteresis response for all remaining 2D unitized composite specimens are given in Figures 151 – 168.

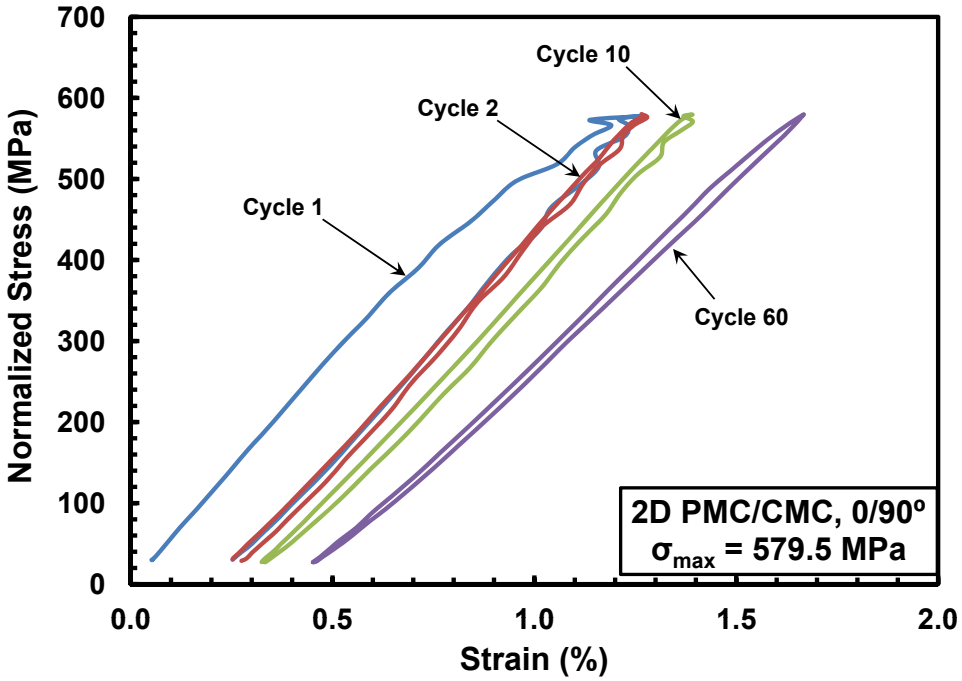

Figure 151: Evolution of stress-strain hysteresis response with fatigue cycles for specimen T5-18 of the 2D PMC/CMC with 0/90° fiber orientation at elevated temperature.

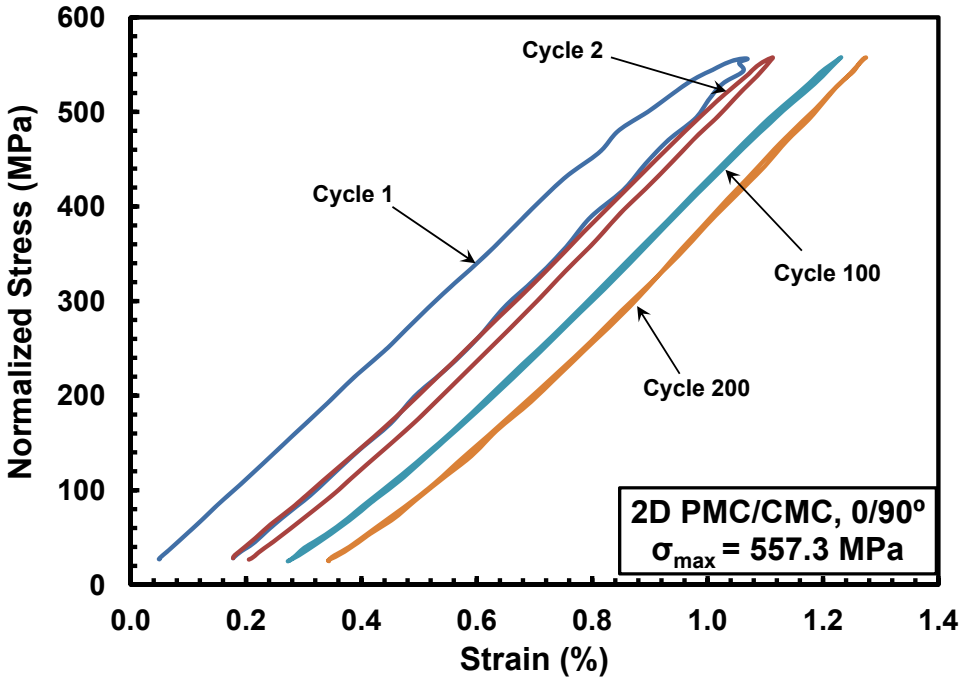

Figure 152: Evolution of stress-strain hysteresis response with fatigue cycles for specimen T5-16 of the 2D PMC/CMC with 0/90° fiber orientation at elevated temperature.

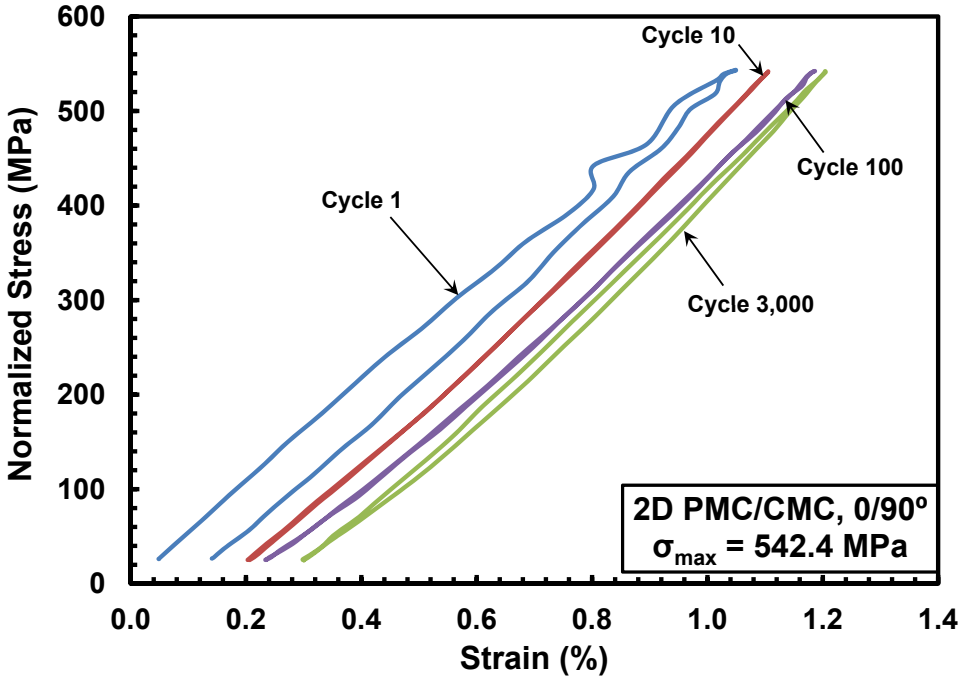

Figure 153: Evolution of stress-strain hysteresis response with fatigue cycles for specimen T5-10 of the 2D PMC/CMC with 0/90° fiber orientation at elevated temperature.

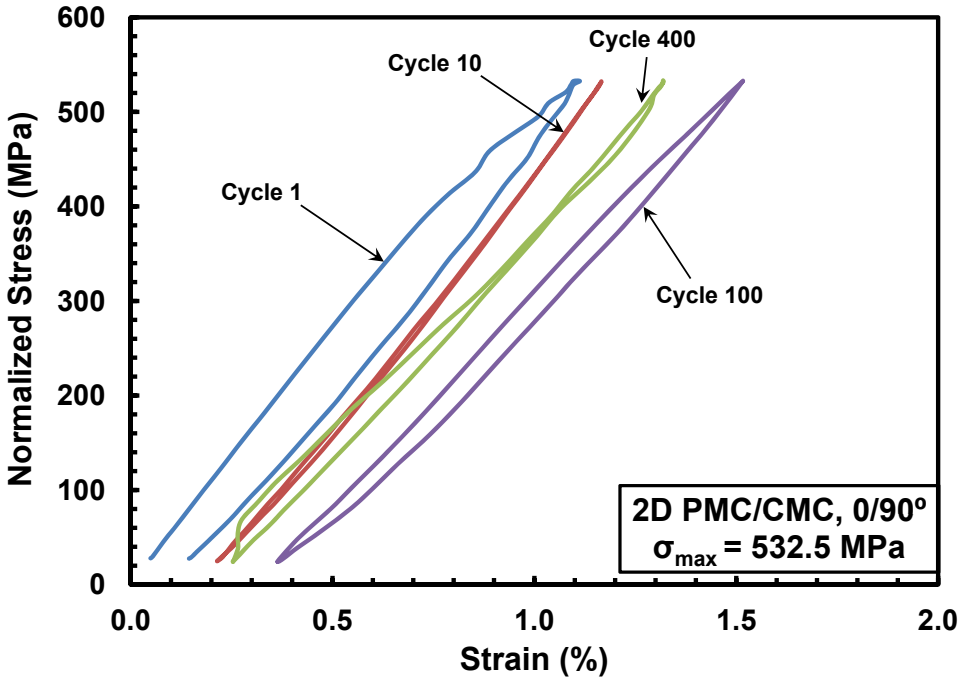

Figure 154: Evolution of stress-strain hysteresis response with fatigue cycles for specimen T5-13 of the 2D PMC/CMC with 0/90° fiber orientation at elevated temperature.

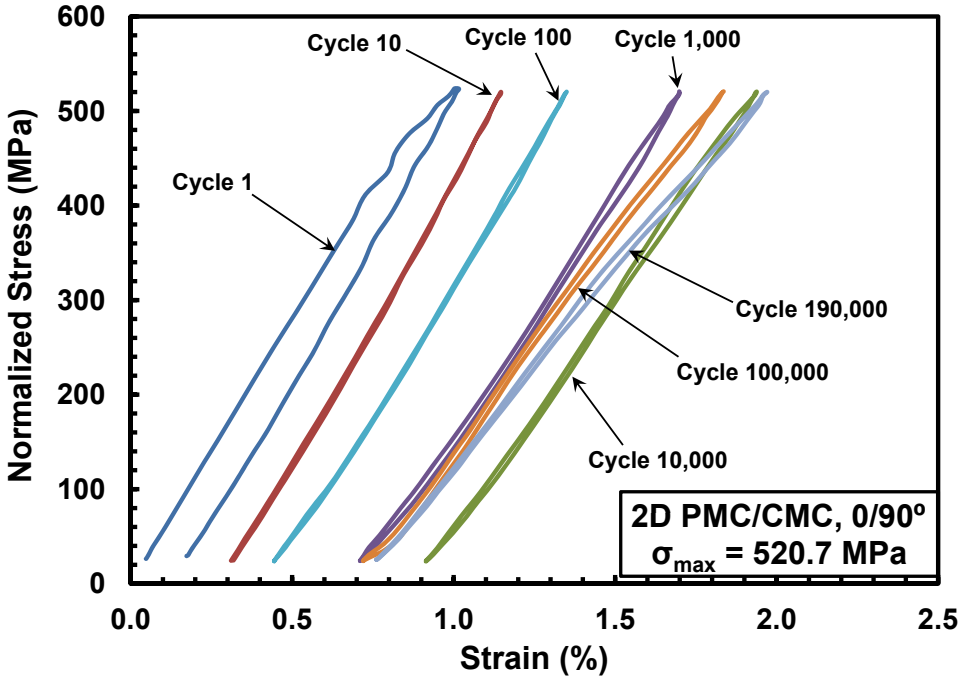

Figure 155: Evolution of stress-strain hysteresis response with fatigue cycles for specimen T5-14 of the 2D PMC/CMC with 0/90° fiber orientation at elevated temperature.

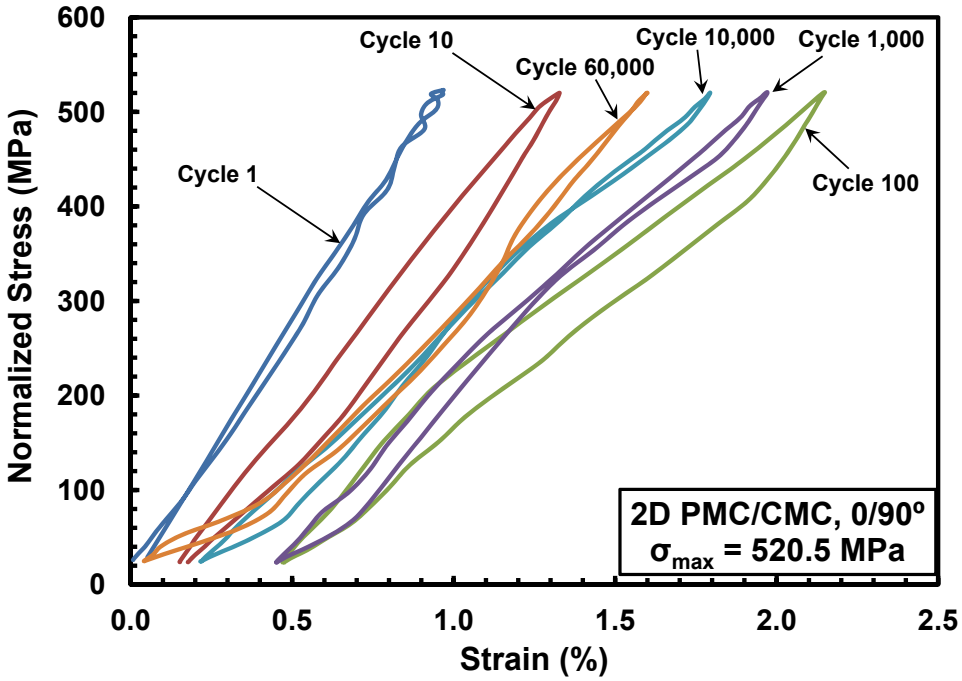

Figure 156: Evolution of stress-strain hysteresis response with fatigue cycles for specimen T5-17 of the 2D PMC/CMC with 0/90° fiber orientation at elevated temperature.

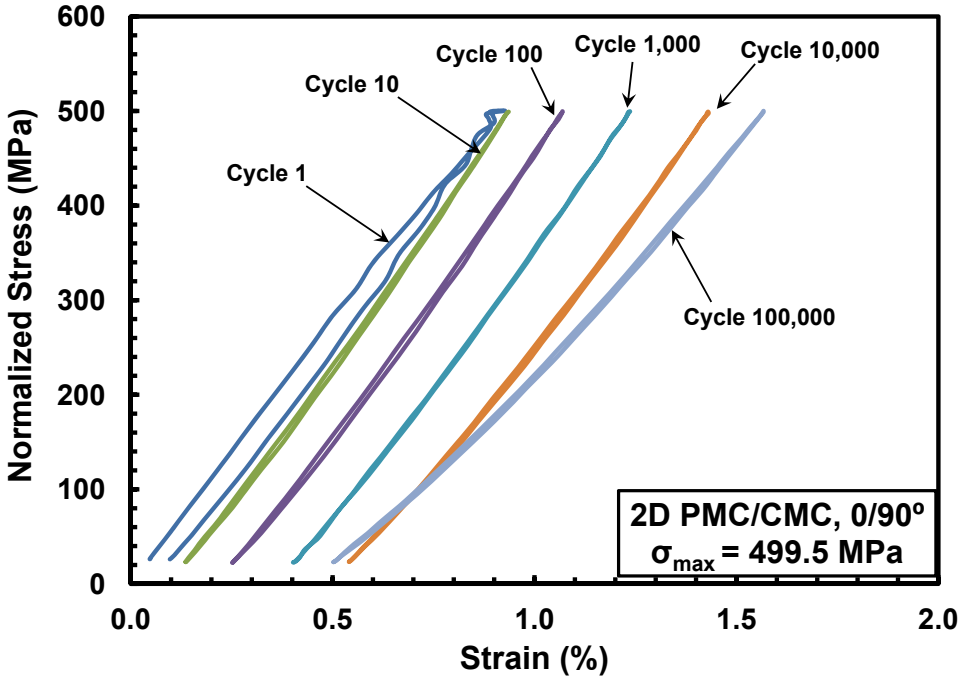

Figure 157: Evolution of stress-strain hysteresis response with fatigue cycles for specimen T5-11 of the 2D PMC/CMC with 0/90° fiber orientation at elevated temperature.

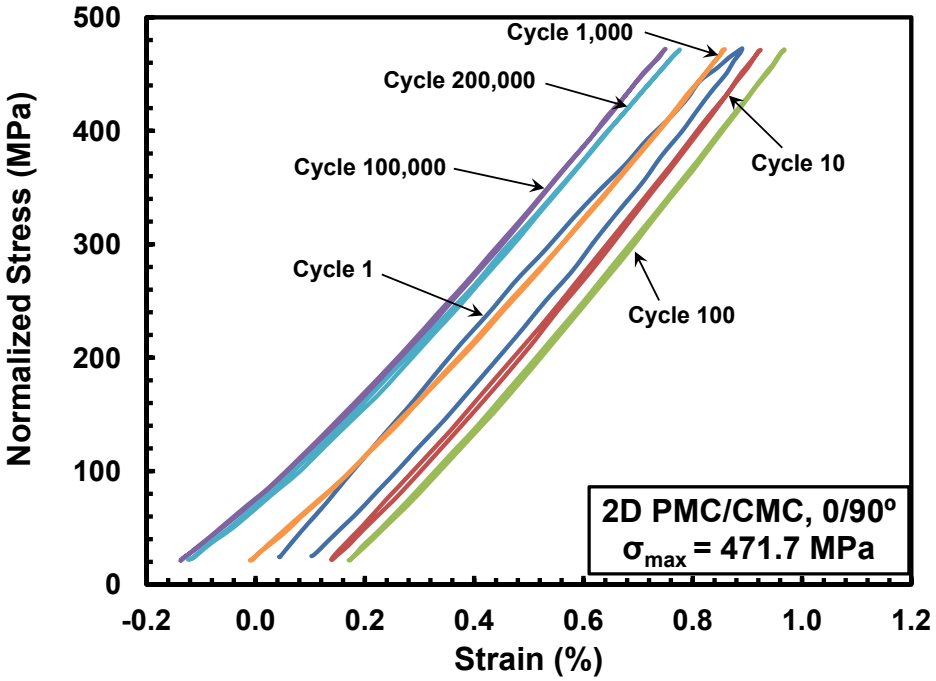

Figure 158: Evolution of stress-strain hysteresis response with fatigue cycles for specimen T5-7 of the 2D PMC/CMC with 0/90° fiber orientation at elevated temperature.

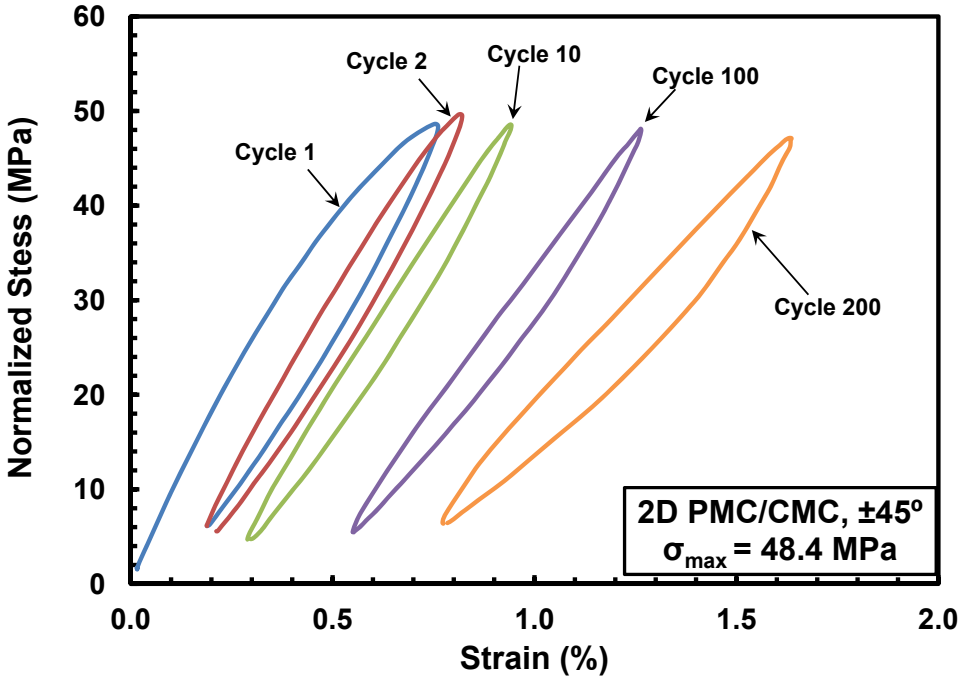

Figure 159: Evolution of stress-strain hysteresis response with fatigue cycles for specimen T6-14 of the 2D PMC/CMC with ±45° fiber orientation at elevated temperature.

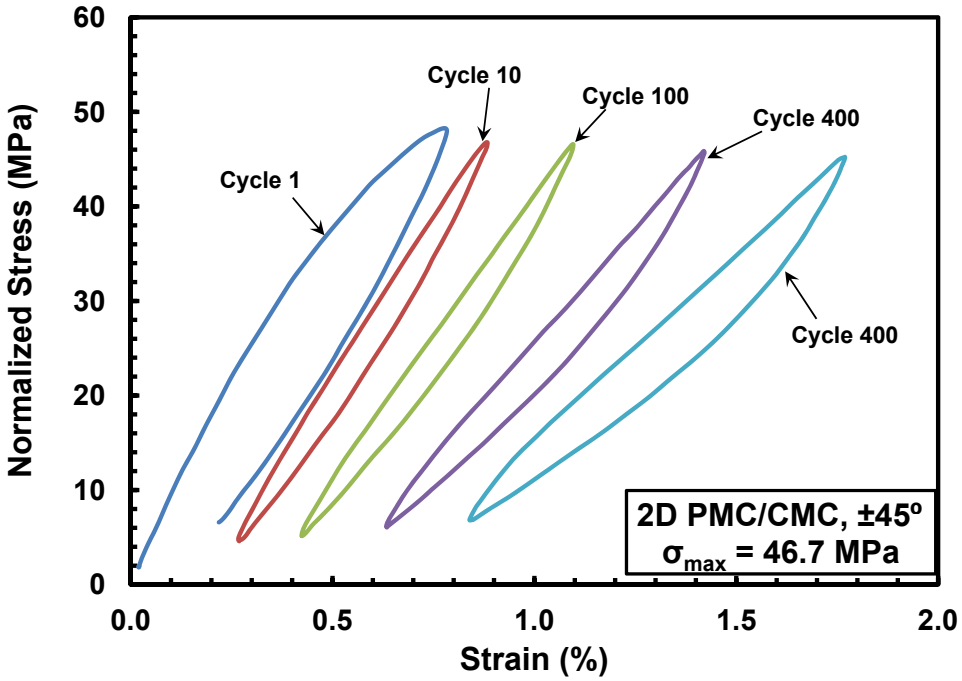

Figure 160: Evolution of stress-strain hysteresis response with fatigue cycles for specimen T6-12 of the 2D PMC/CMC with ±45° fiber orientation at elevated temperature.

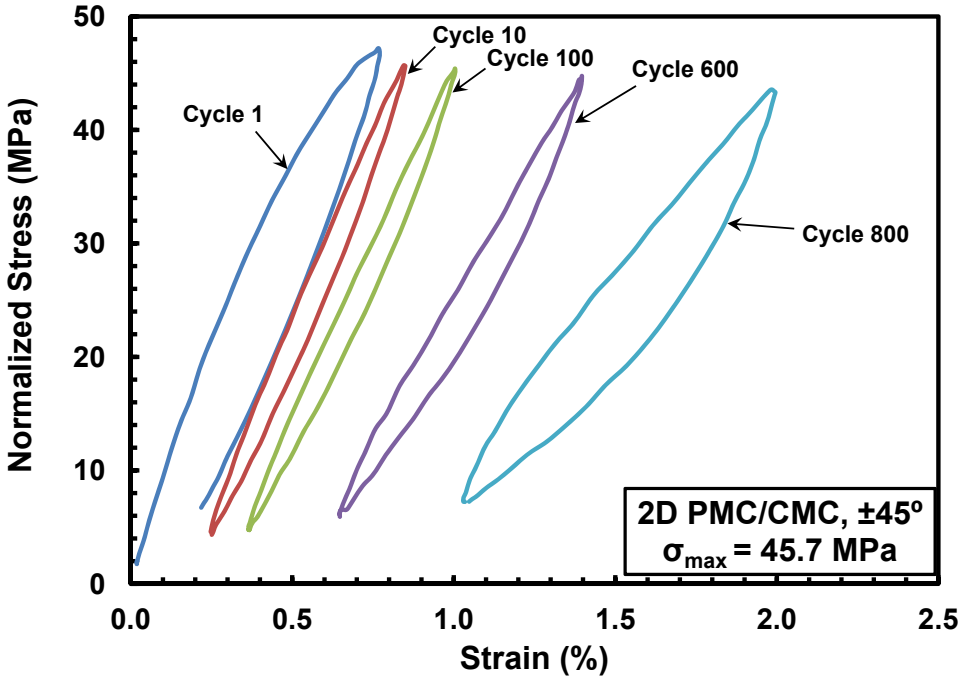

Figure 161: Evolution of stress-strain hysteresis response with fatigue cycles for specimen T6-6 of the 2D PMC/CMC with ±45° fiber orientation at elevated temperature.

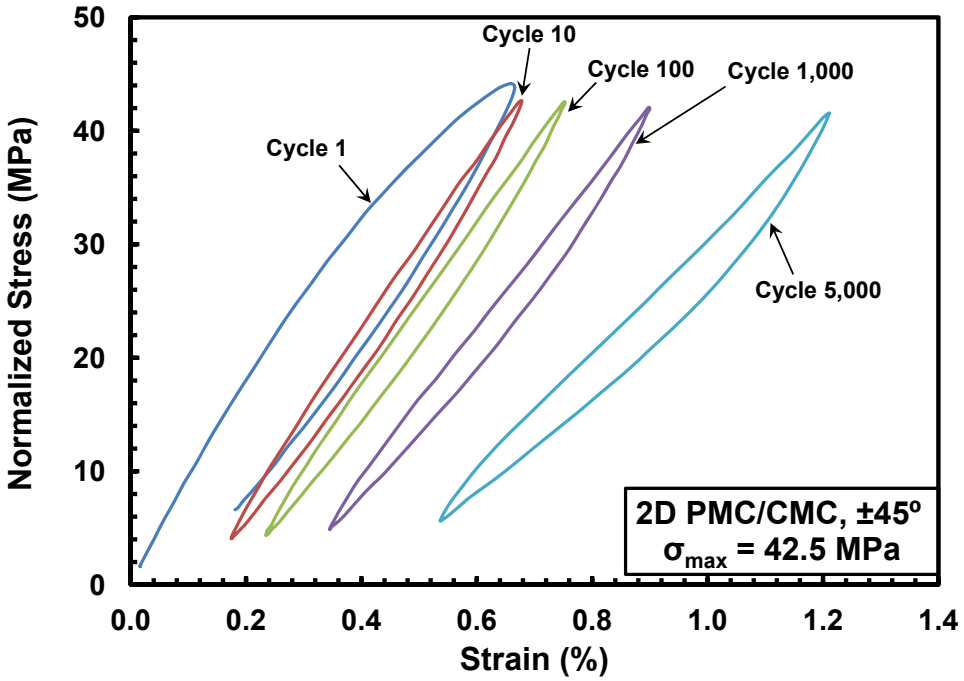

Figure 162: Evolution of stress-strain hysteresis response with fatigue cycles for specimen T6-11 of the 2D PMC/CMC with ±45° fiber orientation at elevated temperature.

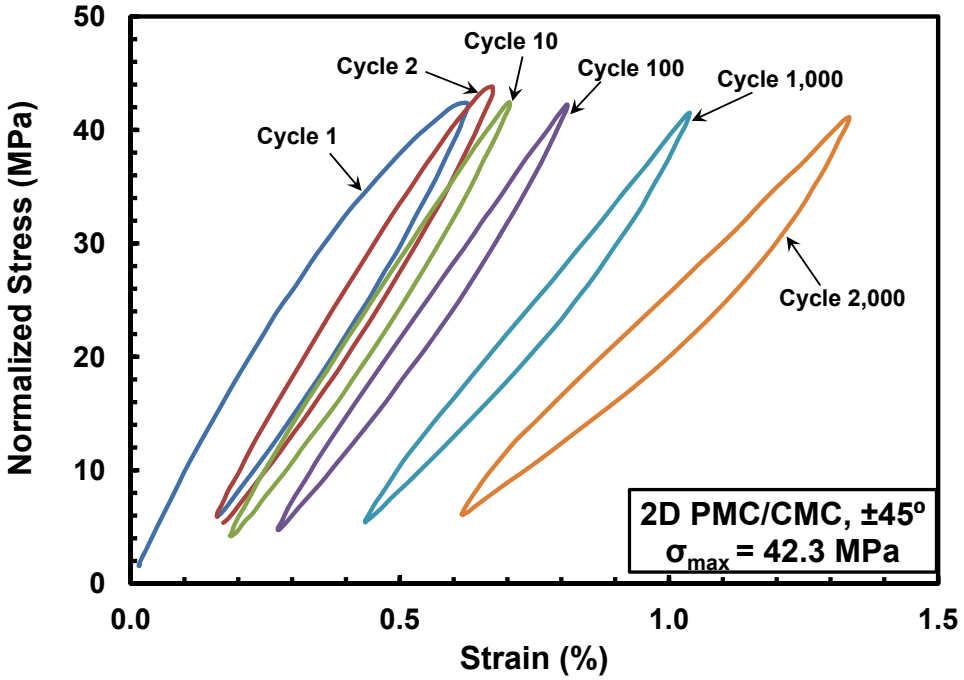

Figure 163: Evolution of stress-strain hysteresis response with fatigue cycles for specimen T6-4 of the 2D PMC/CMC with ±45° fiber orientation at elevated temperature.

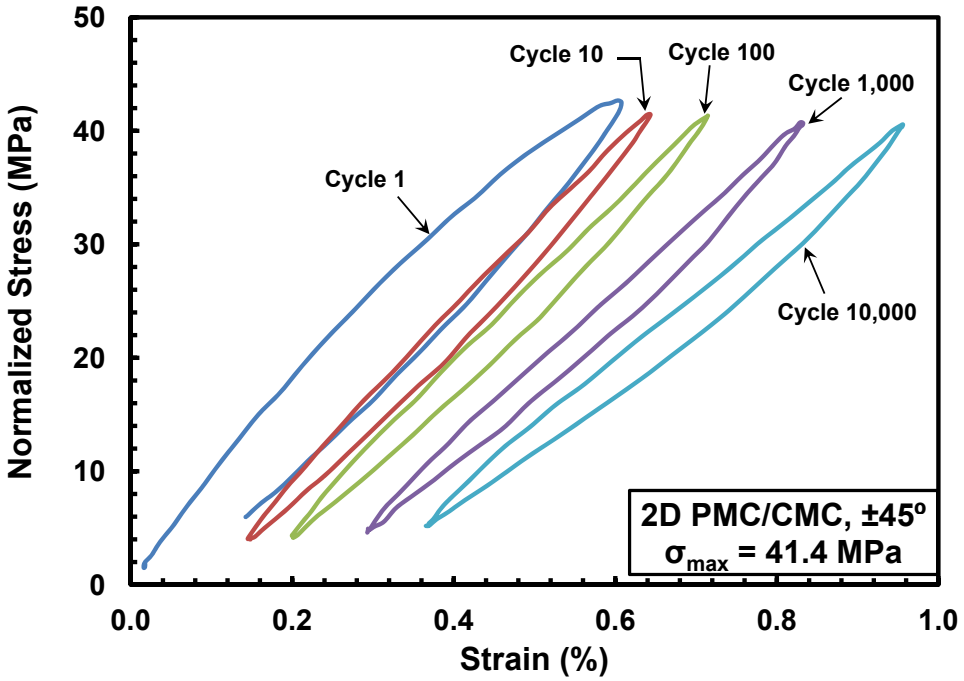

Figure 164: Evolution of stress-strain hysteresis response with fatigue cycles for specimen T6-7 of the 2D PMC/CMC with ±45° fiber orientation at elevated temperature.

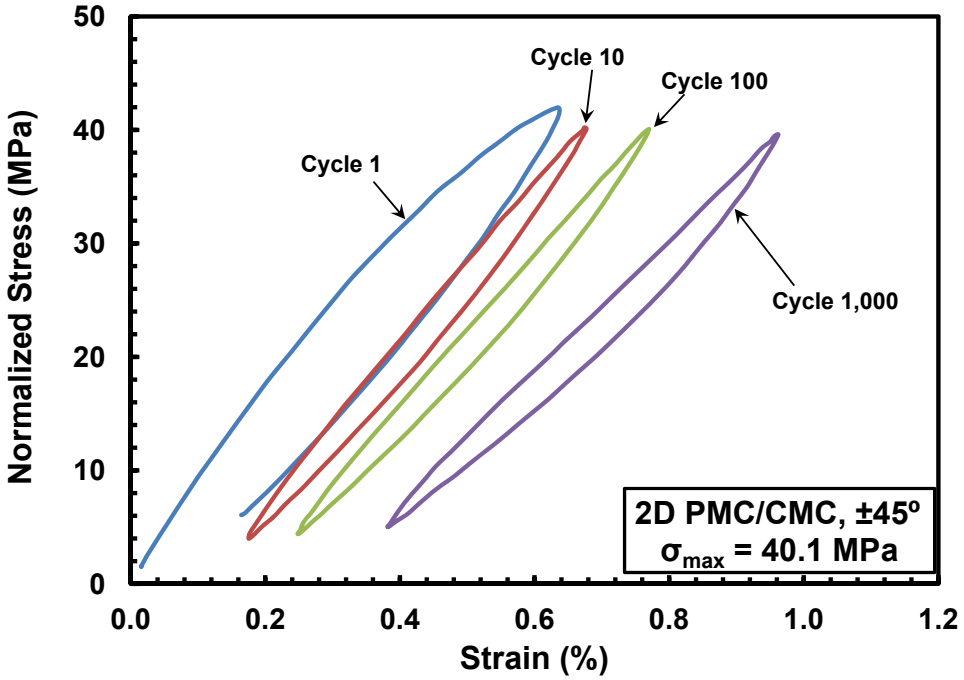

Figure 165: Evolution of stress-strain hysteresis response with fatigue cycles for specimen T6-13 of the 2D PMC/CMC with ±45° fiber orientation at elevated temperature.

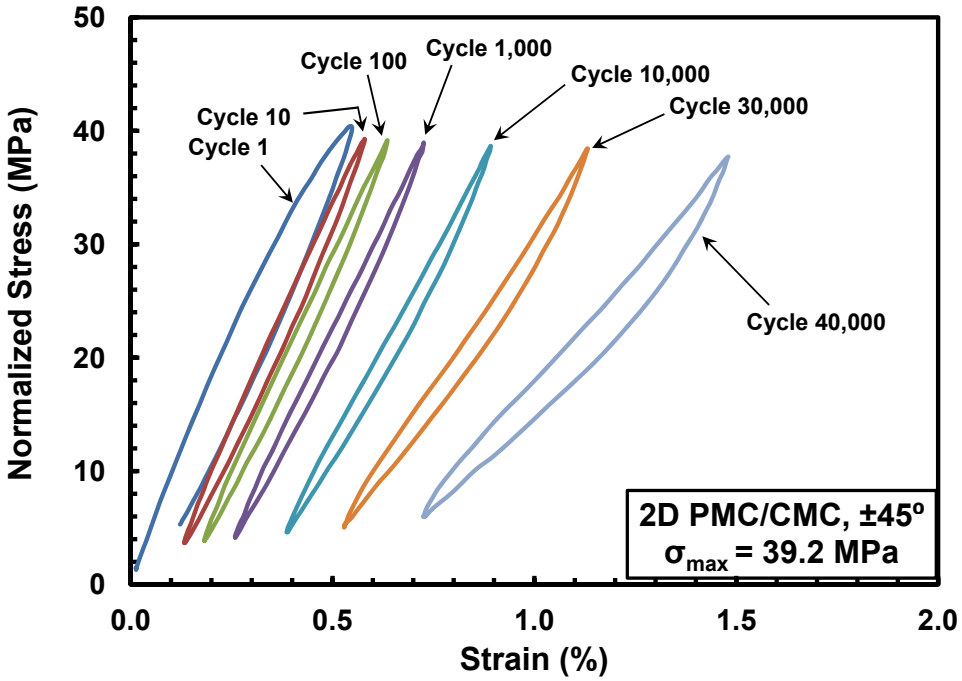

Figure 166: Evolution of stress-strain hysteresis response with fatigue cycles for specimen T6-8 of the 2D PMC/CMC with ±45° fiber orientation at elevated temperature.

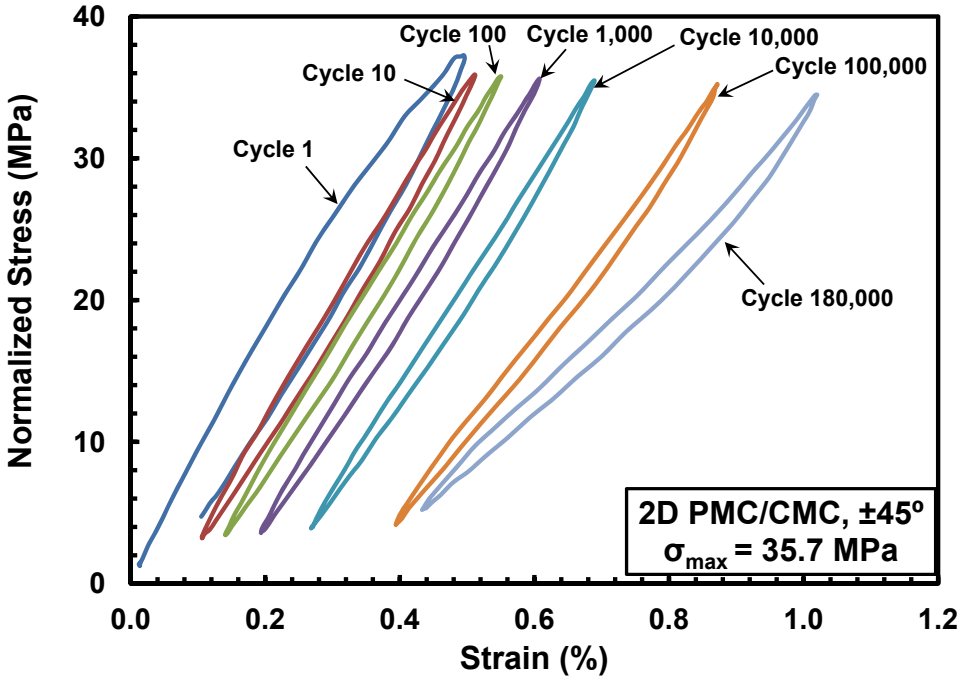

Figure 167: Evolution of stress-strain hysteresis response with fatigue cycles for specimen T6-9 of the 2D PMC/CMC with ±45° fiber orientation at elevated temperature.

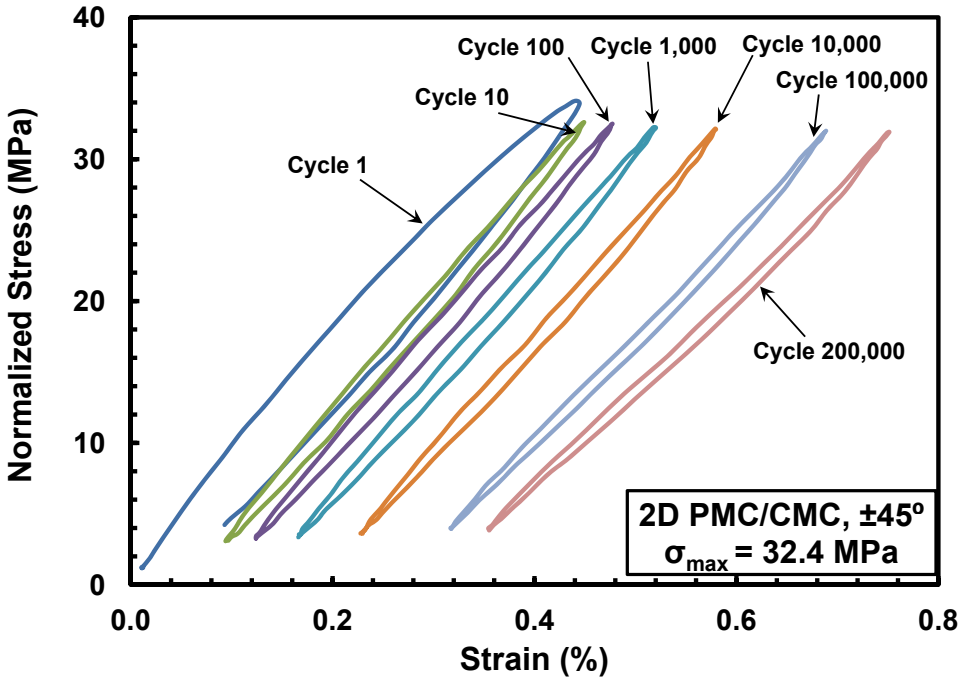

Figure 168: Evolution of stress-strain hysteresis response with fatigue cycles for specimen T6-5 of the 2D PMC/CMC with ±45° fiber orientation at elevated temperature.

Bibliography

[1] Bogdanovich, A. E. and M. H. Mohamed. "Three-Dimensional Reinforcements for Composites". *SAMPE Journal*, 45(6):8 – 28, Nov/Dec 2009.

[2] Bogdanovich, Alexander E., Mehmet Karahan, Stepan V. Lomov, and Ignaas Verpoest. "Quasi-static tensile behavior and damage of carbon/epoxy composite reinforced with 3D non-crimp orthogonal woven fabric". *Mechanics of Materials*, 62(0):14 – 31, 2013. ISSN 0167-6636.

[3] Brandt, J., K. Drechsler, and F.-J. Arendts. "Mechanical performance of composites based on various three-dimensional woven-fibre preforms". *Composites Science and Technology*, 56(3):381 – 386, 1996. ISSN 0266-3538.

[4] Breede, F. and M. Frieß. *Development of Advanced CMC Materials for Dual-bell Rocket Nozzles*. Annual report, Transregional Collaborative Research Center, German Aerospace Center, Institute for Design and Construction Research, Stuttgart, Germany, 2009.

[5] Callister, William D. *Materials Science and Engineering: An Introduction*. John Wiley & Sons, Inc., Hoboken, NJ, 6th edition, 2003.

[6] Cao, Caihua. *Damage and Failure Analysis of Co-Cured Fiber-Reinforced Composite Joints*. Ph.D. thesis, Georgia Institute of Technology, Atlanta, GA, 2003.

[7] Carrillo, J.G. and W.J. Cantwell. "Mechanical properties of a novel fiber—metal laminate based on a polypropylene composite". *Mechanics of Materials*, 41(7):828 – 838, 2009. ISSN 0167-6636.

[8] Carvelli, Valter, Giulia Gramellini, Stepan V. Lomov, Alexander E. Bogdanovich, Dmitri D. Mungalov, and Ignaas Verpoest. "Fatigue behavior of non-crimp 3D orthogonal weave and multi-layer plain weave E-glass reinforced composites". *Composites Science and Technology*, 70(14):2068 – 2076, 2010. ISSN 0266-3538.

[9] Chawla, K. K. *Ceramic Matrix Composites*. Kluwer Academic Publishers, Norwell, MA, 2nd edition, 2003.

[10] Cortes, P., J. Vrabel, and M. Hazel. "Structure-Properties Relations in a Hybrid Laminate Based on a Self-Reinforced Composite Material". 2011.

[11] Daniel, Isaac M. and Ori Ishai. *Engineering Mechanics of Composite Materials*. Oxford University Press, New York, NY, 2nd edition, 1994.

[12] Delapasse, Jacob. *Fatigue Behavior of an Advanced SiC/SiC Composite with an Oxidation Inhibited Matrix at 1200°C in Air and in Steam*. Master's thesis, Air Force Institute of Technology, Wright-Patterson AFB, Ohio, 2010.

[13] Dino, Jonas. "Humans in Space: Thermal Protection System (TPS) and Materials". http://www.nasa.gov/centers/ames/research/humaninspace/humansinspace-thermalprotectionsystem.html, Mar 2008. [Online; accessed 3 Sep 2013].

[14] Federal Aviation Administration. "Aviation Maintenance Technician Handbook". http://www.faa.gov/regulations_policies/handbooks_manuals/aircraft/amt_airframe_handbook/, 2012. [Online; accessed 9 Sep 2013].

[15] Gan, Yong X. "Effect of Interface Structure on Mechanical Properties of Advanced Composite Materials". *International Journal of Molecular Sciences*, 10(12):5115–5134, 2009.

[16] Glass, David E. "Ceramic Matrix Composite (CMC) Thermal Protection Systems (TPS) and Hot Structures for Hypersonic Vehicles". *15th AIAA Space Planes and Hypersonic Systems and Technologies Conference*. AIAA, 2008.

[17] Jones, John. "Polyimide Boosts High-Temperature Performance". http://spinoff.nasa.gov/Spinoff2008/ip_5.html, May 2011. [Online; accessed 2 Sep 2013].

[18] Jones, Tyler. *Tension-Compression Fatigue of Hi-Nicalon/SiC Ceramic Matrix Composite at 1200°C in Air and in Steam*. Master's thesis, Air Force Institute of Technology, Wright-Patterson AFB, Ohio, 2011.

[19] Ladrido, Christine G. *Effect of Prior Aging on Fatigue Behavior of IM7/BMI 5250-4 Composite at 191°C*. Master's thesis, Air Force Institute of Technology, Wright-Patterson AFB, Ohio, 2007.

[20] Lincoln, Jason E. "NRPE Composite Materials". http://www.p2si.com/prepregs/datasheets/NRPE-Public-Release.pdf.

[21] Martin, Rick and Daniel Evans. "Reducing Costs in Aircraft: The Metals Affordability Initiative Consortium". *Journal of the Minerals, Metals, and Materials Society*, 42(3):24–28, 2000.

[22] McDanels, D. L., T. T. Serafini, and J. A. DiCarlo. "Polymer, Metal, and Ceramic Matrix Composites for Advanced Aircraft Engine Applications". *Materials for Energy Systems*, 8(1):80 – 91, June 1986.

[23] Odegard, G and M Kumosa. "Elastic-plastic and failure properties of a unidirectional carbon/PMR-15 composite at room and elevated temperatures". *Composites Science and Technology*, 60(16):2979 – 2988, 2000. ISSN 0266-3538.

[24] Quinn, J.P., A.T. McIlhagger, and R. McIlhagger. "Examination of the failure of 3D woven composites". *Composites Part A: Applied Science and Manufacturing*, 39(2):273 – 283, 2008. ISSN 1359-835X.

[25] Raymer, Daniel P. *Aircraft Design: A Conceptual Approach*. AIAA, New Jersey, 4th edition, 1996.

[26] Rivers, H. Kevin and David E. Glass. *Advances in Hot-Structure Development*. Technical report, NASA Langley Research Center, Hampton, VA.

[27] Ruggles-Wrenn, M. B., D. T. Christensen, A. L. Chamberlain, J. E. Lane, and T. S. Cook. "Effect of frequency and environment on fatigue behavior of a {CVI} SiC/SiC ceramic matrix composite at 1200°C". *Composites Science and Technology*, 71(2):190 – 196, 2011. ISSN 0266-3538.

[28] Ruggles-Wrenn, M. B., J. Delapasse, A. L. Chamberlain, J. E. Lane, and T. S. Cook. "Fatigue behavior of a Hi-Nicalon^{TM}/SiC-B_4C composite at 1200°C in air and in steam". *Materials Science & Engineering*, 534(A):119 – 128, 2012. ISSN 0921-5093.

[29] Ruggles-Wrenn, Marina B. and Vipul Sharma. "Effects of Steam Environment on Fatigue Behavior of Two SiC/[SiC+Si3N4] Ceramic Composites at 1300°C". *Applied Composite Materials*, 18(5):385–396, 2011. ISSN 0929-189X.

[30] Ryther, Chad E. C. *The Effect of Elevated Temperature on the Inelastic Deformation Behavior of PMR-15 Solid Polymer*. Ph.D. thesis, Air Force Institute of Technology, Wright-Patterson AFB, OH, 2012.

[31] Schetz, Joseph A., Alan Baker, Stuart Dutton, and Donald Kelly. *Composite Materials for Aircraft Structures*. AIAA, Reston, VA, 2nd edition, 2004.

[32] Schmidt, S., S. Beyer, H. Knabe, H. Immich, R. Meistring, and A. Gessler. "Advanced Ceramic Matrix Composite Materials for Current and Future Propulsion Technology Applications". *Acta Astronautica*, 55(3 - 9):409 – 420, 2004. ISSN 0094 - 5765.

[33] Stig, Fredrik. *3D-Woven Reinforcement in Composites*. Ph.D. thesis, KTH School of Engineering Sciences, Stockholm, Sweden, 2012.

[34] Stig, Fredrik and Stefan Hallström. "Assessment of the mechanical properties of a new 3D woven fibre composite material". *Composites Science and Technology*, 69(11 - 12):1686 – 1692, 2009. ISSN 0266 - 3538.

REPORT DOCUMENTATION PAGE

Form Approved
OMB No. 0704–0188

1. REPORT DATE *(DD–MM–YYYY)*	2. REPORT TYPE	3. DATES COVERED *(From — To)*
27–03–2014	Master's Thesis	Oct 2012–Mar 2014

4. TITLE AND SUBTITLE

Mechanical Properties and Fatigue Behavior of Unitized Composite Airframe Structures at Elevated Temperature

5a. CONTRACT NUMBER

5b. GRANT NUMBER

5c. PROGRAM ELEMENT NUMBER

6. AUTHOR(S)

Wilkinson, Michael P., Captain, USAF

5d. PROJECT NUMBER

5e. TASK NUMBER

5f. WORK UNIT NUMBER

7. PERFORMING ORGANIZATION NAME(S) AND ADDRESS(ES)

Air Force Institute of Technology
Graduate School of Engineering and Management (AFIT/EN)
2950 Hobson Way
WPAFB, OH 45433-7765

8. PERFORMING ORGANIZATION REPORT NUMBER

AFIT-ENY-14-M-51

9. SPONSORING / MONITORING AGENCY NAME(S) AND ADDRESS(ES)

Air Force Research Laboratory/RQVS
Mr. Michael Falugi
2790 D Street, Bldg. 65
WPAFB OH 45433-7402
(937) 656-8810 michael.falugi@us.af.mil

10. SPONSOR/MONITOR'S ACRONYM(S)

AFRL/RQVS

11. SPONSOR/MONITOR'S REPORT NUMBER(S)

12. DISTRIBUTION / AVAILABILITY STATEMENT

Distribution Statement A: Approved for Public Release; Distribution Unlimited

13. SUPPLEMENTARY NOTES

14. ABSTRACT

The tension-tension fatigue behavior of newly developed polymer matrix composites (PMCs) and that of a unitized composite was studied. The PMCs investigated in this effort consisted of an NRPE (a high-temperature polyimide) matrix reinforced with carbon fibers. Two PMCs consisting of the aforementioned matrix with different fiber architectures were studied: one reinforced with a 2D woven fiber fabric and another reinforced with a non-crimp 3D orthogonal woven fiber fabric. The unitized composite consisted of a PMC co-cured with a ceramic matrix composite (CMC) layer, which acts as a thermal barrier. The PMC portion of the unitized composite had the same constituent properties and weave as the aforementioned 2D PMC. The CMC layer consisted of a zirconia-based matrix reinforced with a 2D woven quartz fiber fabric. For all three material systems (3D PMC, 2D PMC, and unitized composite), material properties were investigated for both on-axis [0/90°] and off-axis [±45°] fiber orientations. Tensile properties were evaluated at (1) room temperature and (2) with one side of the specimen at 329°C and the other side exposed to ambient air. Tension-tension fatigue tests were conducted at elevated temperature at a frequency of 1.0 Hz with a ratio of minimum stress to maximum stress of R= 0.05. Fatigue run-out for this effort was defined as $2{\times}10^5$ cycles.

15. SUBJECT TERMS

Polymer Matrix Composites, Ceramic Matrix Composites, 3D Non-Crimp Orthogonal Weave, Unitized Composites, Fatigue, Mechanical Properties

16. SECURITY CLASSIFICATION OF:			17. LIMITATION OF ABSTRACT	18. NUMBER OF PAGES	19a. NAME OF RESPONSIBLE PERSON
a. REPORT	b. ABSTRACT	c. THIS PAGE			Dr. Marina B. Ruggles-Wrenn (ENY)
U	U	U	UU	196	19b. TELEPHONE NUMBER *(include area code)* (937) 255-3636 x4641 marina.ruggles-wrenn@afit.edu